PROGRESS IN BIOMEDICAL OPTICS AND IMAGING
Vol. 2, No. 3
ISSN 1605-7422

Laser and Noncoherent Light Ocular Effects: Epidemiology, Prevention, and Treatment

Bruce E. Stuck
Michael Belkin
Chairs/Editors

22 January 2001
San Jose, USA

Sponsored by
U.S. Air Force Office of Scientific Research
SPIE—The International Society for Optical Engineering

Proceedings of SPIE
Volume 4246

REPORT DOCUMENTATION PAGE

AFRL-SR-AR-TR-02-

0424

PLEASE DO NOT RETURN YOUR FORM TO THE ABOVE ADDRESS.

1. REPORT DATE (DD-MM-YYYY)	2. REPORT DATE	3. DATES COVERED (From - To)
17-JUL-2002	Final Technical Report	18 JAN 2001 - 17 JAN 2002

4. TITLE AND SUBTITLE

Laser and Noncoherent Light Ocular Effects: Epidemiology, Prevention, and Treatment

5a. CONTRACT NUMBER

5b. GRANT NUMBER

F49620-01-1-0153

5c. PROGRAM ELEMENT NUMBER

6. AUTHOR(S)

Bruce E. Stuck
Michael Belkin

5d. PROJECT NUMBER

5e. TASK NUMBER

5f. WORK UNIT NUMBER

7. PERFORMING ORGANIZATION NAME(S) AND ADDRESS(ES)

Society of Photo-Optical Instrumentation Engineers
PO Box 10
Bellingham, WA 98227-0010

8. PERFORMING ORGANIZATION REPORT NUMBER

Volume 4246

9. SPONSORING/MONITORING AGENCY NAME(S) AND ADDRESS(ES)

Air Force Office of Scientific Research
801 N. Randolph Street, Room 732
Arlington, VA 22203-1977

10. SPONSOR/MONITOR'S ACRONYM(S)

AFOSR/NL

11. SPONSORING/MONITORING AGENCY REPORT NUMBER

12. DISTRIBUTION AVAILABILITY STATEMENT

Approved for Public Release

13. SUPPLEMENTARY NOTES

ISBN 0-8194-3924-X

14. ABSTRACT

This proceedings contains papers on the following topics: ocular hazards, oculr dynamics, ocular damage threshholds, optical coherence tomography, corneal exposures, corneal damage thresholds, laser eye protection research.

15. SUBJECT TERMS

biomedical optics

16. SECURITY CLASSIFICATION OF:			17. LIMITATION OF ABSTRACT	18. NUMBER OF PAGES	19a. NAME OF RESPONSIBLE PERSON
a. REPORT	b. ABSTRACT	c. THIS PAGE			Janice Gaines Walker
Non-Classified			SAR	186	19b. TELEPONE NUMBER (Include area code) (360)676-3290

Standard Form 298 (Rev. 8-98)
Prescribed by ANSI-Std Z39-18

PROGRESS IN BIOMEDICAL OPTICS AND IMAGING
Vol. 2, No. 3

Laser and Noncoherent Light Ocular Effects: Epidemiology, Prevention, and Treatment

Bruce E. Stuck
Michael Belkin
Chairs/Editors

22 January 2001
San Jose, USA

Sponsored by
U.S. Air Force Office of Scientific Research
SPIE—The International Society for Optical Engineering

Published by
SPIE—The International Society for Optical Engineering

Proceedings of SPIE
Volume 4246

Please use the following format to cite material from this book:

Author(s), "Title of paper," in *Laser and Noncoherent Light Ocular Effects: Epidemiology, Prevention, and Treatment*, Bruce E. Stuck, Michael Belkin, Editors, Proceedings of SPIE Vol. 4246, page numbers (2001).

ISSN 1605-7422
ISBN 0-8194-3924-X

Published by
SPIE—The International Society for Optical Engineering
P.O. Box 10, Bellingham, Washington 98227-0010 USA
Telephone 1 360/676-3290 (Pacific Time) • Fax 1 360/647-1445
http://www.spie.org/

Printed in the United States of America.

Contents

Conference Committee

Conference Chairs

Bruce E. Stuck, Walter Reed Army Institute of Research (USA)
Michael Belkin, Tel-Aviv University (Israel)

Program Committee

Jeremiah Brown, Jr., Walter Reed Army Institute of Research (USA)
Randolph D. Glickman, University of Texas Health Science Center at San Antonio (USA)
Amir Langus, Tel-Aviv University (Israel)
David J. Lund, Walter Reed Army Institute of Research (USA)
David O. Robbins, Ohio Wesleyan University (USA)
James B. Sheehy, Naval Air Development Center (USA)
Elmar T. Schmeisser, TASC, Inc (USA)
Steven T. Schuschereba, Walter Reed Army Institute of Research (USA)
David H. Sliney, U.S. Army Center for Health Promotion and Preventive Medicine
Myron L. Wolbarsht, Duke University (USA)
Joseph A. Zuclich, TASC, Inc (USA)
Harry Zwick, Walter Reed Army Institute of Research (USA)

Untoward effects of high dose methylprednisolone therapy on blood-retinal barrier closure, retinal hole repair, and long-term scarring.

S.T. Schuschereba, J. Brown Jr., B.E. Stuck, J. Marshall*
U.S. Army Medical Research Detachment, Brooks Air Force Base, San Antonio, TX 78235;
*The Rayne Institute, St. Thomas' Hospital, London, England.

ABSTRACT

Thirty-seven New Zealand Red rabbits were either dosed with methylprednisolone sodium succinate (MP, n=18) about 20 min before laser irradiation, or they were left untreated (n=19). Dosing with MP was tapered at 30, 30, 20, 20, and 10 mg/kg/day for five consecutive days. Retinas were irradiated with a multi-line argon laser to produce retinal injuries (grid of 16 lesions/eye) near hemorrhaging levels (285 mW/10msec, 290 μm retinal spot size). A variety of funduscopic and histologic assessments were made for hemorrhagic and non-hemorrhagic lesions from 10 min to 6 mo after injury.

Fluorescein angiography showed that non-hemorrhagic control lesions stopped leaking at 3d post injury, but MP-treated lesions leaked for 2-4 days longer. After MP treatment, funduscopic lesion areas were similar to controls during the first 24 h then became smaller by 1 mo. After 1 mo, MP-treated lesions increased in area while controls became reduced. Histologic analysis showed no effect on reduction of neutrophils (PMN) in MP-treated lesions over controls at 3 hr. At 24 hr, retinal PMN values in hemorrhagic lesions of the MP group were elevated ($p<0.05$) while monocyte/macrophage counts were reduced ($p<0.05$) compared to control. At 4d, MP impeded replacement of lost retinal tissue, and contributed to retinal hole development at 1 mo followed by extensive enhancement of chorio-retinal scarring at 6 mo.

In severe laser-induced retinal trauma, the immunosuppressive effects of high dose MP therapy contributed to a variety of untoward wound healing outcomes, thereby suggesting caution in its use to treat similar injuries in humans.

Keywords: laser-induced retinal injury, treatment, methylprednisolone, neuroprotection, immunosuppression, inflammation, neutrophil, retinal hemorrhage, retinal hole, and scarring.

1. INTRODUCTION

Primary laser-induced retinal damage such as photothermal and photomechanical processes induce the onset of early stage secondary damage events such as edema, ischemia-reperfusion injury, lipid peroxidation, and inflammation [1-7]. These early stage secondary processes lead to late stage tertiary damage events such as scarring, scar remodeling and neovascularization, which contribute to retinal traction, retinal hole formation, detachments, and continued tissue degeneration and vision loss[5].

Although damage events responsible for tissue degeneration and vision loss are becoming better understood, no effective or results-based therapeutics can be recommended for therapy to spare vision. One of the main therapeutic candidates for laser injury, which has also been widely used to treat spinal cord and head trauma injuries, has been the steroid, methylprednisolone (MP) [8,9]. Such steroids also have been extensively utilized in suppressing inflammation in a variety of diseases, and they are known to inhibit free-radical-mediated lipid peroxidation and to reduce edema [10,11]. Further, steroids are widely used by ophthalmologists for treating a variety of chronic inflammatory conditions and in some cases have been used to treat laser-induced retinal trauma [12]. Unfortunately, results of therapy for laser ocular trauma have been anecdotal [12] and often controversial [2,3,5,7,13-16], thereby necessitating properly controlled studies to confirm their utility. To gain better insight into the utility of steroid therapy for LIRIs, a controlled morphologic and morphometric study was conducted in rabbits.

The purpose of this study was to test the hypothesis that treatment with methylprednisolone (MP) would reduce short-term secondary injury and therefore, long-term outcomes would also be improved.

Laser and Noncoherent Light Ocular Effects: Epidemiology, Prevention, and Treatment,
Bruce E. Stuck, Michael Belkin, Editors, Proceedings of SPIE Vol. 4246 (2001)

2. MATERIALS and METHODS

Thirty-seven New Zealand Red rabbits were used in this study (Table 1). All animal handling was in accordance with the National Research Council's guidelines on animal use and care. Animals were anesthetized intramuscularly with a mixture of Ketamine HCL 35 mg/kg, Xylazine 4.9 mg/kg, and Acepromazine 0.7 mg/kg.

Animals were pretreated (IV) with methylprednisolone sodium succinate (Solu-Medrol, Upjohn, Kalamazoo, MI), a glucocorticoid (MP, n=18). Controls were untreated (n=19). Fifteen min after the first pretreatment, animals received laser irradiation (16 lesions/eye) from a multiline (454-514.5 nm) cw argon ion laser (Omnichrome, Model 543-600MA, Chino, CA) 4 mm inferior to the medullary streak and temporal to the optic disc. The laser was calibrated with a power meter (Scientech, Boulder, CO) to deliver 285 mW at 7 ms. The laser was co-aligned with a Zeiss fundus camera to facilitate placement and observation of lesions.

Funduscopy and fluorescein angiography were performed at 10 min, 1h, 3h, 1-4d, 1-3wk, and 1-6 mo after laser irradiation. Immediately following fundus photography, fluorescein angiography was performed by intravenous injection into a large lateral ear vein of 1 ml of 10% fluorescein isothiocyanate solution. After 10 min of equilibration, fluorescein angiograms were recorded on Tri-X Pan 400 film.

Histology was performed at 3h, 1d, 1 mo, and 6 mo. The eyes were immediately enucleated and fixed in 50 ml of 3% glutaraldehyde and 2% paraformaldehyde solution, and tissue samples were processed for routine transmission electron microscopy[17]. Blocks of tissue were serially sectioned, in the inferior and superior plane, with a diamond knife (Diatome, Fort Washington, PA) on an Ultracut E (Reichert-Jung, Vienna, Austria) microtome at 1μm.

Changes in lesion characteristics were quantitated from fundus photographs, and histologic sections. All measurement procedures were performed utilizing calibration methods to obtain either arbitrary or actual units. Lesion area measurements were performed using the public domain NIH Image 1.61b7 program (developed by Wayne Rasband at the U.S. National Institutes of Health and available on the internet at http://rsb.info.nih.gov/nih-image/). Maximum RPE diameters were determined for all lesion centers on histology sections prior to any measurements. The lesions were also segregated into nonhemorrhagic and hemorrhagic ($\geq$ 10 red blood cells in any section in the subretinal space) types. Leukocyte counts were performed at 3 and 24 h. Only leukocytes found anterior to the RPE and posterior to the ONL within lesions were counted. At 3 h, polymorphonuclear cells (mainly neutrophils) were counted within lesions. At 24 h, both polymorphonuclear and mononuclear cells (mainly monocytes) were counted in a similar fashion. To determine the extent of photoreceptor sparing, the number of nuclei in the ONL was counted at maximum RPE lesion diameters. Dividing the lesion count/mm by the adjacent normal count/mm and multiplying by 100 determined percent photoreceptor sparing. Choroidal scar areas were measured in a similar manner as the fundus lesion areas at the designated maximum RPE lesion diameters only, and data were collected at 1 and 6 mo from scanned and digitized images on Polaroid 59 film.

Where appropriate, means, standard errors of the mean, and statistical analyses were performed by use of the one-way analysis of variance model, Duncan's t test, at a significance level of $p = 0.05$.

Table 1. Animal dispositions

Treatment	Time	3h	1d	1mo	6mo	Total
Control/No. Animals used		7	6	4	2	**19**
MP/No. Animals used		6	6	4	2	**18**

3. RESULTS

A time course comparison using fluorescein angiography was performed for the control, and methylprednisolone-treated (MP) groups. Treatment with MP showed that leakage persisted at 3 days post injury, while leakage was nearly stopped in the control (Fig. 1). Also, treatment with MP extended the blood-retinal barrier repair time past 4 days after injury and treatment.

The mean percent change in funduscopic lesion areas was compiled from 3h to 6 months after injury (Fig. 2). The two main features of high-dose multi-day treatment with MP on lesion area were 1) that MP had no effect on lesion areas up to 2 days after injury and 2) that lesion areas were returning to near control sizes by 5 and 6 months. From 3h to about 4d the main features comprising measured lesion areas were edema and opacity. From about 4d to about 21d the main features were depigmentation and hyperpigmentation. From 21d to 6 months the main features were pigmentation changes and scar opacity (Fig. 2).

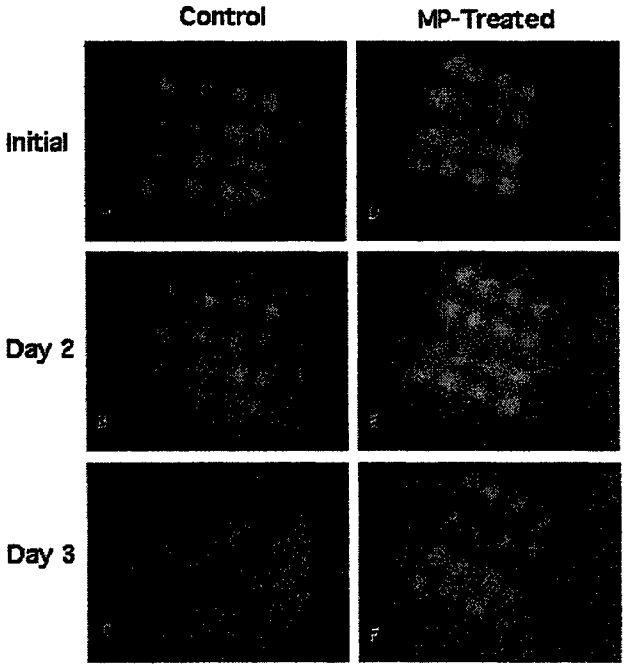

Figure 1. Fluorescein angiograms of Control (A-C) and Methylprednisolone-treated (MP-Treated, D-F) lesions after injury.

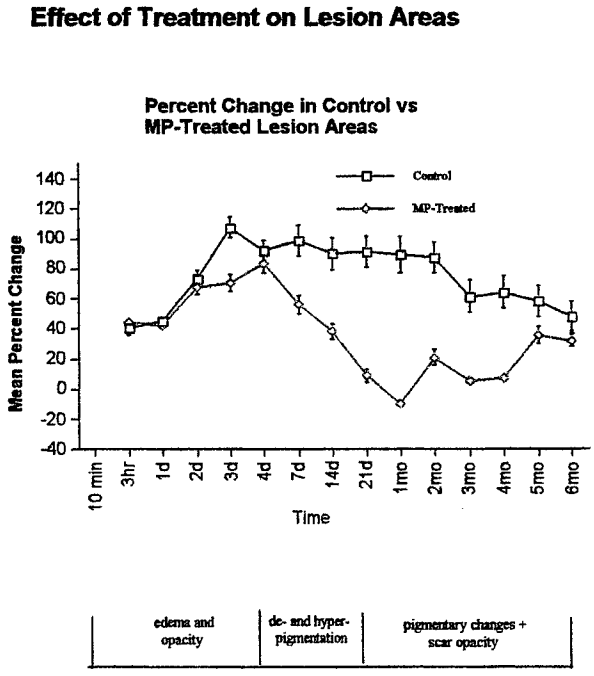

Figure 2. Lesion areas from funduscopic images from 3 hours to 6 months after injury and treatment. Error bars =SEM

A comparison of retinal laser lesions from funduscopy to histologic sections of the same lesion centers was made. The non-treated lesion series (control) indicated the normal progression of wound healing for nonhemorrhagic (type I) to hemorrhagic (type II, subretinal hemorrhage and type III, vitreous hemorrhage) lesions. The centers of funduscopic lesion zones were aligned with histologic centers of lesions (Fig. 3). Controls indicated little scar formation over a time course up to 6 months. With hemorrhagic type lesions (TII and TIII), a greater loss of photoreceptors and larger scar formation occurred (Fig. 3A,B). Therapy with MP indicated fewer lesion macrophages, inhibition of tissue replacement at 4d (note depression in lesion sites, Fig. 3C), retinal hole formation at 1 month (Fig. 3D), and enlarged chorio-retinal scars for all lesion types at 6 months (Fig. 3E).

Mean neutrophil numbers were obtained from nonhemorrhagic vs hemorrhagic lesions at 1, 3, and 24h after injury and treatment (Fig. 4A-D). Values in the retinal compartment were compared to the choroidal compartment. Compared to control (Fig. 4A), treatment with MP elevated neutrophil numbers in the retina from 3 to 24h in hemorrhagic lesions (Fig. 4C). Also at 24h, neutrophil numbers for hemorrhagic and nonhemorrhagic lesions in the choroidal compartment were elevated (Fig. 4B,D). When neutrophil numbers were compared to monocyte/macrophage numbers in the retina at 24 h after MP treatment, hemorrhagic lesions showed higher neutrophil numbers and lower macrophage numbers compared to the control (Fig. 5). Scar areas at lesion center were slightly increased over control in hemorrhagic lesions at 1 month (Fig. 6); however, scar areas were significantly elevated in these lesions by 6 months (Fig. 7). Photoreceptors continued to be lost for all lesion types from 1 to 6 months with no benefit provided by MP-treatment (Fig. 8A). Further, MP provided no neuroprotection or sparing of photoreceptors at 6 months for either nonhemorrhagic or hemorrhagic lesions (Fig. 8B).

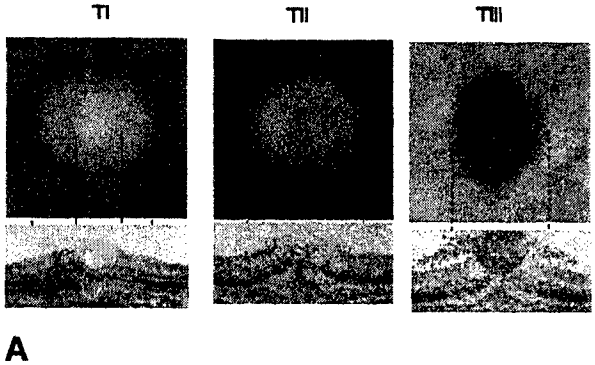

A

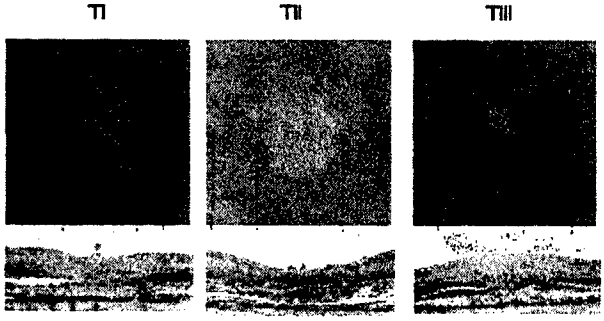

B

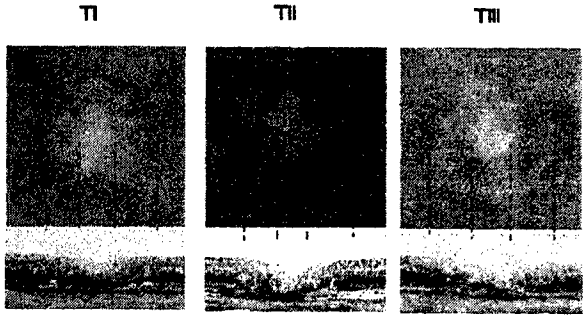

C

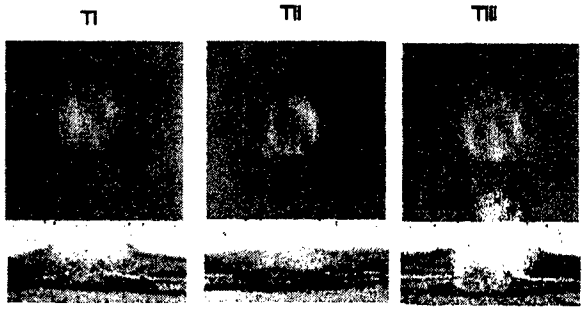

D

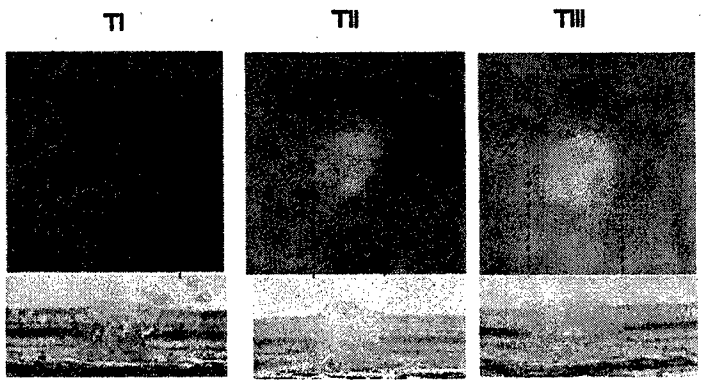

Figure 3. Lesions were compared by funduscopy and histology at lesion centers. All photo enlargements were standardized within figure sets. Vertical dashed lines relate funduscopy to histology. A. Control lesions 3 h after injury for type I-III (TI-III) injuries (type I= opaque lesion, type II = subretinal hemorrhage, and type III = vitreous hemorrhage). Control and MP-treated lesions were similar from 3 to 24 h post injury. B. Control lesions at 4 days post injury. Retinal cell growth has filled in for the lost retinal elements in lesion centers. C. Retinal lesions 4d post treatment with MP showed suppressed cell growth and lack of cell filling in for lost retinal elements. Evidence of early stage retinal hole formation is apparent in all lesion types. D. Retinal lesions 1 month after MP treatment. Retinal glial elements have not filled in for the lost retinal elements and large retinal holes are present. E. Retinal lesions 6 months after MP treatment. Extensive scarring has occurred in both the retina and choroid.

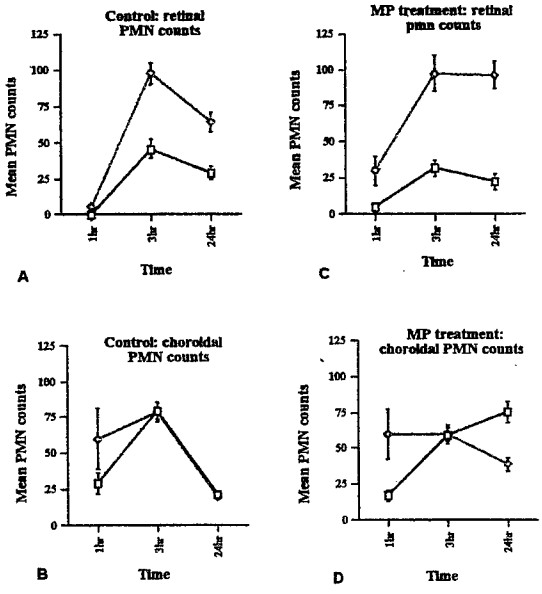

Fig. 4

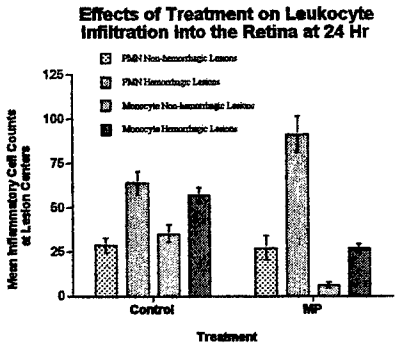

Fig. 5

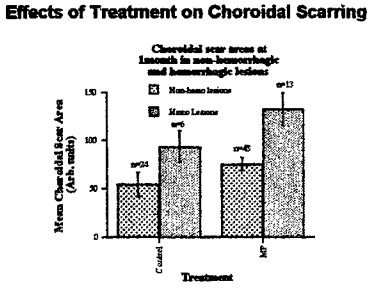

Fig. 6

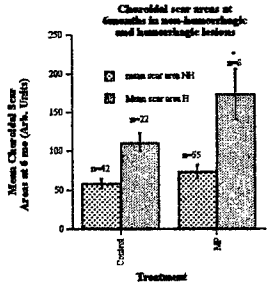

Fig. 7

Fig. 8

Figures 4-10. Fig 4. Neutrophil entry into the choroid and retina of nonhemorrhagic (squares) and hemorrhagic lesions (diamonds) at 3h after injury. Fig. 5. Neutrophil and monocytic cell entry into the retina at 24h. Fig. 6. Choroidal scar areas at 1 month. Fig. 7. Choroidal scar areas at 6 months. Fig. 8A. Photoreceptor sparing in all lesions at 1 and 6 months. Fig 8B. Photoreceptor sparing at 6 months in nonhemorrhagic and hemorrhagic lesions. Error bars = S.E.M.

4. DISCUSSION

It is well known that laser-induced retinal injuries produce a wide variety of tissue responses, but the problem of appropriately defining treatment targets and therapeutics for proposes of augmenting wound healing and sparing vision has been challenging[12]. Due to the wide acceptance of steroids for treating a variety of ocular disorders, clinicians often prescribe steroids such as MP for these injuries[12]. Clinically, however, the rationale for steroid use is anecdotal and no clear human studies have been conducted for this indication. Recently, the use of steroids has been questioned in treating head and spinal cord trauma[10,18,19], and studies on steroid use for treating laser-induced retinal injuries have also questioned the validity of their use[14-16]. Results reported here are extensions of our earlier work and findings continue to indicate that steroid treatment of such injuries needs to be more carefully considered [4,5,14].

Because of delay in blood-retinal barrier repair, as evidenced by persistent leakage in FAs, it can be speculated that RPE cell proliferation has been inhibited through the well-known action of MP suppression of cell growth and replication [20,21]. This effect of MP presumably occurs through the action of inhibiting transcription factor binding to promoter sites on genes, thereby inhibiting the translation of key cytokines and growth factors that are requisite for cell growth[20,21]. The reduction of funduscopic lesion areas from 4d to 1 month by MP, as observed in Fig. 2, may be explained by suppression of RPE cell proliferation and migration, since the main feature of lesion edges at this time was defined by pigmentation changes.

The entry of neutrophils (PMNs) into central nervous system tissues after trauma is generally regarded as not beneficial because injury is often exacerbated [22-25]. It is unclear as to why a lack of effect occurred with MP treatment in curtailing PMN entry into the injury zones of the choriod and retina, but a possible explanation may exist in the fact that MP has been shown to inhibit PMN apoptosis [26,27], and this effect would promote increased numbers at lesions sites. Another explanation for lack of effect of MP in curtailing PMNs at 24 h may be due to its inability to suppress key signals that attract PMNs, such as IL-8, or that therapeutic doses take more than 24 h to be attained.

Therapy with MP also reduced macrophage numbers within lesions. The suppression of macrophages, however, is generally not regarded as being beneficial to wound healing events, since they are thought to augment wound healing by

secreting important agents and mediators [28]. In this sense, treatment of lesions with MP produced two untoward effects on leukocytes, 1) PMN entry was not curtailed and 2) monocyte/macrophage entry was curtailed

Another important observation to steroid use in treating laser-induced retinal injury was the promotion of retinal hole formation. In fact, early stage hole development was detected as early as 4 days after MP treatment (Fig. 3C), and this coincided with debris clearance by both RPE and macrophage-like cells. By this time, however, it was not entirely clear why the high dose MP treatment regimen in rabbits did not curtail all macrophage activity, but dose tapering and refractory effects may have influenced this. Also, injured tissues may have responded by other pathways to attract macrophages into the injury site and these pathways may have included processes not influenced by MP. Two factors appeared to contribute to early stage retinal hole development 1) clearance of dead cells created a retinal gap and 2) lack of cell growth prevented the filling in of the retinal gap. Since the main scar forming cells in the retina are glial cells, inhibition of their growth would significantly reduce filling in for the retinal tissue lost after the initial injury. This effect of inhibiting scar formation was most pronounced by 1 month where many MP-treated lesions showed large and partial-thickness retinal holes. The observation that cell growth was suppressed by MP therapy, up to at least 1month post treatment, has significant implications for retinal wound healing and sparing of vision.

Also surprising was the fact that lesions, by 6 months after injury and MP treatment, demonstrated the formation of large choroidal, chorio-retinal, and retinal scars. In the 6 month hemorrhagic lesions, the scars were larger and seemed to suggest that previously injured and immunosuppressed retina had over-compensated in the scarring response. This concept is supported by previous work, where effects of steroids resulted in over-production of steroid receptors during immunosuppression [29]. This work implied that when normal amounts of endogenous steroid were produced, the effects of low levels of steroid were enhanced, due to the increased number of receptor binding sites [29].

One of the benefits of MP therapy was thought to be neuroprotection, as previously described in both head and spinal cord trauma [30]; however, MP therapy in the rabbit did not spare photoreceptors on the flanks of lesions at 6 months.

In this study, the use of MP for treating LIRIs has indicated that a large variety of negative sequelae occur after treatment of laser-induced retinal injuries and that, in the very least, MP therapy should be used with caution. Although we have confirmed that similar pathology occurs after laser-induced retinal injury in rabbits and humans [31], it must also be pointed out that further work is needed to confirm if similar treatment results occur in non-human primate models and humans.

In conclusion, methylprednisolone therapy resulted in the following deleterious effects 1) repair of the blood retinal barrier was delayed suggesting suppression of RPE cell activity. 2) The acute inflammatory response after trauma, which leads to secondary damage, was not curtailed and the debris clearance rate in the wound may have been impeded due to suppression of macrophage activity. 3) Due to immunosuppressive effects of MP, inhibition of retinal glial elements, which normally replace lost tissue, contributed to retinal hole development around 1 month. 4) At 6 months, immunosuppression enhanced chorio-retinal scarring, and 5) no neuroprotection was provided to photoreceptors. Consequently, neither short-term nor long-term benefits could be attributed to the treatment regimen with MP. Since similar pathological sequelae occur after laser-induced retinal injury in both rabbits and humans, it is possible that effects of treatment in humans may be similar to those observed in rabbits, but this needs to be confirmed.

ACKNOWLEDGEMENTS

The authors thank Michael E. Cross, Donna R. Clarkson, Peter Edsall, Jose Pizzaro, and Andre' Akers for technical support.

DISCLAIMER

In conducting the research described in this report, the investigators adhered to the "Guide for the Care and Use of Laboratory Animals, " as promulgated by the Committee on Revision of the Guide for Laboratory Animal Facilities and Care, Institute of Laboratory Animal Resources, National Academy of Sciences- National Research Council.
The opinions or assertions contained herein are the private views of the authors and not to be construed as official or as reflecting the views of the Department of the Army or the Department of Defense.
Citation of trade names in this report does not constitute an official endorsement or approval of the use of such items.

5. REFERENCES

1. Marshall J, Hamilton AM, Bird AC: Histopathology of ruby and argon laser lesions in monkey and human retina. A comparative study. Brit J. Ophthalmol 59:610-630;1975.

2. Marshall J: Structural aspects of laser-induced damage and their functional implications. Health Physics 56:617-624;1989.

3. Mellerio J, Marshall J, Tengroth B, Anderberg B, Wolbarscht M: Battlefield laser weapons: an assessment of systems, hazards, injuries and ophthalmic resources required for treatment. Laser Light Ophthalmol 4:41-67;1991.

4. Schuschereba ST, Cross ME, Pizarro JM, Ujimori V, Nemeth TJ, Bowman PD, Stuck BE, Marshall J: Pretreatment with hydroxyethyl starch-deferoxamine but not methylprednisolone reduces secondary injury to retina after laser irradiation. Lasers and Light in Ophthalmology. 8:1-14;1997.

5. Schuschereba ST and Scales DK: Current therapy for laser-induced retinal injury: overview of clinical and experimental approaches. In SPIE Proceedings of Laser and Noncoherent ocular effects: epidemiology, prevention, and treatment. Stuck BE, Belkin M (eds) 2974:171-188;1997.

6. Mainster MA: Decreasing retinal photocoagulation damage: principles and techniques. Seminars in Ophthalmol. 14:200-209;1999.

7. Mainster MA: Retinal laser accidents: mechanisms and management. J Laser Applications 12:3-9:2000.

8. Cronstein BN: Clinical use of methylprednisolone sodium succinate: a review. Curr Ther Res 56:1-15:1995.

9. Bracken MB, Shepard MJ, Collins WF et al.: A randomized, controlled trial of methylprednisolone or naloxone in the treatment of acute spinal-cord injury. N Engl J Med 322:1405-1411;1990.

10. Hall ED, Yonkers PA, Taylor BM, Sun FF: Lack of effect of postinjury treatment with methylprednisolone or tirilazad mesylate on the increase in eicosanoid level in the acutely injured cat spinal cord. J Neurotrauma 12:245-256;1995.

11. Young W: Clinical care of brain and spinal cord injury. J. Neurotrauma 8:1-2;1991.

12. Wolfe JA: Laser retinal injury. Military Medicine 150:177-185;1985.

13. Rosner M, Tchirkov M, Dubinski G, Naveh N, Tso MOM: Methylprednisolone ameliorates laser induced retinal injury in rats. Invest Ophthalmol Vis Sci 37:S694; 1996.

14. Schuschereba ST, Cross ME, Scales DK, Pizarro JM, Edsall PR, Stuck BE, Marshall J: High dose methylprednisolone treatment of laser-induced retinal injury exacerbates acute inflammation and long-term scarring in Rol PO, Joss KM, Manns F, Stuck BE, Belkin M (eds) Proceedings of Ophthalmic Technologies IX-SPIE 3591:430-447;1999.

15. Solberg Y, Dubinski G, Tchirkov M, Belkin M, Rosner M: Methylprednisolone therapy for retinal laser injury. Survey of Ophthalmology 44:S85-S92;1999.

16. Berkana Y, Belkin M: Laser eye injuries. Survey of Ophthalmol. 44:459-478;2000.

17. Schuschereba ST, Bowman PD, Ferrando RE, Lund DJ, Quong JA, and Vargas JA: Accelerated healing of laser-injured rabbit retina by basic fibroblast growth factor. Invest. Ophthalmol Vis Sci 35:945-954;1994.

18. Prendergast MR, Saxe JM, Ledgerwood AM, Lucas CE, Lucas WF: Massive steroids do not reduce the zone of injury after penetrating spinal cord injury. J Trauma 37: 576-580;1994.

19. Hurlbert RJ: Methylprednisolone for acute spinal cord injury: an inappropriate standard of care. J Neurosurg (Spine) 93:1-7:2000.

20. Scheinman RI, Cogswell PC, Lofquist AK, Baldwin Jr AS: Role of transcriptional activation of IkB alpha in mediation of immunosuppression by glucocorticoids. Science 270:283-286;1995.

21. Auphan N, DiDonato JA, Rosette C, Helmberg A, Karin M: Immunosuppression by glucocorticoids: inhibition of NF-kB activity through induction of IkB synthesis. Science 270:286-290;1995.

22. Ainsworth TM, Lynam EB, Sklar L: Neutrophil function in inflammation and infection. In: Sirica AE (ed) Cellular and Molecular Pathogenesis pp37-55 Philadelphia: Lippincott-Raven Publishers 1996.

23. Smith D, Lee EK, Saloupis P, Davis JK, Hatchell DL: Role of neutrophils in breakdown of the blood-retinal barrier following intravitreal injection of platelet-activating factor. Exp Eye Res. 59:425-432;1994.

24. Choi M, Rabb H, Armaout MA, and Ehrlich HP: Preventing the infiltration of leukocytes by monoclonal antibody blocks the development of progressive ischemia in rat burns. Plast Reconstr Surg 96:1177-1185;1995.

25. Schoettle RJ Kochanek PM, Magaaree MJ, Uhl MW, and Nemento EM: Early polymorphonuclear leukocyte accumulation correlates with the development of posttraumatic cerebral edema in rats. J Neurotrauma 7:207-217;1990.

26. Liles C, Dale DC, Klebanoff SJ: Glucocorticoids inhibit apoptosis of human neutrophils Blood 86:3181-3188;1995.

27. Cox G: Glucocorticoid treatment inhibits apoptosis in human neutrophils. Separation of survival and activation factors. J. Immunol 154:4719-4729;1995.

28. DiPietro LA: Wound healing: the role of the macrophage and other immune cells. Shock 4:233-240;1995.

29. Weigers GJ and Reul JMHM: Induction of cytokine receptors by glucocorticoids: functional and pathological significance. Trends in Pharmacological Sciences. 19:317-321;1998.

30. Hall ED: The neuroprotective pharmacology of methylprednisolone. J Neurosurg 76:13-22;1992.

31. Schuschereba ST, Scales DK, Cross ME, Pizarro JM, Lund DJ, Stuck BE, and Marshall J: Neutrophils are important treatment targets immediately after severe laser retinal injury in human and rabbit retinas. Investigative Ophthalmol Vis Sci. 38: S85; 1997.

Clinical features of laser-induced macular holes as imaged by optical coherence tomography (OCT)

Jeremiah Brown, Jr.[1,2], Harry Zwick[1], Steven T. Schuschereba[1], Bruce E. Stuck[1]
[1]US Army Medical Research Detachment of the Walter Reed Army Institute of Research, Brooks Air Force Base, TX 78235, [2]Brooke Army Medical Center, Ophthalmology Service, 3851 Roger Brooke Drive, Fort Sam Houston, TX 78234

ABSTRACT

The increasing number of laser applications in military and industrial settings has resulted in a rising number of laser eye injuries. Laser-induced macular holes are one type of injury, usually caused by accidental exposure to radiation from a Q-switched Nd:YAG laser operating at 1064 nm. Laser-induced macular holes share many features with idiopathic macular holes. Optical coherence tomography was employed in the evaluation of two patients with laser-induced macular holes. Tomographic features were compared with those found in patients with idiopathic macular holes. An animal model of laser-induced macular hole was also evaluated in order to elucidate the histologic correlation of the OCT findings.

Keywords: laser injury, optical coherence tomography, OCT, retina, macular hole

1. INTRODUCTION

The growing number of practical applications for the use laser energy has resulted in a dramatic increase in the prevalence of lasers in our daily lives. Military, industrial, medical and recreational uses of lasers have steadily expanded since the first ruby laser was constructed four decades ago[1]. As the prevalence of laser systems has increased, reports of laser eye injuries have also increased. One challenge has been to understand the pathophysiology of laser-induced retinal injury, in order to design rational treatment strategies.

The absorption of the laser energy in the retina depends upon the wavelength, power, spot size, pulse duration and the retinal location. Retinal laser-induced injuries have ranged from mild retinal edema with subsequent changes at the level of the retinal pigment epithelium (RPE) to full thickness retinal holes with vitreous hemorrhage.[2-5] It is this most severe form of retinal injury that has caused the most significant visual complications.

There have been several reports of the surgical[6-7] and medical treatment[3,8-9] of laser-induced macular holes. The visual outcome has been variable in treated and nontreated patients. There is no consensus regarding the need for treatment or the optimal timing and approach to the treatment of laser-induced macular holes. A more complete understanding of the structural abnormalities present in the laser-induced macular holes may reveal similarities and differences between laser-induced macular holes and idiopathic macular holes. This understanding may assist in providing prognostic data for injured patients and developing treatment strategies.

We evaluated two patients with laser-induced macular holes using optical coherence tomography (OCT). OCT is an imaging technique that produces a high-resolution two-dimensional evaluation of retinal anatomy in vivo.[10] In order to provide a histopathologic correlation, we also evaluated previously laser treated nonhuman primates using OCT and performed tissue studies. These results were compared to typical findings in patients with idiopathic macular holes.

Laser and Noncoherent Light Ocular Effects: Epidemiology, Prevention, and Treatment,
Bruce E. Stuck, Michael Belkin, Editors, Proceedings of SPIE Vol. 4246 (2001)

2. SUBJECTS AND METHODS

Two patients with laser-induced macular holes were evaluated using optical coherence tomography. Each patient had sustained a laser injury due to an occupational exposure. A patient with an idiopathic macular hole was also evaluated to provide comparative data. Three nonhuman primates with laser-induced macular holes were studied in order to provide histologic correlation.

2.1 Clinical Examination

The examination included a detailed review of the laser injury accident. The instrument involved in the incident was investigated and measurements of the parameters of the laser energy emission were recorded. Snellen visual acuity was recorded. Slit lamp examination, fundus biomicroscopy and indirect ophthalmoscopy were performed. Static perimetry and contrast sensitivity testing was performed. Optical coherence tomography was performed using commercially available equipment derived from the prototype described by Hee and colleagues[11] and Puliafito and colleagues.[12]

2.2 Animal studies

A mature *M mulatta* was maintained under standard laboratory conditions in accordance with the Association for Vision Research in Ophthalmology Statement for the Use of Animals in Ophthalmic and Vision Research and Federal guidelines. Nine years ago, the animal had received a single 2.5 mJ laser lesion to the macula delivered by a Nd:glass laser. Due to recent medical complications of an unrelated medical disease, the animal was scheduled to be euthanized. The animal was anesthetized for fundus photography and OCT scanning. Ketamine hydrochloride 10mg/kg was given intramuscularly. Under ketamine restraint, intravenous sodium pentobarbital 10-17.5 mg/kg was delivered through a 22 gauge canula to induce anesthesia. Additional sodium pentobarbital, at rates not to exceed 25 mg per dose, was given as needed to maintain anesthesia during the evaluation. The animal's eyelids are held open with a speculum, and the cornea was bathed in isotonic saline solution at intervals of 30 seconds or less to prevent corneal drying. After completion of the photography and OCT studies, the animal was euthanized by using an overdose of sodium pentobarbital, according to the American Veterinary Medical Association guidelines. The ocular tissue was then harvested for histopathologic evaluation.

Two additional animals were studied at 3 and 4 months following the creation of a laser-induced macular hole using a Nd: YAG laser. Fundus photography and OCT scans were performed as above.

2.3 Histopathology

For each animal subject, the macula was oriented for sectioning in the plane of the OCT scans. Serial sectioning (with 10 nm wide glass knives) was performed on an Ultracut E (Reichert-Jung, Vienna, Austria) ultratome at 1 micron thickness. The sections were stained using methylene blue azure II and basic fuchsin (Sigma Chemical Co., St. Louis, MO) coverslipped with immersion oil and rimmed with Permount (Fisher, Fairlawn, NJ), prior to drying.

3. RESULTS

3.1 Case Report 1

A 21 year old Hispanic male Marine reported experiencing a bright white flash after accidentally exposing himself to the exit aperture of a hand held Nd:YAG laser range finder. The soldier was holding the instrument between his knees while attempting to adjust the battery source. The instrument emits a 15 mJ pulse with a pulse duration of 20ns. The total intraocular energy received based on the beam divergence and distance from the eye was calculated to be 1 mJ. The threshold for a retinal minimally visible lesion at this wavelength is 0.1 mJ.

The initial visual acuity was 20/20 OD (right eye) and 20/25 OS (left eye). A full thickness parafoveal macular hole was present OD nasal to fovea. A smaller flat hole was present OS. Over the following six months, the patient developed increasing macular traction and hole enlargement due to epiretinal membrane formation in the right eye. The retinal hole in the left eye sealed. Visual acuity declined to 20/100 OD and improved to 20/20 OS. Pars plana vitrectomy with membrane stripping and placement of 20% C3F8 intraocular gas was performed. Postoperatively, the hole was sealed however visual acuity remained 20/400 OD throughout follow-up.

The patient presented 3 years later noting that the visual acuity in the surgical eye seemed to have declined over the past few months. Visual acuity was found to be counting fingers. On examination, the patient had an open, 1000 micron macular hole with a cuff of subretinal fluid (Figure 1).

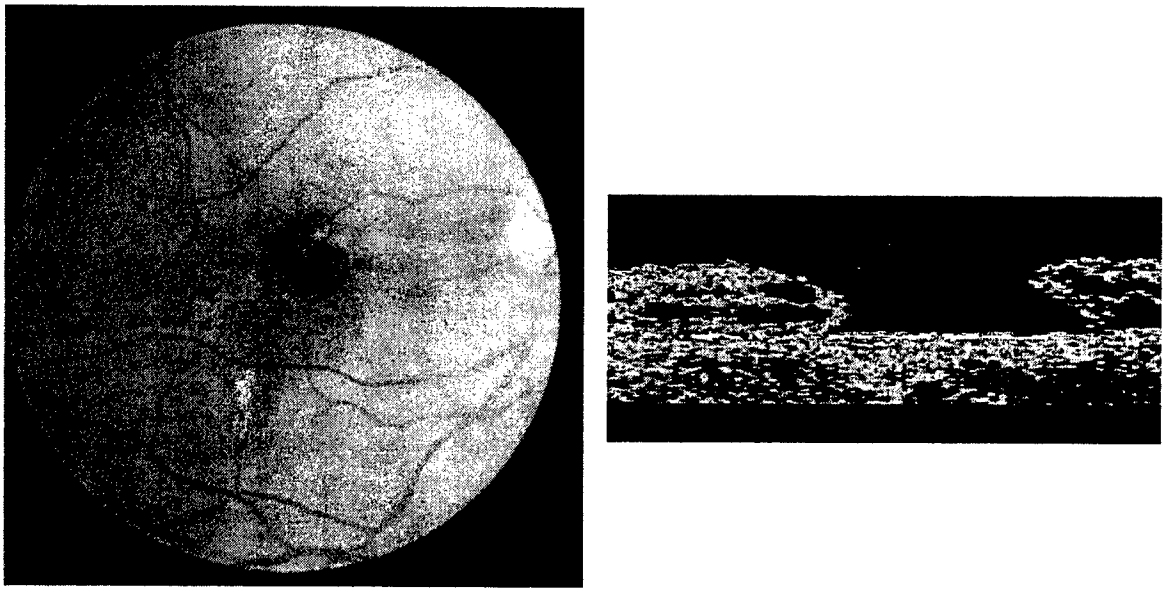

Figure 1. Left. Fundus photograph demonstrates an open, 1000 micron, full thickness macular hole. Right. Horizontal OCT scan through the macular hole shows cyst like hyporeflective zones within the retina at the edges of the hole. The retinal edges are rounded and elevated off the RPE below. Note the increased reflections from the RPE and choroid at the center of the hole.

OCT scans demonstrated the presence of the macular hole and cystoid changes in the surrounding retina. There were strongly reflective signals from the RPE and choroid beneath the hole. This is due in part to the lack of overlying tissue to attenuate the signal. However, this signal is of higher reflectivity compared to patients with idiopathic macular holes that also have this loss of tissue attenuation (see case 3). Cyst like retinal changes were found to extend 1000 microns beyond the edge of the hole.

3.2 Case report 2

A 20 year old white male airman reported an accidental self inflicted laser retinal injury 1 day prior to presentation. The patient was holding a laser rangefinder at arm's length when the laser was activated. The instrument is commonly used to determine cloud height and contains a battery operated 5 mJ Nd:YAG laser operating at 1064 nm. The total intraocular energy was calculated to be 2.5-3 mJ.

On presentation, visual acuity was 20/150 OD and 20/20 OS. The cornea and lenses were clear. The macula of the right eye demonstrated intraretinal hemorrhages and retinal edema surrounding the fovea. There was an overlying vitreous hemorrhage. Three weeks later, visual acuity was 20/60. The vitreous hemorrhage had cleared. A 100 micron full thickness macular hole was present.

Three months after the initial injury, visual acuity was 20/70. On examination, a 100 micron full thickness macular hole was present (Figure 2a). There was a central yellow deposit at the level of the RPE. There was a larger approximately 500 micron zone of RPE depigmentation surrounding the hole. Fundus fluorescein angiography demonstrated a central area of hyperfluorescence corresponding to the area of macular RPE

depigmentation, consistent with a window defect (Figure 2b). There was no evidence of choroidal neovascularization. Indocyanine green angiography demonstrated central hypofluorescence consistent with injury to the choriocapillaris at the base of the hole.

OCT demonstrated a full thickness macular defect with a strongly reflected signal at the level of the RPE and choroid. There were cystic changes in the retina surrounding the hole. The hole edges appeared more angular and irregular compared to the rounded retinal edges found in idiopathic macular holes.

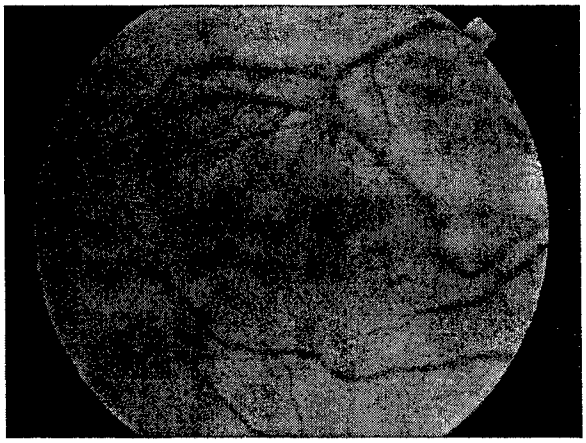

Figure 2a.

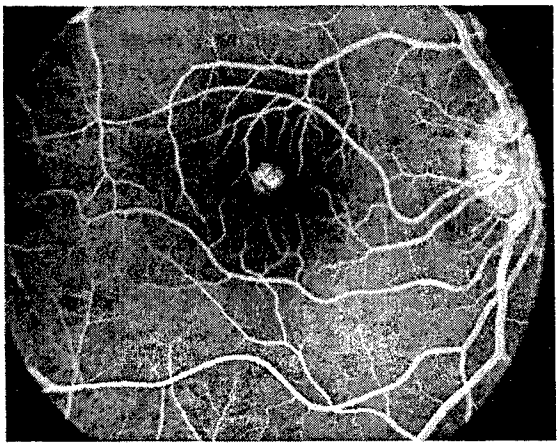

Figure 2b.

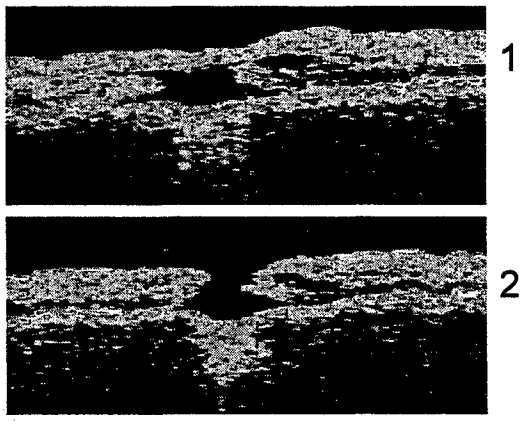

Figure 2c (left).

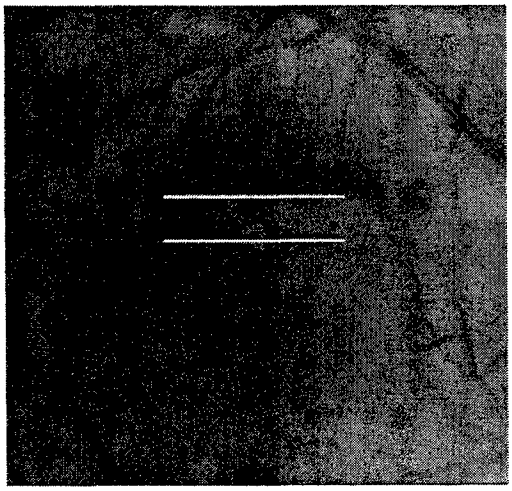

Figure 2c (right).

Figure 2. Fundus photograph (2a) and venous phase fluorescein angiography (2b) of laser-induced macular hole at 3 months following injury. Note the central retinal hole surrounded by a zone of depigmented RPE. Figure 2c left shows the cross sectional appearance of the macular hole on OCT. Horizontal scans have been made as shown in Figure 2c right. The first scan passes just above the edge of the macular hole. Note the hyporeflective zone demonstrating the presence of subretinal fluid in this location. On scan 2, note the somewhat tapered edges of the retina at the center of the hole. The retinal edges are elevated off the RPE and hyporeflective cyst like spaces are noted.

The patient was relatively asymptomatic when viewing binocularly and had noted steady improvement in acuity. Observation and surgical options were discussed. Observation was elected with close follow-up with his local ophthalmologist.

The patient returned for follow-up one year following the injury. He reported that he had steadily improved and he was no longer aware of a deficit when working in binocular conditions. Visual acuity had improved to 20/40 OD.

Fundus examination demonstrated that the macular hole was smaller. Contact lens biomicroscopy identified a less prominent fluid cuff surrounding the hole edges. OCT demonstrated tissue bridging the gap between the edges of the macular hole. The edges of the hole were closer together and fewer cystic changes were identified in the perifoveal retina (Figure 3). These findings were consistent with spontaneous reduction in the macular hole size.

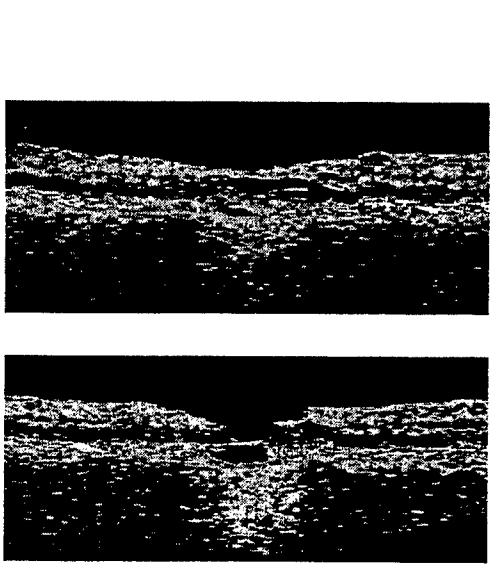

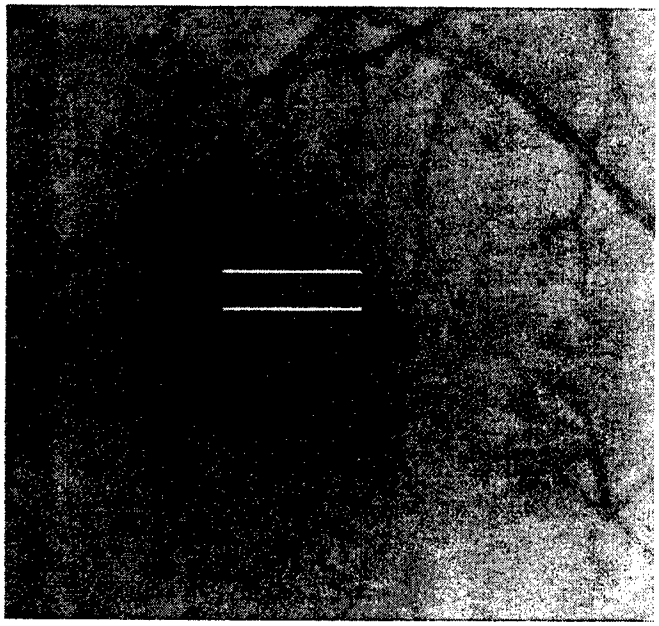

Figure 3 (left)

Figure 3 (right)

Figure 3. A series of horizontal scans through the macular hole were performed on case 2. Scan 1 shows more tissue bridging the zone of hyporeflectivity on the previous scans. Less subretinal fluid was present compared to the previous scans. Scan two shows that the edges of the hole are closer together, although a full thickness defect persists.

3.3 Case report 3

A 73 year old white woman presented with a complaint of progressive metamorphopsia in her left eye for 6 months. Visual acuity was 20/80 OD and 20/50 OS. Anterior segment examination was remarkable for mild nuclear sclerosis of each lens. Fundus examination revealed bilateral full thickness macular holes. The Weiss ring was not identified. Optical coherence tomography demonstrated full thickness macular holes. The hole edges were rounded, elevated and contained hyporeflective cyst like spaces within the tissue (Figure 4).

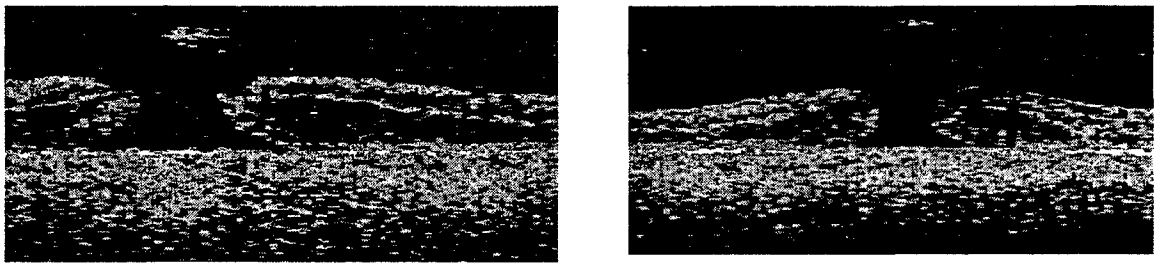

Figure 4. Horizontal OCT scans of right and left eyes of case 3. Note the rounded edges of the retinal hole. Hyporeflective cyst like spaces are noted in the retina surrounding the macular hole. A tuft of tissue is found over the hole in each eye. This represents a glial tuft lying on the detached posterior hyaloid. A perifoveal vitreous detachment was not found on any laser-induced macular hole cases.

3.4 Animal Case Study 1

Nine years earlier, a mature Macacca mulatta received a laser-induced macular hole in the right eye. On examination, a 1000 micron full thickness macular hole was present with a surrounding zone of subretinal fluid and irregular RPE pigmentation (Figure 5). OCT scans demonstrated a full thickness macular hole with elevated thinned retinal edges.

Figure 5a.

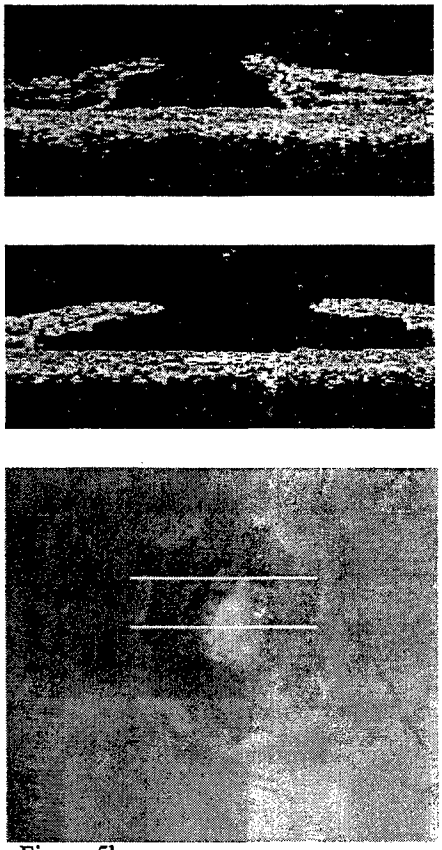

Figure 5b.

Figure 5a. Fundus photograph of animal case study 1 at 9 years following laser-induced macular hole. Note the large zone of irregularly increased pigmentation of the RPE. The macular hole edges are elevated with surrounding subretinal fluid. The full thickness hole is > 1000 microns. Figure 5b demonstrates the cross sectional appearance of the macular hole on OCT. Note the thinned edges of retina, elevated off the RPE.

Histologic sections demonstrated elevated retinal hole edges with loss of photoreceptors. At the base of the hole an area of obliteration of the choriocapillaris was found. Normal vascular channels were replaced with collagen and fibroblasts.

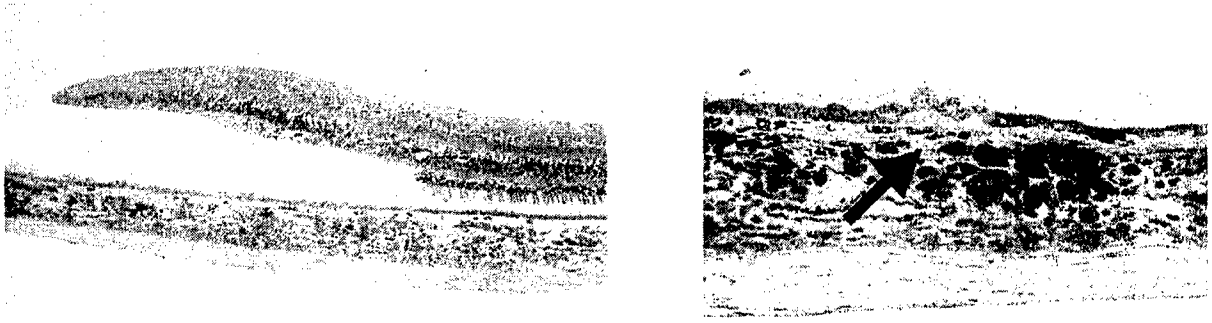

Figure 6. Left. Histologic section through the center of the macular hole in animal case study 1. Note the retinal thinning at the edge of the hole due to loss of photoreceptors. This correlates well with the findings on OCT. Right. Note the replacement of normal choriocapillaris with fibroblasts and collagen at the center of the macular hole. The arrow points to the transition from normal choriocapillaris to scar. The RPE cells are hypopigmented and several drusen are noted.

3.5 Animal Case Report 2

A mature Macacca mulatta with a full thickness macular hole of 4 months duration was previously studied. Histologic sections from the macula were reviewed. A fine epiretinal membrane was found on the retinal surface. Cystic changes were found within the retina surrounding the macular hole (Figure 7).

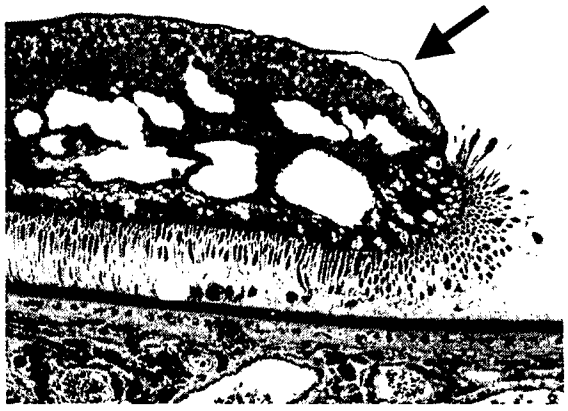

Figure 7. Histologic section of edge of macular hole in animal case report 2. Note the presence of cyst like spaces in the retina at the edge of the macular hole. This correlates well with the hyporeflective spaces found on OCT scans. The retinal edge is elevated off the RPE. Also note the presence of an epiretinal membrane (arrow).

3.6 Animal case report

A mature Macacca mulatta with a full thickness laser induced macular hole of 3 months duration was studied. OCT studies showed a small (<200 micron) full thickness macular hole. Over 6 weeks, tissue was found to bridge the gap resulting in spontaneous closure of the macular hole (Figure 8).

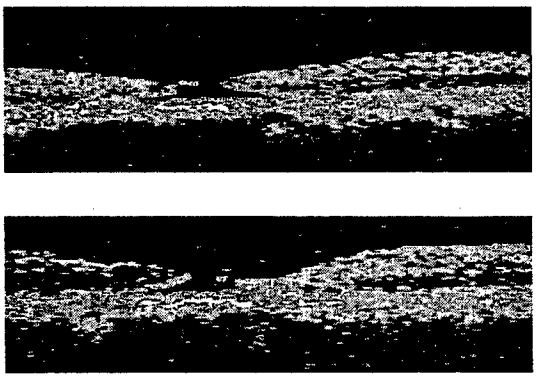

Figure 8a.

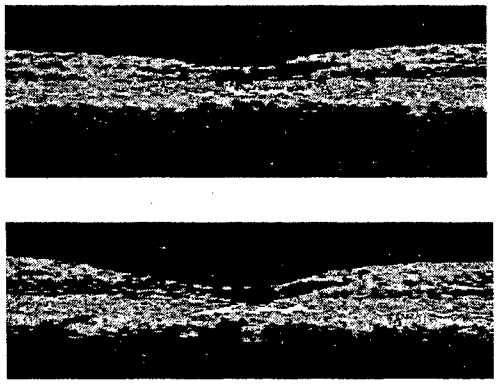

Figure 8b.

Figure 8a (top and bottom). Horizontal OCT scans through laser induced macular hole at 2 weeks. Note the small full thickness defect. Figure 8b (top and bottom) . Horizontal OCT scans through the same macular hole at 6 weeks. Note the presence of bridging tissue. Also note the lack of cyst like spaces in the retina surrounding the hole. The retinal edges are tapered toward the hole center rather than rounded and elevated as in animal case study 1 and human case 1.

4. CONCLUSIONS

Laser induced macular holes are created as a result of the photomechanical tissue disruption caused by a laser exposure of nanosecond or shorter duration. Typically, this injury occurs following exposure of the macula to a Q-switched Nd:YAG laser.[5,8,13] As demonstrated in this study, the natural history of this injury is quite variable ranging from spontaneous closure[9,14] to progressive hole enlargement.[8] The animal model of laser induced macular holes correlates well with the features found in accident cases.

In this study, optical coherence tomography was able to identify features of laser induced macular holes that correlate with histologic findings. Cystic changes were found in the retina surrounding the hole edges as was found in idiopathic macular holes. The edges of the retina appear rounded and elevated in the laser accident cases with persistent macular holes. This morphology is typical of OCT features in idiopathic macular holes. Strong signals from the RPE and choroid layer were found in laser-induced holes and were less prominent in idiopathic macular holes. These signals may represent the scarring at the level of RPE and choroid that was found on histologic section. The lack of perfusion at the base of the hole may result in a limit to long term potential acuity. A posterior vitreous detachment was not found in any patients or study animals with laser induced macular holes.

Idiopathic macular holes are believed to result from a combination of tangential and antero-posterior traction on the perifoveal and foveal retina. Often a partial vitreous detachment is found with persistent attachment and traction on the perifoveal or foveal retina.[15-16] Vitrectomy surgery for macular holes involves removal of the posterior hyaloid, peeling any epiretinal membranes and/or the internal limiting membrane, and placement of an intraocular gas bubble to tamponade the hole.[17] The goals are to remove any traction on the fovea and allow the retinal edges to reapproximate and reattach to the underlying RPE. This results in improvement in sensory function of the foveal photoreceptors. There are two cases in the literature which underwent vitrectomy surgery for laser induced macular holes.[6-7] Improvement in visual acuity to the 20/30 level was obtained. Restoration of baseline preinjury visual acuity is likely limited due to tissue loss and scarring at the level of the RPE and choroid.

Based on a review of the literature and the cases presented here, smaller macular holes (< 250 microns) may seal spontaneously[8,14] and thus, a period of observation is warranted prior to proceeding to surgery. Spontaneous closure of a laser induced macular hole was also identified in the animal model and demonstrated similar OCT characteristics. On OCT, holes that are undergoing this transition show tapered edges. Over time,

tissue begins to bridge the gap and fewer cystic changes are found within the border retinal tissue. Gradually the hole edges move closer together.

The presence of a taut epiretinal membrane may lead to traction and progressive macular hole enlargement Early pars plana vitrectomy and membrane peeling in cases demonstrating this feature may result in a better anatomical outcome. Likewise, large macular holes (>500 microns) are unlikely to seal spontaneously and would likely have a better outcome with vitrectomy surgery.

5. DISCLAIMER

In conducting the research described in this report, the investigators adhered to the "Guide for the Care and Use of Laboratory Animals," as promulgated by the Committee on Revision of the Guide for Laboratory Animal Facilities and Care, Institute of Laboratory Animal Resources, National Academy of Sciences - National Research Council.

The opinions or assertions contained herein are the private views of the authors and are not to be construed as official or as reflecting the views of the Department of the Army or the Department of Defense.

6. REFERENCES

1. Maiman TH. Stimulated optical radiation in ruby. Nature 1960;187:493.
2. Thach AB. Laser injuries of the eye. Int Ophthalmol Clin 1999 Spring:13-27.
3. Wolfe JA. Laser retinal injury. Milit Med 1985;150:177-85.
4. Barkana Y, Belkin MB. Laser eye injuries. Surv Ophthalmol 2000;44:459-78.
5. Bouldrey EF, Little HL, Flocks M, et. al. Retinal injury due to industrial laser burns. Ophthalmology 1981;88:101-7.
6. Ciulla TA, Topping TM. Surgical treatment of a macular hole secondary to accidental laser burn. Arch Ophthalmol 1997;115:929-30.
7. Potthofer S, Foerster MH. Vitrectomy and autologous thrombocyte adhesion of an accidental macular hole caused by Nd:YAG laser. Br J Ophthalmol 1997;81:803-4.
8. Thach AB, Lopez PF, Snady-McCoy LC, et. al. Accidental Nd:YAG laser injuries to the macula. Am J Ophthalmolol 1995;199:767-73.
9. Newman DK, Flanagan DW. Spontaneous closure of a macular hole secondary to an accidental laser injury. Br J Ophthalmol 2000;84:1075.
10. Toth CA, Narayan DG, Boppart SA, et. al. A comparison of retinal morphology viewed by optical coherence tomography and by light microscopy. Arch Ophthalmol. 1997;115:1425-8.
11. Hee MR, Puliafito CA, Wong C et al. Optical coherence tomography of macular holes. Ophthalmology 1995;102:748-756.
12. Puliafito CA, Hee MR, Schuman JS, Fujimoto JG. Optical coherence tomography of ocular diseases. Thorofar, NJ: Slack Inc; 1996.
13. Goldberg MF, Young SLR, Read J, Cunha-vaz JG. Macular hole caused by a 589 nanometer dye laser operating for 10 nanoseconds. Retina 1983;3:40-4.
14. Kusaka S, Fujikado T, Ikeda T, Tano Y. Spontaneous disappearance of traumatic macular holes in young patients. Am J Ophthalmol 1997;123:837-9.
15. Gaudric A, Haouchine B, Massin P et al. Macular hole formation: new data provided by optical coherence tomography. Arch Ophthalmol 1999;117:744-51.
16. Chauhan DS, Antcliff RJ, Rai PA et. al. Papillofoveal traction in macular hole formation: the role of optical coherence tomography. Arch Ophthalmol 2000;118:32-8.
17. Kelly NE, Wendel RT. Vitreous surgery for idiopathic macular holes. Arch Ophthalmol 1991;109:654-9.

Accidental injury to the human retina from a picosecond Ti:sapphire laser

Jeremiah Brown, Jr., David J. Lund, Bruce E. Stuck

US Army Medical Research Detachment of the Walter Reed Army Institute of Research, Brooks Air Force Base, TX 78235

ABSTRACT

The rising number of applications of ultrashort laser systems presents new challenges in laser safety. Retinal damage studies have demonstrated that less energy is required to create a retinal burn for pulses shorter than one nanosecond than for pulses longer than one nanosecond.[1-3] Furthermore, as laser systems become more complex, the potential for accidental injury increases. In this paper we report the accidental injury from a Ti:Sapphire amplifier system delivering 100 picosecond pulses. The circumstances leading to the binocular injury included the use of inadequate eye protection, a defective amplifier crystal and the very dim appearance of 800 nm light. Ophthalmologists evaluating patients with laser eye injury should be prepared to discuss the physiology of the injury and prognosis with their patients.

Keywords: laser injury, ultrashort pulse, picosecond, Ti:sapphire, retina, hemorrhage

1. Case Report

A 29 year-old graduate student was working in a university laboratory performing laser alignment. He was using an ultrashort pulse Ti:Sapphire amplifier system operating at 800 nm delivering 100 picosecond (psec) pulses. The system is driven by a 532 nm Nd:YAG pump laser at 10 Hz with 8 nanosecond (nsec) pulses. He was wearing goggles that protected him from the 532 light, but not the 800 nm light. The eye protection provides an optical density of 4 at 440-514 nm.

The patient was working closely with one of the Ti:sapphire amplifier crystals and sensed a dim flash in his left eye (OS). He sensed no pain and had no audible sensation. He reported that his natural response was to look toward this dim flash to see what it was. He then sensed a flash in his right eye (OD). He had no aversion response to either flash.

He continued to work that evening although it was very difficult due to a central blur most notable in his right eye. He waited for 2 days to see if the symptoms would subside and eventually reported this event to his supervisor. He had concerns regarding his ability to remain in the research program as well as fear of how he would be regarded by his fellow students. He reported feeling psychologically devastated for 2 days until his examination. He was concerned about the potential for permanent blindness and the possibility that he would be forced to abandon his current profession.

On examination he reported a small central scotoma OD and metamorphopsia OS. Visual acuity was 20/30 +2 OD and 20/25 +3 OS. Anterior segment examination of each eye was normal. The lenses and vitreous were clear. Fundus examination of the right eye revealed a small 200 micron area of retinal edema and RPE depigmentation which appeared to be centered on the fovea (Figure 1). There was a second area of depigmented RPE in the temporal macula. There were no

Laser and Noncoherent Light Ocular Effects: Epidemiology, Prevention, and Treatment, Bruce E. Stuck, Michael Belkin, Editors, Proceedings of SPIE Vol. 4246 (2001)

retinal hemorrhages. Fundus examination of the left eye revealed a retinal hemorrhage that extended from the fovea into the inferotemporal parafoveal retina approximately 1500 microns. There was no vitreous hemorrhage. No other lesions were identified.

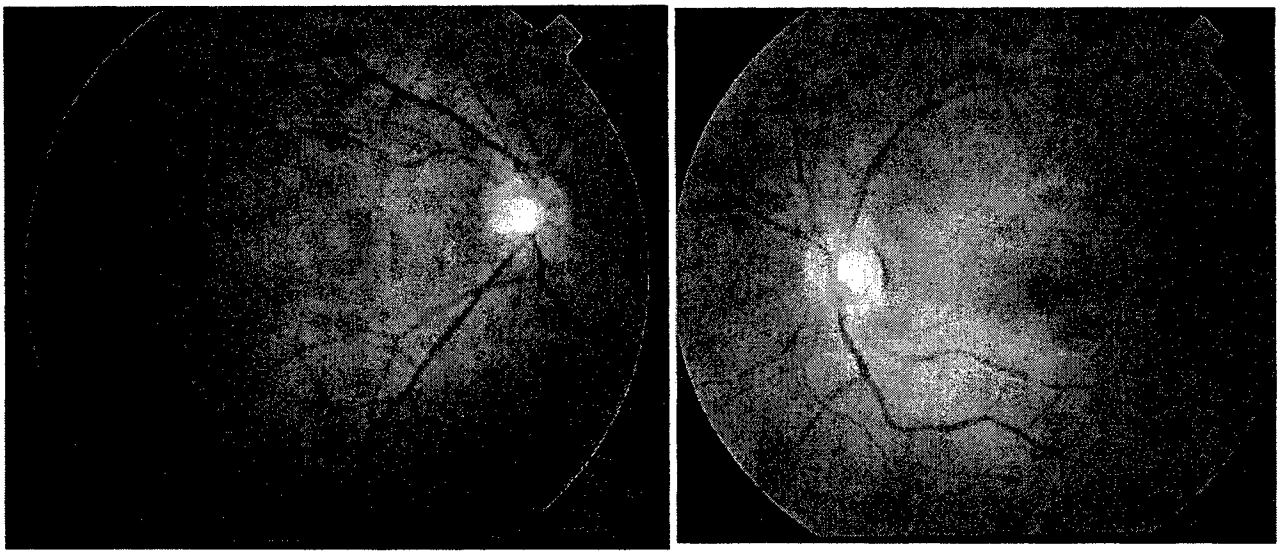

Figure 1. Fundus photographs of macula of right and left eyes taken 2 days following the injury (Left) Note the depigmentation of the perifoveal macular pigment in the right eye. There was surrounding retinal edema (Right) There is an irregularly shaped retinal hemorrhage extending from the fovea, infereotemporally.

No treatment was prescribed. Two weeks later, the patient returned for examination. He reported that the scotoma in the right eye had become more dense centrally surrounded by a ring of light gray distortion. The central scotoma was absolute and reading tasks required eccentric fixation. The patient continued to note metamorphopsia OS, however less dense. He described this zone as being less gray than on previous exam (Figure 2). Best-corrected visual acuity was 20/30 OD and 20/20 OS with eccentric fixation. Static perimetry of the central 10 degrees OD demonstrated that the area of decreased sensitivity had improved, although remained reduced. Static perimetry in the left eye revealed a new area of decreased sensitivity centrally. The anterior segment was normal. Fundus examination of the right eye revealed an atrophic RPE lesion directly below the fovea. There was new pigment clumping within the lesion compared to the previous examination. The fundus of the left eye showed that most of the retinal hemorrhage had cleared revealing a less prominent atrophic lesion at the level of the RPE.

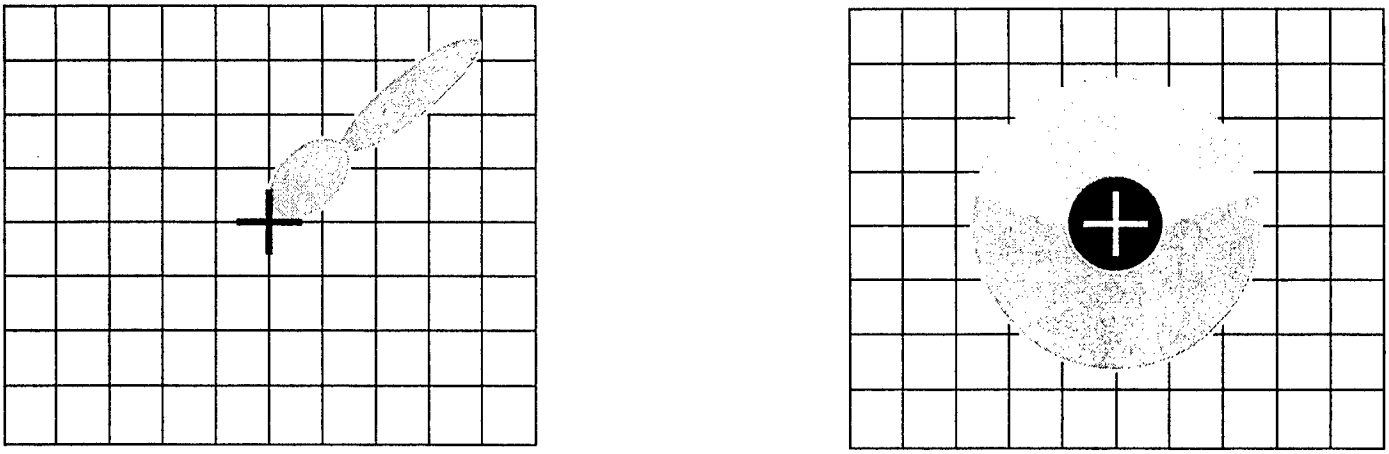

Figure 2. Amsler grid findings of the central 10 degrees as reported by patient 2 weeks following the injury. (Left) Adjacent to the fovea extending superotemporally was a zone of gray distortion. This corresponds to the area of retina hemorrhage. (Right) The patient noted a central round absolute scotoma. This was surrounded by a ring of gray distortion which was clearer superiorly and darker inferiorly.

An investigation of the circumstances of the accidental exposure was conducted. The student had been using the laser system during a weekend evening. The system consisted of a 10 mm diameter, 8 mm long Ti:sapphire rod that is end pumped by 200 mJ of 532 nm light from a 10 Hz, q-switched laser. The emerging light was 800 nm of 35 mJ in 100 ps pulses. The diameter of the 800 nm and 532 nm beams were 3 mm and all beams incident to the crystal were in the plane of the table. A stray beam was detected emanating 30 degrees upward from the second amplifier crystal. This beam was composed primarily of 800 nm light of 10-100 microjoules in energy. The ED50 for a minimally visible lesion is on the order of 0.4 to 4 microjoules incident at the cornea.

The crystal was closely examined and was found to have a bevel on one edge. The bevel was at the bottom of the crystal in a position such that it generated an upward stray refection. Most likely, the bevel was created during a previous polishing of the crystal, presumably to smooth out a chip in the crystal. An additional damage spot in the crystal was identified, however no significant scatter was identified from this location. In the past, the laser table had been oriented in a way such that a wall prevented anyone from standing in the path of the stray beam and it was never detected. Recently, the laser table was repositioned in a way that the stray beam could now cause a hazard.

2. Discussion

Picosecond and shorter duration laser pulses present a unique ocular hazard in that the threshold for creating retinal hemorrhage is closer to the threshold for creating injury than for pulses of longer duration. Thus, retinal hemorrhages have been found with as little as 6-10 microjoules of energy in animal studies.[4] Furthermore, despite the fact that 800 nm light

appears dim, novice researchers should be aware of the potential for injury at these low energies. It is unfortunate that the right eye injury occurred as a result of directing his fixation at the source of the dim flash that he perceived with the left eye. This placed the second injury site directly at the fovea in the right eye.

No treatment was prescribed in this case. This is appropriate as the patient presented two days after the injury and no treatment has been demonstrated to have a consistent beneficial effect on reducing lesion size.[5-8] This patient should retain adequate acuity for driving and performing most tasks. However it is likely that an annoying, permanent, dense small central scotoma will remain in the right eye. He also has a long-term risk of choroidal neovascularization that may complicate the recovery in the left eye.[9]

Proper selection of eye protection requires knowledge of the range of wavelengths covered by the eyewear in use. The challenge is that eyewear incorporating dye technology to absorb from 514 to 800 nm has a very low light transmission and therefore can be difficult to use while performing laser alignment. Newer reflective technologies with narrower cutoff bands will allow greater transmission of light while reflecting the wavelengths of concern. It is also important to be sure that the eyewear provides sufficient protection at short pulse durations. There is evidence that protective eyewear may saturate at picosecond and femtosecond pulses.[10]

Many researchers rely on their ability to know where their beam is at all times. Usually, careful alignment and vigilance can insure safety most of the time. However, the more complex the laser system, the greater the risk that an unpredicted beam may be generated.

It should also be noted that, as in this case, laser workers and students may be reluctant to report accidental injuries out of fear of restriction of activities or impairment of academic reputation. A failure to report this injury may have resulted in additional coworkers being injured on the same laser system. Baseline and annual visual acuity and Amsler Grid testing may identify abnormalities that aid in detection of individuals injured by past exposure. Furthermore, as effective treatment protocols are developed, it will be important to identify treatable lesions and administer the treatment promptly following the injury.

Despite the reluctance to report the injury, the psychological impact of becoming aware of a visual deficit due to a laser can be devastating. Highly educated scientists can express dire fears of blindness that can impair their ability to continue to perform their duties. Physicians evaluating these patients must understand the impact of these experiences and be prepared to provide detailed explanation of the physiology of the injury as well as prognostic information to their patients.

3. DISCLAIMER

The opinions or assertions contained herein are the private views of the authors and are not to be construed as official or as reflecting the views of the Department of the Army or the Department of Defense.

Citation of trade names in this report does not constitute an official endorsement or approval of the use of such items.

4. REFERENCES

1. Cain CP, DiCarlo CD, Rockwell BA, et. al. Retinal damage and laser-induced breakdown produced by ultrashort-pulse lasers. Graefes Arch Clin Exp Ophthalmol. 1996;234 Suppl 1:S28-37.

2. Cain CP, DiCarlo CD, Noojin GD, et. al. In-vivo laser induced bubbles in the primate eye with femtosecond pulses. Laser-Tissue Interaction VII, Steven L. Jacques, Ed., Proc SPIE 1996;2681A:382-8.

3. Rockwell BA, Roach WP, Payne D, et. al. Ultrashort laser pulse retinal damage. Laser and Noncoherent Ocular Effects: Epidemiology, Prevention, and Treatment, Bruce E. Stuck and Michael Belkin editors, Proc SPIE 1997;2974:60-5.

4. Cain CP, Toth CA, DiCarlo CD, et. al. Visible retinal lesions from ultrashort laser pulses in the primate eye. Invest Ophthalmol Vis Sci 1995;36:879-88.

5. Barkana Y, Belkin M. Laser eye injuries. Surv Ophthalmol. 2000 May-Jun;44(6):459-78.

6. Schuschereba ST, Cross ME, Pizarro JM, et. al. Pretreatment with hydroxyethyl starh-deferoxamine but not methylprednisolone reduced secondary injury to retina after laser irradiation. Lasers and Light 1997;8:1-14.

7. Solberg Y, Dubinski G, Tchirkov M, et al. Methylprednisolone therapy for retinal laser injury. Surv Ophthalmolol 1999;44 [Suppl 1]:S85-S92.

8. Lam T, Takahashi K, Fu Jun, Tso MOM. Methylprednisolone therapy in laser injury of the retina. Graefe's Arch Clin Exp Ophthalmol 1993;231:729-36.

9. Roider J, Buesgen P, Hoerauf H, et. al. Macular injury by a military range finder. Retina. 1999;19:531-5.

10. Stolarski DJ, Stolarski J, Noojin GD et. al. Reduction of protection of laser eyewear with ultrashort exposure. Proceedings Laser Tissue Interaction XII: Photochemical, Photothermal, and Photomechanical. Steven L. Jacques, editor. SPIE 2001;4257:-19.

Automated PRL Measurements using a Confocal Laser Ophthalmoscope

Steven Barrett*[a], Harry Zwick**[b],
[a]Department of Electrical Engineering, University of Wyoming, Laramie, WY 82071,
[b]U.S. Army Medical Research Detachment (USAMRD),Walter Reed Army Institute of Research, Brooks AFB, TX 78235-5138)

ABSTRACT

Ocular motility generated by various fixation strategies show a lower propensity to visit laser damaged retinal areas as compared to non-laser damaged sites. This selectivity provides a non-invasive methodology for characterizing retinal pathology by mapping eye movement visitation under various visual function fixation strategies. Ocular motor techniques for imaging eye movement maps of normal and damaged retinal regions are demonstrated with reference to retinal target location at the retina. Eye movement data digitized from a contrast sensitivity task provided video data of eye movement fixation patterns simultaneously with retinal location of target placement during periods of visual fixation required in a Landolt ring contrast sensitivity task. These data were digitized with specialized algorithms that linked target location with retinal morphology and pathology. In one patient with central macular retinal damage, retinal based maps demonstrated strong consistency with measurements made with non-retinal higher resolution Purkinje eye movement apparatus. Such eye movement maps differed primarily eye movement density within a given area but were generally comparable with respect focal areas mapped in retinal space. These data suggest that lower resolution video based imaging can provide a non-invasive assessment of laser induced retinal damage.

KEYWORDS: Macular laser eye injury, Preferred Retinal Location, PRL, Visual Function Recovery, scanning laser ophthalmoscopy retinal tracking algorithms and template matching, laser retinal damage, retinal based fixation eye movements.

1. INTRODUCTION

Investigations of human retinal laser accident cases reveal that long term recovery of visual function may occur [1-6]. Eye movement patterns made independently in a Purkinje eye tracker [7] provide a high resolution image of the fixation eye movement pattern and confirm the location of the preferred retinal location for repeated stable fixation patterns in normal and laser damaged central retinal sites. Preferred Retinal Location (PRL) or development of a pseudo-fovea may occur in certain cases while foveal functionality may return in others. The present experiment continues this line of research by development of a fixation map referenced to the retina. This technique combines the fixation map obtained with the Purkinje eye tracker with a similar map at the retina, allowing a direct determination of the preferred retinal location for visual fixation performance in the normal and damaged retina.

A template matching scheme using blood vessel templates and lesions resulting from accidental laser irradiation was used to track the movement of the retina and derive the PRL location from video acquired of the moving retina using a confocal scanning laser ophthalmoscope. Techniques originally developed to stabilize a laser for therapeutic retinal photocoagulation and retinal safety studies was adapted to obtain the PRL data [8]. In these techniques, the retinal image movement was monitored via a fundus camera equipped with a charge-coupled device (CCD) camera to obtain an image of retinal movement. A brief review of this technique will be provided later in the paper. In this study, we replaced the CCD-equipped fundus camera with a CSLO to obtain the retinal image. The CSLO provides a high resolution image of the retina [9]. Furthermore, fixation targets, such as alpha-numeric characters of varying sizes, may be directly imaged onto the subject retina.

The present study involves the role of small retinal area eye movements involved in visual acuity tasks. Visual inspection of ocular retinal motility indicates fairly minimal disturbance to the retinal image induced by ocular motility. In eyes

Laser and Noncoherent Light Ocular Effects: Epidemiology, Prevention, and Treatment,
Bruce E. Stuck, Michael Belkin, Editors, Proceedings of SPIE Vol. 4246 (2001)

with central retinal pathology; however, small acuity targets that would normally be resolved in the central retina are often placed superior and slightly temporal to the central retina or fovea [6]. In order to quantify such ocular motility with respect to target placement on the retina, we have employed CSLO methods involving visualization of acuity targets at the retina with retinal image tracking techniques to obtain ocular motility quantification of acuity target placement at the retina.

2. METHODS

2.1 Scanning Laser Ophthalmoscope (SLO)

A digitally generated Landolt ring acuity target was displayed on the raster pattern of a Rodenstock Scanning Laser Ophthalmoscope (SLO) via an acousto-optical modulator (Figure 1). Human subjects viewed the Landolt ring with gaps oriented horizontally left or right under conditions of minimal contrast increasing in contrast to a level of contrast where Landolt gap orientation could be discriminated. All sessions were recorded on SVHS video tape and analyzed off line.

2.1.1 Data Collection. Data was selected from a Landolt ring SLO contrast sensitivity test on one laser accident patient. Retinal damage was due to accidental Q-switched exposure from handheld military laser range finder. Ophthalmoscopy and optical coherence tomography (OCT) indicated morphological resolution between 3 and 12 months post exposure. Reduction in retinal traction were observed with Confocal Scanning Laser Ophthalmoscopy , improvement in visual acuity from 20/70 to 20/40, and smaller more symmetric shift in Purkinje fixational eye movement pattern over this same time period. SLO imaging from Landolt ring contrast sensitivity data was examined from the 12 month post exposure test.

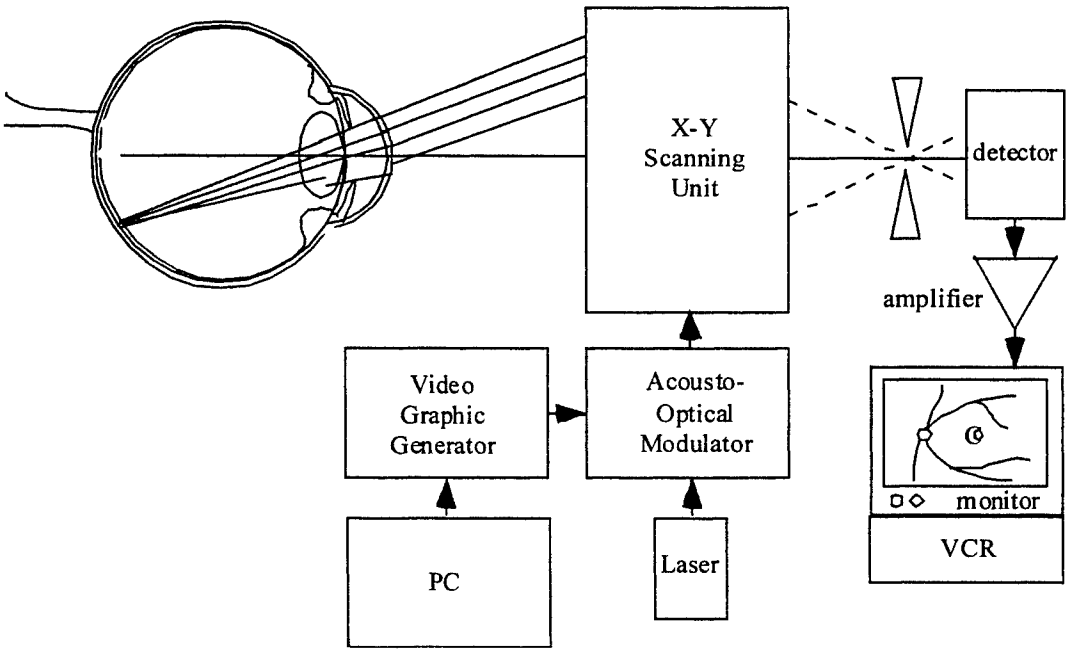

Figure 1. The Scanning Laser Ophthalmoscope (SLO) and technique for writing Landolt ring to SLO via an Acousto-optical modulator (AOM) Diagram shows subject imaging SLO raster pattern and retinal image showing vascular landmarks and Landolt ring positioned on the central macular retina.

2.2 Video Image Registration

Retinal movement was then measured and plotted using a digital imaging-based tracking system. The system was originally designed to stabilize a laser for photocoagulation treatment of various retinal disorders and the development of laser eye safety standards [10 - 14]. It uses video image registration techniques to track and compensate for retinal movements. The image registration technique rapidly digitizes video images to determine the amount of object movement that has occurred in adjacent video frames. A Matrox PIP-1024 frame grabbing board, hosted in a PC, was used to convert the video signal from the SVHS VCR to a series of video "snap shots". The frame grabber provides a snap shot resolution of 512 x 512 pixels with 8-bit pixel gray scale resolution. Video registration consists of : 1) development of a suitable tracking template, 2) choosing an appropriate similarity metric to measure the degree of match (or mismatch) between the template and the tracked object, and 3) selecting a search technique.

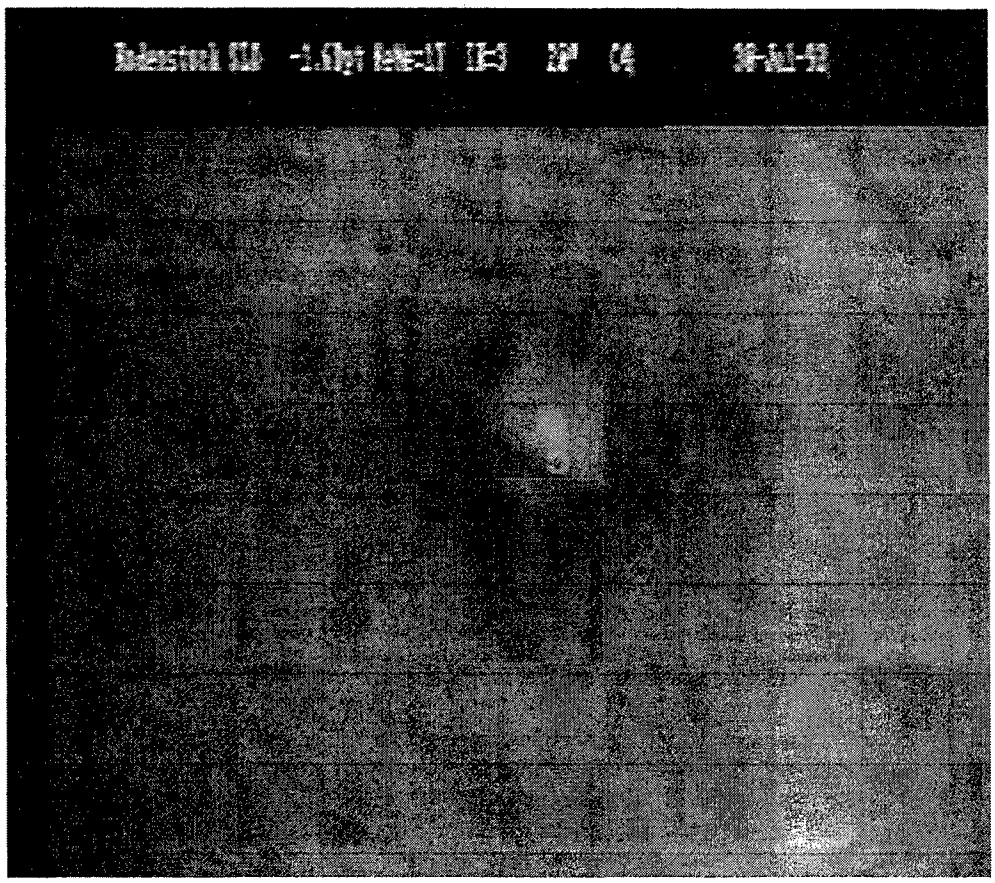

Figure 2. SLO image of retina. Note that the Landolt ring has been imaged directly on the patient's retina by the SLO. Retinal vessels are barely discernible in this small field of view image. The large white lesion resulted from accidental laser exposure to the retina.

2.2.1 Tracking Template. A reference image (the tracking template) of the object is first obtained. The tracking template is a simple mathematical model of the object to be tracked. The template is kept as simple as possible so calculation of the similarity metric does not become computationally exorbitant. The tracking template is swept over subsequent images of the object. When a match has occurred between the tracking template and the object image, object movement information may be derived to determine the amount of object movement that has occurred between adjacent video frames or the point of visual fixation. This template matching is based on having a reference image of the object. For this research task, six one-dimensional blood vessel templates were assembled into a single two-dimensional retinal vessel "fingerprint" template. A pair of horizontal and vertical one-dimensional templates is selected from each third of a retinal area rich in vessels as selected by the user. The horizontal template chosen from the upper third of the reference image is designated as the first horizontal template. All of the other five one-dimensional template locations

are referenced to the first horizontal template's location. This technique results in a computationally efficient model of the subject's retinal vessel pattern. Reference Figure 3 [11]. The individual template response is calculated from ((P1-P2) + (-P3+P4))/(P1+P2+P3+P4) where Pn represents the gray level of the pixel. The entire template response is calculated using the response from all six templates using a minimum absolute value of the difference metric. The difference (P1-P2) detects the leading edge of the vessel while the difference (P4-P3) detects the trailing edge of the vessel. Since the vessel has a darker (lower number gray level) than the surrounding retina (higher number gray level), a larger positive number results when the template is aligned with a retinal vessel. Note that any number of pixels may be inserted between the leading and trailing edge templates to accommodate different vessel widths.

2.2.2 Modified Tracking Template. This retinal vessel tracking template technique worked well for larger retinal fields of view (30-50 degrees) which were rich in retinal vessel features. For smaller fields of view, retinal features suitable for tracking were not always available. In these cases, the actual retinal lesion from the accidental laser irradiation was used as the tracking feature. The tracking algorithm was modified to accommodate this template. The modified template employed is shown in Figure 5. Figure 5 provides a graphic of the retinal surface at a smaller field of view. Although a retinal vessel is present in the image, it does not provide enough distinct features to develop a two-dimensional vessel template. The template response is determined by simply summing the pixel gray levels from the nine pixels forming the lesion tracking template. The highest sum obtained when the template is swept across the image indicates the center of the lesion.

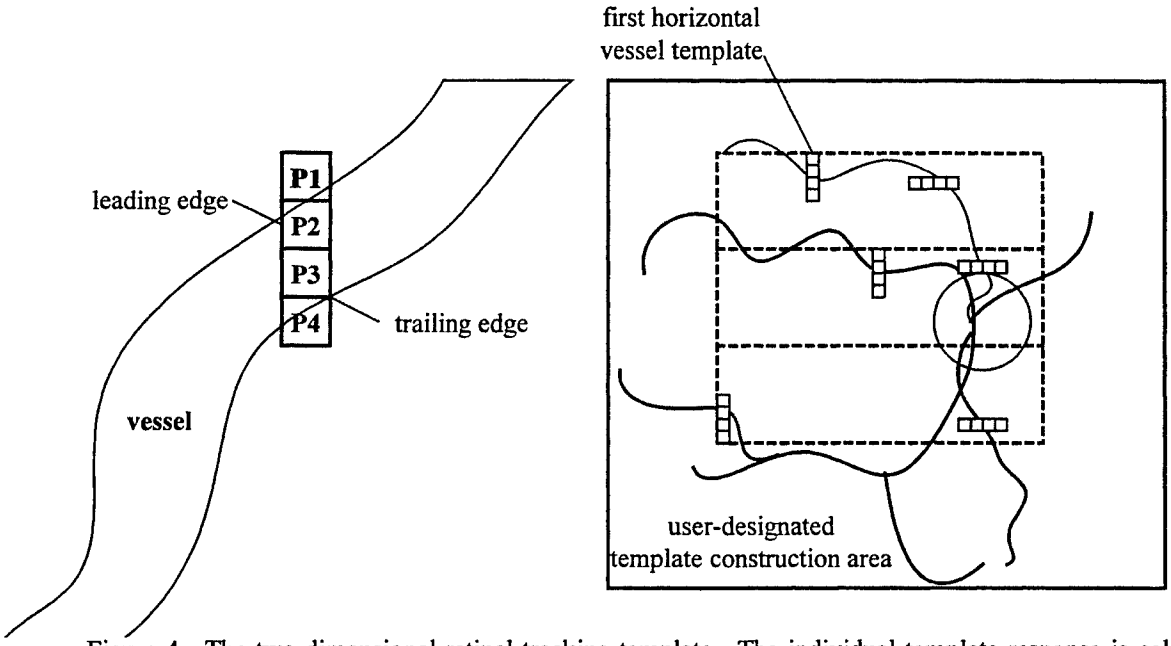

Figure 4. The two-dimensional retinal tracking template. The individual template response is calculated from (P1-P2-P3+P4/(P1+P2+P3+P4) where Pn represents the gray level of the pixel. The entire template response is calculated using the response from all six templates.

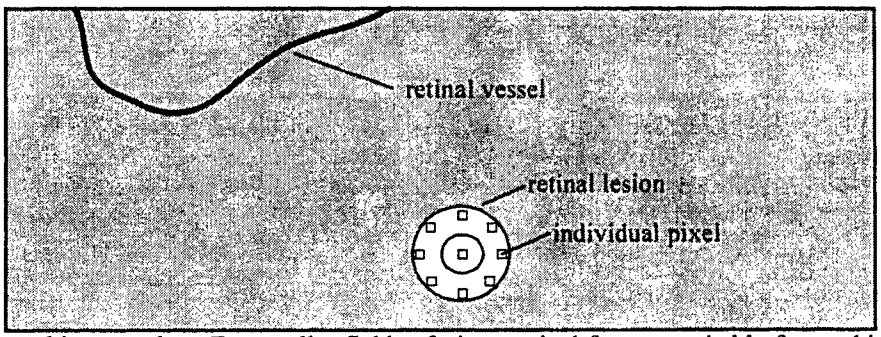

Figure 5. Modified tracking template. For smaller fields of view, retinal features suitable for tracking were not always available. In these cases, the actual retinal lesion from the accidental laser irradiation was used as the tracking feature.

2.2.3 Similarity Metric. With the template defined, the similarity metric to determine the relative goodness of the match between the template and the object image was defined. There are a number of methods of measuring the match (or mismatch) between the tracking template and the image. In this study we employed the absolute value of the difference (AVD) technique. The AVD method uses integer math to calculate the absolute value of the current template response minus the expected template response as a measure of match between the template and the object image. This similarity measure proved to be robust and computationally simple [11]. A "degree of fuzziness" must be incorporated into the template matching metric. As previously discussed, we used the absolute value of the difference (AVD) with integer math to calculate the absolute value of the current template response minus the expected template response as a measure of match between the template and the object image. Due to non-uniform illumination of the retina the template response is not the same at all regions across the surface of the retina. As mentioned previously, the template response is normalized by the sum of the individual pixel gray levels to help compensate for the non-uniform illumination. This normalization technique is based on the assumption that as the illumination of the retina varies, the illumination local to a given individual template will be constant. This assumption held in most cases. Also, recent work by Naess indicates that when a template is built from a static image, and then used to tracking the moving retina, the tracking tends to loose lock a lower retinal velocities as compared to templates derived from a retinal image extracted from a moving retina. We believe this is due to some blur on the image when it moves (even at low speeds). It may be difficult for the human eye to observe that blur on a still image, but it made a significant difference in the ability to track the retina [14]. To compensate for these variabilities, template response was allowed to vary above and below the expected response. When tracking retinal movement using the lesion template illustrated in Figure 5, we simply summed the pixel gray levels from the nine pixels forming the lesion tracking template. The highest sum represented the center of the lesion. (A lighter pixel gray level has a higher integer magnitude).

2.2.4 Search Techniques. There are several different methods of scanning the template over the object image. Ideally, one could calculate the template response at each and every pixel location within the object image--an exhaustive search. Although, this would yield a match on each object image, it is computationally extensive. For this project, this would require calculating the AVD metric at approximately 250,000 pixel locations. The frame grabber providing the image data and the PC could not keep up with such a computational load while maintaining lock on the retina. Another method is to use a coarse-fine technique. In this technique the template is scanned over the image regularly skipping over image rows and columns in a coarse search. As long as the skip dimension of the coarse search is limited to approximately one-half the dimension of the object being searched, this technique should theoretically maintain lock on the object. Based on the template response from the coarse search a fine pixel-by-pixel exhaustive search is performed locally about the coarse match to find the exact location of the object. This technique speeds up the tracking task; however, there is a danger in a real-world implementation that the object may be skipped over during the coarse search [15].

To avoid these concerns, a limited-exhaustive search technique was employed. In this technique, the object's velocity characteristics are used to limit the search in subsequent frames to a small sub-region of the image. For example, for a camera providing images at a standard rate of 30 frames per second, one can calculate how much the object could theoretically move during 33 ms. Since the location of the object is known in the present frame, you need only search a sub-region of the subsequent frame centered about the last known location of the object [16]. This technique tremendously speeds up the tracking task and provides a match using an exhaustive search within the image sub-region. However, should the tracked object moved faster than anticipated, it will not be present within the sub-region on the subsequent frame and loss of tracking lock will occur.

2.2.5 Tracking Algorithm. The flow chart for the tracking algorithm is illustrated in Figure 6. The tracking algorithm was written in Microsoft C, hosted on a Matrox PIP-1024 frame grabber, employed a two-dimensional retinal tracking templates or a lesion template, employed a limited-exhaustive search technique to maintain lock on the retina, and stored fixation point data for analysis. The PIP-1024 is an 8-bit frame grabber connected to the PC's AT (10-12 MHz) bus.

3. EXPERIMENTAL PROTOCOL

Retinal movement was obtained by recording the SLO video output on SVHS tape for several patients who had received vocation-related accidental laser induced or blunt traumatic retinal injury. The CSLO images were videotaped at Brooks AFB, Texas and analyzed at the Image Processing and Optics Laboratory, Department of Electrical Engineering, USAF Academy, Colorado and at the Electrical Engineering Department, University of Wyoming. In previous tests we have

used retinal vessels as tracking templates. Specific test results reported here used the actual retinal lesion as the tracking template due to the absence of clearly definable vessels.

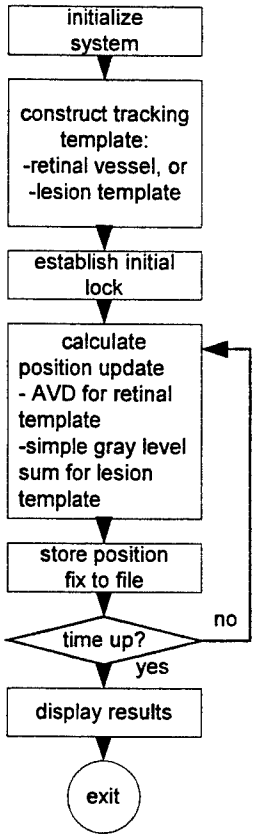

Figure 6. Tracking algorithm flow chart

RESULTS

Figures 7 and 8 shows the results of these tracking episodes. In Figure 7 a lesion template was used to measure retinal movement and hence visual fixation while the Landolt ring was projected onto the patient's retina. The letter Landolt ring is evident in the top diagram in Figure 7. The lower portion of the Figure shows the fixation points as measured by the tracking algorithm during a 10 second fixation episode. The tracking algorithm provided a position update every 165 ms.

In Figure 8 the actual laser macula hole was used to measure visual fixation. The individual fixation points were obtained by the digital image-based tracking system at 165 ms intervals and then plotted on the center of the image field of view.

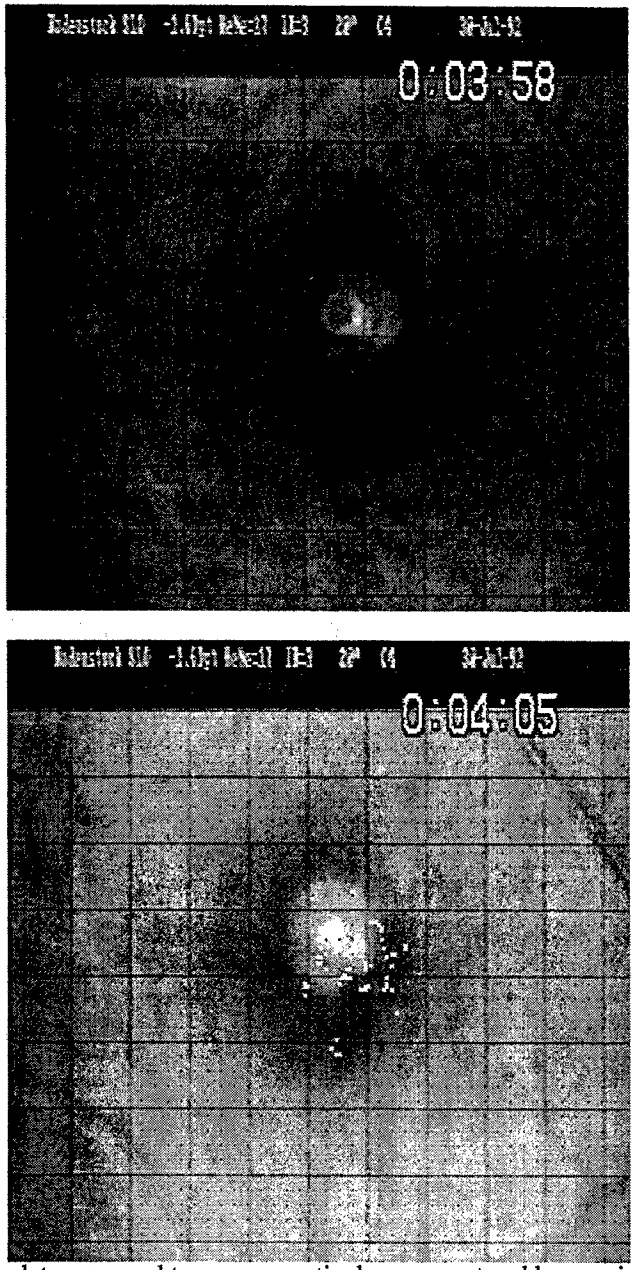

Figure 7. A lesion template was used to measure retinal movement and hence visual fixation while the letter "C" was projected onto the patient's retina. The letter "C" is evident in the top diagram. The lower portion of the figure shows the fixation points as measured by the tracking algorithm during a 10 second fixation episode. The tracking algorithm provided a position update every 165 ms.

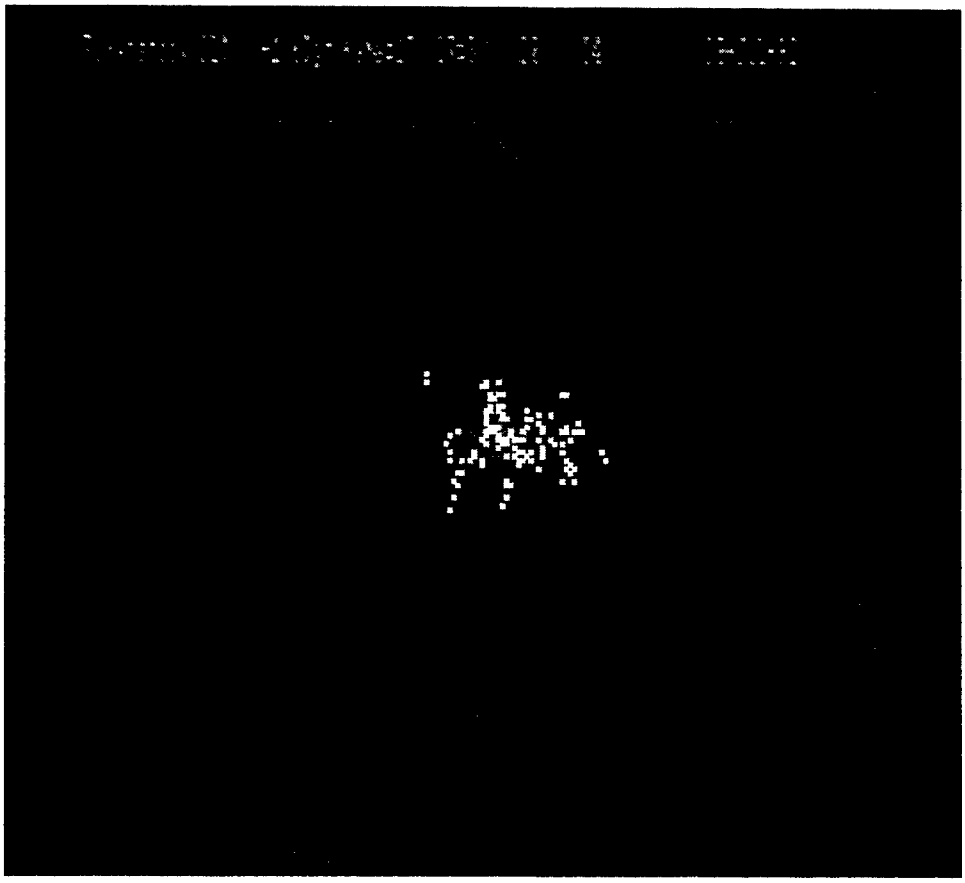

Figure 8. The actual laser lesion was used as the tracking template to measure and plot visual fixation points.

5. DISCUSSION

We have demonstrated that PRL can be quantified and is consistent less direct measurements of PRL. Although not shown, visitations at 12 months involve much more visitations within the laser induced macular hole than at 3 months post exposure. These observations are consistent with indirect retinal based Purkinje measurements made at 3 and 12 months post exposure.

The retinal tracking technique provides for quantifying previous investigations that indicate the PRL is governed by viability and non-viability of retinal areas visited by eye movements and generate a fixational eye movement pattern reflecting normal and non-functional retinal areas within and about lesion sites.

6. CONCLUSIONS

Recent investigations demonstrate that ocular motility in eyes with retinal pathology may show a lower propensity to visit such areas of the retina as compared to non-pathological retinal sites. With the applied method involving rapid image acquisition and registration to obtain an eye movement map, we were able to quantify in real time these images as an eye movement measurement using CSLO images. Preliminary data obtained demonstrate the utility of this technique in quantifying fixation eye movement patterns observed in human patients with vocation-related laser retinal injury.

With the success of this preliminary study we are upgrading the system frame grabber to allow for 30 position updates per second. This will provide a more accurate map of visual fixation points. We also interested in quantitatively comparing the results obtained from a Purkinje eye-tracker and the CSLO technique described in this paper. We have obtained Purkinje eye-tracking plots and CSLO video from three patients. We will be completing this comparative analysis early in 2001.

DISCLAIMER

The opinions or assertions contained herein are the private views of the authors and are not to be construed as official or as reflecting the views of the Department of the Army or the Department of Defense. Citation or trade names in this report does not constitute an official endorsement or approval of the use of such items. Human Volunteers participated in these studies after giving their free and informed consent. Investigators adhered to AR 70-25 and USAMRMC Regulation 50-25 on the use of volunteers in research.

REFERENCES

1. Zwick,H., Ness, J.W., Molchany, J.M., Stuck, B.E. , Loveday, J. "Neural motor ocular strategies associated with the development of a pseudo fovea following laser induced macular damage and artificial macular occlusion: Is the fovea replaceable?" *J. Laser Applications*, 10: 144-147; 1998
2. Ness, J.W., Zwick, H. Stuck,B.E., D.J. Lund, B.J. Lund, J.W. Molchany, D.H. Sliney. "Retinal image motion during deliberate fixation: implications to laser safety for long duration viewing", *Health Physics*, Jan 2000, in press.
3. Delfyett, P., "Emerging Laser Diode Technologies and Applications", *Proceedings of the International Laser Safety Conference*, ILSC'99. Orlando, FL.
4. Zwick, H., Stuck, B.E., Brown, J., Lund, D.J., Scales, D. Ness, J.W., "Long-term evaluation of selected accident cases", *In proceedings of the International Laser Safety Conference*, ILSC' 99. Orlando Fl: ILSC, 1999 p112-122.
5. S.F. Barrett, C.H.G. Wright, A.J. Welch, "Lasers in Ophthalmology", Lasers Applications in Medicine, Kluwer Publishers, 2001.
6. Stuck, B.E., H. Zwick, J.W. Molchany, D.J. Lund, D.A. Gagliano, "Accidental Human Laser Retinal Injuries for Military Laser Systems", *Proceedings of the Laser-Inflicted Eye Injuries: Epidemiology, Prevention, and Treatment, SPIE-The International Society for Optical Engineering,* San Jose , CA, January 1996, 7-20.
7. Crane, H.D. and C.M. Steele, "Accurate Three-dimensional Eyetracker", *Applied Optics*, Volume 17, Number 5, March 1, 1978, pp. 691- 705.
8. C.H.G. Wright, S.F. Barrett, R.D. Ferguson, H.G. Rylander III, and A.J. Welch, "Initial *In Vivo* Results of a Hybrid Retinal Photocoagulation System", *Journal of Biomedical Optics*, Volume 5, Number 1, 2000.
9. Webb, R.H. and G.W. Hughes, "Scanning Laser Ophthalmoscope", *IEEE Transactions on Biomedical Engineering*, Volume BME-28, Number 7, July 1981, pp. 488-489.
10. C.H.G. Wright, R.D. Ferguson, H.G. Rylander III, A.J. Welch, S.F. Barrett, "A Hybrid Approach to Retinal Tracking and Laser Aiming for Photocoagulation", *Journal of Biomedical Optics,* Vol 2, No 2, pp 195-203, 1997.
11. S. F. Barrett, C. H. G. Wright, H. Zwick, M. Wilcox, B. A. Rockwell, E. Naess, "Efficiently Tracking a Moving Object in Two-Dimensional Image Space", *Journal of Electronic Imaging,* accepted for publication.
12. S.F. Barrett, C.H.G. Wright, M.R Jerath, R. Stephen Lewis II, Bryan C. Dillard, H.G. Rylander, and A.J. Welch, "Computer Aided Retinal Photocoagulating System", *Journal of Biomedical Optics,* Volume 1, Number 1, 1996.
13. S.F. Barrtt, M.R. Jerath, H.G. Rylander, and A.J. Welch, "Automated Lesion Placement in the Rabbit Eye", *Lasers in Surgery and Medicine*, Volume 17, pp 172-177, 1995.

14. E. Naess, "Laser Positioning for Retinal Surgery", MSEE Thesis, University of Wyoming, Laramie, WY, December 2000.
15. Rosenfeld and G.J. Vanderbrug, "Coarse-Fine Template Matching", *IEEE Transactions on Systems, Man and Cybernetics*, SMC-7, Feb 1977, pp. 104-107.
16. S.F. Barrett, M.R. Jerath, H.G. Rylander, and A.J. Welch, "Digital Tracking and Control of Retinal Images", *Optical Engineering*, Vol. 33 No. 1, pp 150 - 159, 1994.
17. De Castro, E., G. Cristini, A. Martelli, C. Morandi, and M. Vascotto, "Compensation of Random Eye Motion in Television Ophthalmoscopy: Preliminary Results", *IEEE Transactions on Medical Imaging*, Volume MI-6, No.1 March 1987, pp. 74-81.

Author contact information:
* contact S.F. Barrett at Electrical Engineering Department, College of Engineering, P.O. Box 3295, University of Wyoming, Laramie, WY 82071-3295, steveb@uwyo.edu
** contact H. Zwick at U.S. Army Medical Research Detachment (USAMRD), Walter Reed Army, Institute of Research, Brooks AFB, TX 78235-5138, HSZWICK@aol.com

Effect of Source Intensity on the Variability of Eye Movements During Deliberate Fixation

Brian J. Lund[1], Harry Zwick[2], David J. Lund[2], Bruce E. Stuck[2], James W. Ness[3]
[1]TASC, Inc., 7914 A Drive, Brooks AFB, TX 78235-5138
[2]U.S. Army Medical Research Detachment, Brooks AFB, TX 78235-5138
[3]U.S. Army Medical Research & Materiel Command, 504 Scott Street, Fort Detrick, MD 21702-5012

ABSTRACT

During long-term viewing of a continuous light source, head and eye movements affect the distribution of energy deposited in the retina. Previous studies by this group of eye movements during a fixation task were used in revising the safety limits for long term viewing of such sources. These studies have been continued to determine the effect of source brightness on the nature of fixational eye movements. Volunteers fixated for up to 50 seconds on a HeNe laser (λ = 632.8 nm) masked by a 25 μm diameter aperture to produce a small source subtending ~0.03 mrad in the visual field. The source was attenuated to yield corneal irradiance values in the range 0.6 pW/cm^2 to 6 μW/cm^2. Eye movements were recorded using a Dual Purkinje Image Eye-Tracker. The hypothesis was that eye movements become more erratic as source intensity is increased toward levels that induce an aversion response. This would add a safety margin when viewing a bright source, as the energy deposited in the retina would be spread over a larger area. However, the data do not exhibit any change in the tightness of fixation with increasing source intensity. The area covered by the eye movements during successive 250 ms time slices exhibits a relatively flat trend during the course of the 50 second fixation task for all source intensities considered in this study, suggesting that there was no loss of ability to fixate nor drive to an aversion response during the course of the trials.

Keywords: eye fixation, laser safety, eye movements

1. INTRODUCTION

When viewing a continuous light source, movements of the eye will affect the distribution of energy deposited in the retina. Eye movements scan the image of the source over a portion of the retina, effectively increasing the area illuminated by the source, and thereby decreasing the peak irradiance experienced by any given point of the retina. It is therefore important to understand how eye movements contribute to the distribution of energy when assessing the risk of injury from a continuous light source, or when setting safety standards for the viewing of such sources.

In a previous study, volunteers fixated for 100 s on a point source produced by a light emitting diode (LED)[1]. Each volunteer's eye was subjected to a corneal irradiance of ~1 pW/cm^2. This is a very dim source – it will certainly not produce an aversion response by the viewer. It seemed reasonable to expect that the eye movement pattern would change as source intensity increased. This raises the question: as the source intensity is increased, is there a level at which the eye movement pattern breaks down, i.e., becomes so erratic that the subject is not able to effectively fixate on the source?

We report a study of eye movements during a fixation task designed to assess the effect of source intensity over a seven log unit range on the nature of fixational eye movements. The data are interpreted in terms of the illumination pattern produced on the retina, and the total time a given area of the retina is "visited" during a trial. We have not, for example, tried to extract the frequency or size of saccadic motion.

2. METHODS

2.1 Apparatus

A schematic of the experimental setup is shown in Figure 1. Eye movements were recorded using a version 6 Dual Purkinje Image Eyetracker[2], which is capable of measuring the orientation of the eye to ≤ 1 minute of arc. A head and chin rest was used to hold the volunteer in alignment with the eyetracker. The volunteer used the unity power telescope attached to the eyetracker to bring the fixation spot into best focus.

Laser and Noncoherent Light Ocular Effects: Epidemiology, Prevention, and Treatment,
Bruce E. Stuck, Michael Belkin, Editors, Proceedings of SPIE Vol. 4246 (2001)

The fixation spot was produced by a HeNe laser (λ = 632.8 nm) which was masked by a 25 μm diameter aperture to produce effectively a point source. The aperture was located on the focal plane of the lens indicated in Figure 1. The fixation spot was thus located at optical infinity within the subject's field of view, which eliminated any parallax. That is, any transverse movement of the volunteer within the head/chin rest did not require a rotation of the subject's eye to remain fixated on the spot. In addition, no accommodation was required for viewing an object at effectively a large distance.

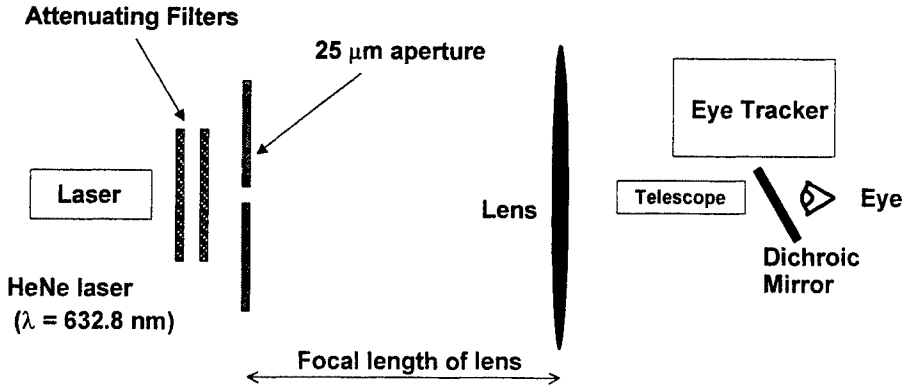

Figure 1: Schematic of system used to measure eye movements during fixation.

All measurements were made in a darkened room (scotopic ambient light conditions).

A series of neutral density filters were located between the laser and the aperture to attenuate the laser output to produce the desired exposure levels at the location of the subject's eye. Measurements were made for corneal irradiances of 0.6 pW/cm^2, 60 pW/cm^2, 6 nW/cm^2, 600 nW/cm^2 and 6 μm/cm^2. At λ = 632.8 nm, this corresponds to a corneal illuminance ranging from 3.5x10^{-8} scotopic lm/m^2 to 0.35 scotopic lm/m^2.

The highest corneal irradiance used in this study, 6 μW/cm^2, was limited by a desire to stay well below the maximum permissible exposure (MPE) as determined from ANSI Z136.1, 1993[3]. The 1993 standard allowed 17.6 μW/cm^2 corneal irradiance for 10,000 s exposures. Although the cumulative daily exposure for any individual was significantly less than 10,000 s, that value was chosen to be conservative (and to facilitate passing the protocol through the review and approval process). It should be noted that the current ANSI Z136.1, 2000 allows exposure to 1 mW/cm^2 for the same viewing conditions[4].

The output of the eyetracker was digitized and recorded by computer, and stored to disk file for later analysis. The subject's horizontal and vertical eye orientations were recorded, as well as the eyetracker's "good lock" signal. The latter signal, in conjunction with a visual inspection of the data, was used to identify the times at which the subject blinked during a trial. Data was recorded at a rate of 1000 measurements/second (The eyetracker has a nominal bandwidth for small amplitude eye movements of 400 Hz).

2.2 Experimental Subjects

Six volunteers ranging in age from 21 to 67 years participated in the study. All volunteers tested normal on a standard ophthalmological eye exam, although they were not required to be emmetropic. At the higher irradiance values (600 nW/cm^2 and 6 μW/cm^2), the constriction of the subject's iris in reaction to the bright stimulus interfered with the fourth Purkinje image, making it impossible for the eyetracker to obtain a good lock. Therefore, at these levels, the subject's pupils were dilated using Alcaine (as a numbing agent) and Mydriacil 1%. The use of a mydriatic prevented the subject's pupils from constricting, but still allowed the eye to accommodate. In order to check that the mydriatic did not have a significant effect on eye movements, several trials were made on dilated subjects at the lower intensity levels.

2.3 Experimental Procedure

For each trial, the subject's left eye was patched for deliberate fixation using the right eye. The data was recorded for a monocular task. The volunteer was instructed to stare at the source "as best they can". A trial consisted of the subject fixating on the laser spot for 50 seconds.

The head/chin rest was adjusted to align the subject with the eyetracker axis as closely as practicable. The subject adjusted the telescope to provide the sharpest focus on the laser spot he or she could attain. The subject was then allowed to relax for a few moments before initiating the experimental trial. During this time the subject could close his or her eyes, or sit back away from the tracker.

The fixation trial began after a stable eyetracker lock was obtained. For the trials run at corneal irradiances of 600 nW/cm^2 and 6 $\mu m/cm^2$, an additional neutral density filter was initially inserted in the beam path to attenuate the laser down to a corneal irradiance < 1 nW/cm^2. This provided a more comfortable level for the subject while the eyetracker was being set up for the trial. The extra filter was removed once an eyetracker lock was obtained, and then data acquisition started.

2.4 Analysis of data

The data was analyzed and interpreted in terms of the location of the image (of the laser spot) on the retina, and the pattern "painted" by the image location as it moves about the retina due to eye movements. In addition, we consider the total time a given point on the retina is "visited" as a result of the eye movements. For tight, stable eye movements, the image will be moved over a relatively small area of the retina, and each area covered will have a relatively large accumulated visitation time. The obverse is true for erratic eye movements - the image location will be moved over a relatively larger area of the retina, and each area covered will have a relatively low accumulated visitation time.

The output of the eyetracker yields the horizontal and vertical eye orientation, θ_H and θ_V, of the subject as he or she fixates on the stimulus. This eye orientation is converted to image position on the retina using an effective focal length of 17 mm for the human eye[5]. This yields an image position measurement resolution of ≤ 5 μm, corresponding to the one minute of arc resolution of the eyetracker. A change in eye orientation of one degree of arc shifts the position of the image on the retina by 297 μm. While using the DPI eyetracker, we do not have a view of the interior of the eye, and therefore cannot specify where the image is located on the retina. However, studies using a Scanning Laser Ophthalmoscope (SLO) show that during a fixation task, the image will be located within the fovea[6].

In keeping with our previous study[1], we define an ellipse centered at the means $\bar{x}$ and $\bar{y}$ of the recorded nasal/temporal and superior/inferior retinal position measurements. The axes of the ellipse are determined by the standard deviations σ_H and σ_V of the data. The area of this one standard deviation ellipse ($A = \pi\sigma_H\sigma_V$) is used as a measure of the "tightness of fixation" of the eye movements. While there is no a priori reason to believe that all of the data will organize along these axes, an examination of the movement patterns seems to suggest a horizontally oriented, roughly elliptical pattern. In addition, this assumption helps to simplify the initial analysis of the data.

We analyze the data in two ways. First, we consider the data as a series of 0.25 s time slices, and construct a time slice one standard deviation ellipse at time t from the eye movement data from time t to $t + 0.25$ s. Second, we examine the growth of the eye movement distribution pattern. We construct a cumulative one standard deviation ellipse at time t from the eye movement data from time 0 to time t (the first t seconds of the trial). An example of this analysis for an artificial eye is discussed below.

2.5 Artificial Eye

To demonstrate the performance of the eyetracker, 50 seconds of data was recorded for an artificial eye mounted on a tripod. The data was converted to retinal space as described above. The visitation time plots of figure 2 show the total accumulated time that the recorded image position fell within a given 10 μm by 10 μm area of the artificial eye's "retina".

The areas of the one standard deviation ellipses calculated for consecutive 0.25 s time slices of the artificial eye data is shown on the right side of figure 3. The average area is computed in the standard way, by summing the areas of the 50/0.25 = 200 time slices, and dividing by the number of time slices. As expected for the stable artificial eye, which exhibits no saccadic motion, gaze shifts or blinks, the areas for the time slices show only a small variation about the mean value of 15.41 μm^2.

A distribution growth plot for the artificial eye is shown on the left side of figure 3. As the artificial eye does not move, successive 0.25 s ellipses will be located very nearly on top of each other. This is demonstrated by the fact that the overall distribution size (area of the one standard deviation ellipse) for the artificial eye quickly settles to a value not much larger than the average area of the time slice ellipses.

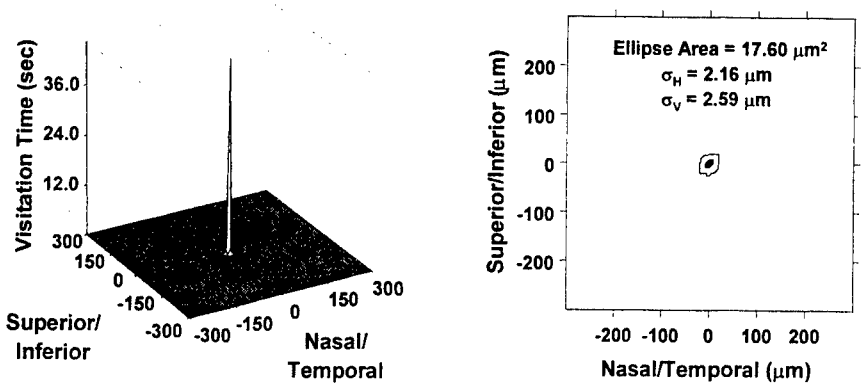

Figure 2: Peak and contour visitation time plots showing the movement pattern recorded for an artificial eye. Data was recorded for 50 s. The cumulative one standard deviation ellipse is too small to be visible on these plots.

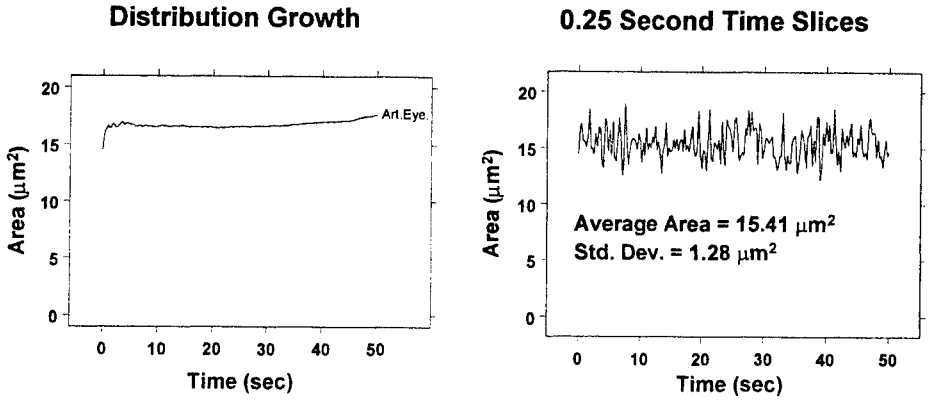

Figure 3: Distribution growth and time slice areas for the artificial eye.

3. RESULTS

Figures 4, 5 and 6 show examples of the visitation time plots obtained from three of the subjects for different values of the corneal irradiance. These plots show the total accumulated time the measured image position fell within a given 10 μm by 10 μm area of the retina during the 50 second trial, and demonstrate some of the range of movement maps observed in this experiment. The one standard deviation ellipse is indicated on the contour plots. Figure 4 shows the results recorded for subject 1 fixating on the 0.6 pW/cm^2 source for 50 seconds, and displays one of the largest ellipse areas obtained. Figure 5, subject 4 fixating on a 60 pW/cm^2 source, illustrates one of the smallest ellipses obtained. Note that the area of the one standard deviation ellipse for the artificial eye is about a factor of 54 times smaller than the ellipse of figure 5.

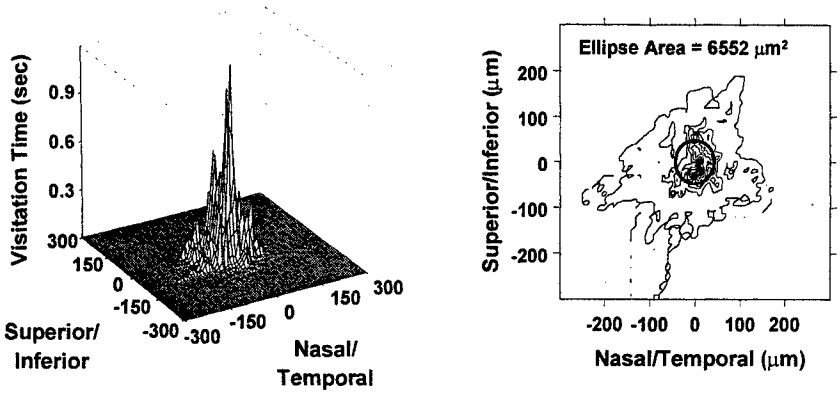

Figure 4: Peak and contour visitation time plots showing the movement pattern recorded for Subject 1 fixating for 50 s at a source of corneal irradiance 0.6 pW/cm^2. The cumulative one standard deviation ellipse is shown on the contour plot. This is an example of one of the larger, more spread-out movement patterns recorded in this study.

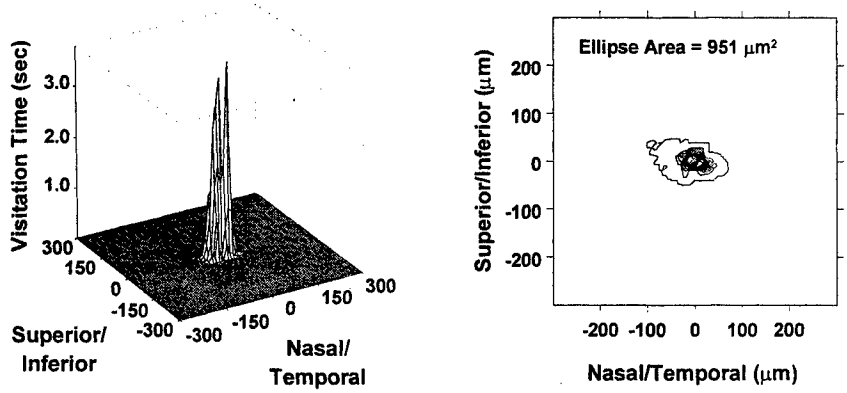

Figure 5: Peak and contour visitation time plots showing the fixation pattern recorded for Subject 4 fixating for 50 s on the 60 pW/cm^2 corneal irradiance source. The cumulative one standard deviation ellipse is shown on the contour plot. This is an example of one of the tightest movement patterns observed in this study.

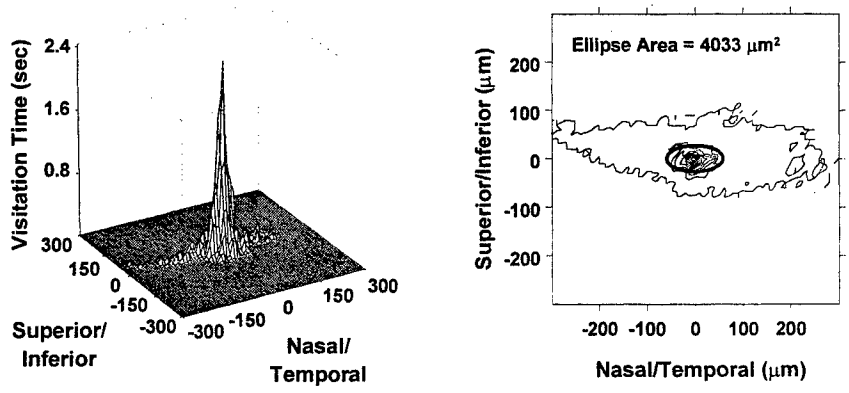

Figure 6: Peak and contour visitation time plots showing the fixation pattern recorded for Subject 6 fixating for 50 s on the 6 μW/cm^2 corneal irradiance source. The one standard deviation ellipse is shown on the contour plot.

An example of the area of the one standard deviation ellipse per each 0.25 s time slice is shown in Figure 7. The data was recorded for subject 3, and includes trials for each of the five corneal irradiance values examined in this experiment. These

data display no obvious trend toward increasing or decreasing area during the 50 second trials. This trend was exhibited by all of the subjects included in the experiment. While the magnitude of the area varied from individual to individual, the ellipses for the 0.25 s time slices show no tendency to increase or decrease in area as the trial progressed.

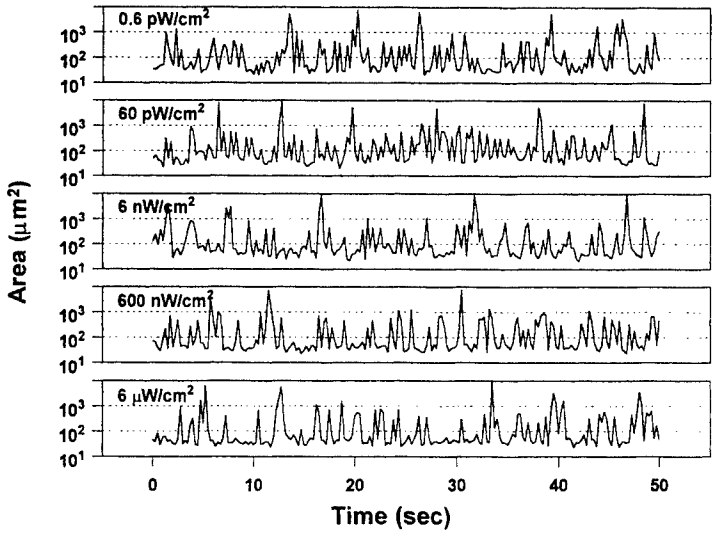

Figure 7: Area of the 0.25 s time slice ellipses for subject 3.

The average area of the ellipse for 0.25 s time slices is plotted vs. the incident corneal irradiance for each of the six subjects in Figure 8. The error bars are ± one standard deviation of the ellipse area for the given trial. The figure clearly demonstrates no dependence on corneal irradiance for the small time scale (0.25 s) eye movements. Subject 5 shows unusually large error bars for the trial at 6 nW/cm^2. During this trial, the subject's eye tended to dry out, causing the subject to blink frequently.

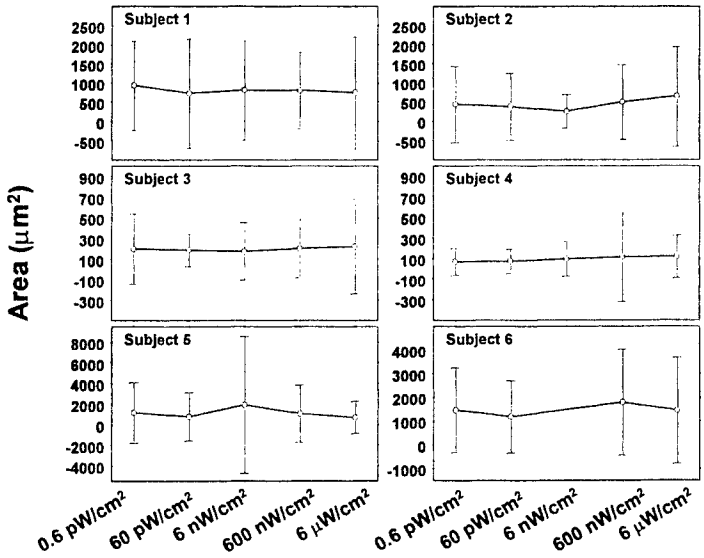

Figure 8: Average area per 0.25 s time slice for the six subjects considered in this experiment. The error bars are ±1 standard deviation of the area for the given trial.

In Figure 9, the evolution of the area of the cumulative one standard deviation ellipse for each of the corneal irradiance values is plotted for subject 3. The time slice data for this subject was discussed above in relation to figure 7. Although there is variation between subjects, this figure serves to illustrate the features displayed by all of the subjects. In particular, sudden

increases in the ellipse area are generally associated with points at which the subject blinked. In recovering from the blink, the subject had to reacquire the location of the fixation source, and will have settled in a location somewhat different from the pre-blink location.

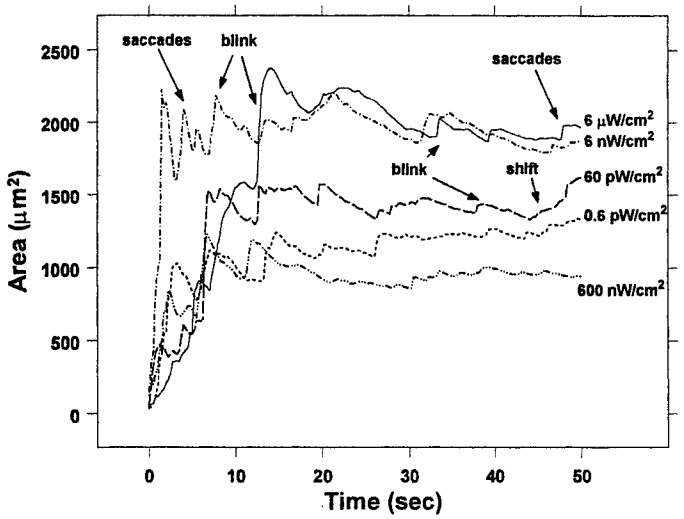

Figure 9: Evolution of the area of the cumulative one standard deviation ellipse during the 50 s trials for subject 3. The curves are labeled at their endpoint by the source corneal irradiance used in the trial. Several points where the subject's eye underwent a series of saccades, or where the subject blinked during a trial area indicated on the figure.

A closer look at the 6 nW/cm^2 trial of subject 3 is shown in Figure 10. A comparison is made between the overall distribution growth (area of the cumulative one standard deviation ellipse) and the area of the 0.25 s time slice ellipses. All blinks that occurred during the run are indicated, as well as a series of large saccades that occurred early in the run (~5 seconds).

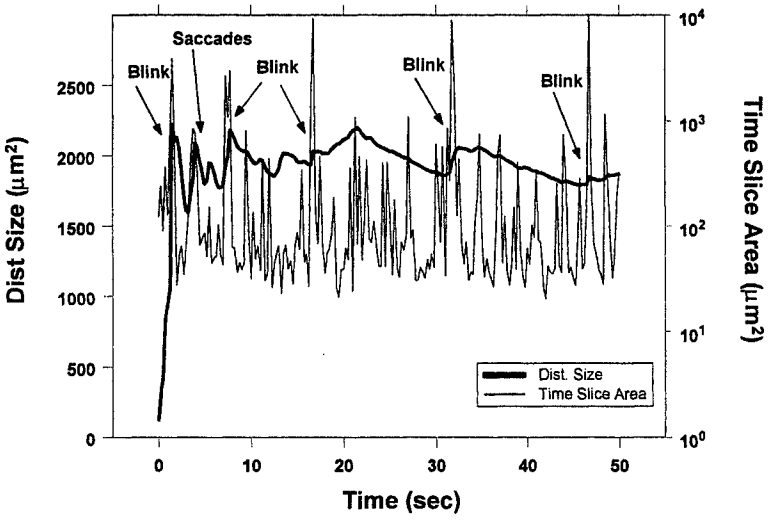

Figure 10: Comparison of the evolution of the area of the cumulative one standard deviation ellipse and the areas of the 0.25 s time slice ellipses for subject 3 fixating on the 6 nW/cm^2 corneal irradiance source. All blinks that occurred during the 50 s run are indicated, as well as a series of large saccades that occurred early in the run.

Figure 11 shows the final distribution size (area of the cumulative one standard deviation ellipse at 50 seconds) for all six subjects vs the source corneal irradiance. There is significant variation from one subject to the next, but there is no obvious trend that can be discerned as a function of the source intensity that would fit all subjects. Indeed, there is no clear trend that can be readily inferred from this data set. Subject 1 is the oldest subject, while subject 5 is the youngest subject in this data set. Subjects 1 and 4 both made concerted efforts to avoid blinking during the runs.

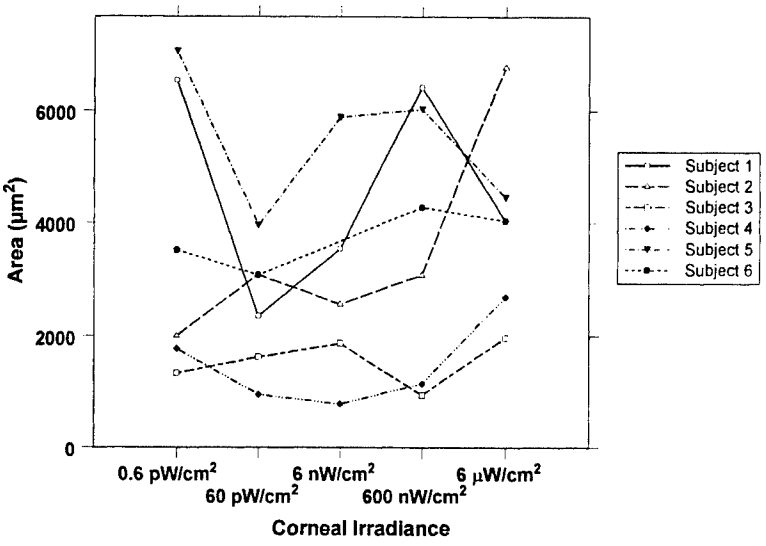

Figure 11: Final distribution size, i.e., the area of the cumulative one standard deviation ellipse at 50 s. These ellipses are illustrated in the contour plots of Figures 4, 5 and 6.

4. DISCUSION

The data do not exhibit any significant systematic change in visited retinal area that can be readily attributed to intensity over the seven orders of magnitude of source intensity considered in this study. In particular, we do not observe a break in the ability to fixate on the point source at higher corneal irradiance. Although staring at the more intense sources might be uncomfortable, individuals can force themselves to fixate on the source, producing an eye movement pattern that cannot be readily differentiated from one recorded for staring at a weak source.

On a 0.25 s time scale the average retinal area over which an image is spread is invariant with respect to the incident source irradiance (figure 8). The final distribution size observed for long term fixation (50 seconds in the case of this study) does exhibit more variation across source intensity (figure 11), but there is no clear source intensity related trend that can be inferred. It is likely that as more data is accumulated on the individuals, the average final 50 second distribution size will exhibit the same flat trend as shown by the 0.25 s time slice data.

While there is no distribution size dependence that can be readily attributed to the source intensity, there is a significant variation between individuals. This is clearly demonstrated in both the 0.25 s time slice results (figure 8) and the long fixation time results (figure 11). This variation will be due to the physiology of the given individual, but may also involve factors such as the age of the individual or the experience and training of the individual.

For an individual with a tight fixation spot, incident laser light entering the eye will be spread over a smaller area than for an individual with a looser fixation spot. Correspondingly, the peak energy deposited in the retina will be higher for the tightly fixated individual than for the more loosely fixated individual. This indicates that the tightly fixated individual may be at somewhat greater risk of injury (lower damage threshold) from an incident laser beam.

We have investigated the influence of irradiation at a single wavelength (632.8 nm). We recognize that because of the spectral sensitivity curve of the human eye, light of longer wavelengths will require a greater irradiance to achieve the same visual response. While the damage potential of the exposure is determined by the irradiance of the laser, the potential to evoke an aversion response is determined by the illuminance of the laser. Based on the photopic sensitivity of the human eye[7], a laser pointer at 670 nm would require 7 times the irradiance, or 42 $\mu W/cm^2$, to achieve the same illuminance as the 6 $\mu W/cm^2$ HeNe laser used in this experiment. A laser at 700 nm would require an irradiance of 360 $\mu W/cm^2$ to match the 6 $\mu W/cm^2$ HeNe laser and a laser at 800 nm would require an irradiance of 36,000 $\mu W/cm^2$. This latter irradiance would exceed the MPE for exposure to a collimated 800 nm laser in about 40 μs and would exceed the threshold for retinal damage in about 0.5 seconds[8, 9]. Thus, even if the aversion response could be shown to affect the irradiated area on the retina, it would not be effective in mitigating the retinal effects of near infrared but still visible laser sources.

5. CONCLUSION

The eye movement maps for a given individual show no change that can be readily attributable to source intensity for sources producing a corneal irradiance up to 6 $\mu W/cm^2$ at a wavelength of 632.8 nm. We conclude that the more intense source does not induce an eye movement pattern that will spread the incident light over a larger area of the retina, as compared to the less intense sources.

6. DISCLAIMER

The opinions or assertions contained herein are the private views of the authors and are not to be construed as official or as reflecting the views of the Department of the Army or the Department of Defense.

Citation of trade names in this report does not constitute an official endorsement or approval of the use of such items.

Human Volunteers participated in these studies after giving their free and informed voluntary consent. Investigators adhered to AR 70-25 and USAMRMC Regulation 50-25 on the use of volunteers in research.

7. REFERENCES

1. James W. Ness, Harry Zwick, Bruce E. Stuck, David J. Lund, Brian J. Lund, Jerome W. Molchany, and David H. Sliney, "Retinal image motion during deliberate fixation: implications to laser safety for long duration viewing," Health Physics 78 (2):131-142; 2000.

2. Hewitt D. Crane, "The Purkinje Image Eyetracker, Image Stabilization, and Related Forms of Stimulus Manipulation,", In: D.H. Kelly, ed., Visual Science and Engineering, Models and Applications, Marcel Dekker, Inc., 1994.

3. ANSI (American National Standards Institute), Safe Use of Lasers, Standard Z-136.1, Cincinnati: Laser Institute of America, 1993.

4. ANSI (American National Standards Institute, Safe Use of Lasers, Standard Z-136.1, Cincinnati: Laser Institute of America, 2000.

5. U.S. Defense Department, Optical Design. Military Handbook 141. 5 October 1952.

6. H. Zwick, D.J. Lund, D.A. Gagliano and B.E. Stuck, "Functional and Ophthalmoscopic Observations in Human Laser Accident Cases Using Scanning Laser Ophthalmoscopy," SPIE Vol. 2126 (1994), 144-153.

7. G. Wyszeski and W.S. Stiles, *Color Science*. John Wiley & Sons, New York, 1967.

8. D.J. Lund, D.O. Adams, C.C. Carver, *Ocular hazards of the gallium arsenide laser*, Presidio of San Francisco, CA: Letterman Army Institute of Research, 1976. Institute Report No. 30.

9. D.J. Lund, B.E. Stuck, E.S. Beatrice, *Biological research in support of project MILES*, Presidio of San Francisco, CA: Letterman Army Institute of Research, 1981. Institute Report No. 96

Ocular Hazards of Q-switched Blue Wavelength Lasers

David J. Lund*[a], Peter Edsall[b] and Bruce E Stuck[a]

[a]U.S. Army Medical Research Detachment, Walter Reed Army Institute of Research
7914 A Drive, Brooks AFB, TX 78235-5138

[b]TASC, Inc, 7914 A Drive, Brooks AFB, TX 78235-5138

ABSTRACT

The threshold for laser-induced retinal damage in the rhesus eye was determined for 14 wavelengths from 410 nm to 580 nm. The laser source was a tunable Optical Parametric Oscillator (OPO) pumped by the 3rd harmonic of a Nd:YAG laser. The laser pulse duration was 3.5 ns. The wavelength dependence of the injury threshold was consistent with the prediction of a model based on the transmission of the preretinal ocular media, absorption in the retinal pigment epithelium, and variation of irradiance diameter resulting from chromatic aberration of the eye optics. The threshold for 24-hour observation was only slightly lower than the threshold for 1-hour observation. The laser-induced retinal hemorrhage threshold was less than a factor of two greater than the minimum visible lesion (MVL) threshold for wavelengths from 442 nm to 410 nm. This results from the presence of a dense capillary network in the inner retina and a large hemoglobin absorption peak.

Keywords: Laser bioeffects, retinal damage, retinal hemorrhage, ocular thresholds, thermal model, action spectrum

1. INTRODUCTION

Ham et al have shown that the eye is more susceptible to damage by light in the blue end of the spectrum as compared to longer wavelengths [1-4]. They subjected 500 μm diameter retinal areas in Rhesus eyes to long duration exposures (1 to 1000 s) and determined damage thresholds for laser irradiation and filtered xenon lamp irradiation for wavelengths from 325 nm to 1064 nm. For wavelengths shorter than 600 nm and durations longer than 10 s they ascribe the damage to photochemical mechanisms. Their data for 100 s exposures are shown in **Figure 1**. The threshold for damage, computed at the retina, continues to decrease with decreasing wavelength to the shortest wavelength tested. In light of this retinal sensitivity curve for photochemical damage, there is interest in the spectra for laser-induced thermal damage in the blue spectrum. The availability of an Optical Parametric Oscillator capable of providing useful pulse energy throughout a tuning range from 400 nm to 2200 nm has made it possible to determine the wavelength dependence of retinal damage for short (3-4 ns) pulses throughout the visible and NIR spectrum. While laser-induced retinal damage from such short pulses are thermal-mechanical in nature, still the damage results from thermal conversion of the incident laser irradiation and we have shown that the action spectrum for laser induced retinal damage between 530 nm and 1300 nm via nanosecond duration pulses is not different than that for 100 ms duration exposures which are purely thermal in nature [5-7]. This paper reports results obtained for retinal exposure to OPO wavelengths from 410 to 580 nm.

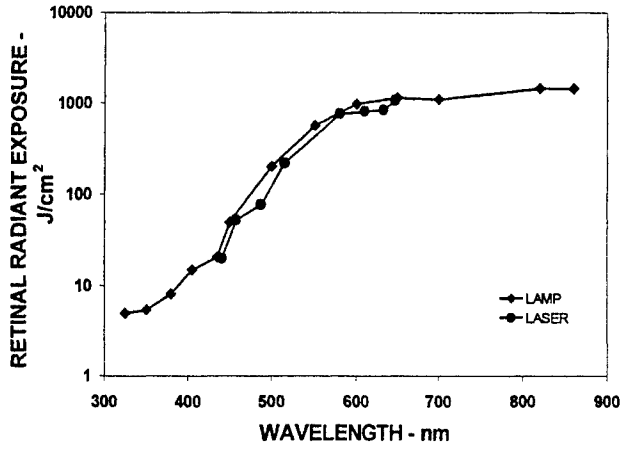

Figure 1. Action spectrum for retinal injury in the Rhesus Monkey for 100 s exposures to laser irradiation (circles) and narrow band pass filtered xenon arc lamp irradiation (diamonds) (After Ham [1-4]). Ham ascribes this spectrum to a photochemical damage mechanism.

Laser and Noncoherent Light Ocular Effects: Epidemiology, Prevention, and Treatment,
Bruce E. Stuck, Michael Belkin, Editors, Proceedings of SPIE Vol. 4246 (2001)

2. MATERIALS AND METHODS

Figure 2 shows a representative exposure system used to measure laser induced retinal damage thresholds. A Continuum Surelite Optical Parametric Oscillator (OPO), pumped by the 355 nm output of a Continuum Surelite Nd:YAG laser provided useful pulse energy throughout a tuning range from 400 nm to 600 nm. A portion of the OPO output was directed by a beam splitter into an Oriel INSTASPEC spectrometer to accurately tune the laser and monitor the wavelength.

The OPO emitted 3.5 ns duration pulses at 20 Hz and a shutter was used to select single pulses for exposure. A beam splitter deflected a constant proportion of the pulse energy into a reference detector while the remainder of the energy passed through attenuators and onto a mirror that directed the laser beam into the eye to be exposed. The mirror was mounted on a translation stage so it could be moved to permit observation and accurately repositioned for exposure. A fundus camera permitted observation of the retina and selection of sites for exposure. The fundus camera, mirror, and laser beam were aligned so that the laser energy reflected by the mirror passed through the center of the ocular pupil and struck the retina at the site corresponding to the crosshairs of the fundus camera viewing optics.

Before the rhesus monkey was positioned, a calibrated detector was placed to directly receive the energy that would normally enter the eye. The ratio of the energy at this position to the energy at the reference detector was obtained with the attenuator removed. Subsequently, when the eye was exposed, the energy entering the eye for each exposure was determined by multiplying the energy at the reference detector by the ratio previously determined and by the transmission of the attenuating filter chosen to give the desired energy.

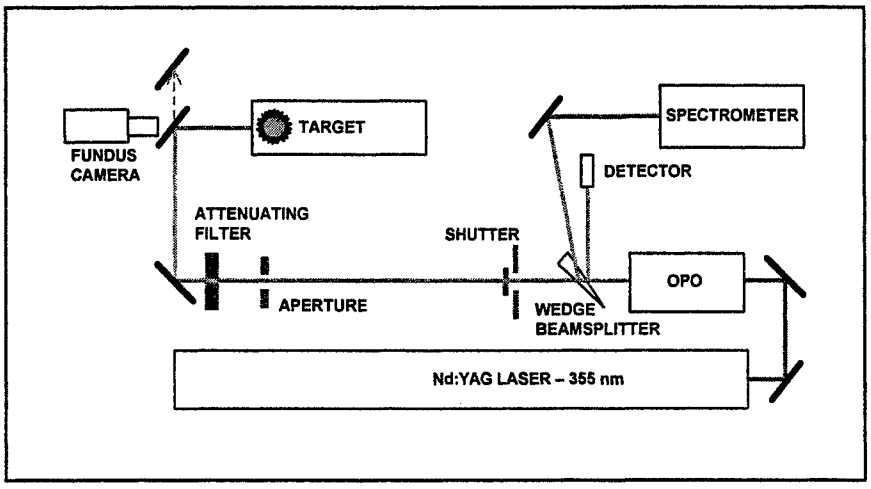

Figure 2: Schematic of laser exposure system employed to expose rhesus monkey eyes. The frequency-tripled Nd:YAG laser pumped the Optical Parametric Oscillator (OPO). An optical wedge directed portions of the beam into a reference detector and a spectrometer. A shutter controlled the exposure duration. After passing through attenuators, the beam was directed by mirrors into the target (animal eye or calibrated detector). The mirror in front of the fundus camera was translated to permit observation of the retina.

Rhesus monkeys were used in this study. Each animal was sedated and anesthetized for exposure. Cycloplegia and full pupil dilation were pharmaceutically induced in the eye to be exposed. The eye was held open by a lid speculum and the cornea was periodically irrigated with physiological saline solution to maintain clarity. For each test, an animal was positioned and 30 exposures were placed in an array in the extramacular retina. The initial row of six exposures in each sequence was at a dose high enough to produce an immediate visible tissue response. Subsequent exposures were at lower doses so that the range of doses in the array varied by about a factor of ten. The exposure sites were examined by ophthalmoscope one hour and 24 hours after exposure and the presence or absence of a minimum visible lesion (MVL) noted for each site. Also noted was the presence or absence of acute retinal hemorrhage at the exposure site. The response at each site was correlated to the dose at that site. The data relating the probability of damage to the exposure energy was processed by the statistical technique of probit analysis[8] to determine the ED_{50}, that incident energy having a fifty percent probability of producing alteration. For each wavelength, the data obtained by exposure of four eyes, one each in four animals, were statistically evaluated to determine the ED_{50} and associated 95% confidence limits.

3. RESULTS

Dose-response data were obtained for 14 wavelengths in the blue spectrum. All exposure durations were 3.5 ns. The laser beam at the eye was 4 mm in diameter and gaussian in profile. The beam divergence was 0.3 mr. The ED_{50} and associated

95% confidence limits were determined for a one hour MVL endpoint, a 24 hour MVL end point and an acute retinal hemorrhage endpoint. These data are shown in **Table 1** and **Figure 3**. Included in **Table 1** are the slopes of the damage probability curves defined as the ED_{84}/ED_{50}.

TABLE 1. ED_{50} FOR RETINAL ALTERATION INDUCED BY 3.5 ns EXPOSURE TO OPO LASER IRRADIATION

WAVELENGTH (nm)	ED_{50} (μJ) *(95% RANGE)*, SLOPE		
	1 Hr Endpoint	24 Hr Endpoint	Retinal Hemorrhage Endpoint
410	76.5 *(58.9-104)*, 1.38	48.8 *(24.5-59.6)*, 1.26	110 *(82.7-147)*, 1.52
420	27.1 *(31.0-24.0)*, 1.43	24.4 *(21.4-28.0)*, 1.51	30.7 *(26.9-36.1)*, 1.52
430	17.6 *(15.7-20.0)*, 1.22	14.9 *(13.1-17.0)*, 1.29	25.5 *(21.8-29.9)*, 1.48
442	16.8 *(14.1-20.0)*, 1.52	12.9 *(10.8-15.4)*, 1.51	21.2 *(17.3-26.1)*, 1.78
450	8.41 *(7.02-10.0)*, 1.45	6.89 *(5.81-8.20)*, 1.38	32.3 *(22.1-58.6)*, 3.84
458	6.30 *(5.14-7.62)*, 1.76	6.20 *(5.19-7.32)*, 1.56	63.2 *(46.3-130)*, 1.98
476	4.76 *(3.15-6.86)*, 1.53	4.61 *(2.75-7.16)*, 1.50	24.4 *(20.4-33.1)*, 1.64
488	3.91 *(2.87-4.98)*, 2.19	4.47 *(3.83-5.20)*, 1.38	74.8 *(59.8-xxx)*, 1.74
493	8.85 *(7.19-10.6)*, 1.33	5.26 *(4.09-6.66)*, 1.74	43.3 *(34.7-68.9)*, 1.59
500	7.73 *(6.60-9.06)*, 1.41	5.12 *(4.26-6.08)*, 1.52	74.4 *(57.9-202)*, 1.48
510	6.90 *(5.49-8.75)*, 1.24	5.25 *(3.86-6.68)*, 1.83	72.3 *(54.9-571)*, 1.66
520	5.93 *(4.54-7.70)*, 2.45	4.01 *(3.09-5.03)*, 2.09	49.5 *(38.7-83.5)*, 1.61
530	4.23 *(3.46-5.21)*, 1.46	3.32 *(2.29-4.76)*, 1.53	69.7 *(48.7-xxx)*, 1.54
580	5.87 *(4.89-6.42)*, 1.15	4.23 *(3.66-4.89)*, 1.32	63.4 *(51.5-99.4)*, 1.54

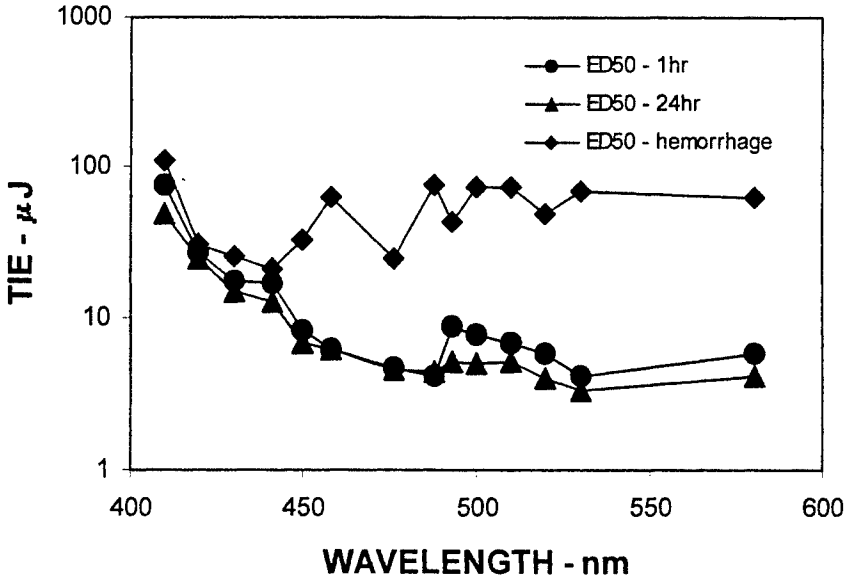

Figure 3. One hour, 24 hour, and retinal-hemorrhage ED_{50} values for extramacular exposure in the rhesus monkey to single 3.5 ns pulses from the OPO. Total Intraocular Energy (TIE) is defined as the energy incident at the cornea within the ocular pupil.

4. DISCUSSION

The data of **Table 1** and **Figure 3** show that the ED_{50} for a 24-hour MVL is only slightly lower than the ED_{50} for a 1-hour MVL. This is consistent with a thermal damage mechanism as opposed to a photochemical damage mechanism. The ED_{50} is minimum in the blue green spectrum and increases with decreasing wavelength below 500 nm. **Figure 4** compares these data to the 100 s data of Ham. The total intraocular energy from **Table 1** was multiplied by the ocular transmission at each wavelength to determine the energy incident on the retina. A retinal irradiance diameter of 70 μm was assumed to determine the retinal radiant exposure. The choice of retinal irradiance diameter does not affect the shape of the curve; 70 μm was chosen based on the examination of available spot size dependence data [9,10]. No correction was made for chromatic aberration. Previously determined ED_{50}'s for 15 ns dye laser exposures were included to complete the short pulse spectrum[11-13]. Clearly two different spectra are shown for wavelengths shorter than 600 nm, The thermal curve can be explained based on the transmission of the ocular media, absorption in the retinal pigment epithelium (RPE), and chromatic aberration of the eye. The photochemical curve results from incompletely understood non-thermal interactions.

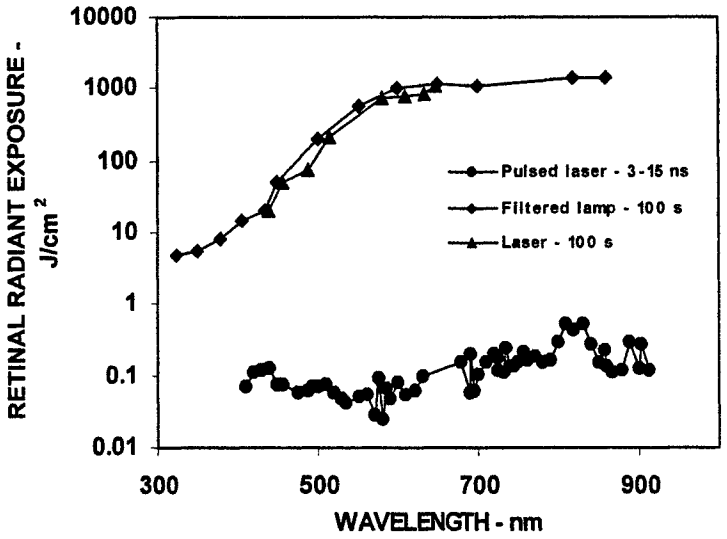

Figure 4. A comparison of the wavelength dependence for photochemical retinal damage to the wavelength dependence for thermal retinal injury. Retinal radiant exposure data for 100 s exposures to irradiation from a narrow-band-pass-filtered xenon lamp (diamonds) and for 100 s laser exposures (triangles) are from Ham[1-4]. The data for the 3-15 ns laser exposures (circles) were corrected for ocular transmission and the retinal irradiation diameter to obtain the retinal radiant exposure. A 70 μm beam diameter at the retina was assumed for the pulsed exposures.

Threshold laser-induced thermal retinal damage is localized to the retinal pigment epithelium that lies at the focus of the eye optics (**Figure 5**). The RPE is a monolayer of cells containing melanin granules. Melanin is a strong absorber of optical radiation to the extent that much of the radiation incident on the retina is absorbed in a 5 μm layer of melanin granules. An action spectrum for thermal retinal damage has been modeled based on the wavelength dependent transmission (**Figure 6**) and absorption (**Figure 7**) of ocular tissue and chromatic aberration of the eye optics.[5-7]

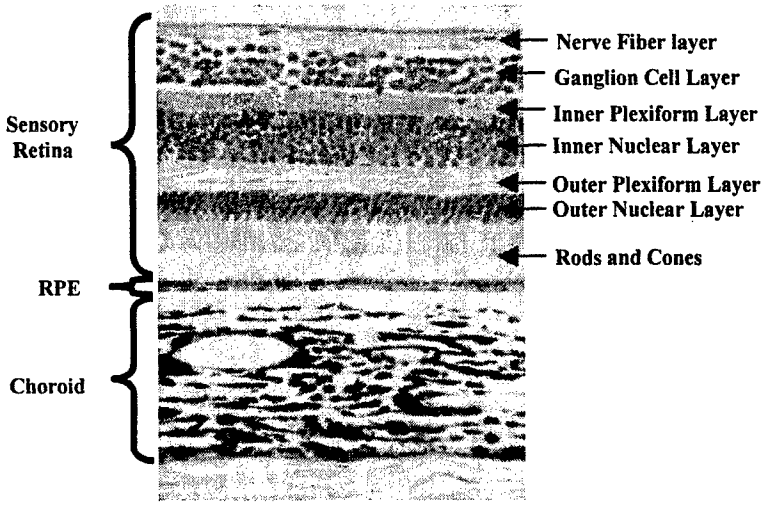

Figure 5. Section through a Rhesus monkey retina. Light is incident from the top and passes through the sensory retina before impinging upon the Retinal Pigment Epithelium (RPE) and the choroid. The RPE is a monolayer of cells containing strongly absorbing melanin granules. Retinal capillaries are found in the nerve fiber layer and between the inner nuclear layer and the outer plexiform layer

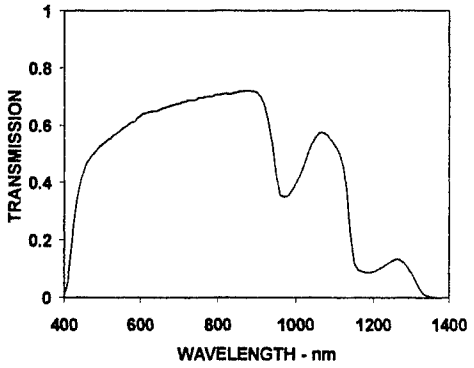

Figure 6. T_λ - Direct Transmission of the preretinal ocular media of the rhesus eye (After Maher [14], Boettner[15,16]).

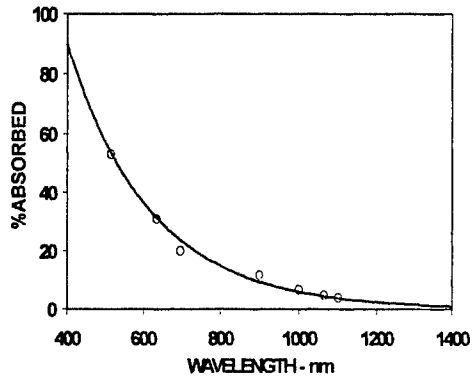

Figure 7. A_λ - Absorption of light in the Retinal Pigment Epithelium (RPE) of the rhesus eye (After Gabel[17,18]).

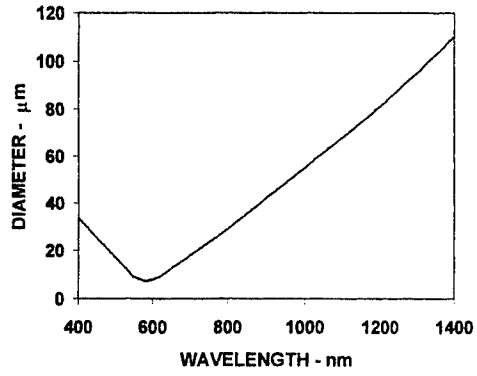

Figure 8. d_λ –Chromatic aberration - induced variation of laser beam diameter at the RPE of the rhesus eye (After Rockwell [19]).

The energy absorbed by the RPE, Qr_λ is:

Eq. 1) $$Qr_\lambda = Qp_\lambda * T_\lambda * A_\lambda$$

where Qp_λ is the energy at the cornea within the area of the pupil,
T_λ is the transmission of the pre-retinal ocular media at wavelength λ,
A_λ is the absorption of the RPE at wavelength λ.

Because of chromatic aberration, the irradiated area at the RPE varies with the wavelength of the incident light[19] **(Figure 8).** Current understanding holds that the threshold varies as the diameter of the irradiated area. The absorbed energy, Qr_λ, required to produce thermal tissue damage is therefore:

Eq. 2) $$Qr_\lambda = Qr_0 * d_\lambda / d_0$$

Where Qr_0 is the required energy for a minimum spot size, d_0,
d_λ is the chromatic aberration induced diameter at wavelength λ.

From equation 1 and equation 2:

$$Qp_\lambda = k * d_\lambda / (T_\lambda * A_\lambda) \text{ where } k = Qr_0 / d_0$$

If the values of Qr_0 and d_0, were known the solution would be complete. In theory, d_0 can be as small as 5-7 µm. In practice, experimenters have always reported a minimum lesion diameter of 25 µm or larger. An examination of the dependence of ED_{50} on retinal irradiation diameter shows that the ED_{50} does not change for retinal irradiation diameters smaller than 70 µm[9-10]. The calculation of Qr_0 is the province of more sophisticated eye damage models. For our purpose, it is adequate to choose the value of k to match the data at a given wavelength and observe the match of the curve $Qp_\lambda = k * d_\lambda / (T_\lambda * A_\lambda)$ to the data across wavelengths. **Figure 9** compares the nanosecond duration ED_{50} data to the computed action spectra. The value of k was chosen to match the 700 nm data point. These results show remarkably good agreement between the ED_{50} data and the model based on the energy absorbed in the pigment epithelium. The match of the computed action spectrum to the ED_{50} data for 100 ms duration laser exposures is closer still, supporting the contention that threshold thermal laser-induced retinal damage results from energy absorbed in the RPE [7].

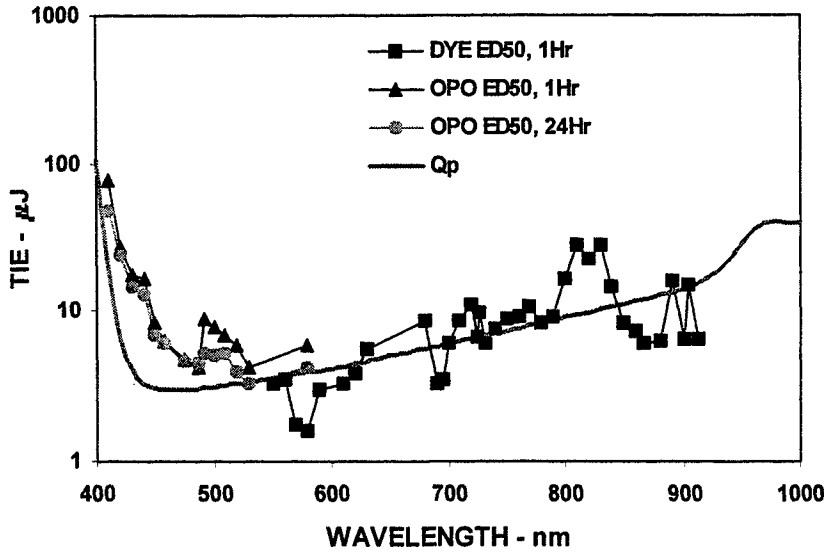

Figure 9. Ophthalmoscopically determined retinal injury ED_{50} values for extramacular exposure in the rhesus monkey to Q-switched laser exposures. Total Intraocular Energy (TIE) is defined as the energy incident at the cornea within the ocular pupil. The line is $Qp_\lambda = k * d_\lambda/(T_\lambda * A_\lambda)$ where k is chosen to so that $Qp_\lambda = ED_{50}$ at 700 nm and d_λ has been set to 25 μm where otherwise it would have been less than 25 μm.

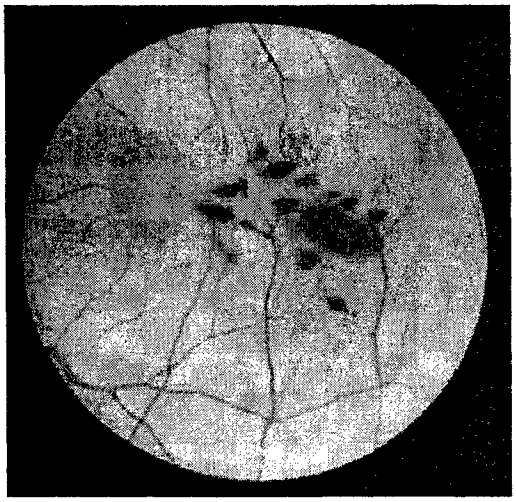

Figure 10. Photograph of rhesus retina following exposure to a 6x5 array of 3.5 ns, 442 nm laser exposures. Retinal hemorrhage was observed in 19 of 30 exposures.

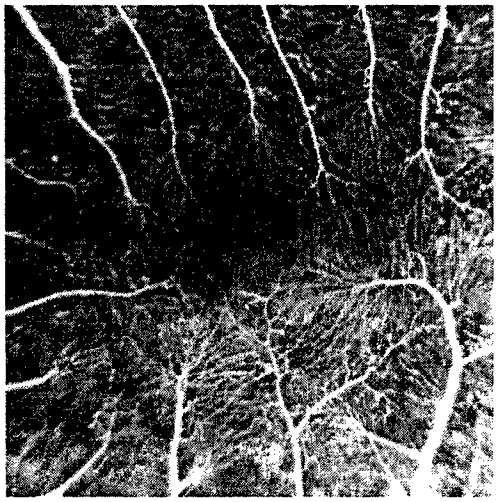

Figure 11. Fluorescein angiogram of a rhesus eye showing the capillary net of the retinal circulatory system. The vessel free area which includes the fovea is about 200 μm in diameter. The entire imaged area is 1 mm square.

The ED_{50} for an acute hemorrhagic lesion is only slightly higher than the 1-hour ED_{50} for wavelengths of 442 nm and shorter. At these short wavelengths, essentially every exposure that resulted in a lesion also produced retinal bleeding (**Figure 10**). **Figure 11** is a fluorescein angiogram of the posterior pole of a rhesus eye showing the capillaries of the retinal circulatory system. These capillary reside in the sensory retina[20-22]. A superficial net is found in the nerve fiber layer and a deep net is found between the inner nuclear layer and the outer plexiform layer. In the posterior pole the capillary net in the nerve fiber layer becomes more complex and forms a two layer net. In addition a fourth net is found in the superficial nerve fiber layer in the area surrounding the optic nerve head. Thus in the macula and the region around the macula, light must traverse three or four layers of capillaries before reaching the RPE. In man, the mesh size of the deep net in the posterior retina is 20 to 100 μm with an average of 45 μm [20]. The average capillary diameter is 5 μm. Thus the fill factor for the deep net is about 22%. If one can assume that the fill factor for the other nets is also ~22% and that the nets are uncorrelated, then the total fill factor is 66% to 88% depending on the number of nets traversed. It is unlikely that an incident beam will traverse all these nets without striking at least one capillary. **Figure 12** shows the absorption in 5 μm of oxy-hemoglobin (HbO^2) and deoxy-

hemoglobin (Hb) compared to the absorption spectrum of the RPE. The strong absorption of Hb and HbO^2 between 400 nm and 450 nm is comparable to the absorption of the RPE. It is not unreasonable to assume that energy absorbed within a retinal capillary is sufficient to rupture that capillary.

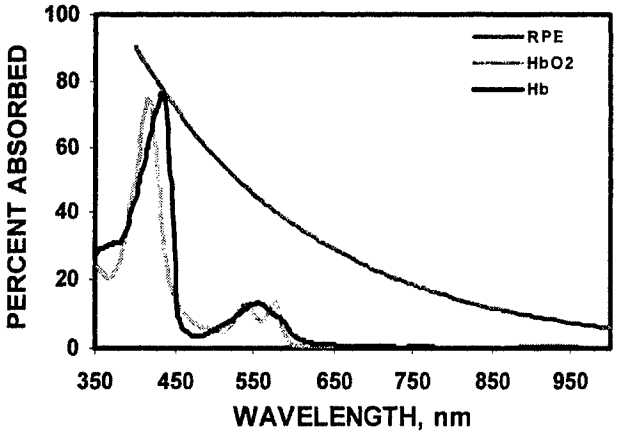

Figure 12. Absorption spectrum for 5 μm of oxy-hemoglobin (HbO^2) and 5 μm of deoxy-hemoglobin (Hb) compared to the absorption spectra of rhesus RPE.

The spectrum for equal absorbed energy in the RPE was given by:

$$Qp_\lambda = k/(T_\lambda * A_\lambda).$$

Where A_λ is the absorption of the pigment epithelium. An equivalent expression can be written for equal absorbed energy in the retinal capillaries by replacing A_λ by B_λ where B_λ is the absorption of Hb or HbO^2 from **Figure 12.** An absorption path length of 5 μm was assumed.

Figure 13 compares

$$Qp_\lambda = k'/(T_\lambda * B_\lambda)$$

computed for the Hb absorption curve and for the HbO^2 absorption curve to the OPO-induced retinal hemorrhage data. For both curves, k' was set to match the data at 430 nm (chosen because the absorption of Hb and HbO^2 are equal at 430 nm). This plot shows that below about 600 nm, the ED_{50} for retinal hemorrhage is reasonably predicted by capillary blood absorption. Above 600 nm, blood absorption is not significant. Hemorrhages induced by exposures at wavelengths longer than 600 nm are typically sub-retinal, resulting as a sequela to energy absorption in the RPE.

The action spectra for thermal retinal damage was defined to be $Qp_\lambda = k * d_\lambda/(T_\lambda * A_\lambda)$. This expression assumed unity transmission in the retina anterior to the RPE. This is not a valid assumption; retinal blood has significant absorption, thus reducing the transmission of the retina. Light absorbed in the retinal capillaries can be accounted for by including an additional term in the denominator. The corrected action spectra is:

$$Qp_\lambda = k * d_\lambda/(T_\lambda * A_\lambda * Tb_\lambda)$$

where Tb_λ is the transmission of Hb or HbO^2 and once again a 5 μm absorption path was assumed. Both Hb absorption and HbO^2 absorption modify the action spectrum below 450 nm **(Figure 14).** Above 450 nm the effect is minor. The data is matched most closely by the action spectrum modified by the transmission of Hb. Michaelson points out that the capillary net is denser at the venous end of the capillary than at the arterial end [20]. Because blood at the venous end has a lower oxygen concentration, the higher density of vessels is required to compensate.

5. CONCLUSIONS

The action spectrum for laser-induced thermal retinal damage differs from the action spectrum for laser induced photochemical retinal damage. The thermal action spectrum is well explained by a model based on absorption in the RPE. For wavelengths shorter than 530 nm, absorption by blood in the retinal capillaries must be accounted for, both in terms of the production of retinal hemorrhage and the screening effect that decreases the energy at the RPE. Though the data set is too sparse to say conclusively, the action spectra for photochemical damage does not appear to be influenced by retinal blood.

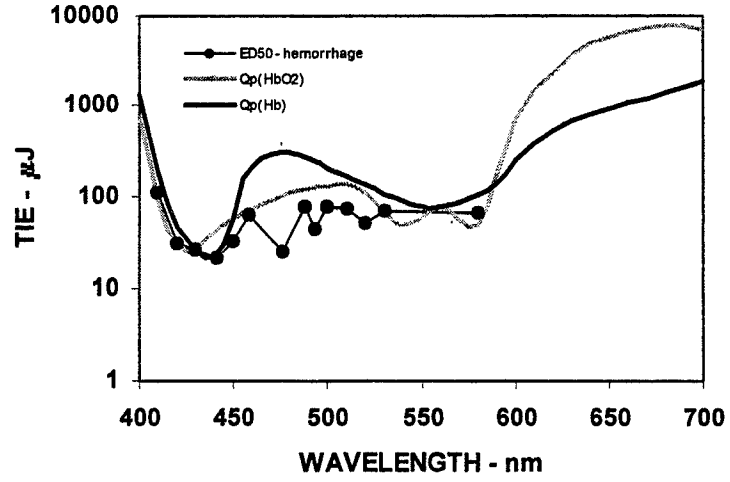

Figure 13 Action Spectrum for laser-induced retinal hemorrhage, $Qp_\lambda = k'/(T_\lambda * B_\lambda)$, compared to the OPO retinal hemorrhage data. Qp_λ was computed for Hb absorption and for HbO^2 absorption. For both cases, k' was set to match the data at 430 nm (chosen because the absorption of Hb and HbO^2 are equal at 430 nm)

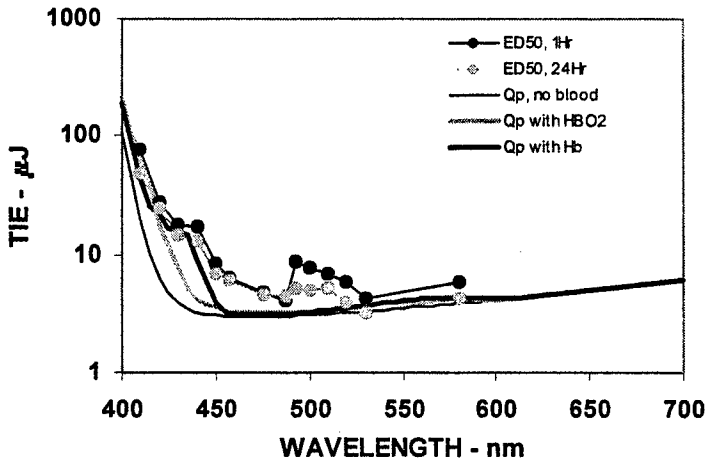

Figure 14. Action spectrum for thermal injury corrected for retinal blood absorption, $Qp_\lambda = k * d_\lambda/(T_\lambda * A_\lambda * Tb_\lambda)$. Curves are shown for Tb_λ = Hb transmission, $Tb_\lambda = HbO^2$ transmission, and for $Tb_\lambda = 1$ (no blood absorption). The action spectra corrected for Hb absorption best fits the data.

6. DISCLAIMER

In conducting the research described in this report, the investigators adhered to the "Guide for the Care and Use of Laboratory Animals," as promulgated by the Committee on Revision of the Guide for Laboratory Animal Facilities and Care, Institute of Laboratory Animal Resources, National Academy of Sciences - National Research Council.

The opinions or assertions contained herein are the private views of the authors and are not to be construed as official or as reflecting the views of the Department of the Army or the Department of Defense.

Citation of trade names in this report does not constitute an official endorsement or approval of the use of such items.

7. REFERENCES

1. WT Ham Jr, HA Mueller, JJ Ruffolo Jr., D Guerry III, and RK Guerry. Action Specrum for retinal injury from near-ultraviolet radiation in the aphakic monkey. *Am J of Ophthal* 93:299-306, 1982

2. WT Ham Jr, HA Mueller, JJ Ruffolo Jr., and AM Clarke. Sensitivity of the retina to radiation damage as a function of wavelength. *Photochem. Photobiol.* 29:735-743, 1979

3. WT Ham Jr, HA Mueller, and DH Sliney. Retinal sensitivity to damage from short wavelength light. *Nature* 260:153-155, 1976

4. WT Ham Jr, JJ Ruffolo Jr, HA Mueller, and D Guerry. The nature of retinal radiation damage dependence on wavelength, power level, and exposure time. *Vision Res.* 20:1105-1111 1980;

5. DJ Lund. The action spectrum for retinal thermal injury. In: . R Matthes and D Sliney, eds. *Measurements of Optical Radiation Hazards.* 209-228 ICNIRP 6,98, Märkl-Druck, Munchen, 1999

6. DJ Lund and PR Edsall. Action spectrum for retinal thermal injury. IN: Ophthalmic Technologies IX, SPIE Vol. 3591: 324-334 1999

7. DJ Lund, PR Edsall, and BE Stuck. Spectral dependence of retinal thermal injury. IN: Laser-induced damage in optical materials. SPIE Vol 3902: 22-33, 1999

8. DJ Finney. *Probit Analysis.* New York: Cambridge University Press, 19528 WJ Geeraets and ER Berry. Ocular spectral characteristics as related to hazards from lasers and other light sources. *Am J Ophthalmol* 66:15-20, 1968.

9. JA Zuclich, DJ Lund, PR Edsall, RC Hollins, PA Smith, BE Stuck and LN McLin. Experimental study of the variation of laser-induced retinal damage threshold with retinal image size(microsecond pulsewidths). *Nonlinear Optics* 21:18-27, 1999

10. JA Zuclich, DJ Lund, PR Edsall, RC Hollins, PA Smith, BE Stuck, LN McLin, PK Kennedy, and S Till. Variation of laser-induced retinal damage threshold with retinal image size. *JLA* 12(2):74-80, 1999

11. DJ Lund and ES Beatrice. Near Infrared laser ocular bioeffects. *Health Physics* 56(5): 631-636. 1989

12. DJ Lund, PR Edsall, DR Fuller, and. SW Hoxie. Bioeffects of near infrared lasers. *JLA* 10(3)140-143, 1998

13. DJ Lund, PR Edsall, DR Fuller, and SW Hoxie. Ocular hazards of tunable continuous-wave near-infrared laser sources. IN: Laser-inflicted Eye Injuries: Epidemiology, Prevention, and Treatment. . SPIE Vol. 2674:53-61, 1996

14. EJ Maher. Transmission and absorption coefficients for ocular media of the rhesus monkey. Report SAM-TR-78-32, San Antonio, Texas: Brooks Air Force Base, April 1978.

15. Boettner, EA. And Wolter, JR. Transmission of the ocular media. *Invest Ophthalmol* 1:776-783, 1962.

16. Boettner, EA. and Dankovic, D. Ocular absorption of laser radiation for calculating personnel hazards: Determination of the absorption coefficients in the Rhesus monkey. Final Contract Report F41609-74-C-0008, University of Michigan, Ann Arbor, MI, November 1974. [Available from NTIS as ADA 009 176]

17. VP Gabel, R Birngruber, and F Hillenkamp. Die lichtabsorption am, augenhintergrund. GSF-Bericht A 55, Gessellschaft Fur Strahlen-Und Umweltforschung, MbH, Munchen. August 1976

18. VP Gabel, R Birngruber, and F Hillenkamp. Visible and near infrared light absorption in pigment epithelium and choroid. *International.Congress Series. No. 450: XXIII. Concilium. Ophthalmologicum,. Kyoto.* Amsterdam, Oxford: Excerpta Medica. 1978

19. BA Rockwell. The focusing of infrared laser beams in the eye. Project Summary. Brooks AFB, TX 1993

20. IC Michaelson. *Retinal Circulation in Man and Animals*. Springfield IL. Charles C Thomas. 1954

21. A Kestenbaum. *Applied anatomy of the Eye*. New York. Grune& Stratton 1963

22. FH Adler. *Physiology of the eye*. St Louis. CV Mosby 1959

A comparative study of ocular damage thresholds from continuous-wave and femtosecond mode-locked lasers

Robert J. Thomas[a], Gary D. Noojin[a], David J. Stolarski[a], Rebecca T. Hall[a], Clarence P. Cain[a], Cynthia A. Toth[b] and Benjamin A. Rockwell[c]

[a]Litton-TASC, San Antonio, TX, 78228, USA

[b]Duke University Eye Center, Durham, NC, 27710, USA

[c]Air Force Research Laboratory, Brooks AFB, TX, 78235, USA

ABSTRACT

In order to provide a direct comparison of the damage thresholds for mode-locked systems to those with continuous-wave (CW) or non-pulsed output, we have performed an experiment with lasers possessing otherwise identical output characteristics. Our work presents an in-vivo minimal visible lesion (MVL) study. Titanium:Sapphire lasers produced 800-nm output for either mode-locked (76 MHz repetition rate, 120 femtosecond) or continuous-wave exposures. Alternating laser exposures were delivered to the paramacular retinal region of rhesus subjects. Laser exposure duration was set to one-quarter second for both types of exposures. Through ophthalmoscopic examination of the fundus, an MVL threshold for damage is established with probit analysis. Approximately 75 data points for each type of exposure were collected. The laser dosage thresholds and confidence intervals for minimal visible damage at twenty-four hours postexposure are reported for mode-locked and CW exposures. Results are compared with published studies conducted at similar pulse duration and similar CW wavelengths.

Keywords: Ultrashort Pulse Laser, Mode-Locked Laser, Laser Damage, Retina, Laser Safety

1. INTRODUCTION

In the past seven years, an effort has been conducted to revise current national and international laser safety standards. An important part of this revision includes the establishment of ocular exposure limits to address lasers that emit pulses of less than one-nanosecond duration. Laser pulses in this time regime are often termed "ultrashort" pulses. They have become increasingly commonplace in research, medical and machining applications.

The establishment of a laser safety standard for ultrashort pulse durations includes the examination of the biological effects of laser pulses, not only as a function of pulse duration. The list of important variables expands to create a large matrix of possible experimental conditions. Specifically, the establishment of a safety standard in a new pulse temporal range requires knowledge of the damage threshold as a function of wavelength and retinal image diameter. In addition, there must be a method for addressing lasers which emit a number of pulses during a given exposure time.

Laser and Noncoherent Light Ocular Effects: Epidemiology, Prevention, and Treatment, Bruce E. Stuck, Michael Belkin, Editors, Proceedings of SPIE Vol. 4246 (2001)

2. BACKGROUND

Effects of repetitive laser pulse exposures have been studied for years,[1] for pulses of greater than one-nanosecond duration. These studies have characterized the threshold for damage as a function of the number of pulses in the exposure and as a function of the time interval between pulses. Trends in the biological data have led to the establishment of general rules, which dictate how exposure limits vary as a function of the number of pulses within the exposure. Here we will discuss the recently released standard for laser safety, the ANSI Z136.1-2000 American National Standard for Safe Use of Lasers.[2] This is the United States' national consensus user standard for laser safety.

The Z136.1 Standard establishes three rules for determining maximum permissible exposure (MPE) limits for multiple pulse lasers. The first rule establishes that any single pulse emitted must be safe, implying an exposure limit based upon the pulse duration and wavelength of the laser.

The second rule establishes an exposure limit based upon the average power emitted by the laser over some nominal accidental exposure duration. For example, this exposure duration may be ten seconds for an infrared wavelength laser. The average power emitted by the laser over a period of ten seconds is then compared to the exposure limit from a continuous-wave ten-second exposure. This rule was designed to provide a margin of safety from heat build-up in tissues during the exposure time, and to provide a safety margin in the case of toxic photochemical reaction processes, which may occur from ultraviolet or blue portions of the spectrum. Commonly this is the applicable MPE for mode-locked lasers in which the biological effects including damage thresholds are similar to those from a continuous-wave laser.

The third rule establishes an intermediate exposure limit trend between the single-pulse limit and the average power exposure limit. Previous studies of pulsed lasers have indicated that the damage threshold goes roughly as the number of pulses to the negative one-quarter power.[3] This was found to be the case for laser wavelengths that produce thermal damage, as opposed to photochemical damage. The third rule in the ANSI standard therefore establishes a trend for the single-pulse thermal damage permissible exposure limit to be reduced by the number of pulses to the negative one-quarter power. This rule is altered slightly by establishing that the single-pulse exposure limit used is based upon some t_{min} and implies that the thermal single-pulse limit employed will be that from a pulse duration no shorter than one nanosecond. It goes on to establish that if multiple pulses fall within the time interval t_{min}, they are to be treated as a single pulse in the computation of the exposure limit. This leads to an interesting prediction regarding the anticipated damage threshold trends for ultrashort pulses. Over some interval of exposure conditions where the number of pulses is relatively few, the single pulse permissible exposure limit will apply as it will be smaller than the single pulse limit for a one-nanosecond pulse corrected by the number of pulses to the negative one-quarter power.

Our laboratory has for many years supported the collection of data for the update of the Z136.1 Standard. Specifically, we have collected ocular damage threshold data for pulse durations shorter than one nanosecond over a variety of retinal hazard wavelengths.[4,5,6]

Most recently we have worked to provide data[7] to establish the proper trends in MPE limits in the case of multi-pulse exposures to pulses which are approximately 100-150 fs in duration at a wavelength of 800 nm, common in Ti:Sapphire laser systems. For these very short pulses (< 150 fs) the predictions of the ANSI Standard for damage threshold trends seem to be

born out. Exposures to a 1-KHz pulse repetition rate train of pulses with 120 fs pulse duration exhibit only a small decrease in damage threshold as the duration increases, and the number of pulses increases proportional to the exposure time.

This is a very interesting result. It is contrary to what the number of pulses to the negative one-quarter trend anticipated. Speculation as to the cause in this difference has included a variety of explanations. The most probable explanations rely on the damage mechanism being related to the occurrence of laser-induced breakdown (LIB) being the primary damage mechanism to the retina.[8] The threshold for LIB occurrence has been linked to the threshold for retinal damage for pulses near 100 fs in other studies.

With this unusual observation in hand, we conducted a study at a higher pulse repetition rate, which should provide damage thresholds near those of a continuous wave exposure. Our goal was to determine if unexpected damage threshold trends would be demonstrated. A mode-locked laser was employed to provide a pulse repetition rate of approximately 76-MHz. A direct comparison to exposure from a CW laser of the same wavelength was conducted. The results of the study are summarized here.

3. METHODS

3.1. Experimental Setup

Here we have designed a direct comparison of CW and mode-locked exposures with identical beam diameters, beam divergence and wavelength. The creation of ultrashort pulses requires increased bandwidth when compared with the CW exposure, but both are centered at the same wavelength. We believe that this is one of the most direct comparisons to date in an MVL threshold experiment.

The laser system employed for the experiment consisted of a mode-locked Ti:Sapphire oscillator operating at 76 MHz pulse repetition frequency, 800 nm center wavelength, and a laser pulse duration of 120 fs. Spectral bandwidths and pulse widths were continually monitored with a spectrometer and autocorrelator while tuning the Ti:Sapphire laser for minimum pulse width. The laser was converted to CW by opening slits required for Kerr lens mode-locking. CW operation was confirmed by observation with a fast (< 300ps rise time) photodiode and digital oscilloscope.

The Ti:Sapphire output was spatially filtered in both CW and mode-locked configurations. Laser beam divergence and beam diameter at the range of the eye were monitored and recorded at each change of configuration. A laser profiler with CCD camera was used to monitor these beam parameters. This ensured that both types of exposures were performed with equivalent parameters.

For this study, the cornea was positioned approximately 1 cm from the final beam splitter so that the reflected portion of the beam entered the eye. The retina was placed in the focal plane of the fundus camera. The transmitted portion of the beam was directed to a photodiode so that the exposure duration could be recorded by digital oscilloscope.

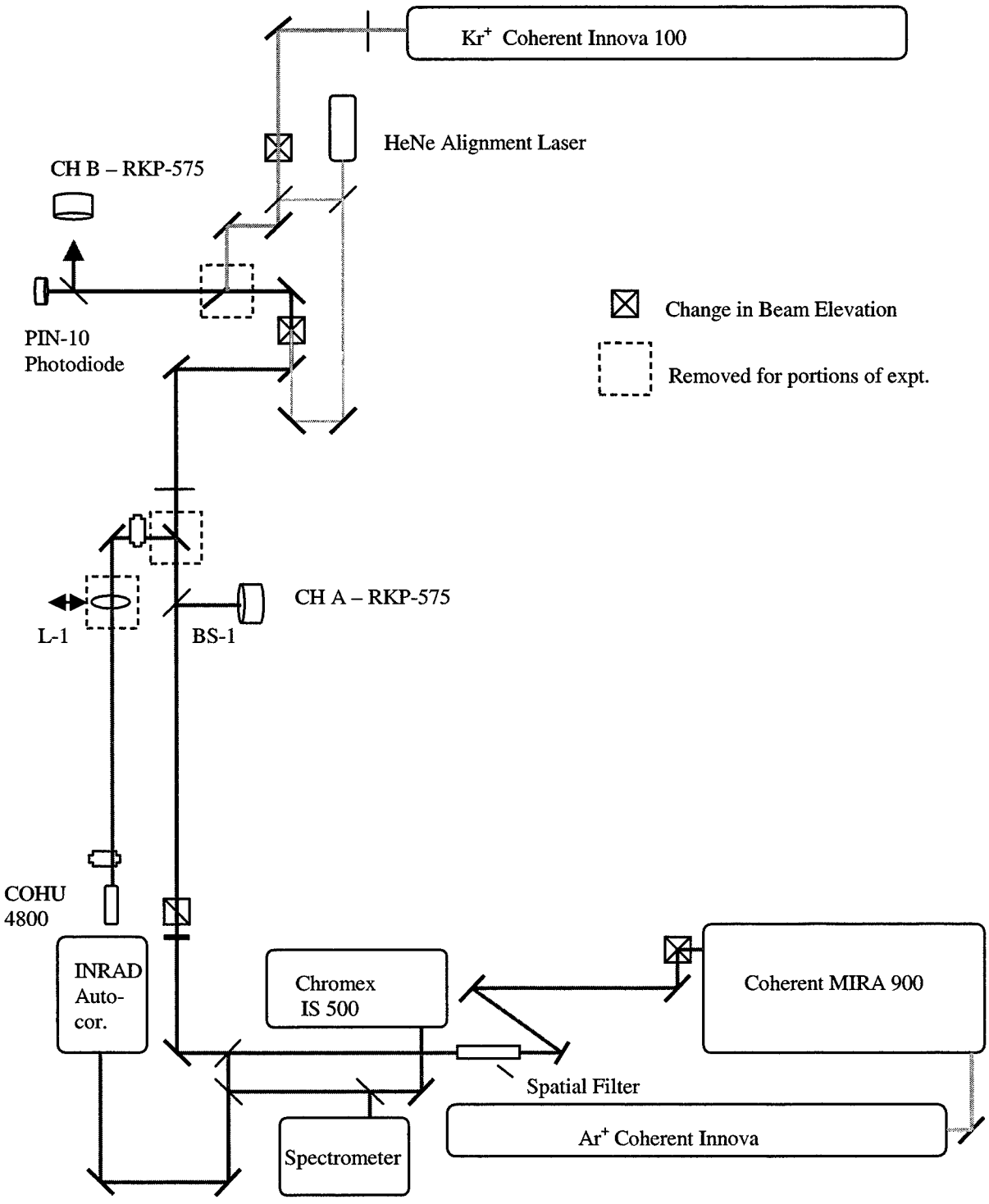

Figure 1: Experimental Configuration

Prior to subject placement, the ratio of power delivered to the eye to the amount measured at the monitor detector at the beam splitter marked BS1 (see Figure 1) was recorded. This ratio remained constant as a function of power delivered for both CW and mode-locked

configurations. This ratio of the reflected and transmitted portions of the beam was measured for each day's exposure and recorded. Average power and ratios were measured with a Laser Precision model RM6600 laser power meter equipped with model RKP-575 detectors. All detectors were independently calibrated to NIST-traceable standards.

3.2. In Vivo Model

Mature *Macaca mulatta* primates from 2.2 to 6.9 kilograms (kg) were maintained under standard laboratory conditions (12 hours light, 12 hours dark). All primates were screened pre-exposure to ensure that no eye was more than one-half diopter from being emmetropic.

All animals were chemically restrained using 10 mg/kg ketamine hydrochloride (HCl) intramuscularly. Once restrained, 0.25 mg atropine sulfate was administered subcutaneously. Two drops of proparacaine HCl 0.5%, phenylephrine HCl 2.5%, and tropicamide 1% were each placed in both eyes. Under ketamine restraint, the subject had intravenous catheters placed for infusion of propofol and an initial induction dose of propofol (5 mg/kg) was administered to effect. The state of anesthesia was maintained using 0.2 - 0.5 mg/kg/min of propofol via syringe pump. The animal was intubated with a cuffed endotracheal tube. A peribulbar injection of 2% lidocaine was administered to reduce extraocular muscular movement. The subject was securely restrained in a prone position on an adjustable stage for the fundus photography, laser exposure, and fluorescein angiography (FA). Prior to FA, 0.6 ml of Fluorescite 10% (Alcon Laboratories) was administered as an intravenous bolus. The subject's blood pressure, temperature, and pulse were continuously monitored throughout the experimental protocol. Normal body temperature was maintained by the use of circulating warm water blankets.

The retina was viewed with a fundus camera and all laser exposures were delivered to the eye in the paramacular region. Exposures were placed laterally, temporal to the macula in a four by five grid, and also in two rows below the macular grid. All eyes were evaluated at 1 hr and 24 hrs postexposure and visible lesions at a given exposure site were reported as a "yes" only if at least two examiners identified a lesion.

Measurements were taken to eliminate the relative sensitivities of the paramacula and inter-subject variations to these ultrashort laser pulses by using alternating rows of CW and mode-locked exposures in the paramacular grids. Rows selected for each type of exposure were also alternated between subjects.

4. RESULTS

The fundoscopic damage thresholds were obtained at 24-hr postexposure using direct ophthalmoscopic observation. Energy delivered along with a "yes" or "no" value was recorded if a lesion was or was not observed on the retina at each laser delivery point. A probit data analysis technique[9] was applied to the "yes/no" recorded as a one or zero for each dosage applied. This analysis provides the estimated dosage to cause a MVL with 50% probability (ED_{50}) and fiducial limits.

The results for one-quarter second exposure to CW and mode-locked pulse trains at 76 MHz are summarized in Table 1. Values are reported for readings taken at 24 hours postexposure. Also tabulated are the fiducial limits for the ED_{50} numbers. These represent confidence intervals at 95%.

The final column indicates the slope of the probit curve calculated at the ED_{50} value point. In each case, the slope is greater than 2.0 for the 24-hr data which is characteristic of good data. This was one of the criteria for ending the experiment. The second of the criteria was that the fiducial limits, as computed at the 95% confidence interval, were within a factor of ±50% of the ED_{50} value. As is illustrated by the data, both criteria are met for the 24-hr postexposure data.

Table 1. Experimental Results – Ophthalmoscopic Observations

Laser Mode	Exposure Duration (s)	Wavelength (nm)	24-hour ED_{50}	Fiducial Limits (95% Confidence)	Probit Slope
Mode-Locked 130 fs, 76 MHz 5 Eyes 75 Exp	0.25	800	5.90 mJ 23.6 mW	5.23 – 6.60 mJ 20.9 – 26.4mW	7.9
CW 5 Eyes 74 Exp	0.25	800	5.84 mJ 23.4 mW	5.23 – 6.58 mJ 20.9 – 26.3 mW	8.0

5. CONCLUSIONS

We report a final value for our study of 5.90 mJ (5.23 – 6.60 mJ) and 5.84 mJ (5.23 – 6.58 mJ) for mode-locked and CW paramacular exposures, respectively, at 24 hrs postexposure. The equivalent CW exposure average powers are 23.6 and 23.4 mW for the same thresholds. We find that these values represent equivalent (to within experimental uncertainty) MVL thresholds for the two exposure conditions at one-quarter second exposure. The difference is less than 0.1 mJ (~ 1 %) and the confidence intervals overlap significantly.

The MVL thresholds presented here represent an excellent agreement with previous CW and mode-locked laser studies. In order to make the best comparison with published data, we have examined studies with exposure times near the one-quarter second value of our study.[3,10,11,12,13,14,15,16,17,18,19,20,21,22,23,24,25,26] Table 3 lists several MVL values that were selected for comparison. The studies were selected based upon exposure duration, retinal image size, wavelength, and subject.

To our knowledge, there is no data at one-quarter second, 800 nm in the open literature. Several studies exist at nearby wavelengths, particularly 632 nm (HeNe), 647 nm (Kr+), 1060 (Nd:Glass), and 1064 nm (Nd:YAG). Several values extracted from the literature have been assembled for Figure 2. The comparable data largely consists of CW exposures of 0.1 to 1 second in duration. In each case, we have normalized the data to a one-quarter second exposure duration by applying the ANSI Z136.1-2000 Standard's trend of MPE's following a trend of time to the three-quarter's power. Figure 2 illustrates the data obtained from the literature. This normalization brought the various studies into good agreement, with variations of up to about a factor of two at a given wavelength. Other variations can be attributed to lesion placement in macular or paramacular regions of the retina, observation times, while some variations in the data can be attributed to variation in retinal spot size due to the beam diameter and divergence characteristics of the particular laser used.

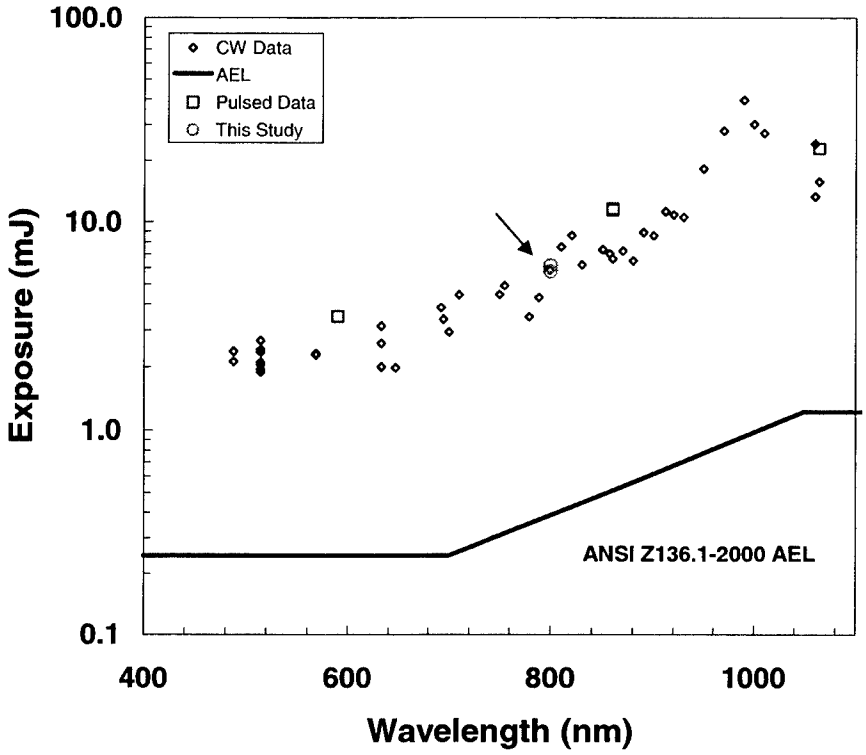

Figure 2. A comparison of MVL study results normalized to a 0.25-second exposure time

We could find no data for mode-locked, sub-picosecond exposures for rhesus subjects. Studies for longer pulse widths can be examined, however. The most directly comparable is the data available for 1064 nm. The references from Lund et al.,[25] Connoly et al.,[18] Skeen et al.,[19] and Birngruber et al.[22] contain values for 1064-nm and 1060-nm exposures, both mode-locked (300 ps, 200 MHz) and CW. Figure 5 shows that at that wavelength the different studies compare well. There, the mode-locked point is normalized from a one-second exposure, the largest difference extrapolated.

Also available are the studies by Courant et al.[24] who performed an MVL study using 8-ps, 590-nm, laser pulses in a 0.2-second, 1-MHz PRF pulse train. That study did not make a direct comparison with CW exposures. Another study documented by Lund et al.[3] using a GaAs diode laser (860 nm) repetitively pulsed at 120 kHz PRF, with 500-ns pulses also determined an MVL threshold for 0.125-second and 0.5-second exposures. These two studies are represented by the circles in Figure 3. Again, no direct comparison was made with CW exposures.

From Table 3 and Figure 5, we see that our study follows closely the CW trends as a function of wavelength at one-quarter second exposure duration. The two adjacent wavelengths, 647 nm and 860 nm, have lower and higher MVL thresholds when normalized to 0.25-second

exposure times. This is expected, following the prescribed wavelength dependence in Maximum Permissible Exposure (MPE) from the ANSI Z136.1 Standard.

In conclusion, our data indicate that average power dictates the damage threshold for the 800-nm, 76-MHz mode-locked, 100-fs laser. This experiment has provided the most direct comparison of damage thresholds possible, with nearly identical beam propagation parameters for both laser exposures. These results point to a thermal damage mechanism as has been described in prior work with CW lasers. However, histopathological studies will follow and determine more precisely if damage mechanisms are the same for both the CW and mode-locked femtosecond pulse train cases. Differing damage sites within the retina with contrasting effects may point to improved clinical techniques or treatment methods.

ACKNOWLEDGEMENTS

The research reported herein was supported by AFOSR #(2312A1012312A103), U.S. Air Force Research Laboratory, and Contract: F33615-92-0017 and AFOSR Grant No. F49622-98-1-0412.

Animals involved in this study were procured, maintained, and used in accordance with the Federal Animal Welfare Act, the Guide for the Care and Use of Laboratory Animals prepared by the Institute of Laboratory Animal Resources, National Research Council, and the ARVO Resolution for the Use of Animals in Ophthalmic and Vision Research.

REFERENCES

1 D. Sliney and M. Wolbarsht, *Safety with Lasers and other Optical Sources*. New York, N.Y. 10013: Plenum Press, 1980.

2 ANSI, "Z136.1 American National Standard for Safe Use of Lasers,". Orlando, Florida: Laser Institute of America, 2000.

3 D. J. Lund, B. E. Stuck, and E. S. Beatrice, "Biological Research in Support of Project MILES," Letterman Army Institute of Research Institute Report No. 96, 1981.

4 C. P. Cain, C. M. Toth, C. A. DiCarlo, C. D. Stein, G. D. Noojin, D. J. Stolarski, and W. P. Roach, "Visible retinal lesions from ultrashort laser pulses in the primate eye," *Investigative Ophthalmology and Visual Science*, vol. 36, pp. 879-888, 1995.

5 W. P. Roach, T. E. Johnson, and B. A. Rockwell, "Proposed maximum permissible exposure limits for ultrashort laser pulses," *Health Physics*, vol. 76, pp. 349-354, 1999.

6 C. P. Cain, C. A. Toth, G. D. Noojin, V. Carothers, D. J. Stolarski, and B. A. Rockwell, "Thresholds for visible lesions in the primate eye produced by ultrashort near-infrared laser pulses," *Investigative Ophthalmology and Visual Science*, vol. 40, pp. 2343, 1999.

7 D. J. Stolarski, C. P. Cain, C. A. Toth, G. D. Noojin, and B. A. Rockwell, "Multiple pulse thresholds in live eyes for ultrashort laser pulses in the near-infrared," presented at Laser-Tissue Interaction X, San Jose, California, 1999.

8 C. P. Cain, C. D. DiCarlo, B. A. Rockwell, P. K. Kennedy, G. D. Noojin, D. J. Stolarski, D. X. Hammer, C. D. Toth, and W. P. Roach, "Retinal damage and laser-induced breakdown produced by ultrashort pulse lasers," *Grafes Archives of Clinical Experimental Ophthalmology*, vol. 234, 1996.

9 D. J. Finney, *Probit Analysis*, 3rd ed. New York, NY: Cambridge University Press, 1971.

10 W. T. Ham, W. J. Geeraets, H. A. Mueller, R. C. Williams, A. M. Clarke, and S. F. Cleary, "Retinal burn thresholds for the helium-neon laser in the rhesus monkey.," *Archives of Ophthalmology*, vol. 84, pp. 797-809, 1970.

11 Y. Onda and T. Kameda, "Studies of Laser Hazards and Safety Standards (Part 2: Retinal Damage Thresholds for Helium-Neon Lasers)," U. S. Army Intelligence and Information Agency USAMIIA-K-9991, 1980.
12 Y. Onda and T. Kameda, "Studies of Laser Hazards and Safety Standards (Part 3: Retinal Damage Thresholds for Argon Lasers)," U. S. Army Intelligence and Information Agency USAMIIA-K-9992, 1980.
13 E. S. Beatrice and G. D. Frisch, "Retinal laser damage thresholds as a function of image diameter," *Archives of Environmental Health*, vol. 27, pp. 322-326, 1973.
14 D. J. Lund, "Bioeffects Data," in *Laser Induced Acute Ocular Bioeffects: A Summary*, vol. Chapter 6, Vol 1,: Letterman Army Institute of Research, 1984, pp. 111-148.
15 G. D. Frisch, E. S. Beatrice, and R. C. Holson, "Comparative study of argon and ruby retinal damage thresholds," *Investigative Ophthalmology and Visual Science*, vol. 10, pp. 911-919, 1971.
16 W. D. Gibbons and R. G. Allen, "Retinal damage from long-term exposure to laser radiation," *Investigative Ophthalmology and Visual Science*, vol. 16, pp. 521-529, 1977.
17 H. W. Hemstreet, J. S. Connolly, and D. E. Egbert, "Ocular hazards of picosecond and repetitive-pulsed lasers; Volume I: Nd:YAG laser (1064 nm)," USAF School of Aerospace Medicine SAM-TR-78-20, 1978.
18 J. S. Connolly, H. W. Hemstreet, and D. E. Egbert, "Ocular hazards of picosecond and repetitive pulsed lasers, Vol II: Argon-Ion laser (514.5nm)," USAF School of Aerospace Medicine SAM-TR-78-21, 1978.
19 C. H. Skeen, W. R. Bruce, J. H. Tips, M. G. Smith, and G. G. Garza, "Ocular Effects of Near Infrared Laser Radiation for Safety Criteria, Final Report," Technology Inc. 1972.
20 A. Vassiliadis, R. C. Rosan, and H. C. Zweng, "Research on Ocular Laser Thresholds," Stanford Research Institute Final Report, 1969.
21 G. H. Bresnick, G. D. Frisch, J. O. Powell, M. B. Landers, G. C. Holst, and A. G. Dallas, "Ocular effects of argon laser radiation (I. Retinal damage threshold studies)," *Investigative Ophthalmology and Visual Science*, vol. 9, pp. 901-910, 1970.
22 R. Birngruber, V.-P. Gabel, and F. Hillenkamp, "Experimental studies of laser thermal retinal injury," *Health Physics*, vol. 44, pp. 519-531, 1983.
23 J. A. Zuclich and M. F. Blankenstein, "Additivity of retinal damage for multiple-pulse laser exposures," USAF School of Aerospace Medicine USAFSAM-TR-88-24, 1988.
24 D. Courant, C. Naudy-Vives, J.-C. Perot, J. Garcia, and D. Dormont, "Experimental determination of retinal damages thresholds induced by multiple picosecond laser pulses," presented at 1997 International Laser Safety Conference, Orlando, Florida, 1997.
25 D. J. Lund, D. O. Adams, and C. Carver, "Ocular Hazard of the GaAs Laser," Letterman Army Institute of Research Final Report, 1976.
26 D. J. Lund, P. R. Edsall, D. R. Fuller, and S. W. Hoxie, "Ocular Hazards of Tunable Continuous-Wave Near-Infrared Laser Sources," presented at Progress in Biomedical Optics (BiOS), San Jose, CA, 1996.

Ocular Dynamics and Visual Tracking Performance After Q-Switched Laser Exposure

H.Zwick, B.E. Stuck, D.J. Lund, M. Nawim
Walter Reed Army Institute of Research
US Army Medical Research Detachment
San Antonio TX

ABSTRACT

In previous investigations of q-switched laser retinal exposure in awake task oriented non-human primates (NHPs), the threshold for retinal damage occurred well below that of the threshold for permanent visual function loss. Visual function measures used in these studies involved measures of visual acuity and contrast sensitivity. In the present study, we examine the same relationship for q-switched laser exposure using a visual performance task, where task dependency involves more parafoveal than foveal retina. NHPs were trained on a visual pursuit motor tracking performance task that required maintaining a small HeNe laser spot (0.3 degrees) centered in a slowly moving (0.5deg/sec) annulus. When NHPs reliably produced visual target tracking efficiencies > 80%, single q-switched laser exposures (7 nsec) were made coaxially with the line of sight of the moving target. An infrared camera imaged the pupil during exposure to obtain the pupillary response to the laser flash. Retinal images were obtained with a scanning laser ophthalmoscope 3 days post exposure under ketamine and nembutol anesthesia. Q-switched visible laser exposures at twice the damage threshold produced small (about 50μm) retinal lesions temporal to the fovea; deficits in NHP visual pursuit tracking were transient, demonstrating full recovery to baseline within a single tracking session. Post exposure analysis of the pupillary response demonstrated that the exposure flash entered the pupil, followed by 90 msec refractory period and than a 12 % pupillary contraction within 1.5 sec from the onset of laser exposure. At 6 times the morphological threshold damage level for 532 nm q-switched exposure, longer term losses in NHP pursuit tracking performance were observed. In summary, q-switched laser exposure appears to have a higher threshold for permanent visual performance loss than the corresponding threshold to produce retinal threshold injury. Mechanisms of neural plasticity within the retina and at higher visual brain centers may mediate the stability of visual function and performance metrics. Long term repeated exposure to the retina, however, may eventually dampen the ability of higher visual brain centers to detect declining retinal neural output from cumulative retinal damage. Individuals chronically exposed to such laser sources should have more frequent ophthalmic retinal surveillance.

Keywords: Laser bioeffects, laser safety, visual function, visual performance, q-switched laser, diagnostics, treatment

I. INTRODUCTION

The increased utilization of q-switched laser sources in industry, academia, and the military requires that our understanding of how q-switched time domain laser induced retinal damage differs in its relationship to visual function vs. that for longer time domains (msec), where mechanisms of damage are primarily thermal[1,2]. Previous visual function investigations in non-human primates (NHPs), utilizing visual acuity and Landolt ring contrast sensitivity, have demonstrated that to achieve q-switched induced permanent functional threshold requires energy levels 15 to 16 times that of the retinal damage threshold.[3,4] In comparison, the threshold energy required for permanent visual function loss is nearly the same as that required for threshold retinal damage in the millisecond time. [5,6,7]

In the present investigation, we continued the investigation of q-switched laser exposure on measures of both visual performance and ocular dynamics. Visual pursuit target tracking is a visual performance task heavily dependent upon visual system guidance and more likely to be mediated by parafoveal retinal sites rather than foveal retinal sites, as is the case in visual acuity metrics. Comparisons of visual pursuit tracking in human and non-human primates demonstrate close agreement between human and NHP mechanisms of visual function[8, 9] involved in visual guidance of such tasks.
Alterations in ocular dynamics from bright light flashes are known to induce an attenuation in pupillary aperture following a refractory period of about 200 msec. [10] As q-switched pulses are short enough to precede the pupillary refractory period, one might expect minimal protection from pupillary dynamics.

Laser and Noncoherent Light Ocular Effects: Epidemiology, Prevention, and Treatment,
Bruce E. Stuck, Michael Belkin, Editors, Proceedings of SPIE Vol. 4246 (2001)

In this paper, we extended our examination of the q-switched laser suprathreshold retinal damage effects on a visual performance metric in behaviorally trained NHPs. Such performance tasks involve more parafoveal retinal function than spatial visual function measures such as visual acuity but may be closer to occupational work situations. The role of ocular dynamics requires consideration as well, as such mechanisms might afford retinal protection.

2. METHODS

2.1 Subjects and task parameters. Non-human primates (NHPs), Macacca mulatta) were used in this investigation. NHPs were trained on a behavioral task that required maintaining a spot of light from a tripod mounted HeNe laser source. They were trained to move the tripod mounted HeNe laser source in conjunction with a small annulus projected on a curved screen

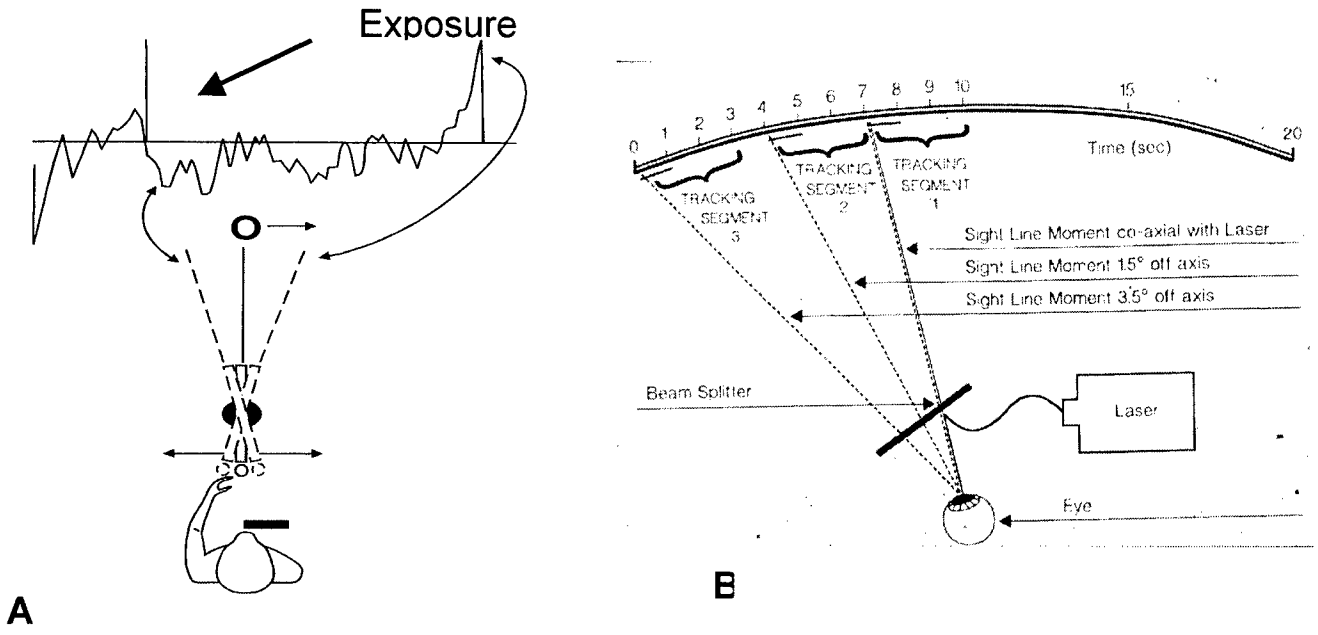

Figure 1 A. *Top down schematic view of NHP manually operating lever directing HeNe laser pointer to stay on slowly moving annulus target. Moving the lever to the left indicates HeNe source is lagging target, producing a downward target movement; moving lever to the right indicates HeNe source is leading target, producing an upward deflection. Figure 1* B. *Laser exposure delivery system for on and off axis exposure. At 7 sec, laser source is in line of site to optimize on-axis exposure. Exposures made prior to 7 sec result in off-axis exposures (1.5 and 3.5 degrees off axis).*

mounted ten feet from the NHP's monocular viewing aperture. A given trial lasted 20 sec. The NHP's task was to maintain the HeNe laser spot in the center of a 0.3 degree annulus (target) while it moved horizontally across the screen at 0.5 cycles/degree. Figure 1 is a schematic depicting tracking through an on-axis exposure and the optical design for delivering the laser energy coaxial with line of site.

In a previous investigation, it was determined that high percentage time on target criteria (about 80 percent) yielded photopic spectral sensitivity curves and that lower criterion spectral sensitivity shifted to broader spectral sensitivity functions and shorter wavelength peaks, about 500 to 520 nm, consistent with mesopic and scotopic spectral sensitivity[7]. These spectral sensitivity functions indicate that pursuit motor tracking provides visual guidance via retinal photoreceptor systems. Damage to such photoreceptor systems should degrade visual tracking performance.

2.2 Laser exposure parameters and Measurement of Pupillary dynamics.

A q-switched laser source (Big Sky Laser, 532 nm, 6 nsec, 45 mJ) operating at a 20 Hz pulse repetition rate was used to produce single q-switched pulses at 6 and 20 microjoules TIE. Figure 1b shows the laser delivery system schematic. At 7 sec into the tracking session, the annulus becomes coaxial with the laser source. All exposures were made in this manner under behavioral task conditions. Pupillary diameter was continuously recorded on VHS video tape under infrared illumination before, during, and after q-switched laser exposure. Real time video images of the pupillary response were derived from SVHS video tape records using a high speed frame grabbing board capable of extracting images at 30 frames per second.

2.3 Ophthalmoscopy of retinal lesion sites pre and post exposure.

Ophthalmoscopy was obtained 3 days post exposure under ketamine and pentobarbital anesthesia.

3.RESULTS

In Figure 2 the effect of a single 6 microjoule q-switched pulse, delivered on-axis is presented showing the corresponding effects of this single q-switched pulsed exposure on a single tracking trial lasting 20 sec (b). The vertical line indicates the occurrence of the q-switched 6 microjoule flash. In A the pre-exposure condition of the exposed retinal site is shown dovoid of damage and in C the presence of a white opacity produced by the exposure. The exposure site is in

.

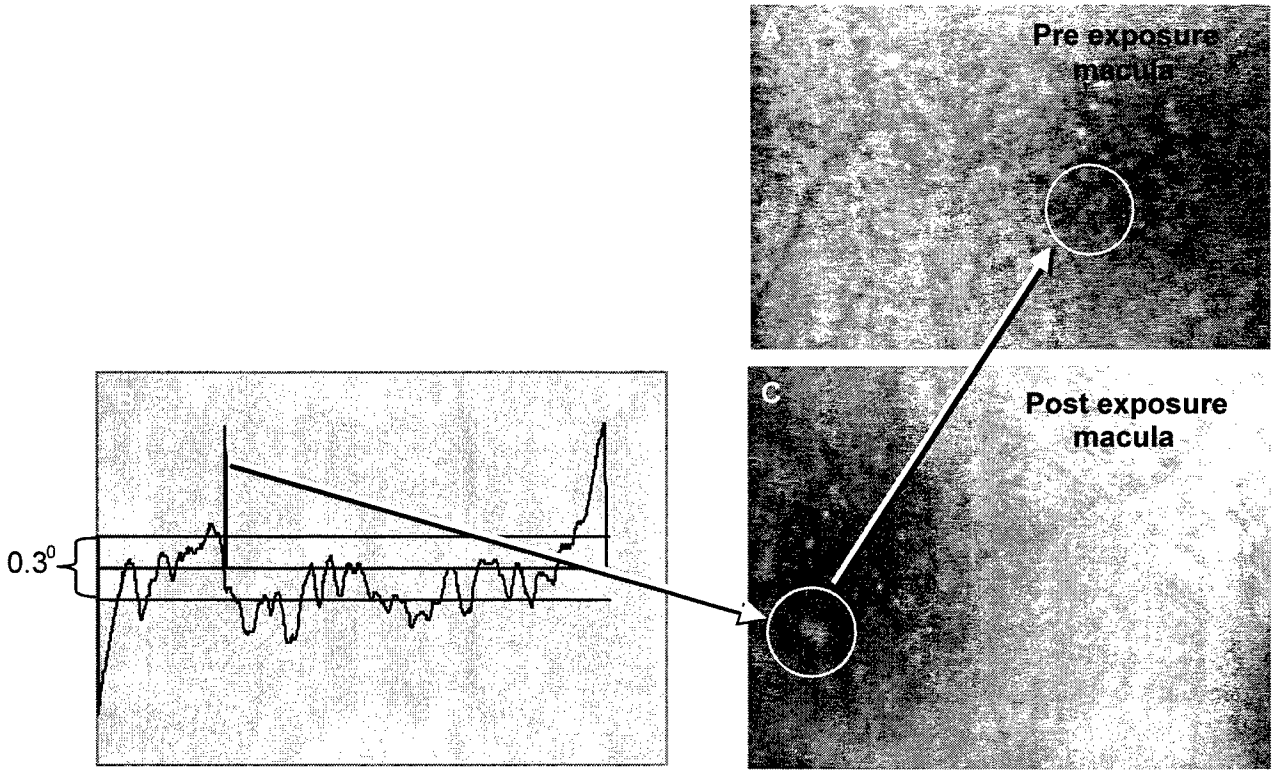

Figure 2. A is the preexposure site; B indicates the occurrence of a single q-switched 6 microjoule exposure during tracking; C is the post exposure site indicating the presence of a retinal lesion 3 days post exposure.

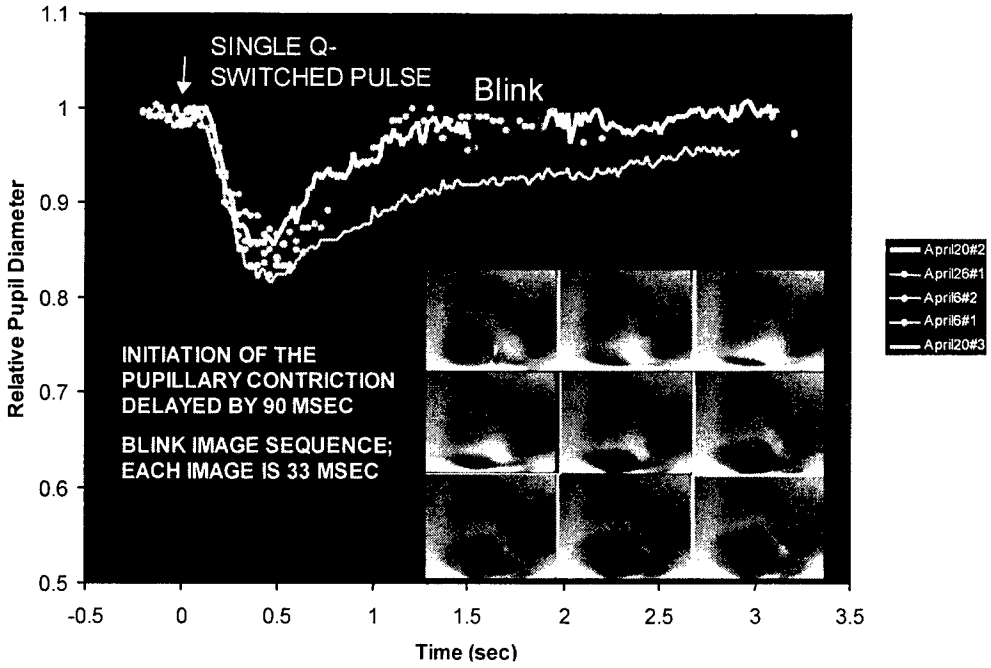

Figure 3. Pupillary contraction resulting from a single 6 microjoule q-switched laser pulse shows a 90 msec refractory period before pupillary contraction onset and real time image separation of a blink response occurring at about 1.5 seconds post exposure.

parafoveal retina temporal to the fovea. Figure 3 shows the effect of a single q-switched exposure on pupillary contraction. About 90 msec of refractory time is required prior to the onset of the pupillary contraction. While a blink response occurs, it does not occur until the recovery of the pupillary contraction response is completed. Figure 4 presents the effect of a single 6 microjoule exposure on NHP pursuit tracking over 4 tracking trials showing significant deficits from baseline during this time but returning to near pre-exposure baseline pursuit tracking at about 673 seconds post exposure.

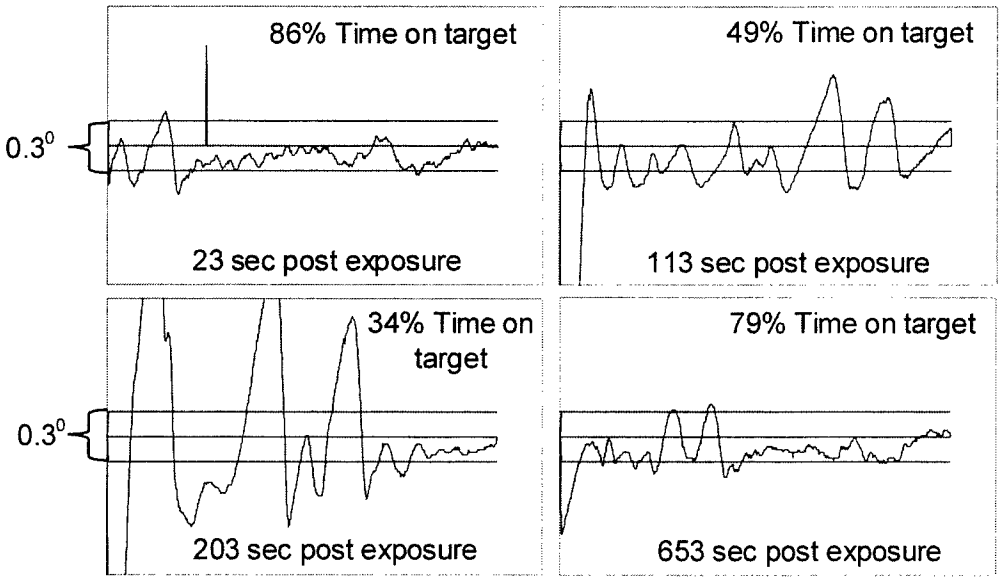

Figure 4 The effect of a single 6 microjoule pulse on subsequent tracking trials measured over a post-exposure period of 673 sec.

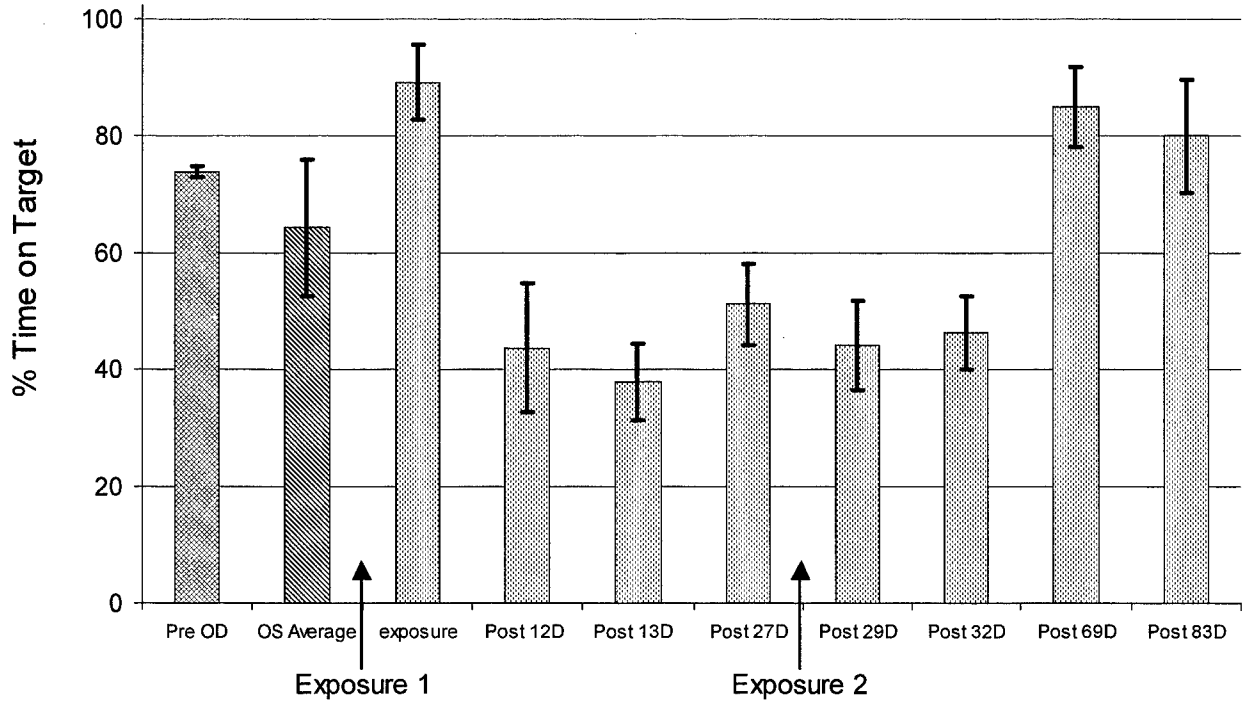

Figure 5 Long term deficit in NHP visual pursuit motor performance induced by 20 microjoule exposure relative to normal baseline and baseline of unexposed eye (OS). Full recovery occurred at 69 days post exposure.

Figure 5 shows a long term deficit in pursuit tracking performance induced by a 20 microjoule q-switched laser exposure. Exposure 1 produced no change in tracking performance during the exposure session. However over the next 5 weeks post exposure percent pursuit tracking performance remained suppressed by about 50 % of pre exposure tracking and about 60 percent relative to the unexposed eye (OS average). A second 20 microjoule exposure was presented at 29 days after the first exposure with no subsequent deficit in tracking performance. Vertical bars indicate plus and minus 1 standard deviation about mean tracking performance for each daily session.

5. DISCUSSION

These results support previous studies in suggesting that permanent loss of visual acuity from q-switched laser exposure requires significantly higher energy levels than those required to produce threshold retinal damage. This study suggests that such a relationship exists, as well, between q-switched retinal damage and NHP visual pursuit tracking performance.

This ineffectiveness of q-switched laser retinal induced damage to depress measures of visual function and performance metrics may reside in visual neural plasticity mechanisms capable of amplifying and modulating residual retinal signals so that neural adjustments can be made at higher order brain centers. Several investigations indicate that receptor fields in higher order brain centers may expand and retune weakened signals from laser damaged retinal sites. [11,12] Moreover, differences in photoreceptor damage between q-switched (7 to 15 nsec) and long pulse (10 msec) also indicate that such plasticity does have differential retinal damage signals. In Figure 6, two photoreceptor lesion sites are shown imaged *in vivo* in the high resolution eye of the garter snake.[13] The q-switched lesion site shows fairly normal sized photoreceptors with larger spacing between photoreceptors while the lesion at the right shows highly reflective photoreceptors over much of the central region. This image suggest that a photoreceptor filling in process. [14] may have occurred in the q-switched damaged lesion site providing a basis for more rapid recovery from q-switched retinal damage than from longer pulse damage.

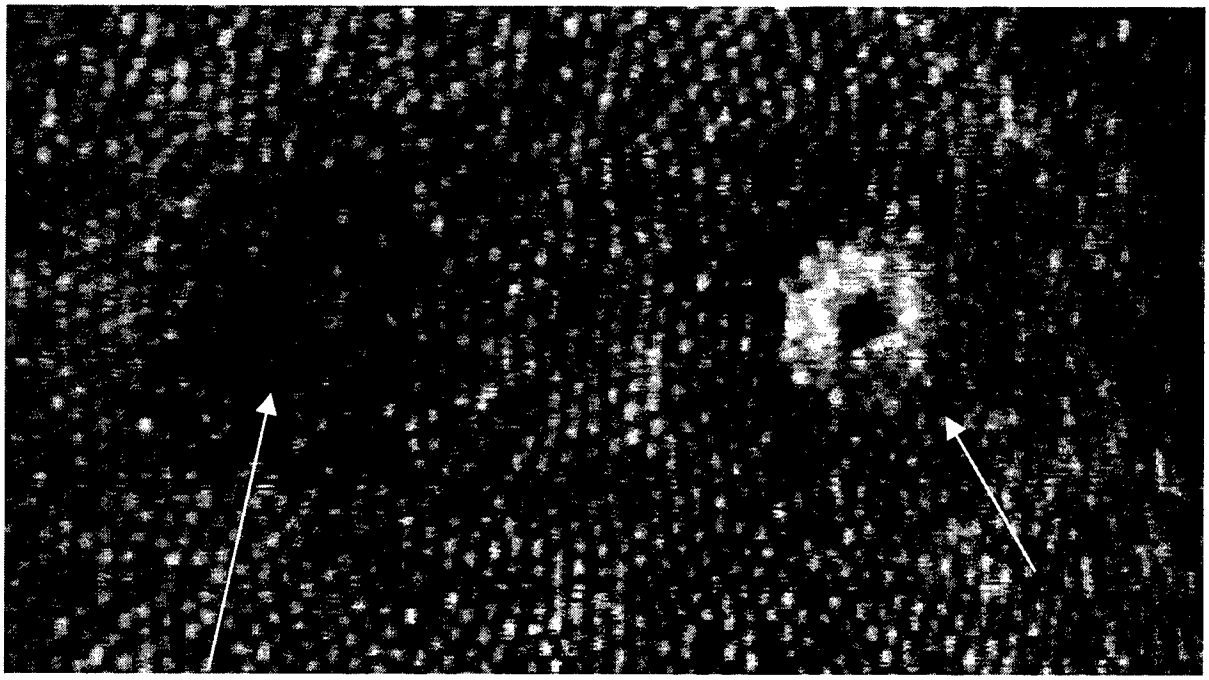

Figure 6 .A scanning laser ophthalmoscope (SLO) image from a small eye at 780 nm.[13] The photoreceptor lesion area at the left was produced with a q-switched 532 nm single pulse; the lesion at the right was produced with and argon laser shuttered at 10 msec. The q switched lesion area shows minimal disruption to the integrity of the photoreceptor matrix alignment within the lesion site: the argon induced lesion shows highly reflective, swollen photoreceptors.

Visual function recovery in human laser accident cases provide additional evidence for recovery via the neural visual plasticity mechanism. At least one q-switched laser accident case demonstrated that even after severe q-switched injury involving vitreous hemorrhage, the damaged fovea might regain functionality.[15] In some cases a *pseudofovea* may develop near the damaged foveal region.[15,16] Limitations on the recovery process seem to occur with intraretinal scar formation, retinal traction, and retinal nerve fiber layer damage.[17]

At lower doses, repeated q-switched exposure below hemorrhagic levels have been demonstrated to induce long term effects in both visual acuity and contrast sensitivity. In the present investigation, we have observed that pupillary contraction is deferred upto 90 msec. In studies with q-switched repetition rates of 20 Hz, multiple pulse exposures of 2 or more pulses have been observed to increase transient effects and may contribute to lower energy thresholds for long term effects.[3,4] This possibility will be evaluated in future NHP visual performance studies.

Because the visual system's neural plasticity mechanisms may mask cumulative retinal damage, a more intensive long-term surveillance program for laser workers is suggested. Occupational specialties where q-switched laser sources are routinely encountered in the work place should be considered for more than routine ophthalmic surveillance.

5. SUMMARY

As is the case in q-switched studies of visual function, q-switched single pulse investigations indicate a similar disconnect between morphological retinal damage threshold and the threshold for permanent loss in visual performance. Multiple suprathreshold exposures at twice the morphological damage threshold do not produce more than transient effects and generally recover within a single hour test session with no residual effects on performance in successive sessions. Evaluation of pupillary dynamics for these exposures demonstrated both a refractory period of 90 msec and a pupillary contraction of about 12 percent lasting a total time of 1.5 seconds. Ophthalmoscopic observations made several days post exposure revealed single punctate lesions in the parafoveal retina, consistent with parafoveal spectral sensitivity measurements made with this task in previous NHP baseline investigations. More permanent effects were obtained at higher dose exposures, about 6 times morphological threshold levels, which required about 69 days for full recovery. The recovery process may occur for both long (10-100msec) and q-switched pulse domain because of the presence of retinal and higher order neural plasticity mechanisms in the visual system. However, it may be more deceptive for q-switched exposure because the visual system provides little indication that retinal damage is being incurred until a visible retinal punctate lesion pattern is apparent. The possibility that such long term cumulative damage to the retina may occur suggests that occupational risk factors regarding q-switched laser exposure be reevaluated with respect to increased ophthalmic surveillance.

6. ACKNOWLEDGMENTS

Mr. Andre.Akers is gratefully acknowledged for his graphics design and graphics format support. Sgt. Janice Loveday is gratefully acknowledged for her support in data reduction.

7. DISCLAIMER

In conducting the research described in this report, the investigators adhered to the "Guide for the Care and Use of Laboratory Animals," as promulgated by the Committee on Revision of the Guide for Laboratory Animal Facilities and Care, Institute of Laboratory Animal Resources, National Academy of Sciences - National Research Council. The opinions or assertions contained herein are the private views of the authors and are not to be construed as official or as reflecting the views of the Department of the Army or the Department of Defense. Citation of trade names in this report does not constitute an official endorsement or approval of the use of such items.

8. REFERENCES

1. B.E. Stuck, H. Zwick, J.W. Molchany, D.J. Lund, and D.A. Gagliano, "Accidental human laser retinal injuries from military laser systems," *SPIE Proc. of Laser-Inflicted Eye Injuries: Epidemiology, Prevention and Treatment* **2674**, pp. 7-20m 1996.
2. P.H. Custis, D.A. Gagliano, H. Zwick, S.T. Schuschereba, and C.D. Regillo, "Macular hole surgery following accidental laser injury with a military range finder," *SPIE Proc. of Laser-Inflicted Eye Injuries: Epidemiology, Prevention, and Treatment* **2674**, pp. 166-174, 1996.
3. H. Zwick, K.R. Bloom, and E.S. Beatrice "Permanent visual change associated with punctate foveal lesions," Colour Vision Deficiencies, Eds B.Drum and G. Verriest, **IX**, pp.251-260,1989.
4. .D.O. Robbins, H. Zwick, B.D. Bearden, B.S. Evans, and B.E. Stuck, "Visual Acuity Changes in Rhesus Following Low Level Q-Switched Exposures," *SPIE Proc on Laser and Nonchoerent Light Ocular Effects: Epidemiology, Prevention, and Treatment,* **2974**, pp. 94-104, 1997.
5. D.O. Robbins, H. Zwick, and G.C. Holst, "A method for producing foveal retinal lesions," Be*hav. Res. Meth. Instr.* **5**, pp. 457, 1973.

6. D.O. Robbins and H. Zwick, "Subthreshold functional additivity occurring at the transition zone between temporary and permanent laser-induced visual loss," *SPIE Proc. of Laser-Inflicted Eye Injuries: Epidemiology, Prevention and Treatment,"* **2674**, pp. 44-52, 1996.
7. W.T. Ham, W.J. Geeraets, H.A. Mueller, R.D. Williams, A.M. Clarke, and S.F. Cleary. "Retinal burn threshoilds for helium-neon laser in the rhesus monkey." Arch. Ophthal. Pp. 797-809, 1970.
8. H. Zwick, J. Calabrese, M. Cook, J. Molchany and K.R. "Bloom. Visual Functions Associated with rhesus visual pursuit tracking," Colour Vision Deficiencies, Ed. B. Drum, **XI**, pp.143-152,1993.
9. D.A. Stamper, D.J. Lund, J.W. Molchany, J.J. Dembrosky, O.F. Boneta, B.E. Stuck "Validation of the Blaser II Laboratory,"Walter Ree Army Institute of Research, *USArmy Medical Research Detachment, BAFB, TX, Technical Report, Institute Report*, **463**, 1991.
10. E. Alexandridis "The Pupil" Springer-Verlag New York, 1985.
11. H. Zwick, D.O. Robbins, T. Westgate "Nonselective changes in receptive field organizaton induced by laser irradiation," Letterman Army Institute of Research, Presidio of San Francisco, Lab. Note **# 86-62**, 1986.
12. C.D. Gilbert, T.N. Wiesel, "Receptive field dynamics in adult primary visual cortex," Nature, **356**,150-152,1992.
13. H. Zwick, W.R. Elliott, S.T. Schuschereba, D.J. Lund, B.E. Stuck, "*In vivo* confocal scanning laser ophthalmoscopic characterization of retinal pathology in a small eye animal model," SPIE, Vol. 2974, pp 44-50, 1997.
14. M.Tso, "Photic maculopathy in rhesus monkey, A light and electron microscope study,".*Invest. Ophthal.* **12**, pp. 17, 1974.
15. H. Zwick, B.E. Stuck, W. Dunlap, D.K. Scales, D.J. Lund, and J.W. Ness, "Accidental bilateral Q-switched neodymium laser exposure: treatment and recovery of visual function," *SPIE Proc. of Laser-Tissue Interaction IX* **3254**, pp. 80-89, 1998.
16. H. Zwick, J.W. Ness, J.M. Molchany, B.E. Stuck, and J.Loveday, "Neural motor ocular strategies associated with the development of a pseudofovea following laser-induced macular damage and artificial macular occlusion. Is the fovea replaceable?," *J. of Laser Applications,* **10**, pp. 144-147, 1998.
17. H. Zwick, B.E. Stuck, D. Gagliano, V.C. Parmley, D.J. Lund, J. Molchany, J.J. Kearney, and M. Belkin, "Two informative cases of Q-switched laser eye injury," *Presidio of San Francisco* (CA) *Letterman Army Institute of Research, Institute Report*, **463**, 1991.

Laser Flash Effects on Tracking Performance and the Aversion Response

David A. Stamper, David J. Lund, Jerome W. Molchany, Bruce E. Stuck
US Army Medical Research Detachment, Brooks Air Force Base, TX

ABSTRACT

Introduction: For an accidental laser exposure, the duration of the incident radiation on a specific retinal site depends on the initial fixation, the kinetics of the aversion (blink reflex) and the orienting response (eye movement) toward or away from the light image. Pupilary constriction during the exposure will attenuate the retinal irradiance. **Methods:** In this study, tracking performance was measured in eight volunteers exposed to 0.1, 1.0, and 3.0 second laser flashes while tracking a dynamic target (0.28 deg/s) through a monocular telescope equipped with a miniature video camera to monitor eye response. The collimated 514 nm argon laser beam produced corneal radiant exposures of 0.16, 0.33, and 1.0 mJ/cm^2 for the 0.1, 1.0, and 3.0 second conditions respectively. Total time off target and maximum absolute error scores were measured for bright (430 nits) and dim (4.3 nits) ambient luminance conditions. Eye response (blink and pupilary response) was assessed by evaluation of the video from the eye camera. Volunteer reports of the visual experience were recorded. **Results:** Total time off target (> 0.5 mrad) was maximal for the 3 second exposure condition and minimal for the 0.1 second conditions. Analysis of the data indicated that there was no photic induced blink reflex for the 0.1 second condition under the bright light condition. For some volunteers, blinks did occur during the longer duration exposures but were not classic reflex blinks. Pupil responses following the laser presentation showed pupil diameters decreased from initial values of approximately 6 mm to 2-3 mm which reduced the total energy into the eye at that point by a factor of 10. Volunteers reported smeared and multiple afterimages for the 3 second condition, however, only a single, focal, afterimage was reported for the 0.1 second condition. This information reflects a history of eye movements during the exposure; **Summary:** For durations of 100 msec or less, physiological mechanisms that would limit the retinal radiant exposure are not operative for the conditions investigated in this study. For the 0.1 second exposure condition, tracking performance was not affected for the bright light trials and only minimally affected foe the dim light trials.

1. INTRODUCTION

The retinal and perceptual effects following an accidental or purposeful laser exposure are dependent on the initial fixation point, the kinetics of the aversion response (blink reflex) and the orienting response (eye movement). The pupilary constriction will attenuate the total energy entering the eye (TIE). Earlier studies have shown that the disruptive effects of longer exposure durations (i.e., 5 sec vs. 3 sec) persist longer than shorter durations (1). The patterns of post-laser exposure images following exposure to the laser light has been proposed to be related to the duration of the laser source and reflect a history of eye blink, eye movement, and pupilary response during the period the laser was on (2).

Laser exposures which last longer than the normal eye blink reflex (250 msec) provide the opportunity to reduce the occurrence of post-flash images appearing in the visual field (or permanent damage), by closing the eyelid and/or moving the laser energy to a different retinal location. During this initial appearance of the laser light the pupil will also constrict. All of these mechanisms serve to reduce the energy entering the eye and/or impact on a specific retinal location. However, if a relatively bright laser light is presented in less than 250 msec, all of the energy will likely be deposited in a relatively small retinal area. The mechanisms that would normally serve to reduce light energy entering the eye will not have time to respond.

For exposures where the laser light fills the entire pupil the TIE will vary according to the diameter of the pupil. At energy levels where prolonged exposure could produce damage to the retina, rapid pupil constriction could prevent retinal damage. Additionally, laser exposures below that which produce

Laser and Noncoherent Light Ocular Effects: Epidemiology, Prevention, and Treatment,
Bruce E. Stuck, Michael Belkin, Editors, Proceedings of SPIE Vol. 4246 (2001)

damage, rapid pupil constriction can reduce the disruptive effects of prolonged exposure. Additional information describing pupil dynamics following laser exposure and its' effect on performance is needed.

2. METHODS

2.1 Volunteers: This study was initially reviewed by Human Use and Scientific Review Committees. The conduct and progress of the project was monitored by an ophthalmologist. Ages of the volunteers ranged 20 to 62 yrs. Each volunteer was given a preliminary ophthalmic screen and fundus evaluation to insure good ocular health prior to beginning the study. The test performed were visual acuity (Snellen Wall Chart) contrast sensitivity (NIC Optronics (CS-2000), color matching (Spectrum Color Vision Meter 712, Reyleigh and Morland), and night vision, night vision flare testing (MCT 8000). All volunteers were required to be within normal limits on these tests prior to their participation in the study. The medical monitor prior to their participation in the study performed Opthalmoscopy and tonometry. Volunteers using long-term medications were not included in the study. At the conclusion of the study the visual screening battery and ophthalmologic examination done prior to entry in the study were repeated.

2.2 Apparatus:

BLASER Simulator: The BLASER simulator (Fig. 1) is a 26 x 30 terrain board simulator presents a desert-type scene. A computer station for data collection and an 8 x 8 ft bunker which contains an in-house constructed, viscous damped, dual pistol handle, monocular eyepiece tracking device were located adjacent to the terrain board. The tracking device with its' mechanical and optical enhancements provided tracking data appropriate for a 2-km distance and visually simulated a 10 X sight at that distance. A television camera mounted coaxially with the optics of the tracking device imaged an infrared light-emitting diode (IR LED) located in a center-of-mass position on the target. The IR LED was invisible to the operator but provided a reference point for the microprocessor and associated software to determine and store aiming error data at frame rate.

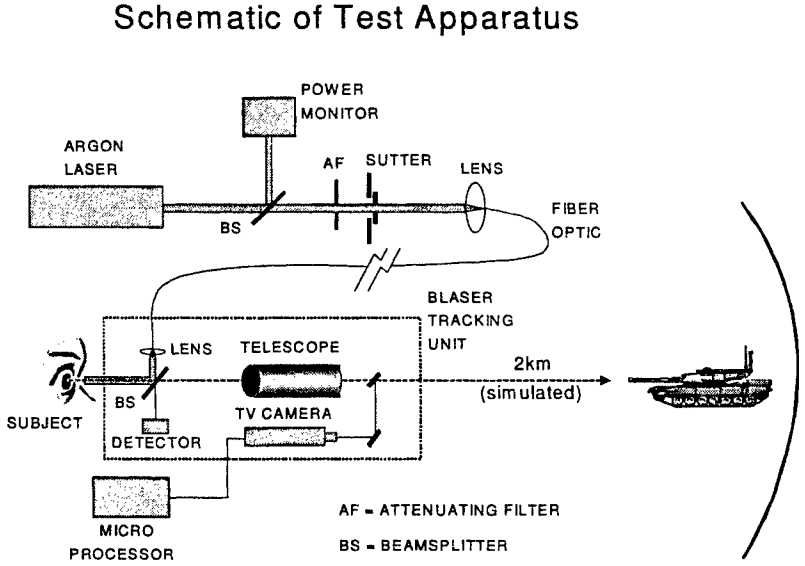

Fig. 1. Schematic of BLASER simulator

The target, a 1/35th scale Russian T-72 tank was track-mounted and traversed an arc on the terrain at the simulated distance of 2 km. It was driven alternately in the left-to-right and right-to-left direction at a constant angular velocity of 5 mrad/sec. Luminance measurements of the camouflaged tank and background were taken with an imaging Spectrophotometer. The calculated contrast of target to background was 23%. The terrain luminance was 430 cd/m^2. The dawn/dusk condition was simulated by inserting a Neutral Density (ND) filter with an optical transmission of 1% (2 OD) that reduced the terrain luminance to 4.3 cd/m^2.

2.2.2 Laser Source: The 514.5 nm laser light was obtained from an argon-ion laser. The laser source was located outside the bunker was brought into the bunker and the optics of the tracking device with a fiber optic cable. The laser light was made coaxial with the cross hairs of the sight. A shutter was activated during each flash trial for one of the three flash durations (0.1, 1.0, or 3.0 seconds). While the 3.0 sec exposure was selected to provide a reference point to compare to earlier work, the one-sec exposure at this dose level has not been previously studied. The 0.1 sec flash duration provides critical information concerning the effects of a flash that occurs prior to the onset of a normal reflexive eye blink. The collimated 514 nm argon laser beam produced corneal radiant exposures of 0.16, 0.33, and 1.0 mJ/cm^2 for the 0.1, 1.0, and 3.0 second conditions respectively

2.2.3 Video Recording of Pupil Dynamics: An infrared light source mounted inside the tracking device provided illumination for the CCD camera that imaged the eye as the volunteer tracked the target. The images of the pupil were recorded on a Mitsubishi video recorder for later analysis. The video images were transferred onto the computer's hard drive using the Kalcium Acquire 3.0 Approximately ten sec of video was acquired at a 30 Hz frame rate and stored as .tif files which were individually viewed. Each file was viewed and a measurement of the pupil's diameter was made using the Corel Photo Paint-8 by calculating the difference in the Y coordinates at the top and bottom edges of the pupil. These data were converted into mm and plotted on to X and Y scatter plots. Following the initial 5-10 data points every fifth frame is used to create a smooth-line plot of each flash trial.

2.3 Procedure: Following the initial eye examination all volunteers received two practice days using the tracking device in the simulator. The first day consisted to twenty-two, 1-min trials and the second day thirty, 15-sec trials. This mass-distributed practice schedule has been shown to produce stable tracking performance (3). Half of the trials were presented under bright ambient light conditions and half under simulated dawn/dusk conditions. The dawn/dusk condition was created by inserting a 2.0 ND filter into the optical pathway of the tracking device.

On each of the two test days each volunteer was told that periodically during the thirty trials they would experience a bright flash and they were to maintain the cross hairs on the target to the best of their ability. They received six flash trails during thirty trials at a rate of 1/5 trials. The flash trials were randomly presented during each group of five trials so that the person tracking was unaware of when the flash would be presented or how long it would last. Three of the flash trials were presented during the bright condition and three during the dawn/dusk condition. The twelve flash trials yielded a total of 2 trials for each flash duration and ambient light condition.

Verbal responses describing what each volunteer experienced during and following the laser light were obtained for each flash trial. The questions asked were, "What color was the laser?", "What color and shape was the image immediately following the flash?", and after one-minute "Has the image changed and what does it look like now?". Responses were entered into a database for later analysis.

2.4 Data Analysis: The error scores determined for each flash trial were the total time off-target scores. These scores represent the amount of time that the crosshairs were off a 0.5 mrad square target patch located on the side of the tank target. The terrain on the simulator was flat and required essentially no change in the vertical component. Visual inspection of the vertical tracking error scores was unremarkable

and showed almost no change during each trial. The results presented represent only the time off target on the horizontal axis.

3. RESULTS

3.1 Pupilary Response: The analysis of the pupil images from videotape to date has provided complete results for three individuals. Figures 2 and 3 show the pupil response of the 0.1, 1.0, and 3.0 flash exposure trials under bright light and simulated dawn/dusk conditions respectively for one individual.

Fig 2. DCB1

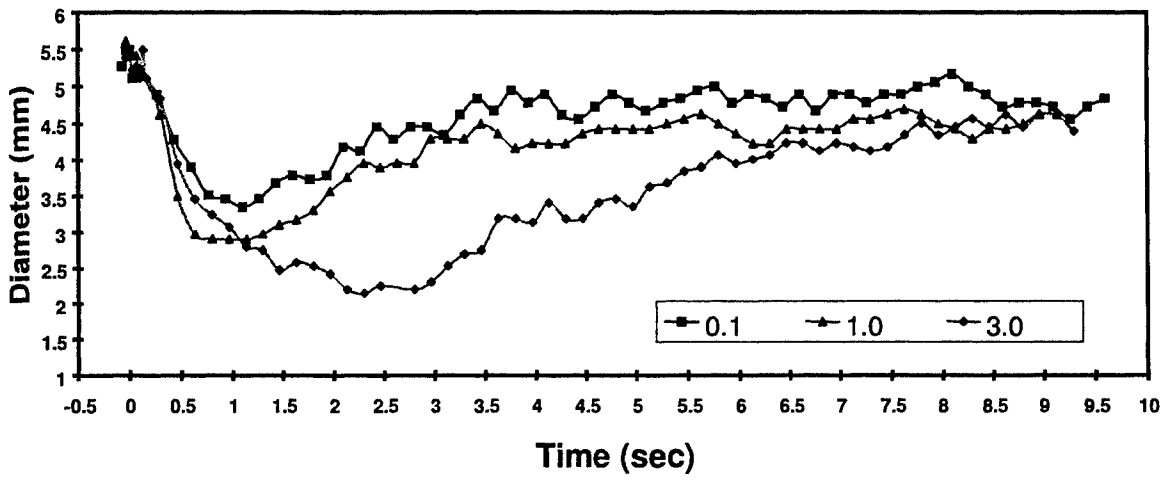

Fig 3. DCD1

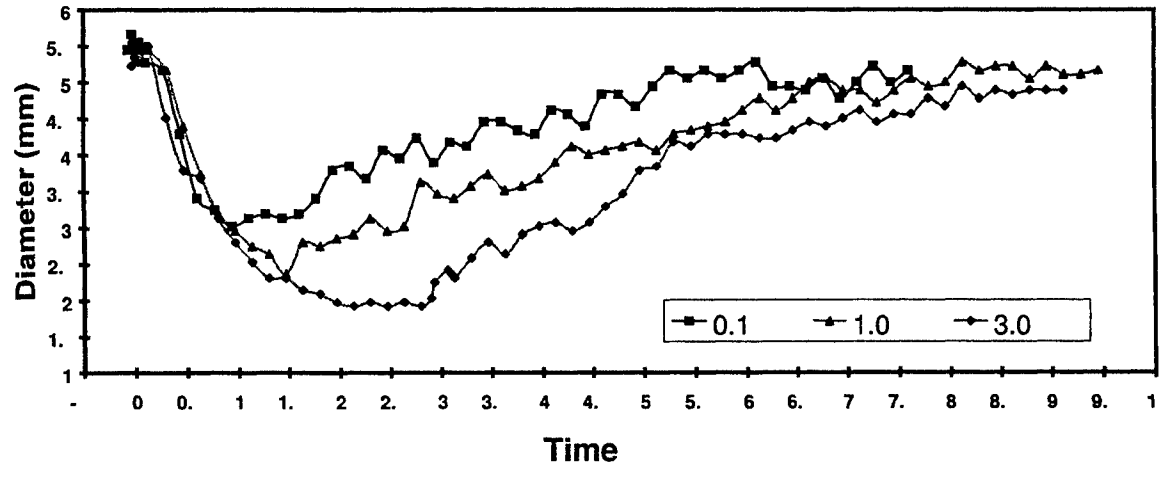

Initial pupil diameters for this individual were approximately the same for the bright and dawn/dusk conditions. The diameters following the flash became increasingly smaller as flash duration increased for both the bright and dawn/dusk trials. The time to reach these smaller diameters also increased as duration increased. Table 1 summarizes these results for the three individuals completed to date.

3.2 Post-Flash Images: The subjective reports by volunteers, which described the appearance of the post flash, images indicated that they observed different patterns for the three durations. The shortest flash, 0.1 sec, produced a small well-defined green image that was the same color as the laser source, Fig 4b. The 1.0 sec image shown in Fig 4c was describe as slightly larger the 0.1 sec images and sometimes had a small comet-like tail as they began to make an aversive response. The images seen following the 3.0 sec exposures (4d) was similar to previously reported images which resembled a large blob or many small spots scattered across the visual field.

Fig 4. Post-Laser Exposure Afterimage Patterns
(Immediate)

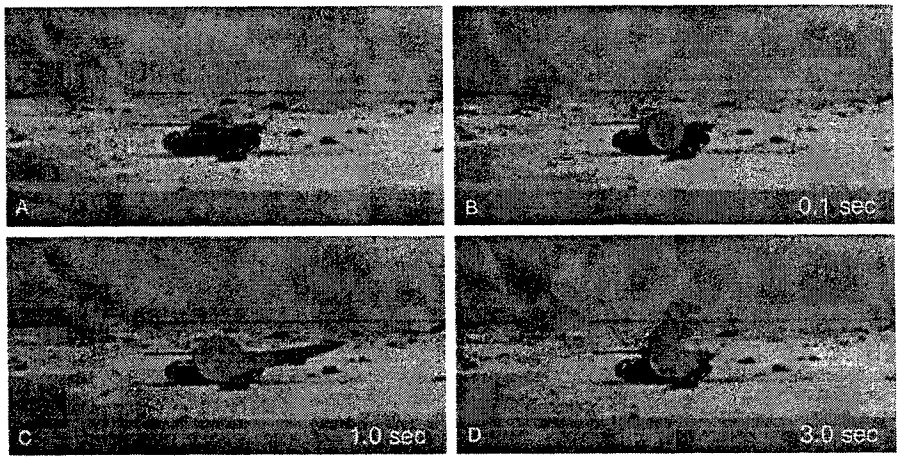

Fig 5. Post-Laser Exposure Afterimage Patterns
(One Minute Post)

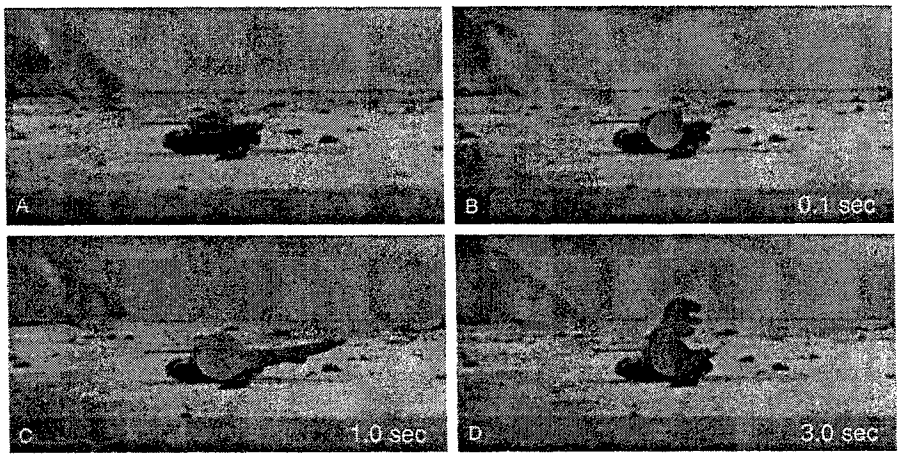

The one-minute post-flash images (Fig 5) remained in shape much like the immediate post-flash images. The form of the image when present retained the shape that was first observed after the flash. However, in some cases the color of the image changed from green to the complimentary colors of red or purple (Fig 5 d). The edges of the images sometimes also appeared as a bright red Fig. 5d).

Table 1. PUPIL DIAMETERS*

	BRIGHT 0.1 SEC	BRIGHT 1.0 SEC	BRIGHT 3.0 SEC	DIM 0.1 SEC	DIM 1.0 SEC	DIM 3.0 SEC
Maximum Diameter	4.81	4.68	4.73	5.38	5.35	5.39
Minimum Diameter	2.73	2.37	1.84	2.52	2.29	1.76
Time To Minimum	1.21 sec	1.25 sec	2.64 sec	1.62 sec	1.75 sec	2.93 sec

N = 3
* diameter in mm

3.3 Total Time Off-Target Scores:. The mean total time off target scores for each of the three flash durations under bright and simulated dawn/dusk ambient light conditions are presented in Fig 6. First, for each of the three flash durations the dawn dusk conditions always produced higher off target scores. Second, the 1.0 sec scores were higher than the 0.1 sec scores and the 3.0 sec scores were always higher that the 0.1 and the 1.0 scores.

Figure 6.

Total Time Off Target

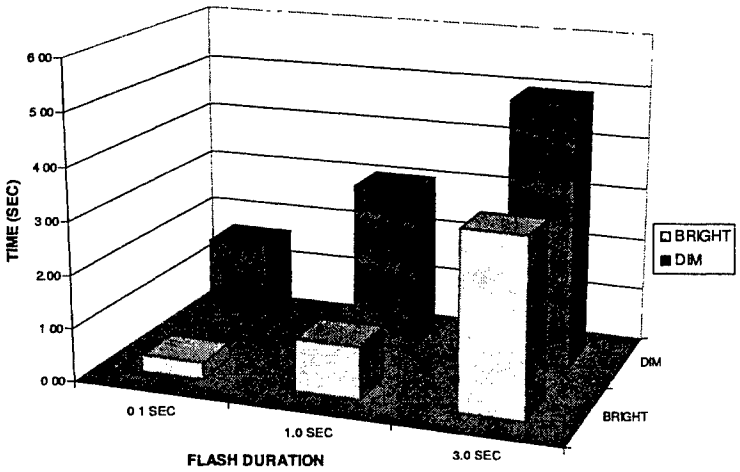

4. DISCUSSION

4.1 The pupil constriction continued after the 0.1 sec flash until approximately 1.0 sec, although it did not reach the levels of the 1.0 and 3.0 second exposures. The amount of constriction was directly related to the duration of the flash and the final recovery during the remainder of the 10 sec period was approximately the same for both the bright and dawn/dusk trials.

4.2 The general appearances of the post-flash images were unlike full-field flashes such as those produced by a photoflash unit. The intense, well-focused laser light painted a pattern on the retina and seen in the visual field, which indicated a history of the eye movements and eyelid openings and closings during the 3-sec glare periods. The appearance of these lingering primary images and afterimages (see Stamper et al., 2000), often surrounded by a brilliant red border, provided a spectacular visual experience.

4.3 The total time off-target scores indicated that the 0.1 sec exposures were the least disruptive of the three exposure conditions. In this study the 0.1 sec exposures were made at approximately 50% of the maximum permissible exposure (MPE) limits while the 1.0 and 3.0 sec exposures were at less than 40% of the MPE.

5. DISCLAIMER

The opinions or assertions contained herein are the private views of the authors and are not to be construed as official or as reflecting the views of the Department of the Army or the Department of Defense.

Citation of trade names in this report does not constitute an official endorsement or approval of the use of such items.

Human Volunteers participated in these studies after giving their free and informed voluntary consent. Investigators adhered to AR 70-25 and USAMRMC Regulation 50-25 on the use of volunteers in research.

6. REFERENCES

1. Stamper DA, Lund DJ, Molchany JW, Stuck BE. Transient disruption of human pursuit tracking performance for laser exposures below permissible exposure limits. In B. E. Stuck and M Belkin (Eds.), *Lasers and noncoherent ocular effects: epidemiology prevention and treatment.* San Jose, CA: *Proceedings of the International Society for Optical Engineering.* 1997, Vol. 2974. Pp. 117-128.

2. Stamper DA, Lund DJ, Molchany JW, Stuck BE. Laser-induced afterimages in humans. *Perceptual and Motor Skills*. 2000: 91, 15-33.

3. Stamper DA, Levine RR, Best PR. Effects of practice schedule on two-hand pursuit tracking performance. *Perceptual and Motor Skills* 1987; 65:483-92.

High-power lasers in the 1.3-1.4 μm wavelength range: ocular effects and safety standard implications

J. A. Zuclich[a], D. J. Lund[b], P.R. Edsall[a], B.E. Stuck[b] and G.Hengst[c]
[a]Litton/TASC, San Antonio, TX. 78228-1330; [b]US Army Medical Research Detachment, Brooks AFB, TX. 78235-5138, [c]Optical Radiation Branch, Air Force Research Laboratory, Brooks AFB, TX. 78235-5215

ABSTRACT

This manuscript details recent studies of ocular effects of pulsed and cw laser radiation at wavelengths of 1.315 and 1.318 μm, and compares corneal, lens and retinal damage thresholds. The results indicate that for the exposure conditions studied, relatively minor changes in pulsewidth and/or wavelength can substantially alter threshold levels and change the tissue site(s) exhibiting the lowest damage threshold. The discussion suggests that these data may be applied to re-assess laser safety standards in the near-IR to far-IR transition-region. Also discussed are unique aspects of the laser-tissue interaction for these penetrating wavelengths where the incident laser radiation is relatively evenly absorbed throughout the ocular medium and the retina. In such cases of "volumetric" absorption observable manifestations of laser insult may be delayed (hours to days) and may ultimately involve inflammatory responses or other disruption of tissue not directly irradiated by the laser.

Keywords: Laser, infrared, eye, damage, threshold, retina, cornea, lens, safety standard

1. INTRODUCTION

The last few years have seen development of numerous pulsed and high power continuous wave (cw) lasers operating in the 1.3-1.4 μm wavelength range, including chemical oxygen iodine or COIL lasers (e.g., the USAF Airborne Laser) and various Neodymium and diode solid-state lasers. In addition, tunable laser system (OPO's) now can generate appreciable pulse energies in this wavelength range. These developments present opportunities for new IR laser applications in medicine, telecommunications and the military. However, bioeffects studies of laser-tissue interactions in this wavelength range remain relatively few in number and there is a paucity of ocular damage threshold data to support laser safety standard maximum permissible exposure (MPE) levels.[1,2] Because, as illustrated in Figure 1, ocular absorption coefficients vary rapidly with wavelength across the 1.4-μm transition between the near-IR and far-IR spectral ranges, the MPE's also vary abruptly and discontinuously with wavelength.[1,2] And due to the absence of ocular threshold data, the safety standards were conservatively drawn, perhaps unnecessarily inhibiting applications of 1.3 to 1.4-μm laser sources.

Earlier studies from this laboratory reported observation of corneal, lens, iris and retinal damage following cw Nd:YAG laser exposures at 1.318 and 1.356 μm.[3-5] Exposure durations were of the order of ~0.25 sec. It was noted that with the wavelengths, exposure durations and corneal irradiance levels used, the damage thresholds for each of the ocular tissues were of comparable magnitude, spanning a range of approximately a factor of two[3]. The simultaneous production of laser-induced damage in several ocular tissues is understood by schematizing the distribution of laser energy absorption at representative wavelengths as the beam propagates through the ocular medium. This is done in Figure 2, which compares the absorption of a visible wavelength (0.514 μm) as depicted in Figure 2a to that for ~1.32-μm radiation (Figure 2c). Penetration into the eye is measured along the horizontal axis as shown by Figure 2b. The solid lines in Figures 2a and 2c represent the absorption coefficients of each ocular component from the cornea through the vitreous. Using these absorption coefficients and treating each ocular component as a homogeneous layer, the percent of corneal incident radiation penetrating to a given depth is calculated and plotted as the dotted curves in Figures 2a and 2c. Thus, at 0.514 μm the greater percentage of the corneal incident radiation reaches the retina but at 1.32 μm, the transmission to the retina is only ~5%. Taking the focusing power of the eye into account, the relative laser irradiance at any point along the optical path or horizontal

Laser and Noncoherent Light Ocular Effects: Epidemiology, Prevention, and Treatment,
Bruce E. Stuck, Michael Belkin, Editors, Proceedings of SPIE Vol. 4246 (2001)

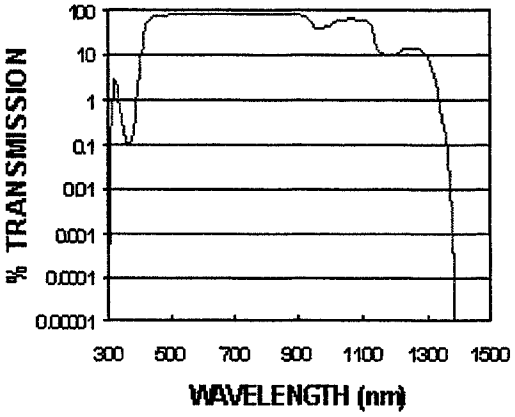

FIGURE 1 Transmission of the pre-retinal ocular medium in the rhesus.

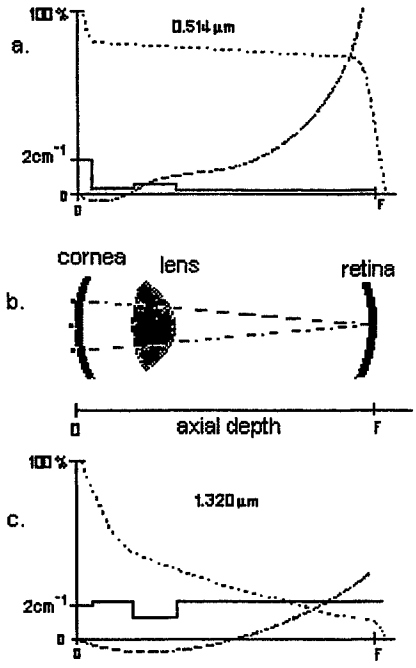

FIGURE 2 Schematic depiction of penetration of 0.514 μm and 1.32 μm radiation (2a and 2c, respectively) into the eye with focal length, F (2b). The vertical axis is, in turn, absorption coefficient in cm-1 (solid lines); percent of corneal incident radiation reaching a given depth into the eye (dotted lines) and relative irradiance at a given depth (dashed lines).

axis is approximated by the dashed curves in Figures 2a and 2c. For visible wavelengths, the retinal hazard is readily appreciated due to the high relative irradiance reaching the retina coupled with a high retinal absorption coefficient. At ~1.32 μm, on the other hand, the retinal irradiance barely exceeds that incident at the cornea and, in fact, the irradiance varies relatively little throughout the ocular medium. Coupled with comparable absorption coefficients for each ocular component at this wavelength, this schematic explains the earlier reports that the damage thresholds for each ocular component are of comparable magnitude and that the relative sensitivities of the ocular components can be re-ordered by seemingly minor changes in wavelength and/or exposure duration.

In this report, we further characterize the laser-tissue interactions at ~1.3 μm and quantify ocular damage thresholds for two exposure scenarios which seem likely to be encountered in the field and which, therefore, have the greatest relevance in assessing safety standard MPE's. In particular, a cw Nd:YAG laser emitting at 1.318 μm was used to examine the "worst-case" exposure scenario for an invisible laser beam when no reaction-time aversion response is anticipated. Accordingly, a 10-sec exposure duration was chosen to match the ANSI standard guidance for the anticipated worst-case IR exposure.[1] A second exposure scenario anticipated a field environment with a high-power IR laser propagated through long distances of the atmosphere and momentarily intercepting (either directly or via a reflected beam) an unintended target. Assuming that the target and/or the laser source are in motion, the dwell time on the target is likely to be quite short and a representative exposure scenario was achieved by using a pulsed Nd:YLF laser emitting at 1.315 μm (coincident with the COIL laser wavelength) and having a pulsewidth of ~350 μsec.

2. METHODS

Ocular exposures were accomplished with cw and pulsed Nd lasers operating at wavelengths selected to be as close as possible to the 1.315-μm emission of the COIL laser. The cw source was a Nd:YAG laser equipped with mirrors and an intracavity etalon which together were tuned to optimize the emission line at 1.318 μm while suppressing other Nd:YAG wavelengths. Maximum cw output of the laser was ~2W. The output was attenuated in incremental steps while determining the ocular damage thresholds for 10-sec exposures.

The pulsed source was a Nd:YLF laser emitting ~350 μsec pulses at a pulse repetition frequency (prf) of 1 Hz and with a maximum pulse energy of ~1 J. The emission wavelength was tunable over a narrow range and was set at 1.315 μm for the experiments reported here.

For both the cw and pulsed lasers, beam profiles were determined using 2-D beam analyzers and were used to define the laser spot size incident at the corneal plane and to measure the beam divergence. Electronically controlled shutters were used to control the exposure duration for the cw case and to select single pulses from the repetitively-pulsed source.

The experimental subjects were rhesus monkeys (Macaca mulatta) used only when retinal effects were being evaluated and Dutch Belted rabbits (Oryctolagus cuniculus), which served as an acceptable animal model for evaluating laser-induced damage in the anterior ocular tissues. All animals used in this study were procured, maintained, and used in accordance with the Animal Welfare Act and the "Guide for the Care of Use of Laboratory Animals" prepared by the Institute of Laboratory Animal Resources, National Research Council; and the ARVO Resolution on the Use of Animals in Research. All experiments involving animals used appropriate levels of anesthesia so the subjects did not experience pain or distress.

Pre-exposure screening of subjects to insure clear ocular media and normal ocular tissues generally consisted of a slit-lamp examination, a fundus camera examination, fluorescein angiography, baseline photography taken while the subject was still in position at the fundus camera, and refraction to the nearest 0.25 diopter. In the case of rabbit subjects scheduled only for anterior ocular tissue exposures, the pre-exposure screening was limited to the slit-lamp and fundus camera examinations. In cases where laser-induced retinal/choroidal effects were detected or suspected, the subjects were also examined with a scanning laser ophthalmoscope (SLO) capable of projecting several visible and near-IR laser wavelengths ranging from 0.488 μm to 0.780 μm. The SLO exams included fluorescein and Indo-cyanine green angiographies and were recorded on videotape. An imaging processing system allowed individual video frames to be digitized and printed.

For exposures to anterior ocular tissues, the laser beam was focused to a 1-mm spot size at the corneal plane, and directed to the selected corneal site at normal incidence. In general, nine exposures were delivered to the cornea forming a 3 x 3 grid of exposed sites with ~2 mm between adjacent exposure sites. The grid was centered on the cornea. To insure that the IR beam was delivered to the selected corneal site, two HeNe beams of ~1-mm diameter were made to cross at the corneal plane. The spot where the two HeNe beams crossed was coincident with the passage of the IR beam through the corneal plane. Thus, positioning the cornea with regard to the 1-mm spot defined by the crossing HeNe beams, insured that the selected spot was irradiated by the IR laser.

For retinal exposures, several changes in procedure were implemented. The subjects were placed on an adjustable stage in front of a fundus camera. Laser exposures were delivered to the eye by deflecting the beam off of a sliding gold mirror mounted in front of the fundus camera and adjusted so that when the mirror was in place, the deflected laser beam was collinear with the optical axis of the fundus camera. Sliding the mirror to the side allowed normal viewing of the fundus immediately before and after each laser exposure. A gold mirror was chosen because of its high reflectivity to the IR wavelengths being studied. Marker lesions were placed on the subject's retina by means of an air-cooled argon laser using 15-msec exposures with ~60 mW incident at the cornea. For rhesus subjects, the marker lesions were placed outside of the pigmented macula in a grid pattern which defined the macular sites for the subsequent IR laser

exposures. For rabbit subjects, the marker lesions, when used, were placed below the visual streak again to define retinal sites (also below the streak) for the IR exposures. In order to avoid, or at least minimize corneal and/or lens damage while delivering multiple exposures to the retina, the IR laser beam diameter at the corneal plane was ~5 mm instead of 1 mm. The laser beam was directed so that it passed through the dilated pupil (generally 7-8 mm) without clipping the iris.

Following each exposure session, lesion/no lesion determinations were made for each exposure site in each potentially affected ocular tissue. Although a 1-hr postexposure criterion is standard when reading eyes for laser-induced thermal damage, such a fixed criterion was not presupposed to be adequate in this instance since we had previously shown[4] that some of the visible consequences of penetrating IR wavelengths were not visualized via slit-lamp, fundus camera, or SLO examination until several days postexposure. Thus, selected subjects were periodically examined at times up to 3-months postexposure to document the temporal development of the various types of observed ocular lesions. When lesion/no lesion data were sufficient, ED_{50} thresholds and confidence limits were calculated by probit analysis[6].

3. RESULTS

Results from three series of experiments are reported. The pulsed Nd:YLF laser was capable of inducing immediate thermal damage to the anterior ocular tissues or, if incident at the eye with a lower corneal irradiance (sub-threshold for corneal and lens damage) the pulse energy could damage the retina. Thus, the first series of experiment examined the retinal effects from single 350-μsec pulses of 1.315-μm radiation when incident at the eye at relatively low corneal irradiance levels (5-mm beam diameter). The second series of experiments studied corneal, lens and iris effects of the 350-μsec Nd:YLF pulses when focused to smaller spot sizes (≤1 mm) at the cornea. The third series of experiments utilized the cw 1.318-μm output of the Nd:YAG laser to determine anterior ocular tissue damage thresholds for 10-sec exposure durations. We did not find retinal damage in rhesus or rabbit subjects following the 10-sec, 1.318-μm ocular exposures.

Figure 3 shows examples of retinal lesions induced in the rhesus by the pulsed Nd:YLF source. The fundus photograph was taken at ~one hour following delivery of a sequence of paramacular exposures (single-pulse, 1.315 μm) with total intraocular energies (TIE) ranging from ~200 mJ to 1 J. Several distinct lesions are seen at exposure sites to the right of and below the pigmented macula. Figure 4 shows the same eye at 1-week postexposure. By this time, secondary retinal effects had appeared in the form of whitish streaks piercing several of the otherwise circular lesions. The funduscopic appearance of the streaks suggested that they reflected localized edema similar to that, which initially developed at the supra-threshold exposure sites. It was noted that in each of several subjects, this secondary effects developed at a number of lesion sites, both macular and paramacular, and consistently had the appearance (as seen in Figure 5) of streaks pointing towards the fovea. In a few cases, the streak appearance was first visualized at 1-hr postexposure but in most cases it was 24-hrs or longer before the effect was noticed. In all cases, the streaks developed only at lesion sites where there had been a distinct white (edematous), circular lesion visible immediately following exposure. With further passage of time, the segments of the whitish streaks running in the direction towards the fovea began to thicken and darken while the segments on the distal sides of the lesion sites tended to fade without exhibiting further development (Figure 6).

Secondary effects aside, the ED_{50} retinal damage threshold (in rhesus) for production of the primary (circular) lesions was assessed by applying probit analysis following ~180 exposures to both macular and paramacular regions of six eyes. The macular threshold was 326 mJ (TIE) with fiducial limits of 305-353 mJ, while the paramacular threshold dose was 334 mJ with fiducial limits of 324-349 mJ. The laser-induced primary lesions were observed immediately or within minutes following exposure and, so, the previously expressed concerns[3-5] regarding lesion/no lesion determinations at 24-hr or longer postexposure as opposed to 1-hr postexposure were not an issue in this case. For the beam diameter utilized, the retinal threshold dose equates to ~1 J/cm^2 incident at the cornea. With this exposure configuration (~5-mm diameter beam incident at the cornea and passing through the dilated pupil) no damage was noted to the anterior ocular tissues, even after 30 or more exposures to each eye (approximately half of the exposures

FIGURE 3 Fundus photograph showing rhesus retinal lesions induced by pulsed Nd:YLF laser. Photograph taken at ~1-hr postexposure.

FIGURE 4 Fundus photograph showing same eye seen in Figure 3, but taken at 1-week postexposure.

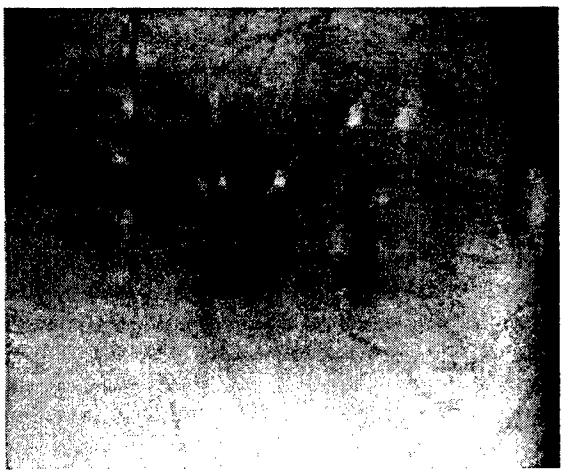

FIGURE 5 Fundus photograph showing a representative array of primary retinal lesions (circular spots) with numerous examples of secondary lesions (streaks piercing circular lesions and pointing towards fovea) which developed over the 24-hr period following exposures.

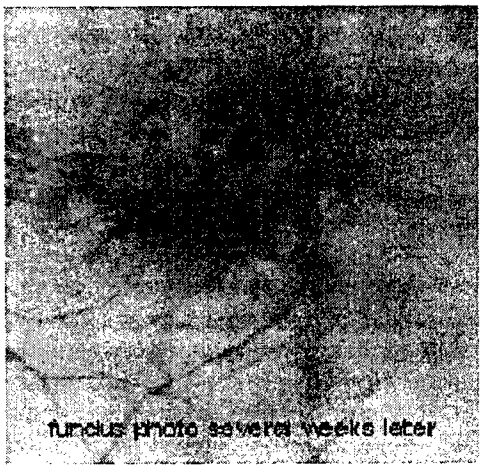

FIGURE 6 Fundus photograph taken at ~1-month postexposure showing late appearance of primary and secondary retinal lesions induced by pulsed Nd:YLF laser.

having pulse energies greater then the retinal threshold dose). Only when the incident laser beam was focused to a small spot (≤1 mm at the corneal plane), did we detect damage in the anterior ocular tissues.

The second series of experiments studied corneal, lens and iris damage effects in rabbits using the same Nd:YLF laser but with the beam focused to ≤1-mm spot diameter incident at the corneal plane. Representative examples of each type of observed lesion are shown in Figure 7. The ED_{50} corneal threshold for minimal clouding, as detected by slit-lamp observation, was 390-mJ pulse energy which, using an exposed area of 0.0092 cm^2 measured by the beam profiler, equates to 42 J/cm^2 incident at the cornea. Fiducial limits were 39-46 J/cm^2.

Damage to the rabbit lens in the form of anterior surface cataract was found in only a few instances where the highest available pulse energy was directed to the eye. In each such case, the laser pulse had also induced a substantial full thickness corneal lesion. In contrast to the earlier studies[3-5] where considerably longer exposure times had been used (0.25 sec vs 350 μsec in this study), the cataracts showed no

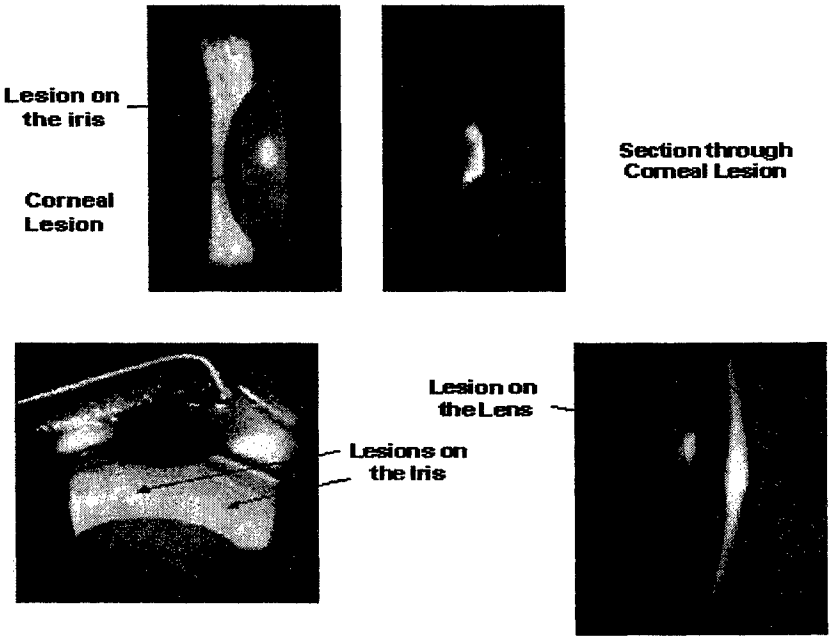

FIGURE 7 Slit-lamp photographs of rabbit anterior ocular component lesions induced by pulsed Nd:YLF laser.

appreciable depth below the anterior surface and apparently had a threshold dose several times greater than the corneal threshold. The lens threshold was not further quantified.

Although the corneal and retinal threshold data were collected from subjects with dilated pupils, testing for iris damage was conducted in two rabbits with undilated pupils. The laser beam was focused using the same optics as for the corneal threshold experiments but the subject was translated relative to the focusing lens so that the focal plane now fell on the iris target site(s). Visible disruption of the irradiated iris was found whenever the corneal radiant exposure exceeded ~32 J/cm^2 (compared to the 42 J/cm^2 corneal threshold dose), suggesting that at this wavelength and exposure time, pigmented tissues (the iris and likely the skin) are at somewhat greater risk than the unpigmented ocular components.

The final series of experiments for this study was an examination of anterior ocular tissue effects induced by 10-sec exposures to the cw Nd:YAG laser emitting at 1.318 μm. With the beam focused to an ~0.8-mm diameter spot at the corneal plane, lenticular damage (and in most instances overlying corneal lesions) was found when the cw laser power was ≥0.95 W. In terms of incident radiant exposure, the threshold for inducing a cataract was 1890 J/cm^2 with fiducial limits of 910-2060 J/cm^2. The threshold for corneal damage was marginally higher. Attempts to induce retinal damage by allowing a large spot-size (≥5 mm) collimated beam to be directed through he pupil (as had been done with the Nd:YLF laser) were not successful.

4. DISCUSSION

The threshold dose levels and the appearance to the ~1.315-μm induced laser damage in the cornea, lens and iris are consistent with a thermal damage mechanism. The representative illustrations of such anterior component lesions shown in Figure 7, can be compared to analogous photographs which were printed and discussed in detail in earlier publications from this laboratory[3-5] and, so, are not discussed further in this report. The appearance of the secondary retinal effects induced by the pulsed Nd:YLF laser, by contrast, is unique and bears further scrutiny.

Although the initial ophthalmoscopic appearance of the IR-laser induced retinal lesions (reflective circular spots) was also consistent with a thermal damage mechanism, the secondary effects which developed over

a timeframe of hours to days following exposure, appear to involve degeneration of tissue not directly exposed to the laser radiation (Figure 4-6). In an attempt to delineate the nature of the secondary effects and their potential consequences for visual function, we tracked the temporal development of the effects via standard ophthalmoscopy and confocal SLO for up to six months following exposure to 350-μsec, 1.315-μm pulses. In addition, we conducted a histopatholigical investigation, at both the light and electron microscopic levels, of representative retinal lesions in tissue fixed at 24-hr postexposure; and are in the process of further pathological evaluation of lesioned tissue fixed at several weeks and longer postexposure.

Figure 8 is an SLO image of the same eye seen in the fundus photograph of Figure 6. The SLO image was captured one month following the time that the pulsed 1.315-μm exposures were delivered. The SLO image was taken with 0.488-μm illumination and so emphasizes relatively shallow features within the retinal layers. The temporal development of the initial whitish streak into the dark, thicker segment running between the lesion site and the fovea is seen even more dramatically than in the fundus photograph of Figure 6. Further, several instances of dark banding running parallel to the retinal nerve fibers (and usually associated with post-laser attrition in the nerve fiber layer[7,8]) can be seen running through several of the supra-threshold lesion sites near the bottom of the image. Finally there are also a few instances of dark banding, interpreted as bridging,[7,8] running between adjacent pairs of supra-threshold experimental lesions or between an experimental lesion and a marker lesion. All of these delayed IR-induced damage features are best visualized with short-wavelength SLO illumination and, hence, are interpreted as involving degeneration in the inner retina and NFL layers.

FIGURE 8 SLO image of same eye seen in the fundus photograph of Figure 6. The SLO image was captured at 1-month postexposure and, so, also shows the mature appearance of the retinal effects induced by the pulsed Nd:YLF laser.

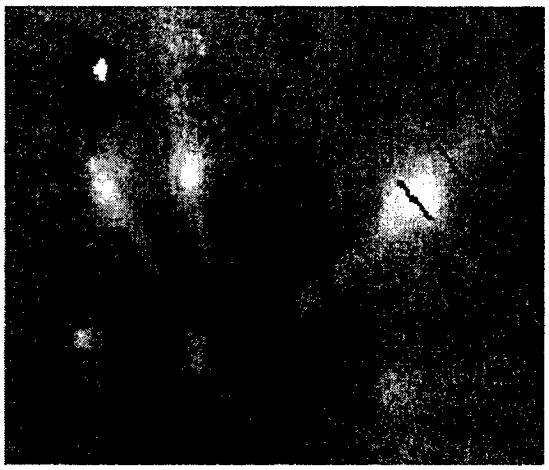

FIGURE 9 Photograph of a block of retinal tissue cut following fixation from the eye shown in the fundus photograph of Figure 5. The markers "1" through "4" show where section cuts were made in preparing the histologic slides shown in the following figures.

Figure 9 is a photograph of a block of fixed retinal tissue cut from the eye shown in the fundus photograph of Figure 5. The tissue was fixed at 3-weeks following exposures to the 1.315-μm pulsed source. Slides were cut at micron intervals including cuts at the points indicated by markers "1" through "4" on Figure 9. As the cuts progressed from marker "1" towards the center of the circular lesion (marker "3") damage was first detected in the innermost retinal layers, specifically in the NFL (Figure 10) and gradually progressed to involve the deeper layers. At the center of the lesion site (marker "3"), the retinal involvement was full thickness as seen in Figure 11. Progressing further in the direction towards the fovea, the tissue again showed no disruption of the deeper retinal layers. At marker "4" and closer to the fovea, the damage was restricted to the inner retina, as seen in Figure 12. This disruption is assigned to the fiber layer of Henly which offers the anatomical explanation for the whitish streaks emanating radially through the lesion sites to the fovea[9]. While NFL dropout bands and Henly layer streak disruptions have been noted is a few

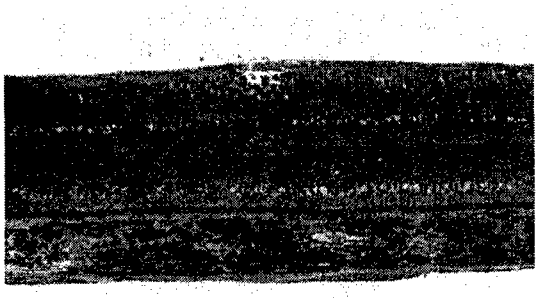

FIGURE 10 Histologic section of retinal tissue cut at marker "1" on eye shown in Figure 9. This section shows the appearance of the retinal disruption at the distal edge of the laser lesion.

FIGURE 11 Histologic section of retinal tissue cut at marker "3" on eye shown in Figure 9. This section shows the appearance at the central portion of the laser lesion.

FIGURE 12 Histologic section of retinal tissue cut at marker "4" on eye shown in Figure 9. This section shows the appearance of the retinal disruption on the inside (nearer the fovea) edge of the laser lesion.

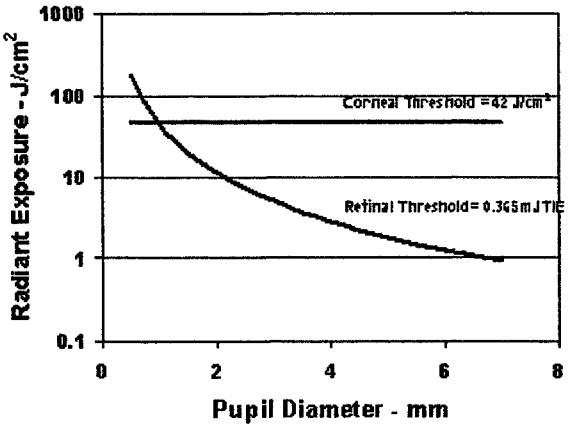

FIGURE 13 Corneal and retinal damage thresholds (in terms of corneal incident radiant exposure) as a function of pupil diameter for pulsed Nd:YLF exposures.

instances following visible-wavelength laser-induced retinal insult at levels much greater than the threshold for inducing ophthalmoscopically visible lesions (2-3 orders of magnitude greater than threshold), the unique aspect of the current observations is that these delayed degenerative features are found following exposure doses that are no greater than ~2x the ED_{50} threshold for a minimal retinal lesion.

Tables 1-3 compare the ED_{50} threshold determinations from the current studies to previously published threshold data and safety standard MPE levels. Table 1 lists retinal damage thresholds for comparable pulse durations but spanning the visible and near-IR wavelength ranges. The dramatic increases in ED_{50} with wavelength is apparent and it is seen that the TIE threshold for 1.315 μm is ~4 orders of magnitude greater than those for visible wavelengths and even close to 2 orders of magnitude above the Nd threshold at 1060 μm. However this behavior is still consistent with the absorption properties of the ocular components and with a thermal damage mechanism when the following factors are taken into account: increasing absorption of the ocular medium with increasing wavelength into the IR (see Figure 1); increased chromatic aberrations of the eye (and therefore increased retinal spot-size) as the wavelength moves further from the optimum focusable wavelength in the green; and more gradual "volumetric" absorption of the laser energy throughout the retinal and choroidal layers for longer IR wavelengths as compared to the abrupt strong absorption at the RPE layer for visible and nearer-IR wavelengths.

TABLE 1: Retinal ED_{50} damage thresholds for 200-800 μsec pulsed laser exposures in the rhesus.

WAVELENGTH	PULSE DURATION	ED_{50}	SOURCE
530 nm	600 μs	0.038 mJ	Vassiliadis
530 nm	600 μs	0.074 mJ	Vassiliadis
694.3 nm	200 μs	0.08 mJ	Vassiliadis
755.4 nm	320 μs	0.118 mJ	Lund
755.4 nm	760 μs	0.135 mJ	Lund
1060 nm	600 μs	4.7 mJ	Vassiliadis
1315 nm	300 μs	325 mJ	This study
1315 nm	300 μs	335 mJ	This study
1318/1338 nm	650 μs	356 mJ	Lund

Corneal ED_{50} threshold data for ~1.315-μm wavelengths is summarized in Table 2. Of course, the safety standard MPE levels for wavelengths between 0.4 and 1.4 μm are based only upon recognition of the potential for retinal damage. The current study suggests that for a 350-μsec pulse duration, the retinal hazard, in terms of energy density incident upon the eye, is, indeed, considerably more appreciable than the corneal hazard (the ED_{50} for the retina is 1 J/cm^2 compared to 42 J/cm^2 for the cornea). However for 10-sec exposure durations at 1.318 μm, the cornea is the primary damage site and no retinal effect was found. Finally, an earlier study[3-5] found that for ~0.28 sec exposure durations at 1.318 μm, the corneal and retinal damage thresholds were comparable.

TABLE 2: Corneal ED_{50} damage thresholds for 1.3-1.4 μm laser exposures in rabbit and rhesus.

WAVELENGTH	PULSE DURATION	ED_{50}	DIAMETER	SOURCE
1315 nm	300 μs	42 J/cm^2	1.0 mm	This study
1318nm	10 s	1890 J/cm2	0.8 mm	This study
1318 nm	0.28 s	175 J/cm2	1.0 mm	Zuclich
1356 nm	0.33 s	87 J/cm	0.7 mm	Zuclich
1318/1338 nm	5.0 s	212 J/cm2	1.4 mm	Lund
1318/1338 nm	0.25 s	45 J/cm2	0.4 mm	Lund

Table 3 summarizes this comparison of corneal (c) and retinal (r) ED_{50} levels. Figure 13 depicts how the retinal threshold (TIE) for the 350-μsec pulsewidth case varies with pupil diameter when quoted in terms of corneal radiant exposure and indicates that the retinal threshold lies well below the corneal threshold for the same pulse duration and wavelength unless the pupil diameter is restricted to its minimum size (~2 mm). On the other hand, the data indicate that for 0.28 sec exposures, the retinal and corneal thresholds cross at the largest pupil diameter (≥5mm) and otherwise the retinal ED_{50} level is higher and the cornea is damaged first. For still longer exposure durations (e.g. the 10-sec data of the current study) the retinal ED_{50} curve lies well above the corneal threshold level for all pupil diameters and the ocular risk is only to the anterior ocular tissues.

Table 3 also lists the ratios of ED_{50} threshold dose to MPE for each exposure condition studied. The corneal comparisons are based on the corneal MPE for 1.4 μm, as the corneal MPE is not defined for shorter wavelengths. Recognizing that the corneal and retinal ED_{50}s vary rapidly with wavelength over the wavelength range covered in this study, an extensive analysis included in the earlier publications from this laboratory[3-5] suggested how the MPE levels could be relaxed (in some cases by 2-3 orders of magnitude) and still maintain an adequate margin of safety relative to the experimented ED_{50} data. This earlier analysis[3-5] continues to be supported by the high ED_{50}/MPE ratios listed in Table 3. The remaining caveat is the delayed retinal effects found following pulsed-IR laser exposures and the fact that they involve NFL and Henly fiber layers with potentially serious implications for visual function. The continuing retinal imaging, angiography and histopathological studies in our laboratory are aimed at assuring that the inner retinal and neural retinal layers are not affected at dose levels lower than those reported as ED_{50} thresholds for ophthalmoscopically visible lesions.

TABLE 3: Corneal (c) and retinal (r) ED_{50} damage threshold for three pulse durations used for 1.315-μm laser exposures and comparisons to laser safety standard MPE levels.

WAVELENGTH	PULSE DURATION	ED_{50} (J/cm2)	MPE (J/cm2)	ED_{50}/MPE
1315 nm	300 μs	42 (c)	0.1*	420
1315nm	300 μs	1 (r)	0.00016	6250
1318 nm	0.28 s	175 (c)	0.41*	426
1318 nm	0.28 s	>~175 (r)	0. 028	>~6250
1318 nm	10.0 s	1890 (c)	1. 0*	1890

* Corneal MPE for >~ 1400 nm

ACKNOWLEDGMENTS

The research reported here was supported by contract F41624-97-D-9000 (Littion/TASC) let by the Optical Radiation Division, Air Force Research Laboratory, Brooks AFB, TX. Steven Schuschereba and Harry Zwick of the US Army Medical Research Detachment, Brooks AFB, TX provided support for the histopatholigic and SLO procedures, respectively.

REFERENCES

1. American National Standards Institute, "American national standard for the safe use of lasers", New York, ANSI Standard Z136.1, 2000.
2. Department of the Air Force, "Exposure to laser radiation", Washington D.C., AFI 48-10, 1999.
3. J. A. Zuclich, D. A. Gagliano, F. Cheney, B. E. Stuck, H. Zwick, P. Edsall and D. J. Lund, "Ocular effects of penetrating IR laser wavelengths," SPIE, **2391**, pp. 112-125, 1995.
4. J. A. Zuclich, S. T. Schuschereba, H. Zwick, S. A. Boppart, J. G. Fujimoto, F. E. Cheney and B. E. Stuck, "A comparison of laser-induced retinal damage from infrared wavelengths to that from visible wavelengths," Laser Light Ophthalmol. **8**, pp. 15-29, 1997.
5. J. A. Zuclich, H. Zwick, S. T. Schuschereba, B. E. Stuck and F. E. Cheney, "Ophthalmoscopic and pathologic description of ocular damage induced by infrared laser radiation", J. Laser Appl. **10**, pp. 114-120, 1998.
6. D. J. Finney, *Probit Analysis*, Third Ed., Cambridge University Press, 1971.
7. H. Zwick, D. J. Lund, B. E. Stuck, J. A. Zuclich, R. Elliott, D. A. Gagliano, M. Belkin and R. D. Glickman, "Confocal scanning laser ophthalmoscopic imaging of secondary retinal effects induced by laser radiation", SPIE, **2732**, pp. 187-198, 1996.
8. H. Zwick, M. Belkin, J. A. Zuclich, D. J. Lund, S. T. Schuscheraba and D. K. Scales, "Laser induced nerve fiber layer injury in the non-human primate", SPIE, **2674**, pp. 89-96, 1996.
9. J. Marshall, A. M. Hamilton and A. C. Bird, "Histopathology of ruby and argon laser lesions in monkey and human retina", Brit. J. Ophthalmol. **59**, pp. 610-630, 1975.

Corneal Exposures from 1540 nm Laser Pulses

W.P. Roach[1], T.E.Eurell[2] and Thomas E. Johnson[1]

[1]Department of Preventive Medicine and Biometrics Uniformed Services University, 4301 Jones Bridge Road, Bethesda MD, 20814
[2]Department of Veterinary Biosciences, University of Illinois at Urbana-Champaign, Urbana, IL, 61802

ABSTRACT

Dutch Belted rabbit corneas and corneal equivalent (CE) tissue were exposed to 0.8 millisecond pulses of 1540 nm laser light. We report the single pulse ED_{50} for Dutch belted rabbits and for in-vitro corneal equivalent tissues. A histological comparison between the two tissues is presented. Remarkable similarities between the two models in both location and extent of damage are noted. We postulate which cellular energy absorption mechanisms are significant at 1540 nm and how this relates to the histopathology presented.

Keywords: Cornea, ED_{50}, 1540 nm, "eye safe", rabbit, and corneal equivalent

1. INTRODUCTION

This work supports the theory that 1540 nm laser light is completely absorbed in the cornea between the epithelial and endothelial layers when damage is observed. Ham et al.[1] indicated that 1540 nm laser light energy is absorbed at the cornea prior to reaching the retina of the eye, while other studies have provided inconsistent results in the quantity of radiant energy required to cause corneal damage[1-4]. It is postulated that these discrepancies are in part a function of incident beam area or spot size dependence.

Laser and Noncoherent Light Ocular Effects: Epidemiology, Prevention, and Treatment,
Bruce E. Stuck, Michael Belkin, Editors, Proceedings of SPIE Vol. 4246 (2001)

We examine both the Dutch-belted rabbit[5] corneal model using 1540 nm exposure and a corneal equivalent (CE) model, for contrast and comparison with exposures to the same 1540 nm laser source under similar laboratory conditions as the in-vivo model case. Our collaborators at the University of Illinois at Urbana-Champaign prepare the CE's and they are shipped to us for exposure.[6] One aim of our work is to consider the use of in-vitro CE's as a potential aid in the reduction and eventual replacement of in-vivo corneal tissues.

The Dutch-belted rabbit model has a cornea very similar to that of humans with the exception of a Bowman's Membrane[7, 8]. A clear and concise description of the structural anatomy of the cornea is given in previous work[9] and highlights similarities and differences when comparing animal and human corneal anatomy. We present the estimated dose to 50%, ED_{50}, injury at 95% Fiducial Limits for both the in-vivo (Dutch-belted rabbits) and in-vitro models (CE's), using the $1/e^2$ incident beam areas, and discuss the impact of this work on ANSI -Z136.1-2000[10] is also given.

2. Materials and Methods

2.1 Exposure procedure, sample collection and preparation

As previously indicated by Clarke et al.[11] a total of 7 Dutch Belted rabbits were used to determine ED_{50}'s in-vivo. Rabbits were positioned with the eye held behind a fixed, "ring" target to insure consistent placement of the laser beam on the cornea, indicated in Figure 1. Each cornea was exposed in four locations, producing a total of 28 exposure sites. The animals were maintained under general anesthesia during laser exposure procedures and maintained on buprenorphine for the 24-hour post procedure.[12] Corneas were examined opthalmoscopically and with a slit lamp biomicroscope.

As described in detail by Fletcher et al.[9], live in-vitro CE's produced from rabbit corneas obtained from the University of Illinois at Urbana-Champaign [6]. Transwell containers shipped over night to our lab, containing 12 CE's per tray were exposed the same day. One control CE well was saved from each tray to compare against exposed equivalents. Equivalents were removed from the tray but remained in isolated transwells while being exposed. Only one exposure per equivalent was performed because of histological constraints.

A total of 72 transwells were examined and a total of 60 CE's were exposed to 1540 nm laser light for study. Once exposure levels had been recorded and post exposure experiments performed, the CE's were cold packaged and shipped for histology and genomic expression studies at the University of Illinois at Urbana-Champaign and the United States Air Force Academy, respectively.

Laser beam delivery was accomplished using an Er:Glass laser system producing 1540 nm of light for 0.8 ms in single pulse per exposure and is described in detail elsewhere.[9] The focal point was measured at the $1/e^2$ points for both the in-vivo and in-vitro set ups shown in Figure 1 using a knife edge technique previously described by Cain et al.[13]

For the in-vivo model, exposures were made at 26.7 cm from the 1540 nm focusing lens for an elliptical area of 0.002 cm^2, at the $1/e^2$ points. Rabbit corneas were exposed to between 14.4 and 133.7 J/cm^2. For the in-vitro model of CE's in transwells, exposures were made at 25.4 cm from the 1540 nm focusing lens for an average elliptical area of 0.003 cm^2, at the $1/e^2$ points. CE's were exposed to between 56.4 and 124.2 J/cm^2.

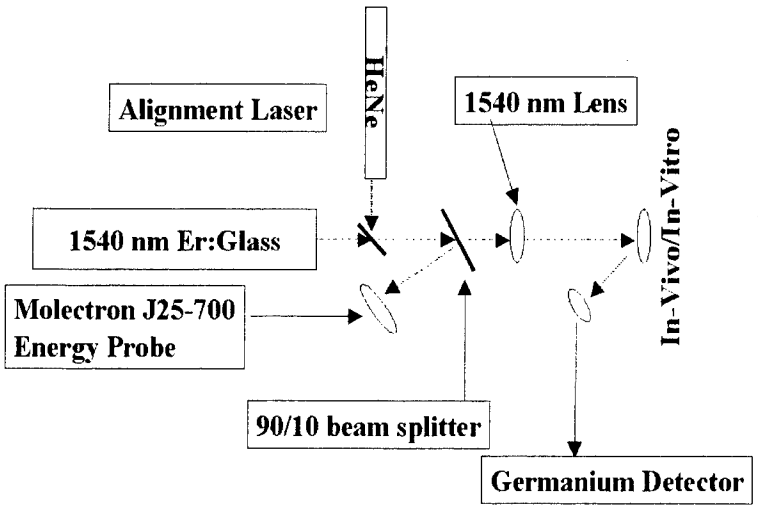

Figure 1: Simple schematic of current laser set up for 1540 nm delivery to *in vivo* and *in vitro* models.

2.2 Sample evaluation

Rabbit corneas were examined both pre- and post exposure opthalmoscopically, and using slit lamp biomicroscopy at acute, 1 and 24-hours post exposure. Damage sites were easily distinguished from normal tissue upon acute exposure examination. Histological examination of the cornea was accomplished by sectioning and staining with hematoxylin and eosin (H&E). Similarly, each CE was visually examined prior to exposure and immediately after exposure. CE's were then sent to the University of Illinois at Champaign-Urbana.

Probit analysis using Easy Probit[14] statistical package was used to determined the estimated dose for 50% probability of laser induced damage, ED_{50}, for both the corneal equivalents and the in-vivo corneal models. Grading of each lesion was performed using three independent readers as described elsewhere[9].

3. Results

Lesions produced in-vivo at the cornea by single pulse, 0.8 ms, 1540 nm laser were clearly visible upon examination. No lesions noted initially or at one hour appeared

to decrease or resolve over a 24-hour period. Ophthalmoscopic and slit lamp examination of the corneas did not identify any lesions that were not seen with careful, examination. Under slit lamp examination, lesions were well demarcated with a sharp border and no apparent damage outside the area of beam intersection with corneal tissue.

Exposed rabbit corneas based on our Probit analysis produced an ED_{50} of 56.7 J/cm^2 at the 95% Fiducial Limits. The Probit curve for the Dutch-belted rabbit cornea exposure to 1540 nm light for 0.8 ms is given in Figure 2.

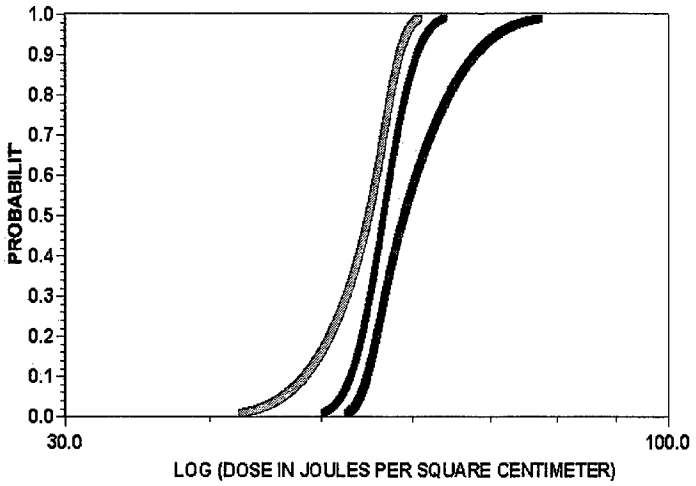

Figure 2. Probit Curve at the 95% Confidence Level For In-Vivo Corneal Exposure To 1540 nm

Similarly, lesions produced at in-vitro CE surfaces by single pulse, 0.8 ms, 1540 nm laser light were clearly visible upon examination. Acute lesions were analyzed using and produced an ED_{50} of 83.7 J/cm^2 at the 95% Fiducial Limits. The Probit curve for the CE exposure to 1540 nm light for 0.8 ms is given in Figure 3. A summary of the results obtained is given in Table 1.

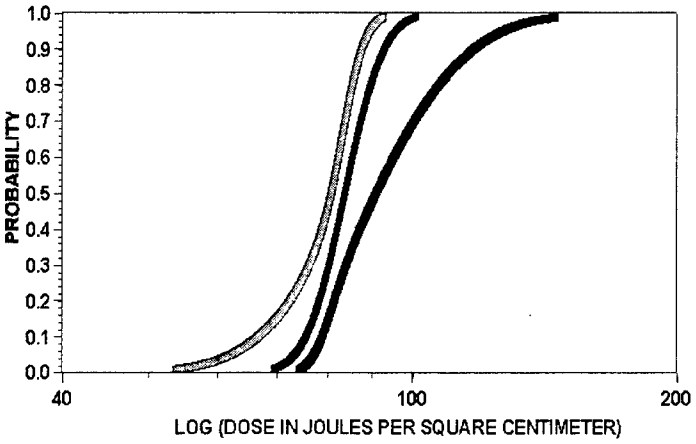

Figure 3. Probit Curve at the 95% Confidence Level For Corneal Equivalent Exposure To 1540 nm

Table 1. Summary of Probit analysis results for 1540 nm exposure at 24 hr.

Subject	No. of Subjects	No. of Data Points	Lower FL (J/cm^2)	ED_{50} (J/cm^2)	Upper FL (J/cm^2)
In-Vivo Dutch-belted Rabbit	7	28	54.9*	56.7*	58.9*
In-Vitro Corneal Equivalents	72	60	80.5*	83.7*	90.6*

* Values are calculated at the $1/e^2$ incident average beam area of 0.002 cm^2 for the Dutch-belted rabbits and 0.003 cm^2 for the Corneal Equivalents.

4. Discussion and Conclusions

The data clearly shows that 1540 nm laser light causes significant in-vivo and en-vitro corneal damage at reproducible energy levels. The ED_{50} for the CE's was found to be 83.7 J/cm^2 an the in-vivo corneal ED_{50} was found to be 56.7 J/cm^2, both at 95% fiducial limits with reproducible statistical significance. We note that the fiducial limits centered about the ED_{50} do not overlap between the in-vivo and in-vitro models. This leads to the proposal that either a mathematical factor exists that will allow us to extrapolate from in-vitro exposures to in-vivo, or the CE's are not a reasonable replacement model for in-vivo study at this time.

CE's and in-vivo corneas showed remarkably similar histological findings in the stroma as evidenced by the extensive damage to collagen. This leads us to believe that the in-vitro model is very close to mimicking the in-vivo model as a replacement for in-vivo laser exposure study. Continued research is clearly necessary. Limited studies using non-human primate models should be done to insure that the presence of Bowman's membrane does not significantly alter the in-vivo corneal injury pattern. Further, once the correct scientific connection between the in-vitro and in-vivo model is delineated, studies to compare the in-vitro to non-human primate study must be accomplished.

ACKNOWLEDGMENTS

This research was supported by the Air Force Office of Scientific Researchunder Grant # FQ8671-9900412 (PMB # G687HQ-04), the Uniformed Services University of the Health Sciences Departments of Preventive Medicine and Biometrics and Laboratory Animal Medicine.

References

1. W. T. Ham and H. Mueller, "Ocular effects of laser radiation," *Journal of Laser Applications* **3**, p. 19, 1991.

2. D.J. Lund, M.B. Landers, G.H. Bresnick, J.O. Powell, J.E. Chester, C. Carver, "Ocular hazards of the Q-switched erbium laser," *Investigative Ophthalmology*, 1970, **9**, pp. 463-470, 1970.

3. B. E. Stuck, D. J. Lund, and E. S. Beatrice, "Ocular effects of holmiun (2.06 um) and erbium (1.54 um) laser radiation," *Health Physics* **40**, pp. 835-846, 1991.

4. W.T. Ham, H.A. Mueller, *Ocular effects of laser infrared radiation*, Research Report to Bell Telephone Laboratories, Virginia Commonwealth University, Virginia, 1989.

5. The animals involved in this study were procured, maintained and used in accordance with the Animal Welfare Act and the "Guide for the Care and Use of Laboratory Animals" prepared by the Committee on Care and Use of Laboratory Animals of the Institute of Laboratory Animal Resources, National Research Council. The Uniformed Services University of the Health Sciences has been fully accredited by the Association for the Assessment and Accreditation of Laboratory Animal Care, International since 1982.

6. T. Eurell, DVM, PhD, University of Illinois at Urbana-Champaign College of Veterinary Medicine, Urbana, Illinois. Protocol established in 1998 for corneal equivalent work.

7. D. Slatter, *Fundamentals of Veterinary Ophthalmology*, W.B. Saunders, Philadelphia, 1990.

8. W. Spencer, *Ophthalmic Pathology: An Atlas and Textbook*, W.B. Saunders, Philadelphia, 1996.

9. D.J. Fletcher, T.E. Johnson, M.A. Mitchellb, T.E. Eurell, P.J. Rico, W. P. Roach, "Corneal Equivalents: a Replacement Model for In-vivo 1540 nm Laser Exposure Studies", Procedings of SPIE Vol. 3907-E-69, (2000).

10. ANSI, *American National Safety Standard for Safe Use of Lasers (ANSI Z136.1-2000)*, Laser Institute of America, Inc., Orlando, 2000.

11. Thomas F. Clarke, W.P. Roach, Bryan Ketzenberger, and T.E. Johnson "Corneal Injury Threshold And Public Health Implications Of The 1540 Nm Laser (Infrared Laser Eye Injury)" submitted to the Journal of Aviation Space and Environmental Medicine, Nov 2000.

12. W.P. Roach, T.E. Johnson, T.A. Eggleston, and M. Mitchell, "Risk Assessment of the "Eye Safe Laser" Wavelength for Cornea and Skin (Rabbits, Pigs)" Animal Use Protocol, G387HQ, April 1996.

13. C.P. Cain, C.A. Toth, C.D. DiCarlo, C.D. Stein, G.D. Noojin, D.J. Stolarski, and W.P. Roach, "Visible Retinal Lesions From Ultrashort Laser Pulses In the Primate Eye", Inves Oph and Vis Sci, 36, 5, 879 (1995).

Corneal damage thresholds for multiple-pulse exposures to 2.02 μm radiation from a Tm:YAG laser[†]

Russell L. McCally*[1,2] and C. Brent Bargeron*[1]

[1]The Johns Hopkins University Applied Physics Laboratory, [2]The Wilmer Ophthalmological Institute of the Johns Hopkins Medical School

ABSTRACT

Corneal epithelial damage thresholds were determined for exposures to sequences of pulses from a Tm:YAG laser (wavelength 2.02 μm). Pulse repetition frequencies were 1, 10, 20, and 100 Hz and individual pulse durations were 0.300 sec at 1 Hz, 0.025 sec at 10 and 20 Hz, and 0.005 sec at 100 Hz. Threshold damage is correlated by an empirical power law of the form $I_{th} = CN^{-\alpha}$, in which I_{th} is the threshold irradiance and N is the number of pulses. The constant C differs depending on the pulse repetition frequency and individual pulse duration. The exponent α varies between 0.22 and 0.29. For some exposure conditions the empirical power law underestimates the damage threshold for small numbers of pulses.

1. INTRODUCTION

The spectral region for wavelengths greater than about 1.4 μm is often called "eyesafe" because the cornea and aqueous humor have sufficient absorption to prevent damaging levels of radiation from reaching the retina. However, because of its absorption, the cornea itself can sustain thermal damage. Much of the work that has been done investigating corneal damage thresholds in the infrared has been for CO_2 radiation at 10.6 μm.[1-5] Radiation at this wavelength is strongly absorbed, having an absorption depth of only ~10 μm[6] (the absorption depth is the depth at which the irradiance is diminished to 1/e or 37% of its incident level). Therefore CO_2 radiation would be almost entirely absorbed within the 50 μm thick human corneal epithelium [1, 7]). A few studies have been conducted for more penetrating radiation. Stuck et al [8] investigated thresholds for Holmium laser radiation at 2.06 μm (absorption depth ~250 μm [6]) for exposure durations of 100μsec and 42 nsec and for Erbium laser radiation at 1.54μm.(absorption depth greater than 900 μm [6]) for an exposure duration of 930 μsec;. Thresholds have also been determined for Tm:YAG laser radiation for exposure durations between 0.08 and 4.3 sec.[9] The absorption depth of Tm:YAG radiation is 182 μm,[6] thus 94 % of this radiation would be absorbed in a 520 μm thick human cornea.

Many laser systems emit sequences of pulses; however the only investigations of corneal damage thresholds for multiple-pulse exposures have been for CO_2 laser radiation.[1, 10, 11] These investigations showed, that over a wide range of exposure conditions, thresholds could be correlated by a power law that relates the threshold irradiance in Watts per square centimeter (or radiant exposure in Joules per square centimeter per pulse for short pulses) to the number of pulses in the sequence. In view of the widely varying absorption properties of the cornea for wavelengths greater than 1.4 μm it is important to extend investigations of threshold damage for sequences of pulses to more penetrating wavelengths. Such investigations provide a rational scientific basis for setting laser safety standards. In this study we have determined epithelial damage thresholds for sequences of pulses Tm:YAG laser radiation.

[†] In conducting the research described in this report, the investigators adhered to the "*Guide for Care and Use of Laboratory Animals*" prepared by the Committee on Care and use of Laboratory Animals of the Institute of Laboratory Animal Resources, Commission on Life Sciences, National Research Council.
The views, opinions and/or findings contained in this report are those of the authors and should not be construed as an official Department of the Army position, policy, or decision unless so designated by other documentation.

* Russell.McCally@jhuapl.edu, phone-443-778-6201; FAX 443-778-5889; The Johns Hopkins University Applied Physics Laboratory, 11100 Johns Hopkins Road, Laurel, MD 20723-6099 USA; Brent.Bargeron@jhuapl.edu, phone 443-778-6240; FAX 443-778-6904

Laser and Noncoherent Light Ocular Effects: Epidemiology, Prevention, and Treatment,
Bruce E. Stuck, Michael Belkin, Editors, Proceedings of SPIE Vol. 4246 (2001)

2. METHODOLOGY

2.1 Laser System

A continuous wave diode pumped Tm:YAG laser was used for the exposures. This laser emits mid-infrared radiation at a wavelength of 2.02 μm and operates in the TEM_{00} mode. The laser's wavelength was verified by measuring its output with a SPEX Minimate spectrometer with a 300 line/mm grating. Mode quality was verified by directly viewing of the beam on a fluorescent screen and by profiling with a knife-edge.[12, 13] The irradiance profile for a laser operating in the TEM_{00} mode has a Gaussian shape. The power measured as a knife-edge is scanned in the x direction across a Gaussian beam is given by

$$P(x) = \frac{P}{2}\left\{1 - erf\left[\frac{(x - x_0)}{r_{1/e}}\right]\right\}, \qquad (1)$$

where x_0 is the position of the center of the beam, P is the total laser power and $r_{1/e}$ is the 1/e radius of the beam and *erf* is the error function.[12, 13] We use the program Mathematica to obtain a non-linear least squares fit to Equation 1 in terms of the three parameters $r_{1/e}$, x_0, and P. The results of a typical beam scan are shown in Fig. 1. The value of χ^2 for the fit indicates that the beam quality is excellent.

The nominal 1/e radius of the laser beam was 1 mm (cf. Fig. 1). The actual beam diameter at the position of the cornea surface was controlled with a quartz lens and was determined at each experimental session. Beam power was adjusted

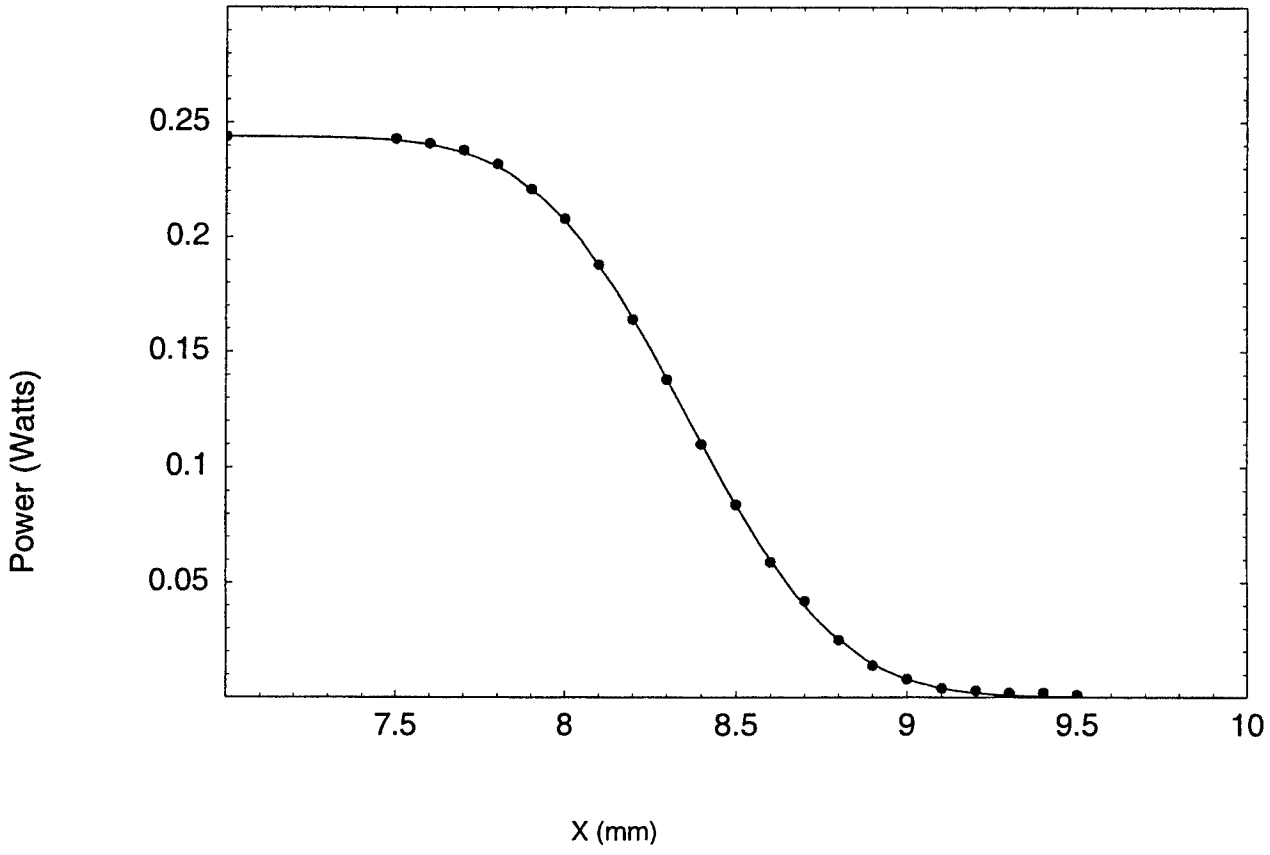

Figure 1: Profile of the Tm:YAG laser beam using a scanning knife edge. The solid line is a best least-squares fit to Equation 1, for which $r_{1/e}$ = 0.492 mm, x_0 = 8.359 mm, and P = 0.244 W. For this fit, $\chi^2 = 1.7 \times 10^{-6}$, which indicates that the fit is excellent.

using a circular linear wedge neutral density filter that varies continuously from 0 to 1.0 OD and was measured with a Scientec detector before and after each exposure. Exposure duration and pulse rate for exposures at pulse repetition frequencies of 10, 20, and 100 Hz were controlled with a Princeton Applied Research chopper. The chopper was used in conjunction with a Uniblitz shutter that acted as a gate to allow passage of the desired number of pulses.[14] Pulse durations and pulse repetition frequencies were measured using a LeCroy 9354M digital oscilloscope. For exposures at a frequency of 1 Hz, the pulse duration and frequency were controlled with the Uniblitz shutter which was calibrated using the digital oscilloscope.

2.2 Animals

New Zealand white rabbits of either sex weighing 1.8 – 2.3 kg were used for the experiments. The rabbits were anesthetized with an intramuscular injection of a mixture of xylazine (12 mg/kg) and ketamine hydrochloride (40 mg/kg). A topical anesthesia (proparacaine hydrochloride 1/2%) also was applied to each eye and a drop of homatropine bromide 5% was instilled to dilate the pupil. Homatropine facilitates examining the exposed corneas for minimal lesions. The anesthetized animals were placed in a conventional holder where they were positioned with the aid of a He-Ne laser whose beam was aligned to be coaxial with the Tm:YAG laser beam. The eyes were positioned so that incident beam from the Tm:YAG laser would be perpendicular to the central cornea. A speculum was inserted in the eye about one minute prior to exposure. In order to create a reproducible tear film, the eye was irrigated with a small amount of physiological saline solution (BSS - Alcon Surgical) that was at room temperature. Irrigation was stopped about 20 sec before exposure and the excess fluid was blotted at the limbus. The corneal surface was assumed to have returned to its normal temperature at the time of exposure. One-half hour after exposure, the rabbits, still under anesthesia, were sacrificed with Beuthanasia-D (100 mg/kg) administered in an ear vein. The eyes were enucleated and immediately examined for damage using a Nikon FS-3 photo slit-lamp.

2.3 Damage Determination

The criterion used to determine minimal epithelial damage was the presence of a superficial, barely visible, gray-white spot that develops within one-half hour after exposure.[2] In these experiments the damage threshold is well defined. Only rarely is there any overlap between exposures that produce minimal lesions and those that do not. Therefore statistical procedures such as probit analysis were not used to determine the threshold, as these would require using more animals than necessary.[1, 9] One exposure was made per eye, initially attempting to find broadly bracketing exposures above and below threshold. The bracket was then narrowed until there was only about a 10% difference in irradiance between an exposure that produced a minimal lesion and one that did not. The threshold exposure was taken to be at the center of the bracket.

3. RESULTS

Epithelial damage thresholds were measured for sequences of pulses at frequencies of 1, 10, 20, and 100 Hz. The duration of the individual pulses was 0.300 sec at 1 Hz, 0.025 sec at 10 and 20 Hz, and 0.005 sec at 100 Hz. The threshold for a single 0.300 sec pulse also was determined. All damage thresholds are compiled in Table 1. The threshold for the single 0.300 sec pulse is consistent with single-pulse damage thresholds that were determined for Tm:YAG radiation in an earlier study (cf., Fig. 2).[9] All lesions, even those produced by exposures above threshold, were circular and well defined.

The threshold irradiances for the exposures at 1 Hz (0.300 s pulse duration) are plotted in Fig. 3 as a function of the number of pulses. The line is a least-squares fit to a power law of the form, $I_{th} = CN^{-\alpha}$ where $C = 33.8$ W/cm^2 and $\alpha = 0.287$ ($R = 0.997$). The value of the constant C is within 4 percent of the threshold irradiance of the single 0.300 sec pulse. As will be shown below, this contrasts with the results obtained for sequences of 0.025 sec pulses at frequencies of 10 and 20 Hz and sequences of 0.005 sec pulses at 100 Hz.

The threshold irradiances for the exposures at 10, 20 and 100 Hz listed in Table 1 are plotted in Fig. 4 as functions of the number of pulses. It is evident that a power law of the form $I_{th} = CN^{-\alpha}$ also can relate the data for these three exposure conditions, at least for the values of N for which thresholds were measured. The values of the parameters C and α

Table 1: Threshold irradiances for sequences of pulses of Tm:YAG radiation at 2.02 μm.

Number of Pulses	Pulse Repetition Frequency (Hz)	Pulse Duration (sec)	I_{th} (W/cm^2)	$d_{1/e}$ (mm)
1		0.300	32.5	0.938
8	1	0.300	19.6	0.946
32	1	0.300	12.9	1.040
128	1	0.300	8.04	1.032
25	10	0.025	35.0	0.936
50	10	0.025	29.2	0.984
200	10	0.025	19.6	1.010
999	10	0.025	15.5	1.018
25	20	0.025	25.4	1.016
50	20	0.025	22.2	0.984
200	20	0.025	17.4	0.972
999	20	0.025	11.2	0.984
150	100	0.005	26.1	0.974
200	100	0.005	26.0	0.928
500	100	0.005	19.0	0.934
999	100	0.005	15.5	1.016

[a] Calculated on the beam axis, 10 μm beneath the anterior tear surface.

obtained from the least squares fits are respectively: 70.0 W/cm^2 and 0.22 for the thresholds at 10 Hz (R = 0.99); 52.7 W/cm^2 and 0.22 for the thresholds at 20 Hz (R = 0.99); and 116 W/cm^2 and 0.29 (R = 0.99) for the thresholds at 100 Hz.

The fits for the 10 and 20 Hz exposures have the same value of the parameter α, but have different values of the parameter C (i.e., they are parallel on the log-log plot). Therefore, the power law relationships must break down for smaller numbers of pulses, because they do not converge to the same value for the single-pulse threshold. Indeed, on the basis of previous data[9] and the threshold for a single 0.300 sec pulse that was determined in this study, the values of the parameter C for both sets of data are much lower than the threshold that would be expected for an exposure to a single 0.025 sec pulse. . The single-pulse data suggest that the threshold for a 0.025 sec exposure with a 1/e beam diameter of 1 mm would be approximately 100 W/cm^2 (c.f., Fig. 2). The maximum power output of the Tm:YAG laser available for this study (~0.3 W, which includes the reflective losses at the quartz focusing lens and the attenuator) precluded obtaining thresholds with 0.025 sec pulses and a 1/e beam diameter of ~1 mm for less than 25 pulses at 10 Hz and for less than about 10 pulses at 20 Hz. Similarly, the value of C for the exposures to 0.005 sec pulses at 100 Hz also is lower than the single-pulse threshold that would be predicted from the data in Fig. 2 (viz., ~190 W/cm^2). Therefore at present, we are not able to determine where the data begin to deviate from the power law dependence as the number of pulses is reduced.

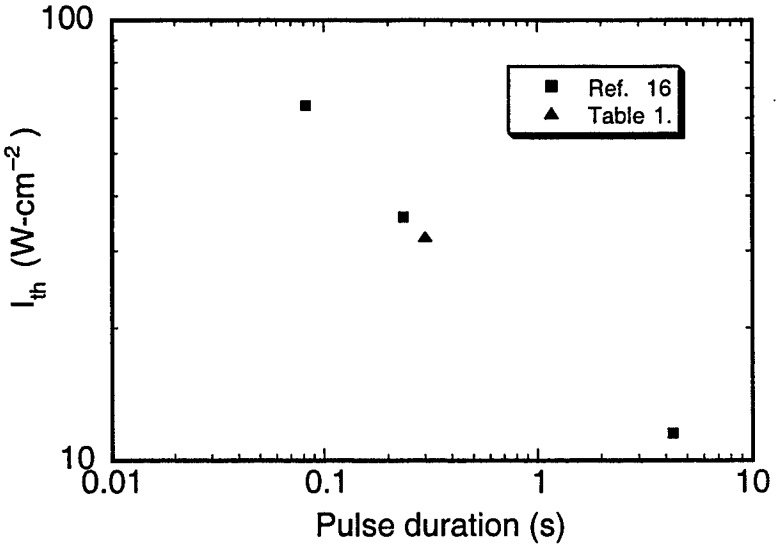

Figure 2: Dependence of the threshold irradiance on on pulse duration for single pulses of Tm:YAG laser radiation.

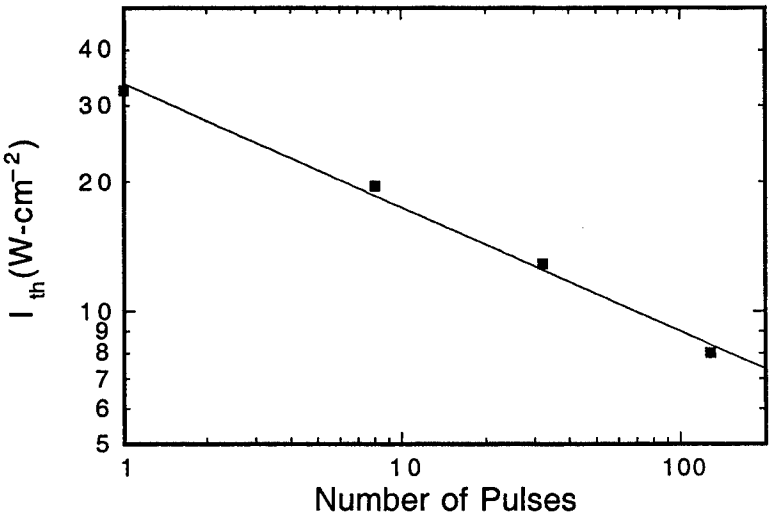

Figure 3: Dependence of the threshold irradiance on the number of pulses at pulse repetition frequency of 1 Hz. The individual pulse duration was 0.300 sec. The line is a least squares fit to a power law of the form $I_{th} = CN^{-\alpha}$.

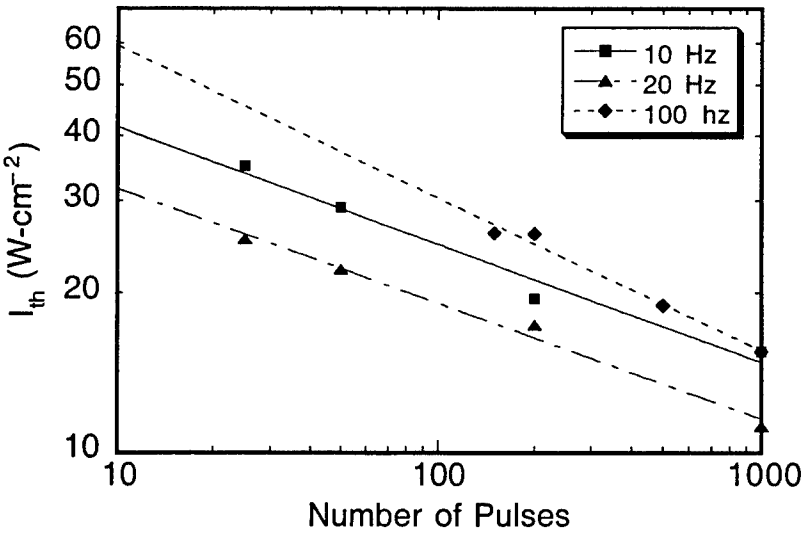

Figure 4: Dependence of the threshold irradiance on the number of pulses at pulse repetition frequencies of 10, 20 and 100 Hz. The lines are least-squares fits to a power law of the form $I_{th} = CN^{-\alpha}$.

The results for Tm:YAG damage show that, for small numbers of pulses, there can be substantial deviations from the predictions of damage thresholds provided by an empirical relationship of the form $I_{th} = CN^{-\alpha}$. The deviations are such that a relationship of this form, which accurately correlates the damage for large numbers of pulses, underestimates the damage threshold for small numbers of pulses and the single-pulse threshold.

4. CONCLUSIONS

Corneal epithelial damage thresholds for multiple-pulse exposures to mid-infrared radiation from a Tm:YAG laser at a wavelength of 2.02 μm are correlated by a power law of the form $I_{th} = CN^{-\alpha}$, which relates the threshold irradiance, I_{th}, to the number of pulses in the sequence. The constant C differs depending on the pulse repetition frequency and individual pulse duration. The exponent α varies between 0.22 and 0.29. For exposures to 0.300 sec pulses at 1 Hz, the value of C is within 4 percent of the threshold for a single pulse. Because of laser power limitations, thresholds could not be determined for fewer than 25 pulses at pulse repetition frequencies of 10 and 20 Hz (pulse duration 0.025 sec), and for fewer than 150 pulses at 100 Hz (pulse duration 0.005 sec). For these exposure conditions the value of C is less than the predicted threshold for single pulses having the same durations. In terms of setting safety standards, the power law determined for larger numbers of pulses will, at least for some exposure conditions, underestimate the damage threshold for small numbers of pulses. This would provide an additional margin of safety for small numbers of pulses. However, if one were to use the measured damage threshold for a single-pulse exposure for the value of the constant C, the resulting relationship would tend to overestimate the damage threshold for large numbers of pulses (i.e., it would lessen the margin of safety).

5. ACKNOWLEDGEMENTS

This work was supported by U. S. Army Medical Research and Materiel Command under contract No. DAMD17-96-C-6005 and by the National Eye Institute under Grant EY 12165. The authors are also pleased to recognize valuable discussions with Bruce Stuck of the U. S. Army Medical Research Detachment, Walter Reed Army Institute of Research, Brooks AFB, TX.

6. REFERENCES

1. C. B. Bargeron, O. J. Deters, R. A. Farrell, and R. L. McCally, "Epithelial Damage in Rabbit Corneas Exposed to CO_2 Laser Radiation," *Health Phys.* **56**, 85-95 (1989).
2. A. S. Brownell and B. E. Stuck, "Ocular and Skin Hazards from CO_2 Laser Radiation," in *Proceedings of the 9th Army Science Conference*, U. S. Military Academy, West Point, NY, 123-138 (1974).
3. D. E. Egbert and E. F. Maher, "Corneal Damage Thresholds for Infrared Laser Exposure: Experimental Data, Model Calculations, and Safety Standards," USAF School of Aerospace Medicine, Brooks AFB (1974).
4. R. R. Peabody, H. Rose, N. A. Peppers, and A. Vassiliadis, "Threshold Damage from CO_2 Lasers," *Arch. ophthalmol.* **82**, 105-107 (1969).
5. N. A. Peppers, *et al.*, "Cornea Damage Thresholds for CO_2 Laser Radiation," *Appl. Optics* **8**, 377-381 (1969).
6. E. F. Maher, "Transmission and Absorption Coefficients for Ocular Media of the rhesus monkey," USAF School of Aerospace Medicine, Brooks AFB (1978).
7. D. M. Maurice, *The Cornea and Sclera*, in *The Eye,* H. Davson (ed.), Academic Press, Orlando (1984).
8. B. E. Stuck, D. J. Lund, and E. S. Beatrice, "Ocular Effects of Holmium (2.06 μm) and Erbium (1.54 μm) Laser Radiation," *Health Physics* **40**, 835-846 (1981).
9. R. L. McCally, R. A. Farrell, and C. B. Bargeron, "Cornea Epithelial Damage Thresholds in Rabbits Exposed to Tm:YAG Laser Radiation at 2.02 μm," *Lasers in Surgery and Medicine* **12**, 598-603 (1992).
10. R. L . McCally and C. B. Bargeron, "Epithelial Damage Thresholds for Sequences of 80 ns Pulses of 10.6 μm Laser Radiation," *Jour. of Laser Appl.* **10**, 137-139 (1998).
11. R. L. McCally and C. B. Bargeron, "Epithelial Damage Thresholds for multiple-Pulse Exposures to 80 ns Pulses of CO_2 Laser Radiation," *Health Physics* **80**, 41-46 (2001).
12. J. M. Khosrofian and B. A. Garetz, "Measurement of a Gaussian Laser Beam Diameter by the Direct Inversion of Knife-edge Data," *Appl. Optics* **22**, 3406-3410 (1983).
13. R. L. McCally, "Measurement of Gaussian Beam Parameters," *Appl. Optics* **23**, 2227 (1984).
14. C.B. Bargeron, R. A. Farrell, W. R. Green, and R. L. McCally, "Threshold Corneal Damage from Very Short Pulses of CO_2 Laser Radiation," *Supplement to Invest. Ophthalmol. and Vis. Sci.* **30**, 217 (1989).

Concepts in dosimetry related to laser safety and optical radiation hazard evaluation

Karl Schulmeister[§]

Austrian Research Centers Seibersdorf, A-2444 Seibersdorf, Austria

ABSTRACT

Concepts in dosimetry pertinent to hazard evaluation of optical radiation and specifically laser radiation are discussed. The basic units of power, energy, irradiance, exposure and radiance will be reviewed, as well as the relation of retinal exposures and experimental data given as intra-ocular energy to exposure limits specified in exposure at the cornea or time integrated radiance.

Averaging apertures and field of views are specified with the exposure limits to be used when exposure values are measured or calculated which in turn are compared to exposure limits for laser radiation or broadband optical radiation. The size of the averaging aperture for irradiance measurements or the size of the averaging field of view for radiance measurements is closely linked to biophysical effects and dimensions such as the diameter of the pupil of the eye or the angular extent of eye movements. In some cases, the specified size of the averaging aperture and FOV result in measured irradiance and radiance values, which are much smaller than the real physical values.

In the latest revision of the international laser safety standard, IEC 60825-1, and in the revised ICNIRP laser limits, blue light limits are split from the thermal limits and are given in irradiance, specifying corresponding measurement criteria for the measurement FOV. The derivation of the irradiance limit from the basic radiance limit as it is specified for the broadband blue light hazard (for instance by ACGIH and ICNIRP) can be understood on the basis of the specification for the measurement FOV.

Keywords: dosimetry, radiometry, laser safety, optical radiation, hazard evaluation, exposure limit, Maximum Permissible Exposure, averaging aperture, field of view, photochemical retinal limit

1. INTRODUCTION

Exposure limits for laser radiation and broadband optical radiation are defined on the basis of animal experiments and on injury data, and the levels are set so that adverse effects or injuries are prevented if the exposure level is below the exposure limit (EL) for a given exposure duration and wavelength.

As the optical and thermal properties of the skin and the eye are different, the ELs for the eye and the skin differ, especially in the retinal hazard wavelength region[*]. Consequently there is a set of ELs for ocular exposure and another one for the skin. The ELs depend on the exposure duration and the laser wavelength and may also depend on the size of the source-image on the retina. This image size is expressed as angular subtense of the apparent source and will be discussed in the body of the paper.

In order to evaluate the potential hazard of exposure to optical radiation, the level of exposure at a given location and for a given exposure scenario, including the exposure duration, need to be assessed, and this value is then compared to the EL for the given exposure duration, wavelength and, if applicable, the angular subtense of the apparent source. This process of hazard evaluation, i.e. of assessing (calculating or measuring) the level exposure on the one hand and comparing this value with the appropriate exposure limit on the other hand is commonplace in health physics. For optical radiation hazard assessments, it is particularly important to keep this concept in mind in order to understand the close link of the measurement and the EL, which is somewhat unique for optical radiation, as will be elaborated in this paper. Wording such as "the EL is measured", can lead to confusion, as it is the *exposure* which is to be measured (with a certain averaging aperture and field of view), and this exposure value is consequently to be compared to the EL.

The internationally accepted committee which defines exposure limits for laser radiation and broadband optical radiation is the International Commission for Non-Ionizing Radiation Protection, which publishes the respective guidelines in the

[§] karl.schulmeister@arcs.ac.at; phone +43 50550 2533; fax +43 50550 2502; http://www.arcs.ac.at/G/GS

[*] The retinal hazard region is the wavelength range between 400 nm and 1400 nm, where the radiation is focused onto the retina of the eye.

Laser and Noncoherent Light Ocular Effects: Epidemiology, Prevention, and Treatment,
Bruce E. Stuck, Michael Belkin, Editors, Proceedings of SPIE Vol. 4246 (2001)

Health Physics journal[1,2,3]. A number of national and international standards adopted these exposure limits for specific purposes, such as the international laser safety standard[4] IEC 60825-1.2, which is mainly a product requirement standard, but also features a section on user guidelines, or the American National Standard[5] ANSI Z136.1, a laser user standard. In both documents, the exposure limits are called maximum permissible exposure limits, MPEs, but they are identical to the EL as published by ICNIRP. Regarding broadband radiation, several document were developed and published in recent years, which made use of the exposure limits as specified by ICNIRP: for lamp safety, the northern American[6] IESNA RP-27 required practice series for lamp manufacturers, a standard developed by the international lighting committee[7] CIE, with the aim to serve as basis for an international lamp product safety standard, and a technical report of the International Electrotechnical Committee[8], IEC 60825-9, where the goal was to summarize the ICNIRP exposure limits for incoherent broadband radiation.

Above documents also specify the measurement requirements which need to be observed when assessing the level of exposure. The goal of this paper is to review the measurement requirements in terms of what could be called "geometrical aspects" of the measurement, i.e. mainly the averaging aperture and the field of view, and to discuss the origin and background to these requirements. This review concentrates on the hazard evaluation of a given exposure szenario of the general public or in the work place, in contrast to product safety requirements, where the emission of a product has to be tested against specified requirements. However, much of the discussion is also applicable to the classification of laser products following the concept of allowable emission limits, AEL, as for instance used in IEC 60825-1 or ANSI Z136.1, since the AELs of Class 1 and Class 2 are directly derived from the exposure limits for the eye by multiplication with the area of the averaging aperture.

2. OVERVIEW OF QUANTITIES AND UNITS

The quantities and units relevant for the definition of exposure limits and for measurements and hazard evaluation of exposure to laser radiation and optical radiation are summarized in Table 1.

Table 1. Quantities and units used to express exposure limits and to measure and evaluate exposures to laser radiation and broadband optical radiation. The letters are the usual symbols used for the respective quantities, as for instance used in IEC 60825-1 and ANSI Z136.1. No specific letter is assigned for the time integrated radiance, and the symbol L·t is used in this paper. It is noted that the units given in the table are the basic SI units, and the usual derived units such as cm^2 and mW are often used in practice.

Power P Unit: *Watt (W)*	Irradiance E Unit: $\frac{W}{m^2}$	Radiance L Unit: $\frac{W}{m^2\,sr}$
Energy Q Unit: *Joule (J)*	Radiant exposure H Unit: $\frac{J}{m^2}$	Time Integrated Radiance L·t Unit: $\frac{J}{m^2\,sr}$
Comment: Basic Quantity	Comment: Averaging over aperture area	Comment: Averaging over aperture area and measurement field of view

2.1 Temporal integration to obtain "dose"

The relationship between the quantities of the first line of Table 1, which could be collectively addressed as "power quantities", with the quantities in the second line, which could be called "energy quantities", is in terms of the quantity "time", as energy equals power multiplied by time. For laser safety and hazard assessment of optical radiation, "time" can have the meaning of exposure duration or pulse duration. The power quantities are usually used for quantification of continuous sources and exposures, however, they can also be used in terms of maximum power levels of pulses, especially for ultrashort laser pulses, where some ELs are given in units of W/m^2. The energy quantities are usually used for quantifying the exposure level** and exposure limit for pulses. However, "energy quantities" are also used for hazard assessment to prevent photochemical damage of the skin or the eye. It is typical for photochemical interaction, that the effect is additive over some duration, which could be called integration duration. For photochemical damage of the eye and the skin by ultraviolet radiation, this integration duration is 8 hours, for photochemical damage of the retina by blue light, the integration duration is 10,000 s, i.e. 2 hours and 47 minutes). Therefore, exposure limits for photochemical damage are

** In this paper, the term "exposure level" is used as general description for the quantity which is assessed for a given exposure situation and which is consequently compared to the exposure limit. It is used as a "catch all" term to represent all relevant quantities as summarized in table 1, including spectral derivatives. Although "intensity" in the everyday use has a corresponding meaning, in optical radiometry it is assigned to the quantity with dimensions power per solid angle (units: W/sr) and is therefore not used in this text in the broad general meaning.

specified as "energy quantity", and the sum of all individual exposures in the sense of a total "dose" need to be compared to the exposure limit. For the case of a constant continuous exposure, the energy quantity is simply obtained by multiplication of the power quantity with the exposure duration. For continuous exposure with varying irradiance or radiance level, the corresponding energy quantity of the exposure is determined by temporal integration over the required integration duration.

The main scope of the paper is to review "geometrical aspects" of the measurement setup and relationship of the quantities as given in table 1 in *horizontal* direction, and these are the same for power and energy quantities. Consequently, in the remainder of the paper, the deliberations apply to both power and energy quantities, even if it is only referred to one of them.

2.2 Broadband radiation, spectral quantities

For laser radiation, where only exposure to discrete wavelengths is an issue, any wavelength dependence of the "effectiveness" of a given level of exposure to produce a lesion, can simply be accounted for in the definition of the exposure limits. For exposure to broadband incoherent radiation, the wavelength dependence is accounted for by action spectra, $s(\lambda)$, which are used to weigh a given (measured) spectral irradiance, $E_\lambda(\lambda)$, measured in units of W m^{-2} nm^{-1} (or spectral radiance, measured in units of W m^{-2} sr^{-1} nm^{-1}) in order to produce an "effective" irradiance, E_{eff} (or radiance) by integration over the wavelength, as is expressed by the equation

$$E_{eff} = E_\lambda(\lambda) \cdot s(\lambda) d\lambda$$

In practice, the spectral irradiance or spectral radiance is measured with spectroradiometers, and the effective irradiance or effective radiance is subsequently calculated numerically. Alternatively, the effective irradiance or radiance can be directly measured with integrating broadband hazard-meters, which feature a spectral sensitivity that mimics the desired action spectrum. The principle of temporal integration of the exposure when the exposure limit is given in energy quantities, as described above, and the geometrical relationships for the measurement as described in the following sections of the paper, apply to spectral quantities in the same way as for non-spectral quantities. Regarding the diameter of the averaging aperture, however, there are differences between the hazard evaluation of broadband radiation in comparison to laser radiation, which will be discussed below.

3. BASIC RADIOMETRIC CONCEPTS

3.1 Irradiance and radiant exposure – averaging over aperture

The text of this paragraph only refers to irradiance, however the dosimetry concept discussed also applies to radiant exposure. For radiation which is absorbed by the surface, irradiance is the appropriate quantity to express the "level of exposure". Irradiance is defined as incident power divided by the area over which the irradiance is determined. If the area to which irradiance is related to becomes infinitesimally small, the irradiance equals the local physical irradiance. For finite areas, the determined irradiance will represent a value averaged over that area. This concept is explained on the basis of the typical practical measurement procedure: a laser radiometer is typically calibrated to measure radiant power or energy incident on the detector with given sensitive area[***]. The sensitive area can also be reduced by an aperture of a given size. In the following, circular apertures or sensitive areas of the detector are assumed and both are generally referred to as aperture. The irradiance is determined by dividing the power as measured with the radiometer by the area of the aperture. If the irradiance profile incident on the detector is not spatially constant over the detector or aperture area, then the resulting irradiance value represents an *value averaged* over the area of the aperture. An example plot of a non-constant irradiance profile and the average value is schematically shown in figure 1. The "averaging" can be conceptualized as "spreading" the total power on the detector over the aperture area.

The aperture area, i.e. measurement area, can also be considered as the smallest spatial *resolution* with which the irradiance can be determined and hotspots in the irradiance profile smaller than the aperture area can not be detected. If the irradiance profile is spatially constant over a given area, then the averaged irradiance is equal to the true physical irradiance value. If the aperture area is decreased, the measured power will decrease correspondingly and the resulting irradiance value remains constant.

In the field of laser safety and for hazard evaluation of broadband optical radiation, specific averaging apertures are specified which are related to biological parameters such as pupil size and eye-movements. In some cases, the specified size of the averaging aperture result in measured irradiance values, which are much smaller than the real physical values.

[***] Some laser radiometers and most spectroradiometers are calibrated to measure irradiance directly. It should be kept in mind that the irradiance value measured is averaged over the sensitive area of the detector for which the calibration has be performed.

However, for hazard evaluations, it is these *biologically effective* values, which have to be compared to the respective exposure limits for optical radiation, as will be discussed further below.

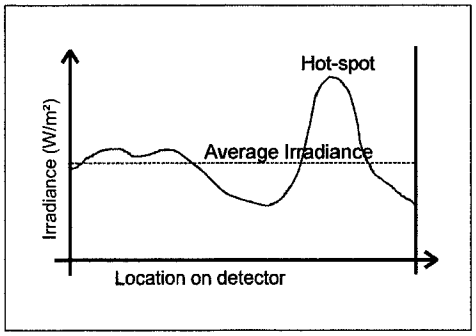

Fig. 1. Example of an inhomogeneous irradiance profile across a detector surface and the corresponding averaged value. If the true irradiance profile is to be determined, then the measurement aperture would have to be correspondingly small.

For completeness it is noted that sometimes power- and energy density are also used instead of irradiance or radiant exposure. Following the document DIN xx, power and energy density should be used to denote power and energy relative to a volume, i.e. they are measured with units of W/m^3 and J/m^3. It is also noted that for optical radiation propagation in scattering media radiant exposure, radiant exposure has a different concept than fluence, as fluence is defined as energy per area passing through a given area from either side of the area, i.e. it not only includes the exposure of the surface to the direct laser radiation, but also includes exposure with radiation scattered within the tissue.

3.2 Beam diameter

For the determination of the irradiance to be compared to exposure limits for laser radiation and broadband radiation, it is not necessary to determine the diameter of the irradiated area or the beam diameter, as the irradiance is averaged over a specified area. However, as basis for the following discussion on retinal image diameter and irradiated spot areas for the cornea or the skin, the definition of beam diameter is reviewed. Usually the term "beam" is used for a well defined collimated beam of optical radiation, i.e. a beam with relatively small divergence, such as a laser beam or a searchlight beam. Here, the term beam diameter is used more broadly to denote the diameter of the irradiated area at a given surface. For a top hat spatial beam profile, the beam diameter is intrinsic in the profile. However, for more general beams, the irradiance will gradually decrease and to define the beam diameter as the diameter where the irradiance actually reaches would not be practical. Therefore, the beam diameter is usually defined as the minimum diameter of the circular area within which a certain percentage of the total power is contained. In laser safety and safety of optical radiation, this percentage is 68 %, which for a Gaussian beam profile corresponds to a that local irradiance at the diameter which is a factor of 1/e = 0.368 from the maximum irradiance of the center of the beam, as is schematically depicted in figure 2.

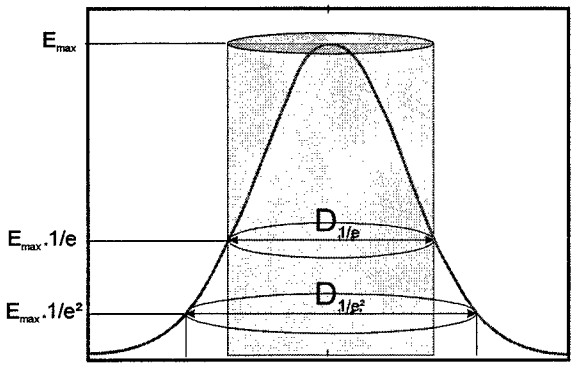

Fig. 2. Concept of beam diameter specified at the 1/e points of a Gaussian irradiance profile, as usual for laser safety purposes, and at the $1/e^2$ points, as usual for technical and engineering purposes.

For technical laser beam specifications, a beam diameter at the $1/e^2$ point is most often used, which results in a beam diameter which for a Gaussian beam which is a factor of $\sqrt{2}$ larger than the 1/e diameter, and the area is a factor 2 larger. The 1/e definition is used in laser safety, as for this diameter, when the irradiance is obtained by dividing the total beam power by the corresponding area (for instance for simple hazard calculations) is equal to the maximum irradiance at the

beam center. If a larger area is used for the determination of the irradiance to be compared to the exposure limit, then the hazard for exposure to the center of the beam is underestimated.

3.3 Imaging onto the retina, angular subtense of apparent source

When the eye is exposed to radiation with wavelengths for which the ocular media are transparent, then the radiation is focused by the cornea and the lens onto the retina[****]. For a characterization of the hazard, the irradiance on the retina is relevant, for which the power or energy and the irradiated area on the retina needs to be quantified. The geometric extent of the irradiated area on the retina is either characterized by the diameter of the irradiated area on the retina, or by the angular subtense subtended by the source at the location of the cornea.

If the eye is assumed to be resting in respect to a source, the diameter of the image on the retina d_r, in μm, can be related very easily to the angular subtense of the source α in mrad (see Fig. 3) by using the standardised focal length of the eye of 17 mm: $d_r = \alpha \cdot 17$

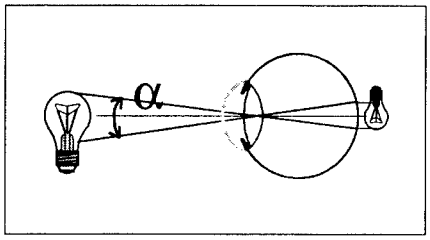

Fig. 3. The angular subtense of the source is directly related to the size of the image on the retina.

The angular subtense is usually measured in radian, (or milliradian, mrad) which is defined as the ratio of the extent of the source to the distance to the source: a source with dimensions of 1 mm and is located at a distance of 1 m from the eye subtends a plane angle of 1 mrad.

Due to the physical limitations of the imaging process in the eye, the minimal angular subtense of the image or spot-size on the retina, termed α_{min}, is about 1.7 mrad, which is equivalent to a spot size on the retina of about 25 - 30 μm. Such a minimal spot size can be realised either by a very small or distant source or by a well collimated laser beam, which, due to the parallel rays, is perceived as originating at a great distance from the viewer. An apparent source with angular subtense smaller than 1.5 mrad is usually referred to as small source, sources larger than this are referred to as extended sources.

The term *apparent* source is a general term and also includes sources where radiation is projected by collimating optics, and the source subtense and location as perceived by the eye when looking at the source does not correspond to the subtense and location of the real physical source. For a source such as a lamp for which the radiation is collimated by lenses, or a laser which produces a collimated beam, the apparent source lies behind the physical source of the radiation, and it lies further back the better collimated the radiation is. This can be understood on the basis of the angle of the rays entering the eye: parallel rays, such as those coming from a distant star, produce a point image on the retina, which is perceived as a small source originating from a long distance. The location of the apparent source can be inferred by following the direction of the rays to where they would intersect. The characterization and measurement of the location and subtense of the apparent source is not in the scope of this review.

3.4 Field-of-view of the detector

Besides the aperture area of the detector, the field-of-view, FOV, is the second geometric property of relevance for the measurement of optical radiation. In simple terms, the FOV is the part of space, quantified as angle, which is "seen" by the detector, or from which the detector (or the input optics) receives radiation.

The FOV can be specified as solid angle (i.e. a "two-dimensional" angle), with the unit of steradian and the symbol for the unit of sr. The solid angle of 1 sr is defined as the solid angle which is subtended by an area of 1 m^2 at a distance of 1 m away from the area, which can also account for a non-circular FOV. In laser safety and hazard analysis of optical radiation, a circular FOV is assumed, and the plane angle, measured in units of radian (or more often mrad) is often used to characterise the FOV. The plane angle ω of a circular object can be converted to a solid angle Ω by the approximation for small angles, $\Omega = (\pi/4)\ \omega^2$.

[****] It is pointed out that the refraction at the air-cornea surface of the eye is responsible for most of the refractive power of the eye, while the lens of the eye is responsible for fine adjustment between accommodation of the eye to a source in infinity to a source very close to the eye.

The term *angle of acceptance* is also often used instead of the term FOV, more often for the definition as plane angle than for the solid angle. In ANSI Z136.1, the term *cone angle* is also used.

Often a tube, also called Gershun tube, is used to limit the field of view (FOV) of a detector[9]. However, as is depicted schematically in Fig. 4, this does not result in a well defined FOV, as different points on the surface of the detector have a different direction and size of FOV and the resulting total FOV of the detector has a central part from which the whole detector surface receives radiation, and an outer part from which only the outer parts of the detector receive radiation.

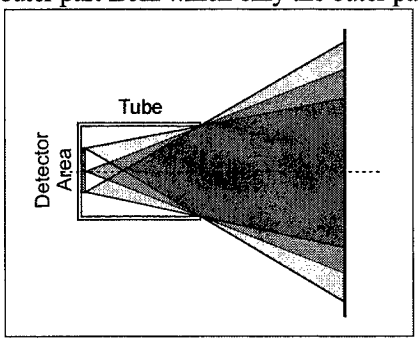

Fig. 4. Using a tube with the detector to limit the field of view results in a central field of view and outer areas of the detector which have a different field of view.

A well defined FOV can be obtained by either of two set-ups, which are depicted in Fig. 5 and Fig. 6. Assuming a circular FOV, in both set-ups the size of the FOV is determined by the size and location of the circular field stop. The FOV can be defined either by placing the field stop at the source and the detector at a corresponding distance (see Fig. 5), where the plane angle - FOV (in units of radian) is given by the ratio of the diameter of the field stop to the distance of the field stop to the aperture stop. This set-up relies on the placement of the field stop at the source or very close to the source, which means that the source has to be accessible. If the field stop is not placed in close proximity to the source, then the FOV is no longer well defined, and the set-up is comparable to a Gershun tube which was shown in Fig. 4. However, it allows to use radiometers with detectors or input optics with a large FOV, which are usually used to measure irradiance. The deliberations regarding the irradiance measurements in respect to the averaging over the aperture area apply here to the aperture stop.

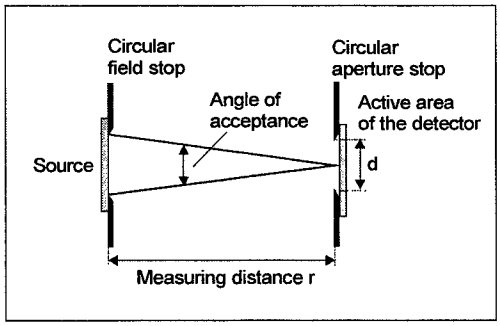

Fig. 5. A well defined field of view can be obtained by placing the field stop at the source.

By imaging the source onto the field stop (Fig. 6), the field stop does not have to placed at the source and therefore this set-up can also be used to measure sources which are not accessible or which employ projecting optics. In order to define a FOV, a lens is used to image the source onto the plane of the field stop. The plane angle FOV is determined by the ratio of the diameter of field stop to the distance of the field stop to the lens. In this case, the averaging measurement aperture for the determination of the irradiance part of the radiance measurement is in front of the lens, i.e. the aperture stop of the input optics. Such a set-up is realized in specialized integrating hazard meters as well as in telescopic input optics of radiometers.

For both set-ups, the diameter and the distance of the field stop to the aperture stop determines the FOV, while the aperture stop is equivalent to the averaging aperture in the sense of irradiance measurement.

For many laser safety measurements and for hazard analysis of optical radiation, the FOV of the detector does not have to fulfil special requirement, as long as all of the source is seen by the detector, i.e. as long as the detector FOV is at least as large as the source size, as the measurement result is not influenced by the size of the FOV as long as the complete source is measured.

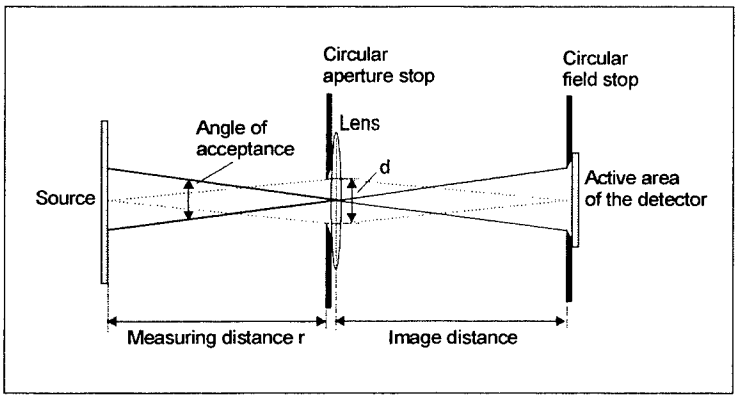

Fig. 6. As the source is imaging onto the field stop in front of the detector, a telescopic radiance-meter can also be used for sources which can not be accessed or which use projecting optics.

3.5 Radiance – concept and measurement

A practical way of conceptualizing radiance (which is measured in units of W m^{-2} sr^{-1}), is to start off with irradiance as discussed above, i.e. with an irradiance measurement, and relating (dividing) the irradiance at a given area to the solid angle of space from which the radiation was received, i.e. the measurement field-of-view of the detector.

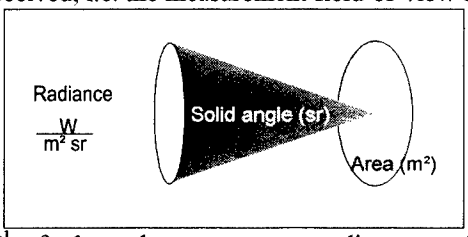

Fig. 7. The unit of radiance is W m^{-2} sr^{-1} – for hazard measurements, radiance can be seen as the irradiance at the detector (averaged over the appropriate area) divided by the field of view of the detector as measured in steradian.

Laser radiation comes from very small angle and together with the typical irradiance values at the cornea can result in a level of radiance much higher than is possible to achieve for any conventional light source. While irradiance is a related to a certain location in the beam, radiance can be conceptualized rather as a field or source property. For instance, radiance is not changed by optical instruments (besides the reflection and absorption losses).

3.6 Relationship of radiance and irradiance

The basic relation between radiance, L, and irradiance, E, is $E = L \cdot \Omega$, where Ω is the solid angle. This relationship appears simple, however due to the intricacies of optical radiation hazard measurements, care has to be taken when calculating irradiance exposure limits (ELs) out of radiance limits and when performing corresponding measurements.

For ocular hazards, two main locations where irradiance is specified, need be considered: the irradiance level at the cornea, where for instance the laser MPEs (also for the retinal hazard wavelength range) are specified, and for wavelengths in the retinal hazard region, the irradiance at the retina, which is the actual location of interaction of laser radiation with biological tissue. The retinal irradiance profile is not directly related to the corneal irradiance. However, when the interocular energy (or power) is known, the irradiance at the retina can be calculated by dividing that energy or power by the area of the image at the retina. The irradiance at the retina E_r can also be calculate from the source radiance L by[10]

$E_r = 0.27 \cdot d_{pupil} \cdot L \cdot \tau$

Where d_{pupil} is given in cm and is the pupil diameter, and τ is the transmission of the ocular media, and the focal length of the eye is taken as 17 mm.

It is also interesting to relate the law of constant radiance with the imaging of a source onto the retina: When an image is formed on the retina for a given source, and magnifying optics are used, then more power is collected by the optics, but with the same ratio, the area of image on the retina is increased, leaving the irradiance on the retina the same. This law of radiometry can however be violated when the radiance is averaged over a FOV and the FOV is larger than the source, as is required for hazard measurements.

3.7 Averaging of radiance

There is a Golden rule of radiance measurements: the source has to underfill the detector's FOV. This is a simplified expression of the requirement that the measurement FOV needs to be small enough to resolve the radiance profile of the source (compare irradiance measurement). Just as for irradiance hotspots, radiance measurements performed with a given FOV can not characterize radiance hotspots (which will become irradiance hotspots in the image plane) which are smaller than the measurement FOV. When the source is smaller than the measurement (averaging) FOV, then the resulting value is smaller than the physical radiance of the source, and can be seen as a *effective* radiance. This effective radiance is directly related to an effective irradiance on the retina.

4. DOSIMETRIC CONCEPTS SPECIFIC TO LASER SAFETY AND OPTICAL RADIATION HAZARD ANALYSIS

4.1 Dosimetry for biomedical studies as basis for exposure limits

Animal studies and some limited information regarding human exposure are the basis for the setting of exposure limits of optical radiation. In animal studies, a number of exposures are performed for a given wavelength, exposure duration and irradiated spot diameter, while varying the exposure level. A threshold is subsequently identified for the given wavelength, exposure duration and spot diameter, where no injury was observed for exposures below the threshold level and injury was observed above the threshold level. However, especially for the retina, due to biological variability in the level of threshold from specimen to specimen or for different locations within one retina, a statistical distribution for the threshold is found rather than a sharp threshold[11]. As representative point of the distribution, the ED50 is usually reported, which is the exposure level which produced an injury in 50 % of the exposures. An exposure limit is set by the responsible committee, which currently is the ICNIRP, following a review of the available experimental data. The exposure limit is set so that it lies below the ED50 as identified by experimental animal studies by introducing a "safety factor", which is typically in the range of a factor 10, however can be somewhat less if the uncertainty about the threshold is small. The difference can also be larger when the wavelength or pulse duration dependence of the EL has been simplified in comparison to the corresponding trend in the experimental data.

For a discussion of the dosimetry regarding experimental studies which are designed to quantify a threshold for injury, and the radiometric relation to the corresponding EL, specific wavelength ranges and consequently the type of tissue at risk need to be distinguished. Generally, the location of the injury corresponds to the location of the (main) absorption of the wavelength. For optical radiation hazards, the tissues at risk are the cornea and the lens of the eye for wavelengths in the ultraviolet and the infrared above 1400 nm, the retina in the wavelength range of 400 nm to 1400 nm, and the skin.

For the cornea and lens, experimental ED50 and threshold values are typically reported as irradiance or radiant exposure at the cornea. In practice, for laser beams, the power or energy per pulse of the laser beam is measured and the irradiated spot diameter on the cornea is determined at the 1/e level. The reported irradiance or radiant exposure value is the result of a division of the power or energy per pulse by the area of the irradiated spot using the 1/e definition of beam diameter. For exposure of the skin, the procedure is equivalent.

For the retina, experimental ED50 and threshold values are usually reported in terms of the power or energy which is incident on the cornea and enters the pupil, which is referred to either as intraocular energy, IOE, or as total intraocular energy, TIE. The energy or power incident on the retina can be determined by considering reflection and absorption losses in the ocular media in front of the retina. Additionally to the power or energy, the diameter of the irradiated spot on the retina is also necessary to fully characterize the level of exposure.

4.2 Aperture averaging for optical radiation hazard evaluation

When an irradiance profile is averaged over a given aperture, then the resulting value represents an *effective* value which is smaller than the maximum physical value of the irradiance profile. For laser safety and hazard evaluation of broadband optical radiation, it is this effective hazard which is to be compared to the exposure limit. The size of the averaging aperture is determined by biological factors such as the optical properties of the eye, body movements and scattering. For the example of skin exposure lasting for several seconds, the movement of the body will average an irradiance profile on the skin over an area of at least several square millimeters, even if the irradiated body part is kept still. Especially in the near-infrared, radiation is penetrating relatively deep into skin and due to scattering, the irradiance profile is averaged over corresponding dimensions. In the laser safety standards, averaging apertures are specified for different wavelength ranges, separately for the eye and the skin.

Table 9 of IEC 60825-1 – Aperture diameter applicable to measuring laser irradiance and radiant exposure

Spectral region nm	Aperture diameter for	
	Eye mm	Skin mm
180 to 400	1	3.5
≥ 400 to 1 400	7	3.5
≥ 1 400 to 10^5	1 for $t \leq 0.35$ s $1.5\ t^{3/8}$ for 0.35 s < t < 10 s 3,5 for $t \geq 10$ s.	3.5
≥ 10^5 to 10^6	11	11

In 1997, ICNIRP published guidelines for optical broadband radiation[2], where maximum permissible exposures are defined alongside with the minimal averaging aperture diameters. An aperture diameter of 25 mm is specified, only for the case of an inhomogeneous field, the averaging aperture size should be reduced to 7 mm.

An extreme example is a laser beam which produces an irradiated area on the detector of, for example, 1 mm^2. Let us further assume that the optical power contained in this laser beam equals 0.1 mW, and that the laser radiation is in the visible spectral range and the aperture of the detector or the detector surface has a diameter of 7 mm, corresponding to an area 3.6 10^{-4} m^2. A radiometer calibrated in Watts would display a value of 0.1 mW – the irradiance obtained by dividing with the area of the 7 mm aperture would give about 2.6 W m^{-2}. However the actual physical irradiance in the laser beam would be (for the simplifying assumption of a top-hat beam) 0.1 mW divided by 1 mm^2, which equals 100 W m^{-2}. It is interesting to note that in this example, the irradiance value obtained by averaging over an aperture of 7 mm diameter is the correct value to be compared to the exposure limit of laser radiation for inadvertent exposure, which is given as irradiance on the cornea of 25 W m^{-2}. The averaging aperture of 7 mm corresponds to the maximum diameter of a dark-adapted pupil and is therefore the biological relevant dimension over which the irradiance is "biologically" averaged. Therefore 2.6 W m^{-2} is the irradiance value which has to be compared to the applicable exposure limit of 25 W m^{-2} and not the actual physical irradiance value which is much larger. This example shows the importance of specifying the appropriate averaging aperture size together with the exposure limit. If the averaging aperture is not specified, the actual physical irradiance might be compared to the exposure limit, which, for the case of hot-spots or small beams, would lead to an unnecessarily-restrictive hazard evaluation.

It is important to note, that values specified for the averaging aperture diameter are the *smallest* apertures to be used to obtain an averaged value of irradiance to be compared with the exposure limits - if smaller averaging apertures were used, for the case of hotspots, the hazard would be *over*-estimated. If the irradiating field is homogenous over a given area which is larger than the minimum aperture size, then the measurement aperture can be larger than the specified minimum value. By way of example, if one did not account for body-movements, a 1 mm diameter aperture would seem appropriate for UV-measurements, however the radiant exposure in the wavelength range of UV radiation will practically never have to be measured with an averaging aperture of 1 mm diameter, as this would be only relevant for hazard evaluation of exposure to pulses produced by ultraviolet lasers. It should be noted that for the measurement of homogeneous irradiation, the usage of a larger aperture is actually advantageous, as the measurement accuracy is improved due to a larger signal.

4.3 Cosine dependence for skin exposure

For the measurement of radiation to be compared to limits concerning irradiation of the surface of the body, i.e. the skin and the surface of the eye, the detector should have a plane angle of acceptance of 2π, and a cosine-response regarding the sensitivity of the detector for different angles of incidence, mimicking the irradiation of a flat surface where the irradiance is decreased with the cosine of the incidence angle, as is schematically shown in Fig. 8.

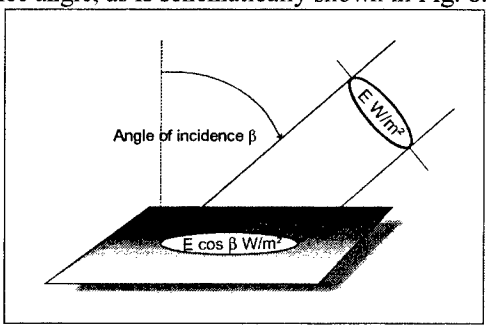

Fig. 8. For measurements of radiation to be compared to exposure limits of the skin, the detector should have a cosine response in regard to the sensitivity as a function of the incidence angle.

The cosine response of a detector however only comes into play when large sources are measured at close distance. If the angle of incidence of the incident rays does not vary much, then also the dependence of the sensitivity of the radiometer as a function of angle of incidence has no influence on the measurement.

4.4 Eye movements

For exposure to flashes of light, the retina appears to be resting in respect to the image on the retina, and the angular subtense α, with a minimal value of α_{min}, can be used to estimate the size of the irradiated area on the retina and the corresponding irradiance. For continuous exposure situations, however, eye-movements will result in the movement of the image on the retina, causing the irradiated retinal area to be larger than the optical image size α, as is schematically depicted in Fig. 9. The extent of the eye-movements is time dependent: for very short exposures, the retina will be fixed in respect to the image for the duration of the exposure. With increasing exposure duration, eye-movements will increase from involuntary tremors to larger, task oriented eye-movement and for very long exposure durations under realistic situations, even head movements would come into play.

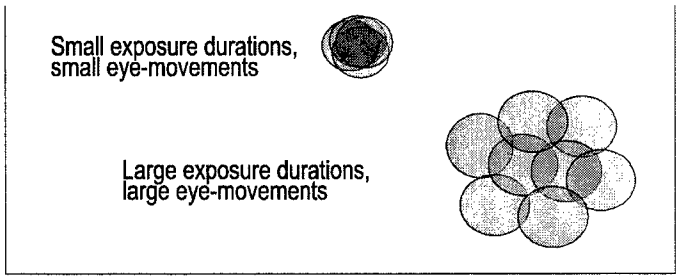

Fig. 9. In this diagram, the image on the retina is represented by a grey disk, and the eye movements are visualised by the location of the image at given time intervals. Eye movements will result in relative motions of the image over the retina, comparable to a photographic film being moved in relation to the image. This however distributes the radiant energy over a larger area, thereby decreasing the hazard.

Such eye-movements will increase the effectively irradiated and therefore also the potentially damaged area on the retina. However due to these eye-movements and the correspondingly increased irradiated area, the *effective* irradiance on the retina as defined by the power entering the eye divided by the effectively irradiated area, will decrease correspondingly, thereby decreasing the level of hazard as compared to the irradiation of a fixated eye for the same exposure duration. The general tendency is:

longer exposure duration → larger eye movements → larger effectively irradiated area → smaller effective irradiance → decreased hazard

Since the retinal photochemical hazard depends on the irradiance on the retina and not on the image size, the concept of accounting for the influence of eye movement by a time dependent averaging FOV is adopted for the specification of the MPEs and measurement requirements for the photochemical retinal MPE, both for laser radiation as well as for broadband radiation.

4.5 FOV averaging for the photochemical hazard evaluation

Usually, if the level of the hazard is decreased, this is expressed by increasing the exposure limit, allowing for a higher exposure level. For the case of a decrease of the hazard due to eye-movements, this relaxation is not expressed as increase of the exposure limit as given in radiance, but by an increase of the averaging FOV. As discussed above, if the FOV is larger than the source, then the measured radiance value will be smaller than the actual physical radiance of the source. An increase of the averaging FOV results in a decrease of the effective radiance measurement value, as this value is derived by division with the averaging measurement FOV. Thereby the decrease of the hazard is not reflected by an increase of the exposure limit, but by a decrease of the measured effective value which is to be compared to the exposure limit. The specification of an averaging FOV results in the measurement of a *biologically effective* radiance value, which might be smaller than the physical radiance value of the source. Therefore, the effective radiance value should be seen as a parameter related to the *exposure* of the retina rather than as a property of the source.

The law of conservation of radiance and the independence of the radiance in regard to the distance to the source also only applies to the physical real radiance, not to effective averaged radiance, as the effective retinal irradiance will remain

unchanged as long as the (magnified) image is smaller than the extent of the eye movements (the effective irradiance on the retina is derived by dividing the intraocular power by the area reflecting the retinal area covered by the eye movements.

In several documents, the Greek letter γ is used to denominate the averaging plane angle FOV to prevent confusion with the source size α and with the minimal retinal spot size α_{min}. In the ICNIRP guidelines for broadband radiation[2], the averaging FOV is specified to be 11 mrad for exposure durations between 10 s and 100 s. It is difficult to quantify the minimal averaging effect of eye-movements for exposure durations greater than 100 seconds and up to 10.000 s, which is about 2 ½ hours. According to the ICNIRP guidelines for broadband radiation, for exposure durations greater than 100 s, the averaging FOV is increased linearly up to 0.2 radian at 10,000 seconds. In the course of the current revision of the laser exposure limits, ICNIRP will specify[3] a square-root dependence of the plane angle averaging FOV, γ, which translates into a simple linear dependence of the solid angle averaging FOV, Γ, on the exposure duration. It is suggested here to adopt this specification, as reproduced below, also for broadband radiation.

Short time exposure	$\gamma = 1.7\ mrad$	$\Gamma = 2.3\ 10^{-6}\ sr$ (relevant for thermal retinal broadband hazard only)
$10\ s - 100\ s$	$\gamma = 11\ mrad$	$\Gamma = 10^{-4}\ sr$
$100\ s - 10\ 000\ s$	$\gamma = 1.1\sqrt{t}\ mrad$	$\Gamma = 10^{-6} \cdot t\ sr$
$t > 10\ 000\ s$	$\gamma = 110\ mrad$	$\Gamma = 10^{-2}\ sr$

It should be noted, that the value of 1.7 mrad is specified by ICNIRP to be the averaging FOV for the retinal thermal hazard for the wavelength range of 380 nm to 1,400 nm, which is relevant for short time exposures. For the blue light photochemical retinal hazard, relevant exposure durations are 10 seconds and longer, and the above values for the averaging FOVs for times greater than 10 seconds apply. For the evaluation of near infrared sources that provide no strong visual stimulus, the exposure limit for thermal damage of the retina is defined for exposure durations larger than 10 seconds, and the radiance measurement has to be averaged over $\gamma = 11$ mrad.

The consequences of the averaging FOV for practical hazard measurements shall be discussed for two FOV sizes in relation to a small and a large source, as schematically shown in Fig. 9.

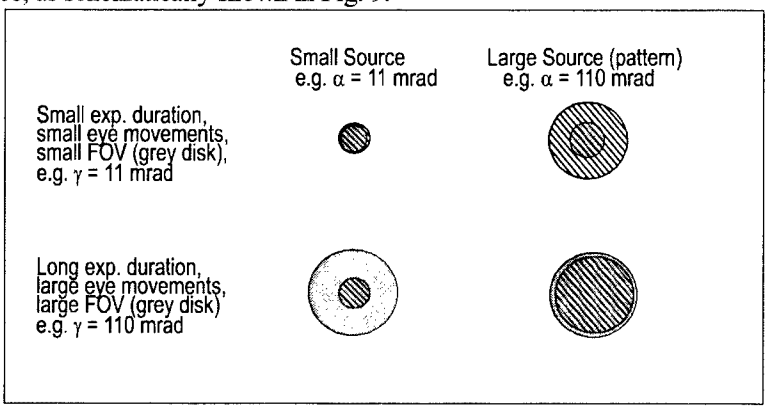

Fig. 10. Possible relations of source size to the averaging FOV as specified for two different exposure durations. If the source is smaller than the FOV, the measured averaged value is smaller than the physical value. if the source is larger than the FOV, the source will be sampled for hot-spots with the specified FOV.

For the example of a source size of $\alpha = 11$ mrad, the averaging FOV for an exposure duration between 10 s and 100 s is $\gamma = 11$ mrad. For a homogeneous source, the measured effective radiance value will be the same as the physical radiance. If the same source is evaluated for longer exposure durations, the averaging FOV increases corresponding to increased eye-movements, thereby the *biologically effective* radiance value as averaged over γ is smaller than the real physical radiance of the source. On the other hand, for the case of a source of for instance $\alpha = 110$ mrad, the specification of an averaging FOV of $\gamma = 11$ mrad means that the source is to be sampled for hot-spots. The examples also show, that for a given exposure duration the specified averaging FOV γ corresponds to a minimal image size, above which the effective averaged radiance is equal to the physical radiance, i.e. there does not seem to be a reduction in the hazard due to eye-movements for sources larger than γ. This can be understood on the basis of Fig. 10, where the image of a small and large source is represented by grey disks and for both sources the distribution corresponds to the same geometrical extent of eye-movements for a given time (i.e. the centres of the disks are at the same positions in both cases).

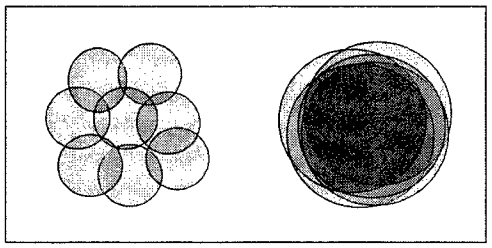

Fig. 11: Comparison of the effectively irradiated retinal area for the same extent of eye-movements for small and large source sizes: for large sources, i.e. images, the extent of the eye-movements is not large to significantly increase the effectively irradiated area.

If the extent of the eye-movements is small compared to the image size, then the irradiated area on the retina will correspond to the image size α. Therefore, for larger image sizes only larger eye-movements can significantly increase the effectively irradiated area on the retina.

4. 6 Photochemical retinal broadband limit "Blue light hazard"

The broadband radiation exposure limit for the photochemical retinal hazard, which is also often referred to as „Blue Light Hazard", is given by ICNIRP as[2]: $L_B \cdot t \le 10^6 \frac{J}{m^2\ sr}$

where L_B is the effective blue-light radiance at the eye and t is the exposure duration.

For t > 10,000 s: $L_B \le 100 \frac{W}{m^2\ sr}$

The term „effective" indicates that the spectral radiance L_λ of the broadband source is weighted with the blue light hazard action spectrum $B(\lambda)$ and is subsequently integrated over the wavelength λ:

$$L_B \cdot t = \sum_{300}^{700} L_\lambda \cdot B(\lambda) \cdot t\, \Delta\lambda$$

4.7 Relation of radiance MPE to irradiance MPE

The basic relation between radiance, L, and irradiance, E, is $E = L \cdot \Omega$ where Ω is the solid angle. This relationship appears simple, however due to the intricacies of optical radiation hazard measurements, care has to be taken when calculating irradiance exposure limits (ELs) out of radiance limits and when performing corresponding measurements.

The most straightforward case is a source with angular subtense α, which is smaller than the averaging FOV, γ. In this case, the measured effective radiance value does not depend on the angular subtense of the source, and it also does not depend on the actual value of the measurement FOV, as long as the FOV is larger than the source, and as long as the radiance value is obtained by dividing the irradiance value by the specified averaging FOV, Γ. Consequently the *radiance*-EL can be multiplied with the averaging FOV to obtain the exposure limit given as irradiance at the cornea, and the measurement can be performed with a regular irradiance detector with an "open", i.e. large, FOV. Specifically, this is done for the photochemical retinal limit, where the basic exposure limit is 10^6 W m^{-2} sr^{-1}. The exposure limit expressed as irradiance is obtained by multiplying with the appropriate averaging FOV Γ (see above), i.e. with $\Gamma = 10^{-4}$ sr ($\gamma = 11$ mrad) for exposure durations from 10 to 100 s:

$$10^6\ J\ m^{-2}\ sr^{-1} \cdot 10^{-4}\ sr = 100\ J\ m^{-2}$$

This value is specified by ICNIRP[2] and ACGIH[12] to be valid for sources with angular subtense smaller than 11 mrad ("small" sources). By multiplying the *radiance*-EL with the averaging FOV, the relaxation of the hazard due to eye-movements is contained in the exposure limit, which is not the case for the *radiance*-ELs, where the averaging is contained in the measurement value, which is to be compared with the *radiance*-EL. This relationship between the ELs and averaging FOV can be seen when the blue light *irradiance*-EL is derived for very long exposure durations[*****], where $\gamma = 110$ mrad, i.e. $\Gamma = 10^{-2}$ sr:

$$10^6\ J\ m^{-2}\ sr^{-1} \cdot 10^{-2}\ sr = 10^4\ J\ m^{-2}$$

A comparison with the value for exposure durations of 10 to 100 s shows, that the EL is larger for very long exposure durations. The relaxation of the hazard due to larger eye-movements results in an *increase* of the *EL*, if the EL is expressed as irradiance. For both evaluations, i.e. for 10 – 100 s and for very long exposure durations, the irradiance measurement

[*****] An equivalent derivation of the blue light exposure limit for a 10,000 s exposure duration is the background for the limit of 0.8 W m^{-2}, as specified in the IESNA lamp safety standards[6] for the exempt group. There a value of $\gamma = 100$ mrad has been used.

value is the same, in contrast to the specification of the EL as a radiance value, where the value of the EL does not depend on the exposure duration, but the relaxation of the hazard is mirrored by a decrease of the effectively measured radiance value. It should be noted that the irradiance blue light limit is fully equivalent to the *radiance*-EL, provided that the radiance measurement is performed with the specified averaging FOV, and it is not a relaxation, as indicated in by ACGIH[12].

The exposure limit for the blue-light hazard for exposure durations greater than 100 seconds up to 30,000 seconds can be given in a simple form when the irradiance MPE is derived from the radiance limit with the averaging field of view as specified as function of time and is subsequently divided by the exposure duration to obtain a value for irradiance:

$$MPE_{irradiance} = 1\ W\ m^{-2}$$

It is mentioned above, that the irradiance limits are valid for sources smaller than the averaging angle, which implies that an "open"-FOV irradiance radiometer, as is common for laser measurements, is used for the hazard measurements. If the source were larger than γ, then one would measure a larger level of radiation, and the hazard would be overestimated as compared to the radiance-case, where the FOV is limited to γ. If the FOV for the irradiance measurement were also limited to γ, for instance by placing an aperture at the source, there would be a full equivalence to radiance measurements and the *irradiance*-ELs could also be applied to sources larger than γ. In this case however, γ is not an *averaging* FOV, but rather a *limiting* FOV, as it prevents that radiation from outside the FOV contributes to the measured irradiance. For the case that the source is homogeneous and an "open" field of view (i.e. larger than the source size α) is to be used, the exposure limits could be corrected for the larger measured value by increasing the exposure limit correspondingly:

$$MPE_{irradiance\ open} = MPE_{irradiance} \cdot \alpha^2 \gamma^2$$

If the source is not homogenous, this method would underestimate the hazard, as it would correspond to averaging over the source size, whereas the usage of the specified averaging field of view would be used to scan the source for hotspots, i.e. for maximised measurement values, which would have to be compared to the exposure limit.

ACKNOWLEDGEMENTS

The author would like to express his appreciation for many spirited and informative discussions with David Sliney US Army Center for Health Promotion and Preventive Medicine, MD, and John Mellerio, School of Biosciences, University of Westminster, London.

REFERENCES

1. ICNIRP "Guidelines on Limits of Exposure to Laser Radiation of Wavelengths between 180 nm and 1,000 μm", *Health Physics* **71**, p. 804-819, 1996.
2. ICNIRP "Guidelines on Limits of Exposure to Broad-band Incoherent Optical Radiation (0,38 to 3 μm)", *Health Physics* **73**, p. 539-554, 1997.
3. ICNIRP, "Revision of Guidelines on Limits of Exposure to Laser Radiation of Wavelengths between 180 nm and 1,000 μm", *Health Physics* **79** p. 431-440, 2001.
4. IEC 60825-1 "Safety of laser products Part 1: Equipment classification, requirements and user's guide", 1997, Amendment A2 2001.
5. ANSI Z136.1 "American National Standard for Safe Use of Lasers", 2000.
6. ANSI/IESNA RP-27.3-96 "Recommended Practice for Photobiological Safety for Lamps – Risk Group Classification & Labeling", 1996.
7. CIE "Photobiological Safety of Lamps and Lamp Systems", to be published 2001.
8. TR IEC 60825-8 "Safety of laser products Part 9, Compilation of maximum permissible exposure to incoherent optical radiation (broadband sources)", 1999.
9. McCluney, R., *Introduction to Radiometry and Photometry*, p. 116 f, Artech House, MA, 1994
10. D. H. Sliney and M. Wolbarsht, *Safety with Lasers and Other Optical Sources*, New York, Plenum Publishing Corp., 1980.
11. K. Schulmeister, G. Sonneck, H. Hödlmoser, F. Rattay, J. Mellerio and D. Sliney, *Modeling of uncertainty associated with dose–response curves as applied for probabilistic risk assessment in laser safety*, SPIE Vol. 4246, San Jose, 2001, Laser and Noncoherent Light Ocular Effects: Epidemiology, Prevention, and Treatment, Ed. B. E. Stuck and M. B. Belkin (these proceedings), 2001.
12. ACGIH, American Conference of Industrial Governmental Hygienists, TLVs® and BEIs® for Chemical Substances and Physical Agents, *Photochemical injury from blue light*, p. 107 f, 1996.

The Accuracy and Relevancy of the Probit Analysis for "In Vivo Dose-Response Laser Tissue Experiments"

Amir Langus*[a], Camil Fuchs[b] and Israel Gannot[a]

[a] Faculty of Engineering, Department of Bio-Medical Engineering,
[b] Faculty of Exact sciences, School of Mathematical Sciences, Department of Statistics and Operations Research,
Tel-Aviv University, Tel-Aviv, Israel 69978

ABSTRACT

The most common method of analysis for "in vivo laser tissue experiments" is the probit regression. The data gathered at these experiments are specific in that there are very few repetitions of the exact stimulus exposure; thus the response frequencies for most stimulus are either '0' or '1'. Though such type of data is acceptable in probit, it seems that such data might not produce robust estimates of the ED_{50} and the slope. The accuracy of the probit's estimation was investigated by the use of Monte-Carlo simulation. Preliminary results suggest that the accuracy of the probit's estimations is conditional and might be biased in a way that raise doubts about the validity of the conclusions based on probit's estimations.

Keywords: probit, experimental data analysis, laser tissue interactions.

1. INTRODUCTION

A typical in-vivo dose-response laser-tissue experiment is carried out by treating several subjects (i.e. animals). Each subject usually is exposed several times at different tissue sites. The exposure energies are varied through out the experiment (while other laser parameters are kept constant). The data gathered are the exposure energies and the exposure results, which are the characteristics of the post-exposure laser lesion. Laser lesions may have many different appearances. It is convenient to define a threshold lesion and to classify the exposure results by a binary quantal grade. If an exposure outcome is a lesion that is similar or more severe than the threshold lesion, the exposure's result is defined as response and coded as "1". If an exposure outcome is a lesion that is less severe than the threshold lesion, the exposure result is defined as no-response and coded as "0". The threshold lesion customarily is defined as the minimal, yet noticeable, change in the exposed tissue site.

A very common statistical method of analysis of the data gathered at the "in vivo laser tissue experiments" is the probit method. The probit procedure measures the relationship between the strength of a stimulus and the proportion of cases exhibiting a response to the stimulus. probit procedure is commonly accepted and widely used in biological assay and clinical trials. For example, one can estimate the effectiveness of a new pesticide at killing ants, and the recommended concentration to use, by performing an experiment in which samples of ants are exposed to different concentrations of the pesticide. The collected data are the concentrations of the pesticide, the number of ants killed and the number of ants exposed. Applying probit analysis to these data, one can estimate the statistical functional relationship between concentration and killing, and can determine the recommended concentration of pesticide to be almost sure to kill, for example, 95% of the exposed ants.

The main assumptions of the probit model are that occurrence or non-occurrence of response depends upon the intensity of the stimulus (e.g. concentration of pesticide or exposure energy). For any one subject there will be a certain level of intensity below which no response occur, and above which there always is a positive response. This level is usually defined as a tolerance. Tolerance value will vary from one subject to another in the population used. Hence, the response probability equals to the probability that a randomly selected tolerance is smaller than the stimulus.

The probit analysis estimates the parameters of these tolerances' distribution. The most meaningful parameter is the ED_{50}, which is the effective stimulus (exposure) dose that corresponds to a 50% response (lesion) probability. Another important parameter is the slope. The slope is defined as the ratio ED_{84}/ED_{50}, where ED_x corresponds to the x% response (lesion) probability.

The procedures for the maximum likelihood estimations of the ED50 (and other parameters) used in probit usually assume aggregated data for every stimulus[1,2]. A case where the experimental response frequencies are either 0 or 1 is considered as an extreme and heterogeneous case[2].

* Correspondence: Email: langusa@eng.tau.ac.il

Laser and Noncoherent Light Ocular Effects: Epidemiology, Prevention, and Treatment,
Bruce E. Stuck, Michael Belkin, Editors, Proceedings of SPIE Vol. 4246 (2001)

However, the data gathered at the "in vivo laser tissue experiments" are specific in that there are very few repetitions of the exact stimulus, thus the response frequencies for most stimulus are either '0' or '1'. Though such type of data is acceptable in probit, it seems that such data might not produce robust estimates of the ED_{50} and the slope.
Moreover, in a previous study[3] we re-analyzed data that was gathered by researchers from the USAMRD-WRAIR. The USAMRD-WRAIR data included information on 47 animals exposed to a single 15-nanosecond pulse emitted from a dye laser operated at 34 different wavelengths[4]. Each animal was treated at about four out of 34 different wavelengths. The data consisted of 211 single specimen vectors of dose and response, a vector for each combination of animal and wavelength. The USAMRD-WRAIR analyzed this data with probit after they concatenated vector of specimens, which pertain to the same wavelength, into a unified specimen batch. The USAMRD-WRAIR report reveals an unexplainable significant variation of the ED_{50} with small changes in wavelength. As a part of our study we analyzed the vectors of the single specimens and detected significant dissimilarity between the specimens. Following this finding, it was suggested that specimens' dissimilarity ungrounded the vectors unification, which should be replaced with a single specimen analysis. The single specimen analysis reveals a spread of the single specimen ED_{50} values, which leads to the assumption that subject dissimilarity might be one of the reasons that caused the unexplainable significant variation of the ED_{50}. However, the relatively small size of the single specimen batch (about 1/5 of the unified specimen batch) raised doubts on the effect of the batch size on probit's accuracy.
These problems start in a study to test the exactness and relevancy of the probit estimation technique for the specific characteristics of the data gathered at in-vivo laser- tissue experiments. The accuracy of probit's estimation was investigated by the use of Monte-Carlo simulations. Preliminary results are reported in the following sections.

2. METHOD

The Monte-Carlo simulations included the following steps:
1) Generating in-silico dose-response vectors from a predefined distribution.
2) Estimating the distribution parameters of these vectors with the probit analysis,
3) Comparing the probit's estimations with the predefined parameters.

1. Generating dose-response vectors

In a real laser tissue dose-response experiment, it is impossible to repeat the experiment under the same identical conditions. Once a tissue site is exposed to laser radiation, its physical properties are probable to change following the interaction with the laser radiation. Accuracy evaluation of a statistical estimation analysis is conditioned to many repetitions. Therefore, the first step in generating the in-silico dose-response vectors was to simulate repetitions of a real in-vivo experiment.
A set of 1000 vectors was prepared for each of the single as well as for the unified experimentally gathered specimen vectors (except for 10 single specimen vectors that had constant response, hence couldn't be analyzed). The dose values in each of the in-silico generated vectors were determined by using same values of the corresponding experimentally measured vectors.
The response values for each of the in-silico generated vectors were determined as follows. For each dose, the probability of response was calculated as the probability that a random tolerance is smaller than that dose. The parameters of the tolerance's distribution function were the parameters that were estimated by the probit analysis for the corresponding experimental in-vivo vector. Next, a random value originated from a uniform distribution ranged from 0 to 1 was generated. The random number was compared to the calculated response probability. The response was set the value of "1" if the random number was smaller then the calculated probability, and "0" otherwise.
For each experimental vector, two sets were prepared. One set was prepared while assuming that the tolerances' distribution type is normal. The second one was prepared while assuming that the tolerances' distribution type is log-normal. The predefined distribution for each set are then defined by the distribution type, the ED50 and slope estimations of the corresponding experimental vector.
Thus, we in all generated 470 different sets of in-silico vectors, 68 sets for the 34 unified experimental vectors and 402 sets for the 201 single specimen experimental vectors (a total of 470000 vectors.).
This procedure of vectors preparation preserve the basic assumption of any regression that the independent variable values are not random, and follow the basic assumptions of the Bio-assay circumstances for which the probit regression analysis is the appropriate analysis method. Moreover, this procedure results in a variety of sets that spans different dose combination, several vector sizes and two types of tolerances' distribution.
Assuming that the characteristics of the data gathered at the in-vivo laser- tissue experiments are such that are fit to be analyzed by the probit method, it is expected that analyzing the in-silico vectors will return estimates of the ED50 and slope values that are close to the ED_{50} and slope of the corresponding experimental vector.

2. Estimating the distribution parameters with the probit analysis

The ED_{50}'s and slopes for all classes of in-vivo and in-silico as well as single and unified vectors were estimated by the probit analysis. The probit algorithms were programmed (using MATLAB) following Finney's[2] instructions and algorithm. This algorithm composed of three steps. The first step is a transformation from response frequency (the number of responses divided by the number of subjects) to a normal equivalent deviation. This transforms observations coming from a normal (log-normal) distribution into a linear scale, which practically transforms a normal (or log-normal) resembling data points scatter into a linear resembling data points scatter. The second step includes a weighted linear (or semi-log-linear) regression done on the linear scatter of the data points. Several iterations are usually needed before the linear probit regression line and the scattered transformed data points are best fitted according to the maximum likelihood criterion. At the third step the tolerances' distribution parameters are calculated, based on the slope and intercept of the probit regression line.

The data of the in-vivo vectors and therefore the data of the in-silico vectors are specific in that the response frequencies are either '0' or '1'. The normal equivalent deviation of response frequencies that are [0, 1] are $[-\infty, \infty]$, respectively. Hence, to avoid numerical crash, limiting values of normal equivalent deviation were forced to the range [-5,5], which is equivalent to the probability range of [2.8E-7, 1- 2.8E-7]. The maximum likelihood iterations were stooped after 30 iterations or after the incremental change, of the parameters of the probit regression line, between two successive iterations was smaller than 1E-6.

Each of the in-silico vectors was analyzed twice. One analysis was preformed with the correct distribution type. That is, vectors that were generated with normal/log-normal distribution were analyzed with normal/log-normal distribution, respectively. The second analysis was done with the incorrect distribution type. That is, vectors that were prepared with normal/log-normal distribution were analyzed with log-normal/normal distribution, respectively.

At the end of this phase we then had 2000 ED_{50} and slope values for each set of in-silico vectors.

3. Comparisons of the probit analysis estimation to the pre-defined distribution

The mean and standard deviation of ED_{50} and slope values, of the 1000 vectors, were calculated for every set and combination of the prepared sets of vectors and conditions of the tolerances distribution type.

The biases of probit's ED_{50} and slope estimations are then the difference between the estimated ED_{50} and slope of the predefined distribution and the mean of the ED_{50}'s and slopes of the corresponding in-silico vectors. Respectively, the standard deviations of probit's ED_{50} and slope estimations are the standard deviation of the ED_{50}'s and slopes of the in-silico vectors.

The method of the result analysis for the comparison is demonstrated with the help of Figure 1 that shows probit's estimations of the 610nm unified vectors set. Graphs 1 and 3 in figure 1 exhibit the ED_{50} estimations. Graphs 2 and 4 in figure 1 exhibit the slope estimations. Graphs 1 and 2 are for the log-normal distribution and Graphs 3 and 4 are for the normal distribution. The vertical solid line in each of the four graphs shows the probit estimation of the in-vivo vector. For example, the ED_{50} value of the in-vivo unified vector that was treated with 610nm laser wavelength and was estimated under the assumption that the tolerances' distribution is log-normal can be read from graph 1. The slope value of the same in-vivo vector that was estimated under the assumption that the tolerances' distribution is normal can be read from vertical solid line in graph 4.

Each of the sigmoid curves displays the cumulative frequency of 1000 estimated values of the in-silico vectors. Solid curves display cases where the estimation was done with the same distribution that was used when the vectors were prepared, and dashed curves display cases where the estimation was done with the other distribution than that that was used when the vectors were prepared. For example, the dashed curve in graph 3 displays the cumulative frequency of 1000 ED_{50} estimations values of in-silico vectors that were generated according to the normal distribution and were estimated on the assumption that the tolerances distribution is log-normal.

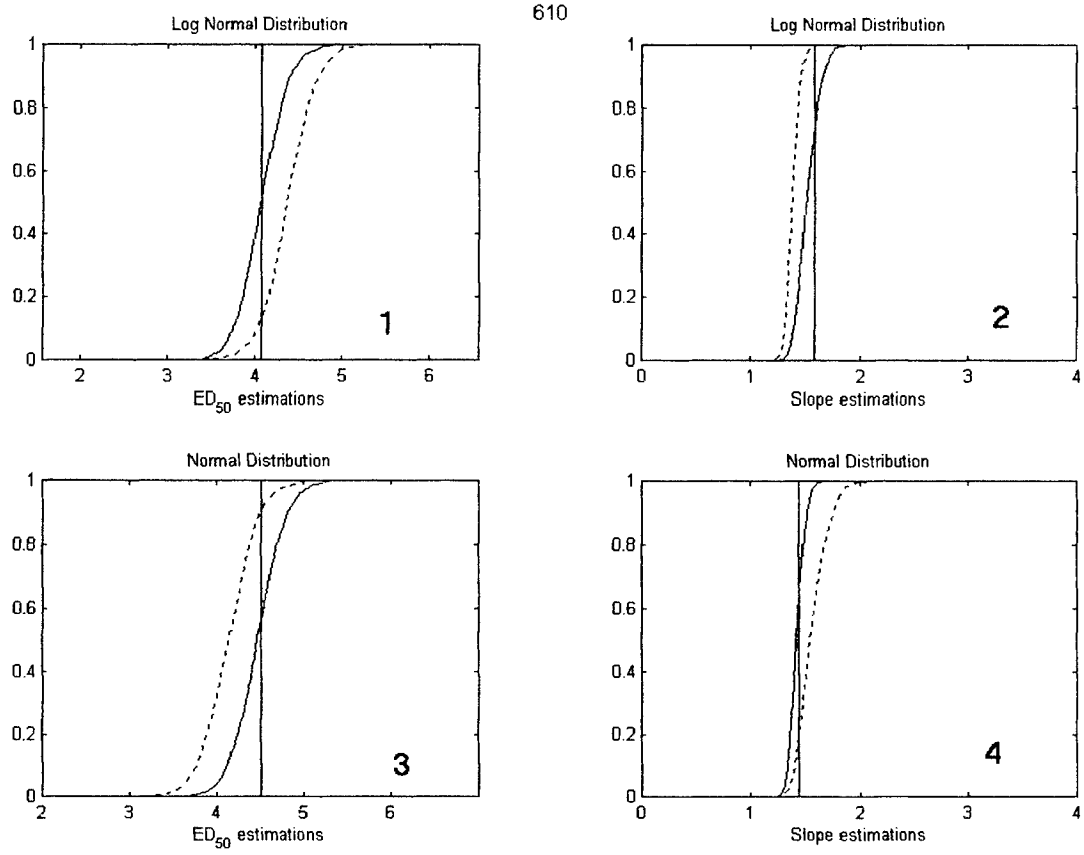

Figure 1: ED_{50} and slope estimations of the 610 nm unified vectors sets.

The bias of all classes of estimations is then the horizontal distance between the vertical solid lines to the means of the values represented by the relevant sigmoid curves. The standard deviation of all classes of estimations is then the standard deviation of the values represented by the relevant sigmoid lines.
Representing the data generated and analyzed at the current study should encompass an impossible presentation that includes 235 figures like figure 1. Therefore, the results section will mainly presents the statistics (mean, standard deviation and range) of the biases and standard deviations of the sets of the in-silico vectors.

probit's estimation exactness and relevancy for each in-vivo vector as well as for the whole experimental data may be examined by those biases and standard deviations.
The effect of vector size may be examined by comparing the estimations' bias and standard deviation of the unified specimen in-silico vectors to those of the single specimens in-silico vectors.
The sensitivity to the correctness of the assumed distribution type can be examined by comparing the effect of analysis with the correct distribution against the incorrect distribution on the bias and standard deviation of the estimations.

3. RESULTS

The mean, standard deviation and range of the biases of the ED_{50} estimation are tabulated in table 1. These statistics relate to the sample of 34 in-silico unified specimens' sets (1000 vectors in each set). Following the units of the in-vivo ED_{50}, the entries in table 1 should be interpreted as microjoules.

		Generating distribution of in-silico vectors					
		Log-normal			Normal		
		Mean	Standard deviation	Range	Mean	Standard deviation	Range
Analysis distribution of in-silico vectors	Log-normal	**0.02**	**0.07**	**-0.1 – 0.25**	-0.85	0.97	-5.5 - 0
	Normal	0.83	1.07	0.06 – 6.5	**-0.06**	**0.07**	**-0.3 – 0.09**

Table 1: Biases' statistics of ED_{50} estimations of the 34 in silico unified specimens' sets

The small mean and standard deviation of biases of the ED50 estimation for the case of where the tolerance's distributions of the vector generated and analysis are the same suggests that a very small mean error is expected when there is a previous knowledge about the correct tolerances distribution type. However, when such previous knowledge does not exist, a sizable mean error might be expected. The mean error when the analysis is done with the wrong assumed tolerances distribution (i.e. normal instead of log-normal or vice versa) might be as large as 2 microjoules or even 5 or 6 microjoules at extreme cases. Another interesting result is that when the vectors were generated with log-normal tolerances distribution and the estimation is done based on the normal distribution, the expected mean error is positive (i.e. real ED_{50} are smaller than the estimated ED_{50}), and vice versa.

The mean, standard deviation and range of the ED_{50} estimations' standard deviations of the 34 in-silico unified specimens sets are tabulated in table 2.

		Generating distribution of in-silico vectors					
		Log-normal			Normal		
		Mean	Standard deviation	Range	Mean	Standard deviation	Range
Analysis distribution of in-silico vectors	Log-normal	**0.73**	**0.62**	**0.1-3.17**	0.73	0.49	0.13 – 2.22
	Normal	0.99	1.54	0.1 – 9.22	**0.79**	**0.77**	**0.12 – 4.37**

Table 2: statistics of standard deviations of ED_{50} estimations of the 34 in silico unified specimens sets

The data in table 2 suggests that a random error in the ED_{50} value of about 1microjoule is quite likely. Moreover, the insignificant differences in the statistics between conditions where the generated and analyzed tolerances distribution are the same to the conditions where they are different, suggests that the random error is robust on the distribution type. Another matter regards the relatively large ranges of the standard deviations of the ED_{50} estimations. Such ranges might be due to differences between different sets of vectors. This issue will be discussed later.

The mean, standard deviation and range of the slope estimations' biases of the 34 in-silico unified specimens sets are in table 3.

		Generating distribution of in-silico vectors					
		Log-normal			Normal		
		Mean	Standard deviation	Range	Mean	Standard deviation	Range
Analysis distribution of in-silico vectors	Log-normal	**0.02**	**0.51**	**-0.11 – 2.89**	0.2	0.35	-0.03 – 2.08
	Normal	-0.39	0.87	-5.33 – -0.08	**-0.02**	**0.04**	**-0.04 – 0.18**

Table 3: Biases' statistics of the slopes of the 34 in-silico unified specimens sets

The data in table 3 presents similar results to those in tables 1 (biases' statistics of the ED_{50} estimations). The slopes mean error is small when the generating distributions for vectors are the same as the analysis distribution. This is especially true when both distributions are normal. When both distributions are log-normal, there is a relatively large standard deviation of the slope biases. Analyzing vectors with the wrong distribution type results with constant error which often might be as large as 0.5 or 1 and even 5 at extreme situations (for example, the estimated slope is 6.5 where the real slope is 1.5). When the tolerances' distribution is log-normal and the analysis is carried based on the normal distribution the mean error is negative (the real slope is larger than the estimated slope). When the tolerances' distribution is normal and the analysis is carried based on the log-normal distribution the mean error is positive (the real slope is smaller than the estimated slope).

The mean, standard deviation and range of the slope estimations' standard deviation of the 34 in-silico unified specimens sets are presented in table 4.

		Generating distribution of in-silico vectors					
		Log-normal			Normal		
		Mean	Standard deviation	Range	Mean	Standard deviation	Range
Analysis distribution of in-silico vectors	Log-normal	**0.87**	**4.2**	**0.06 - 24**	0.2	0.26	0.05 – 1.62
	Normal	2.76	15.57	0.05 - 90	**0.17**	**0.48**	**0.04 – 2.9**

Table 4: Statistics of slopes' standard deviations of the 34 in silico unified specimens sets

The statistics of the standard deviation of the slope estimations exhibits a similar trend to the statistics of the standard deviation of the ED_{50} estimations. The effect of analyzing with the correct distribution type is not significant when the random slope error is considered. A random slope error of 0.5 is quite likely. However, comparing the statistics of the slope random error of vectors that were generated with the log-normal distribution to the statistics of slope random error of vectors generated with the normal distribution, show that vectors generated with the log-normal distribution are associated with a greater random slope error.

We shall move on to the statistics of the estimations of the single specimens in-silico sets. The ED_{50} and slope estimations of 16 of the 201 (8%) in-silico sets were such that their bias and/or standard deviation were illogically large. This means that these 16 sets are not appropriate to be analyzed by probit. There could be several reasons for this inappropriateness. It could be that the predefined tolerances distribution (i.e. the distribution estimated by probit when analyzing the in-vivo vector) was wrong. It also could be due to the rage of doses not including the ED_{50} or too narrow in a way that there were no doses at high and/or low response probability (i.e. doses of ED_{10} ED_{20} and/or ED_{80} ED_{90}), etc'. We have not yet looked for an explanation for the inappropriateness of those 8% of the in-silico sets.

The statistics of the rest 185 (92%) of the in-silico single specimens sets are presented in tables 5 to 8. In order to enable comparison to the statistics of the unified specimens in-silico sets of vectors, the statistics of the unified sets are presented within parenthesis.

The mean, standard deviation and range of the biases of the ED_{50} estimation are presented in table 5. These statistics relates to the sample of 185 in-silico single specimens sets (1000 vectors in each set).

		Generating distribution of in-silico vectors					
		Log-normal			Normal		
		Mean	Standard deviation	Range	Mean	Standard deviation	Range
Analysis distribution of in-silico vectors	Log-normal	**0.09** (**0.02**)	**0.4** (**0.07**)	**-2.29 - 3.69** (**-0.1 – 0.25**)	-0.37 (-0.85)	0.56 (0.97)	-3.3 - 1.52 (-5.5 – 0)
	Normal	0.46 (0.83)	0.76 (1.07)	-2.12 - 5.55 (0.06 – 6.5)	**-0.02** (**-0.06**)	**0.38** (**0.07**)	**-1.94 - 2.8** (**-0.3 – 0.09**)

Table 5: Biases of ED_{50} estimations of the 185 in-silico single specimens sets

From table 5 we conclude that prior knowledge about the tolerances distribution type is beneficial for the single specimens sets as well as for the unified sets. For such cases, the expected mean ED_{50} error of the single specimens sets, though not extremely large (about 0.5 microjoule), is significantly larger than the expected mean ED_{50} error of the unified specimens sets. However, for cases where the assumed distribution type is wrong, the expected mean ED_{50} error of the single specimens sets is not different from the expected constant ED_{50} error at the unified specimens sets.

The mean, standard deviation and range of the ED_{50} estimations' standard deviations of the 185 in-silico single specimens sets are tabulated in table 6.

		Generating distribution of in-silico vectors					
		Log-normal			Normal		
		Mean	Standard deviation	Range	Mean	Standard deviation	Range
Analysis distribution of in-silico vectors	Log-normal	**2.05** **(0.73)**	**7.38** **(0.62)**	**0.05 - 98.4** **(0.1-3.17)**	1.42 (0.73)	1.17 (0.49)	0.07 - 6.9 (0.13 – 2.22)
	Normal	1.76 (0.99)	1.86 (1.54)	0.07 - 14.3 (0.1 – 9.22)	**1.51** **(0.79)**	**1.26** **(0.77)**	**0.08 - 6.8** **(0.12 – 4.37)**

Table 6: Standard deviations of ED_{50} estimations of the 185 in-silico single specimens sets

The results presented in table 6 show that as long as the random ED_{50} error is considered the analysis is insensitive to the distribution type. Moreover, the effect of vector's size is significant only where vectors were generated and analyzed with the log-normal distribution. For the case where single specimens vectors were prepared with the log-normal distribution, it even seems that the preferable distribution for analysis is the normal distribution. However, this result is not significant. For the single specimen vectors common random ED_{50} error is of 1.5 microjoules.

The mean, standard deviation and range of the slope estimations' biases and standard deviation of the 185 in-silico single specimens sets are presented in tables 7 and 8.

		Generating distribution of in-silico vectors					
		Log-normal			Normal		
		Mean	Standard deviation	Range	Mean	Standard deviation	Range
Analysis distribution of in-silico vectors	Log-normal	**3.32** **(0.02)**	**39.2** **(0.51)**	**-0.28 - 524** **(-0.11 – 2.89)**	4.6 (0.2)	46.4 (0.35)	-0.24 - 568 (-0.03 – 2.08)
	Normal	-0.17 (-0.39)	0.27 (0.87)	-2.39 - 1.2 (-5.33 – -0.08)	**-0.04** **(-0.02)**	**0.10** **(0.04)**	**-0.53 - 0.7** **(-0.04 – 0.18)**

Table 7: Biases of slopes of 185 in-silico single specimens sets

		Generating distribution of in-silico vectors					
		Log-normal			Normal		
		Mean	Standard deviation	Range	Mean	Standard deviation	Range
Analysis distribution of in-silico vectors	Log-normal	**107** **(0.87)**	**1238** **(4.2)**	**0 - 16580** **(0.06 – 24)**	144 (0.2)	1466 (0.26)	0 - 17947 (0.05 – 1.62)
	Normal	1.3 (2.76)	6.1 (15.57)	0 - 68 (0.05 – 90)	**0.83** **(0.17)**	**2.69** **(0.48)**	**0 - 23** **(0.04 – 2.9)**

Table 8: Standard deviations of slopes of 185 in-silico single specimens sets

The results presented in tables 7 and 8 shows that regardless of the tolerances distribution that was used in the vectors generation, the preferred distribution for the analysis is the normal distribution. That is as long as the mean and random error of the estimated slope of the single specimen sets is considered.

4. DISCUSSION

The preliminary results of the analysis of the Monte Carlo simulation show that the accuracy and relevancy of the probit analysis, for the case of data gathered at "in vivo dose-response laser tissue experiments", are conditional.

The statistics of the sample of 34 in-silico unified specimens sets suggest that a very small mean error of the ED_{50} and slope values is expected when there is a prior knowledge about the correct tolerances distribution type. However, when the analysis is done with the wrong tolerances distribution (i.e. normal instead of log-normal or log-normal instead of normal) the mean ED_{50} error might be as large as 2 microjoule and the mean slope error might be as large as 0.5 or even 1.

Moreover, a common ED_{50} random error of about 1microjoule and a random slope error of 0.5 is quite likely, where the random errors are insensitive on the prior knowledge of the tolerances distribution type.

Assuming that the estimation's errors' distribution is similar to the normal distribution, and assuming an estimated ED_{50} value is, say, 5 microjoule, the real ED_{50} is quit likely to be in the range of [4.5 – 5.5], if the correct tolerances distribution type was used in the analysis. If the wrong tolerances distribution type was used in the analysis the real ED_{50} value could be in the range of, say, [3.5 - 5] or in the range, say, [4.5 - 7].

The inter-ocular energy of a 3-mm pupil eye that is exposed to the maximal permissible exposure is about 0.04 microjoule and 0.2 microjoule for a 7-mm pupil. Considering that there are ED_{50} values of 2 microjoules, the safety margin is about 1.9 microjoule. According to our results, an ED_{50} error as large as 1.9 microjoule is not likely. However, it is quit clear that even smaller errors might significantly reduce the safety margins.

Considering the previously mentioned USAMRD-WRAIR report, which reveals an unexplainable significant variation of the ED_{50} with small changes in wavelength, we suppose that the matter of probit's accuracy might suggest an explanation for the significant variation of the ED_{50}. The ED_{50} of the in-vivo unified specimen vectors and the mean and standard deviation of the in-silico vectors are plotted in figure 2, versus the laser wavelength.

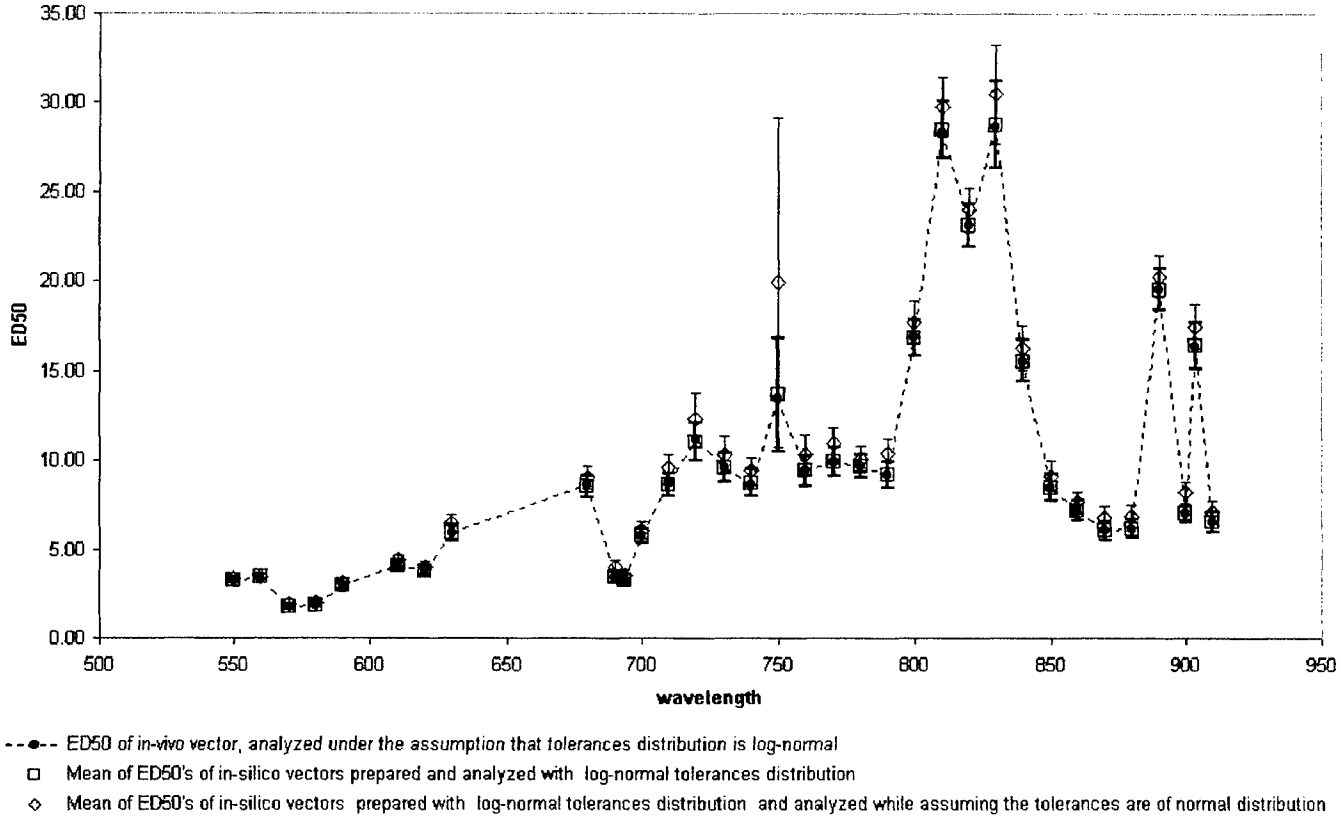

Figure 2: Mean and standard deviation of ED50 estimation, of vector prepared with log-normal distribution.

It is easily seen that there is a large correlation between the larger ED_{50} values, which cause the large variations, to the bias and standard deviation of the in-silico ED_{50} estimations.
Following this, we suspect that the large variations of the ED50 value were caused by the inapplicability of the probit analysis method to the collected data. Further research is needed to determine specifically the factors of the inapplicability.
Regarding the single specimens in-silico sets, 16 out of the 201 (8%) in-silico sets are probably not appropriate to be analyzed by probit. The statistics of the rest 185 (92%) of the in-silico single specimens sets shows that the expected constant ED_{50} error of the single specimens sets is up to 0.5 microjoule. Prior knowledge about the tolerances' distribution type is likely to reduce the mean error. A common random ED_{50} error is of 1.5 microjoules regardless of the correctness of the tolerances' distribution type. However, as long as the slope accuracy of the single specimens vectors is considered, the preferred distribution for the analysis is the normal distribution, which is expected to give a slope error that is similar to the unified specimens slope error.
Though we previously suggested that a single specimen analysis is better than the analysis done on the unified specimens[3], it now seems that such single specimen analysis will probably had to deal with a different problem of poor larger errors in the ED_{50} estimations. Hence, there is a trade off between dealing with specimen dissimilarity and the accuracy of the ED50 estimations.

5. CONCLUSIONS

Preliminary results suggest that probit's estimations might, sometimes, be biased in a way that they raise doubts about the validity of the conclusions based on probit's results. It might be that the assumptions of probit do not fit data gathered at the laser-tissue dose-response experiment.

Therefore, there is a need for another supporting analysis method, which could trace data, which might be inapplicable for been analyzed with probit (such as the simulation presented here). It also could be that another ED_{50} estimation method might return other, maybe more accurate ED_{50} estimations.

ACKNOWLEDGMENTS

We thank the USAMRD-WRAIR for supplying us their comprehensive data and especially Mr. Jack Lund for his invaluable ideas and support during our research.

REFERENCES

1. SPSS algorithm support: "Probit", http://www.spss.com/tech/stat/algorithms/probit.pdf.
2. D. J. Finney: "Probit Analysis", Cambridge University press, 1971.
3. Langus A. Fuchs C. and Gannot I., "Unconsidered Subject Dissimilarity: a Possible Key for Understanding Confusing Laser-Tissue Experiments Results", Proc. SPIE 3591, pp. 359-367, 1999.
4. D. J. Lund, E.S. Beatrice: "Near Infrared Laser Ocular Bioeffects", Health Physics Vol. 56, No. 5, pp. 631-636, 1989.

Implications of using ED-50 and probit analysis in comparing retinal injury threshold data

David H. Sliney[a*], John Mellerio[b], and Karl Schulmeister[c]

[a]U.S. Army Center for Health Promotion and Preventive Medicine, Aberdeen Proving Ground, MD 21010-5403, USA
[b]University of Westminster, School of Biosciences, W1M 8JS London, U.K.
[c]Austrian Research Centers Seibersdorf, A-2444 Seibersdorf, Austria

ABSTRACT

An indication of the level of uncertainty in laser injury studies relates to the slope of the transformed dose-response curve, or the "probit plot" of the data. The most cited threshold in a laser injury experiment is the point on the probit plot that represents a 50 % probability of injury: the ED-50. This value is frequently referred to as the "threshold," even though some experimental damage points exist below this "threshold." An analysis of any number of example data sets reveals that the slope in most experiments could not be explained by biological variation alone. The optical, thermophysical and biological factors influencing the probit plot are critically analyzed. By theoretically modelling an experiment, small errors in focus are shown to produce a substantial change in the ED-50 and the slope of the probit plot. The implications of plotting spot-size dependence with ED-50 values are shown to be significant, and can lead to erroneous conclusions regarding the apparent spot-size dependence.

1. INTRODUCTION

1.1 The Dose Response Curve

In studies of laser-induced injury of biological tissue, a dose response curve is frequently prepared to present the result. Any statistical analysis of uncertainties in retinal threshold studies has traditionally centred on an examination of the slope of the dose response curve expressed as a probit plot of experimental data. It frequently had been thought in some circles that the most important reference point on the probit plot is the exposure that represents a 50 % probability of injury: the ED-50. Indeed, this value is frequently referred to as the "threshold," even though some experimental damage points exist below this "threshold." The steepness of the curve is not only related to the type of damage mechanism and variation among individual animals, but also indicates problems in conducting the experiment. The techniques of probit analysis come from toxicology, and certain inherent assumptions relating to the expected distribution of toxicological threshold data, where each exposure is presumed to be independent,[9] have been carried over to laser safety studies, however the assumptions underlying this technique require some discussion. We define the slope as the ratio of ED-84/ED-50.

The thresholds for injury are normally obtained by exposing laboratory animals under controlled conditions to simulate "worst-case" human exposure conditions[4] and threshold is quoted as a single ED-50 value. Mush[21] and Wolbarsht and Sliney[29] argue that this approach is unsatisfactory and that far too much emphasis is placed on the ED-50 value, rather than also reporting other points on the curve. Nevertheless, quoting the ED-50 is the accepted convention. The value of the ED-50 will be influenced by the choice of experimental endpoint and the delay until examination after exposure. Although the biological change is most frequently determined by direct observation, more sensitive endpoints based upon microscopy or chemical analytical techniques are also employed. In the determination of thresholds of laser-induced injury, direct observation by ophthalmic instruments is most frequently used. For retinal studies, the experimentalist, to observe the retinal location where the laser exposure takes place, uses the ophthalmoscope or slit-lamp microscope. In some cases the visibility of the laser-induced lesion can be improved by a technique known as fluorescein angiography, and some workers have even used light and electron microscopy to examine the exposed tissue[4,5]. These measures claim to have greater sensitivity, but are more costly and less practical. Although fluorescein angiography is frequently used, the detailed histological studies with microscopic examination of thin slices of exposed tissue have only been carried out for specified laser wavelengths and exposure durations to quantify the reduction in the ophthalmoscopically determined ED-50 by the more elaborate techniques. Normally this reduction factor is approximately 2, and the committees deriving the total "safety factor" required to arrive at an MPE take this factor into account.

Laser and Noncoherent Light Ocular Effects: Epidemiology, Prevention, and Treatment,
Bruce E. Stuck, Michael Belkin, Editors, Proceedings of SPIE Vol. 4246 (2001)

Figure 1 shows an example of an early, hand-drawn retinal damage probability curve where the actual bars indicate the absence or presence of damage are recorded above and below the curve. It also shows the lowering of the threshold values when histological criteria for damage are applied. The slope "S" of the dose response curve reflects not only natural biological variation, which may have a lognormal distribution, but also the impact of experimental errors, which may show a different statistical distribution. The class of damage mechanism will also alter the steepness of the curve. When the slope is shallower, this indicates an increased standard deviation, which in turn may be due to increased experimental uncertainties. This illustrates that any derivation of human exposure limits for laser-induced injury requires one to estimate the true biological variation and separate this from the added experimental errors that reduce the steepness of the slope in the probit plot.

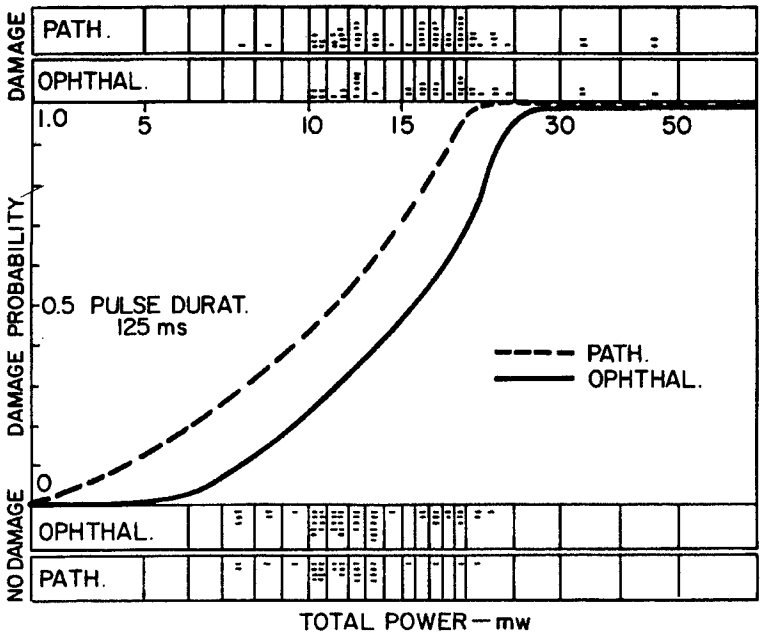

Figure 1. Early, hand-drawn dose-response curve.

We analysed a collection of experimental data reported in a variety of studies of corneal and retinal injury from pulsed laser radiation[26]. The analysis indicates that thermal and thermoacoustic damage mechanisms apparently have an intrinsic slope of approximately 1.05 to 1.15[1,18,25]. Often, however, experimental threshold data have shallower curves with slopes "S" that are numerically much greater, e.g., 1.5 - 1.7, and even up to 2.8[19,27,28]. This is really not surprising because the enormous difficulties of seeing a minimally visible lesion and focusing the laser beam to produce the nearly diffraction-limited image leads to this greater spread of data and shallower slopes. Thus, a probit plot applied during the derivation of exposure limits should have a slope adjusted to be steeper to account for these experimental contributions to the spread of data points.

The slope of the probit plot has generally been considered a good indication of the overall uncertainty and quality of the experimental data, but there has been some disagreement as to whether this slope could be considered an index of risk to a human population.

1.2 Retinal Injury Mechanisms

In an ideal experiment where the experimental errors introduced by the beam propagation through the ocular media were not present, the spread of retinal threshold data would be much smaller than that obtained by current experimental methods. The type of damage mechanism will affect the absolute spread of threshold data. Based upon the current understanding of the retinal injury mechanisms by short-pulsed lasers, thermal photocoagulation dominates for pulse durations of 10 ns to many milliseconds. Injury thresholds appear to vary little from 10 ns to about 18 – 50 μs. At longer durations, the thresholds increase because heat flow occurs during the exposure. At sub-nanosecond exposure durations, other, non-linear damage mechanisms come into play, such as self-focussing and laser-induced breakdown. The thermal and thermo-mechanical mechanisms have sharply defined thresholds in experiments where tissue is directly exposed without confounding factors, as

in CO_2 laser-induced corneal injury[1] or *in vitro* studies of laser induced injury to RPE cell cultures[18]. More stochastic effects appear in the sub-nanosecond regime and the dose-response curves become shallower[24,25].

2. METHODS AND ANALYSIS OF EXPERIMENTAL FACTORS

The calculated value of the ED-50 and the spread of data points can change by varying the experimental exposure or evaluation techniques. We analyzed the major sources of uncertainties in experimentally determined thresholds and dose-response curves for retinal thermal injury. There are a number of factors that influence the spread of data in laboratory experiments and each was evaluated in terms of the impact upon the reported ED-50 values and probit slopes. To explore these factors, we undertook a review of the extensive database from experimental animal threshold ocular injury studies. The methods of this analysis focused on the variation in the slopes as well as the ED-50 values in the dose-response plots, where available. All of the sources of experimental error - other than false-positive data - will increase the ED-50 value and the value of the slope. The published ED-50 data with slopes showed slopes S ranging from about 1.04 to 2.5. As the slope values increase, corresponding to an increased spread of data, one implication is that experimental difficulties have also increased. For example, one early series of experiments to determine ED-50 values for a 30-ns q-switched ruby laser (694.3 nm) had particularly large slopes of 2.2 for the smallest spot sizes, and dropped to 1.3 for large (0.89 mm) retinal image sizes as shown in Figure 2[3]. From a biophysical standpoint, one would not expect the dose response curve (and therefore probit slopes) to vary so much for different retinal image sizes. It is well known that ruby laser beams did not have clean Gaussian profiles and therefore, a consistent, minimal image diameter was difficult to achieve, and the spread of data were particularly great for these small spot sizes.

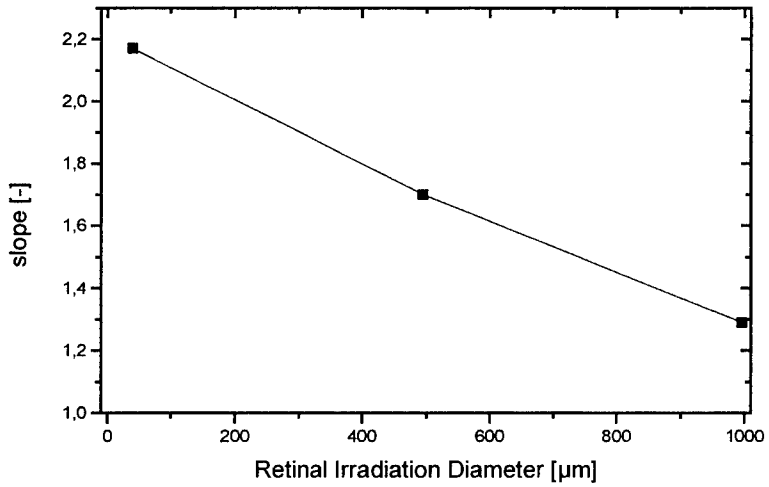

Figure 2. The variation of reported slope of the retinal threshold dose-response curve for one study.

2.1 Time of Examination

One of the most critical elements of the experimental protocol is the delay between laser exposure and time of examination, because biological changes undergo a time course following injury. Typical delays for examination range from 5 minutes to 48 hours, with 1 hour and 24 hours being the most frequently used. Depending upon damage mechanism (i.e., thermal, thermo-mechanical, photochemical, etc.), the optimum period for determining the ED-50 changes as the time-course varies for the biological response and amplification of the initial biophysical tissue insult. For thermal injury this appears to have a very small impact of 1.2 or less, and this was not studied further.

2.2 Animal Model

Another factor that affects the ED-50 value is the choice of experimental animal. One of the most frequently used animals in ophthalmic research is the rabbit, and this is used most often for corneal injury studies, and was used in many early retinal studies. However, the optical quality of the rabbit eye is poor, leading to distorted retinal images and inaccurate threshold determinations[4,25]. There have been studies employing ophthalmic contact lenses and careful optical alignment of the anaesthetised rabbit to eliminate most corneal aberrations in the eye[6]. These conditions produce nearly diffraction-limited retinal images leading to lower threshold values. However, There remains some uncertainty as to how close the contact-lens-rabbit model is to the awake, task-oriented human eye in everyday environments. Hence, the most favored animal model has

become the rhesus monkey for retinal studies for most investigators, and this has greatly increased the cost of the experiment, leading to fewer threshold determinations.

2.3 Retinal Pigmentation

Still another factor, the retinal pigmentation, will determine the fraction of incident energy absorbed at each wavelength and thereby affect the resulting ED-50. Pigmentation in the retinal pigment epithelium (RPE) and choroid varies with the individual subject, the species and the retinal location. Although the color of the rabbit retina appears to more closely resemble that of the human retina[13], it has been argued that since the RPE melanin pigment density is greater in the rhesus monkey compared to that of the human (and the retinal structure more similar), the rhesus monkey is a preferable experimental model for safety studies[20, 25]. Gabel et al[11, 12] showed that the RPE pigmentation had a limited variation of about two-fold across a human population although choroidal pigmentation varied. The macular pigmentation was the most uniform and consistent. To estimate the impact of localized pigment mottling, we scanned micrographs of RPE cells (Figure 3) to determine the pigmentation densities. The variation in relative absorption was approximately 1.3 for a 25 μm spot 1.2 for a 40 μm spot and 1.15 for a 75-μm diameter spot. While this would impact the spread of data, it would not have a very great impact upon the slope of the dose-response curve.

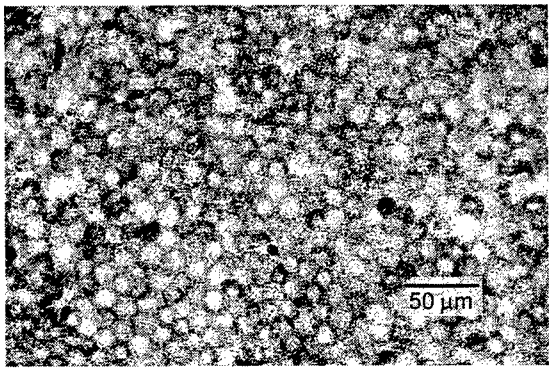

Figure 3. Photomicrograph of a flat-preparation of retinal pigment epithelium showing pigment mottling[11]

2.4 Refractive State

Also of concern is the refractive state of the experimental subject as this determines whether the minimal retinal image size of a collimated laser beam is achieved; this is critical[10]. A one-diopter error in the refractive state can result in an increase in the achieved retinal blur circle from approximately 25 μm to about 120 μm -- a change in image area of 22 times. Investigators therefore normally attempt to correct the animal's state of refraction in the visible, but this does not take into account the chromatic aberrations -- also of the order of one diopter across the visible spectrum. Investigators are able to correct the refraction to within 0.25 D, which leads to an uncertainty in the actually achieved minimal retinal image diameter of approximately 20 μm to 50 μm. Furthermore, during an investigative session, the animal's refractive state will vary slightly from exposure to exposure, the degree depending upon the level of anaesthesia; this increases the spread of data.

2.5 Eye Movements

Eye movements during the experimental exposure will also affect the outcome. These eye-movements will only be of concern for exposures lasting more than 10 ms, particularly in anaesthetised animals[22, 16]. Ness et al.[22] showed that laser energy was concentrated in a much smaller retinal area in the anaesthetized animal.

2.6 Retinal Location

The actual site of retinal exposure will influence the ED-50. This occurs for two reasons. First the optical quality of the eye for off-axis beams is somewhat less than for axial exposures to the macula. Second, the pigmentation and thickness of the neural retina vary from the center of the fovea, through the macula to the paramacular regions. As a general rule, the ED-50 values will be less in the fovea than parafovea or paramacular region. This variation is of the order of two-fold[4, 17, 23].

2.7 Intra-ocular Scatter

The state of the ocular media (cornea, aqueous, lens and vitreous) influences the distribution of radiant energy at the retina. Intraocular scatter diffuses the beam, and depending upon the nature and size of the scattering centers in the ocular media, small-angle forward scatter and diffuse scatter will vary. The age of the eye, the care taken by the experimentalist to preserve

corneal clarity by frequent irrigation of the cornea (or use of contact lens), and the potential for subtle lenticular opacities (early stages of cataractogenesis), all play a role in producing scatter[25].

2.8 Observer Skills and Lesion Detection

The ability of the experimental investigator observing the retina to detect a just-perceptible minimum visible lesion (MVL) also influences the ED-50 value. As investigators have more experience, the reported ED-50 values generally decrease. The visual contrast of the threshold injury is usually low, making the task of correct lesion detection difficult. Furthermore, the chance of scoring the presence of a very small lesion when an injury is actually not present (i.e., false positive) will increase if the retina appears mottled or otherwise exhibits abnormalities that could be mistaken for a laser induced lesion. It may also be difficult to discern the edges of some very large lesions making positive identification difficult. Nevertheless, our review of the published threshold studies that provide dose response slopes show a general trend for a steeper slope (smaller numerical value) for larger images, suggesting that small-lesion experiments are more difficult to perform[3, 31] as shown in Figure 2.

2.9 Beam Quality

The optical quality of the incident laser beam influences the minimal retinal image size. In earlier studies, multi-mode lasers were frequently used, leading to a larger retinal image area and increased values of the ED-50[25]. Today, most lasers used in these experiments have been carefully aligned to achieve a single transverse mode. The presence of apertures in the beam path can also alter the quality of the retinal image.

3. RESULTS

It is evident that aside from false positive identification of a lesion, all of the other aforementioned sources of error will tend to increase the ED-50 values and the spread of the data from which they are derived[25]. This will be discussed in greater detail in the following discussion of the statistical treatment of threshold data.

3.1 Method of Determining a Risk of Injury in Awake Humans

Recent studies typically report slopes of 1.1 to 1.4. Indeed, the choice of the "safety factor" used by committees for derivation of MPEs recognized that experimental difficulties led to a skewed probability distribution and ED-50 values that are too high. The choice of large "safety factor" values, as great as 10 to 20, resulted from this recognition of experimental uncertainties. As experimental techniques improved (often indicated by steeper probit slopes), safety factor values less than 10 have sometimes been applied. It is interesting to note that in deriving exposure limits for skin and cornea, smaller safety factors have been possible because of the reduced uncertainties in experimental determinations of exposure parameters and damage.

An analysis of a number of example data sets reveals that the slope in some experiments could not be explained by biological variation alone. For example, if the reported slope is not very steep due to experimental uncertainties, the laser safety community might assume that a larger-than-necessary safety factor would be required. The consequence of directly applying experimental animal dose-response curves having more shallow slopes (e.g., 2 to 2.5) to estimate risk of injury in humans is that the plot could predict a finite probability for an injury occurring at a dose of as little as 10 % of the ED-50. Yet, from fundamental biophysical principles, this result could be shown clearly to be flawed. If the ED-50 energy corresponds to a retinal temperature elevation of 15°, an energy of 10 % of the ED-50 would correspond to 1.5° (10 % of the ED-50 temperature elevation), which could not produce photocoagulation[7]. This is true despite the fact that individual proteins, although denatured at normal body temperatures, are repaired or replaced by cellular maintenance processes that insure proper cellular function[2, 14, 15] and it also fits with one's own experience, that an elevation of body temperature (as with a mild fever of 1.5° C) although unpleasant, is not fatal. Finney[9] states that "...very extreme probits, say outside the range of 2.5 to 7.5, carry little weight, and may almost be disregarded unless many more subjects were used..." Probit values of 2.5 and 7.5 correspond to probabilities of about 1 % and 99 %, respectively.

The total uncertainty in threshold studies of CO_2 laser corneal thermal injury is frequently reported as 10 % or less. For example, Bargeron and colleagues[1] explained that they did not need to apply probit analysis because the final bracket between a lesion and no-lesion was approximately 10 % of the working power level. As a consequence, they required fewer animals to determine their thresholds[1]. Such corneal studies imply a probit slope less than 1.1 because experimental error is minimal and the underlying biological variation for photocoagulation is revealed. Clearly, a "safety factor" of 10 in deriving MPE limits cannot be justified

3.2 Controlling for Refractive Errors

A review of the data from retinal injury studies shows that probit slopes tended to be smaller for the more recent retinal injury studies where laser quality and experimental techniques have improved. It follows that the distributions of experimental data points are more tightly clustered in these more recent studies and should more closely approach the ideal experimental exposure conditions with minimal experimental error. The steepest slopes reported ranged from 1.01 for a large spot 3 μs threshold to about 1.2 for small images for visible wavelengths[31]. This variation in slope with retinal spot size results for two reasons. There are greater experimental difficulties in consistently achieving the smallest possible retinal image due to variations in corneal clarity and intra-ocular light scattering and achieving optimal refraction. This is aptly demonstrated by the studies of Birngruber and colleagues who employed a contact lens delivery system for exposing both rabbits and monkeys with a contact-lens delivery system which eliminated most of the experimental error related to refraction[8]; they consistently obtained steeper slopes of 1.1 to 1.4 in the visible. Also, the small retinal structural and pigmentary inhomogeneities have dimensions approximately the same size at the minimum retinal image and therefore would influence localised energy absorption from exposure to exposure.

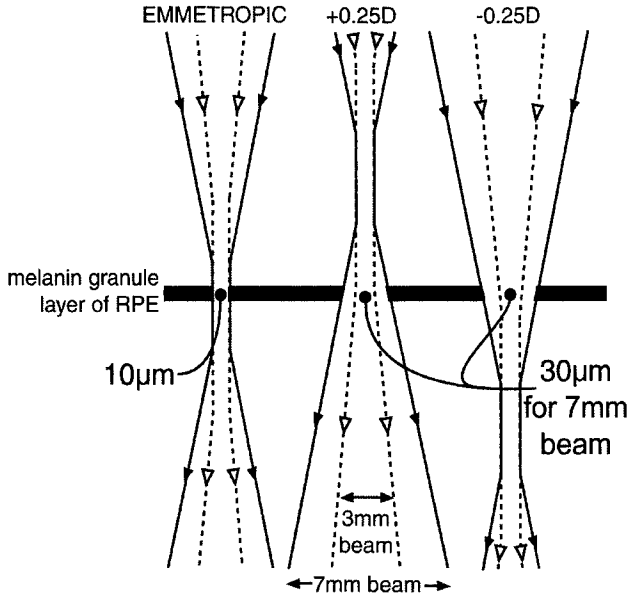

Figure 4. Schematic effect of error in focus for only 0.25 D error. Actual focal error can be greater.

To estimate the magnitude of effect upon the probit slope of refractive errors in an experimental study of retinal thresholds for small images, we mathematically simulated a range of likely refractive errors. It is generally accepted that the best refractive correction in a laboratory setting is approximately 0.25 diopter (0.25 D). In the model, which is schematically depicted in Figure 4, a series of hypothetical exposures were delivered in one primate eye having an effective focal length in air of 15.00 mm and the minimal, nearly diffraction-limited image of 10 μm was achieved for every exposure and the ED-50 was set at 1 μJ with a probit slope of 1.1. Next, a similar series of exposures were made under the assumption that all were delivered with varying degrees of refractive error, but not exceeding 0.25 D. A maximal refractive error of 0.25 D resulted in a retinal image blur circle of 34 μm for a 7-mm pupil. When it was assumed that the thermal injury threshold varied linearly with spot size[3], then the slope increased to 1.6 and the ED-50 increased to 2.5 μJ (for a beam diameter of 7 mm). When it was assumed that the threshold was constant with retinal irradiance (as postulated for some sub-microsecond durations and shown by Lin et al.[18]), then the slope increased to values greater than 2.0 and the ED-50 increased to approximately 6 μJ. Because the rabbit eye has a shorter focal length (about 10 mm) than the monkey eye (about 15 mm), these calculated results would be even more dramatic for a rabbit model. The results are illustrated in Figure 5. Note that there is an inflection in the slope because there is a minimum spot size of 10 μm, which applies to all probabilities below the inflection point. This model actually fits quite well with published experimental laboratory experience. If the beam diameter at the cornea were 3 mm rather than 7 mm, the slope above the inflection point would become steeper than as shown in Figure 5 because of the increased geometrical depth of focus for the 3 mm beam. In addition to this geometrical factor, the greater corneal spherical aberrations over a 7 mm corneal area will further spread the retinal focal diameter of the larger beam; however, we did not add this effect to our simulation.

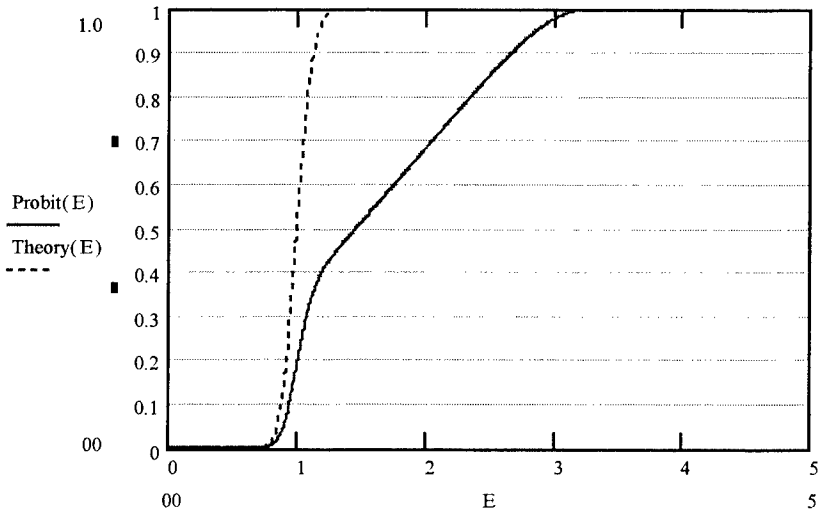

Figure 5. The change in the dose response curve modelled by a slight refractive error of only 0.25 D. Note the increase in the ED-50 value, which can become much greater for a slightly greater refractive error.

4. CONCLUSIONS

By adding the effects of misfocus and the change in the impact of pigmentation variation, we show a reduction in the spot-size dependence. In setting retinal laser safety limits, committees have always agreed that human exposures at levels less than 10 % of the apparent ED-50 assured safe exposure. In other words a "safety factor" of 10 was quite adequate even though the "real safety factor", i.e. the ratio of the "true" ("ideal" experiment) ED-50 and the EL, would be less. In the future, committees deriving human exposure limits must take full account of the impact of improved experimental techniques. As techniques improve and uncertainties reduce, probit slopes will become steeper, and it must be recognised that the former "safety factor" of 10 should be reduced accordingly without sacrificing safety. When all contributing physical factors are considered, the true dose-response function cannot be considered to follow a log-normal distribution at extremes. The slope of the dose-response curve is very steep at low probabilities and becomes shallower for higher probabilities where the physical variables of pigment variation, focusability, etc. strongly influence the slope.

Collective plots of spectral dependence, temporal dependence or spot-size dependence, will be skewed if only ED-50 values are plotted without consideration of the variation in their corresponding slopes. The most obvious impact would relate to plots of the variation of ED-50 values with retinal spot-size, since the slope (and "true ED-50") vary greatly with spot size as was shown in Figure 3 (where the reported ED-50 for the smallest image could be a factor of at least four too large). By adding the effect of misfocus and the variability of pigment mottling, the spot-size dependence of some recent studies of Zuclich et al (2000), can be nearly predicted, as shown in Figure 6. This problem has a direct impact upon setting human exposure limits for extended sources. While both theory and experiment predict a spot-size dependence for CW laser exposures, this is not the case for short-pulse laser exposures, and this review suggests that the value for alpha-max needs to be reduced for short pulses. Finally, we can conclude the "safety factor" applied to IR-B and IR-C (corneal hazard) can be two-fold and not ten-fold.

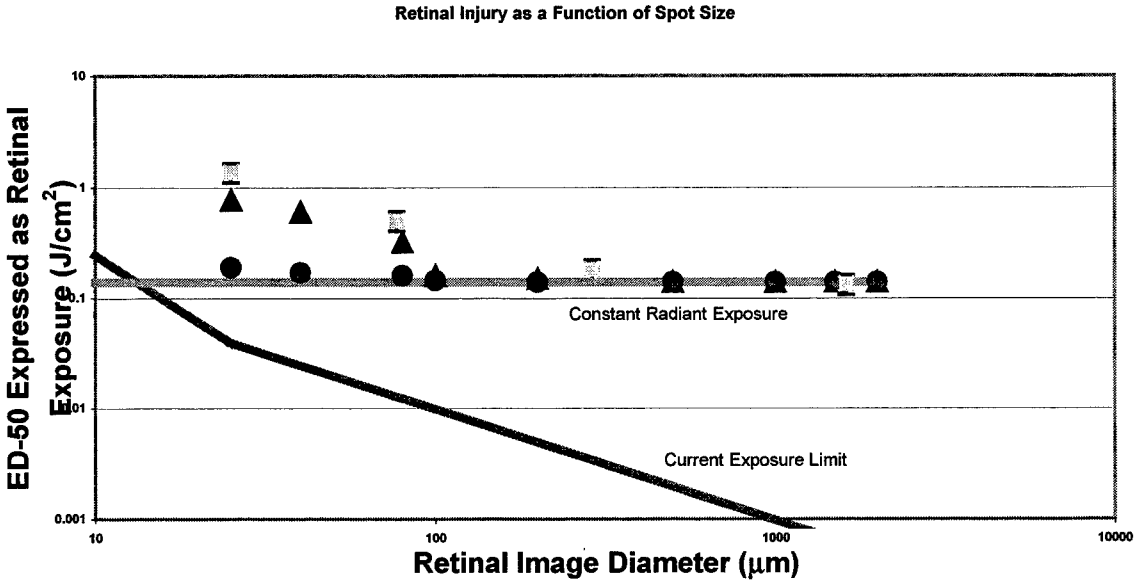

Figure 6. The retinal injury thresholds expressed as radiant exposure calculated at the retina in J/cm^2 (■) reported by Zuclich et al, (2000) are the uppermost data points . The solid sloped line is the current MPE value for visible microsecond pulsed exposures. The horizontal solid line is the theoretically expected spot-size dependence for such a short pulse. The effect of uncertainties and data spread upon the ED-50 due to mottling is shown by the (●) points. Finally, the combined effect of both pigment-mottling and focal errors to increase the ED-50 values for the smaller images is shown as triangular data points (▲). This suggests that past efforts to plot ED-50 values may have led committees to set limits with a spot-size dependence that was largely artifactual.

REFERENCES

1. Bargeron C. B., Deters D. J., Farrell R. A., McCally R.L., "Epithelial damage in rabbit corneas exposed to CO2 laser radiation", *Health Phys*, **56,** pp.85-95, 1989.

2. Barnes, F. S., "Biological damage resulting from thermal pulses", In M.L. Wolbarsht, Ed, *Laser Applications in Medicine and Biology, Vol. 2*, Plenum Press, New York, pp. 205-332, 1974.

3. Beatrice E. S., Frisch G. D., "Retinal laser damage thresholds as a function of image diameter", *Arch Environ Health*, **27**, pp. 322-326, 1973.

4. Beatrice, E. S., Randolph, D. I., Zwick, H., Stuck, B. E., Lund, D. J., "Laser hazards: biomedical threshold level investigations", *Mil Med*, **141**, pp. 889-892, 1977.

5. Borland, R. G., Brennan, D. J., Marshall, J., Viveash, J. P., "The role of fluorescein angiography in the detection of laser-induced damage to the retina: A threshold study for Q- switched neodymium and ruby lasers", Exp Eye Res, 27, pp. 471-493, 1978.

6. Birngruber, R., Gabel, V. P., Hillenkamp, F., "Experimental studies of laser-thermal retinal injury", *Health Physics*, **44**, pp. 519-531, 1983.

7. Birngruber, R., Hillenkamp, F., Gabel, V. P.,"Theoretical Investigations of Laser Thermal Retinal Injury", *Health Physics*,**48**, pp. 781-796, 1985.

8. Birngruber, R., Hillenkamp, F., Gabel, V.P., "Experimentelle und Theoretische Untersuchungen zur thermischen Schadigung des Augenhintergrundes durch Laserstrahlung", GSF-Bericht. AO 251, Munich, Gesellschaft fur Strahlen- und Umweltforschung mbH, 1978.

9. Finney, D. J., *Probit Analysis, 3rd Edn*, Cambridge University Press, Cambridge, 1971.

10. Frisch, G. D., "Retinal laser irradiation diameter estimation", *Appl Opt*, **11**, p. 939, 1972 .

11. Gabel, V. P., Birngruber, R., Hillenkamp, F., "Visible and near infrared light absorption in pigment epithelium and choroids", In: K. Shimizu and J.A. Oosterhuis, Eds, *XXIII Concilium Ophthalmologicum*, International Congress Series No. 450. pp. 662-678, 1978.

12. Gabel, V. P., Birngruber, R., Hillenkamp, F.,"Die Lichtabsorption am Augenhintergrund [Light Absorption in the Retina]", GSF Report A-55, Gesellschaft fuer Strahlen-und Umwelforschung, Neuherberg; 1976.

13. Geeraets, W. J., Berry, E. R., "Ocular spectral characteristics as related to hazards from lasers and other light sources", *Am J Ophth*, **66**, pp. 15-20, 1968.

14. Henriques, Jr. F.C., "Studies of thermal injury V. The predictability and the significance of thermally induced rate processes leading to irreversible epidermal injury", *Amer J Pathol*, **23**, pp. 489-502, 1947.

15. Hillenkamp, F., "Interaction between laser radiation and biological systems, In: f. Hillenkamp, r. Pratesi, C.Z. Sacchi, Eds, *Lasers in Biology and Medicine*, NATO Advanced Study Institutes Series A #4. New York: Plenum Press, 1980.

16. International Commission on Non-Ionizing Radiation Protection (ICNIRP). Revision of guidelines on limits for laser radiation of wavelengths between 310 nm and 1.4 μm. Health Phys. 77:??; 2000.

17. Lappin, P. W., Coogan, P. S., "Relative sensitivity of various areas of the retina to laser radiation", *Arch Ophthalmol*, **84**, pp. 350-254, 1970.

18. Lin, C. P., M. W. Kelly, Sybayan A.B.S., Latina M. A., Anderson R.R., "Selective Cell Killing by Microparticle Absorption of Pulsed Laser Radiation", *IEEE Journal of Selected Topics in Quantum Electronics*, **5**, pp. 963 – 967, 1999.

19. Lund, D. J., and P. Edsall, "Action spectrum for retinal thermal injury", pp 209-228 In r. Matthes, D.H. Sliney, Eds, *Measurement of optical radiation hazards*, ICNIRP Oberschleißheim, 1998.

20. Maher, E. F., "Transmission and absorption coefficients for ocular media of the rhesus monkey", USAF School of Aerospace Med, Brooks AF Base, TX, Report SAM-TR-78-32, 1978.

21. Mush, A., "Dose-time-effect-relationships", In R.J.M. Niesink, J. deVries, M.A. Hollinger, Eds, *Toxicology: Principles and Practice*, CRC Press, Boca Raton, 1996.

22. Ness, J. W., Zwick, H., Stuck, B. E., Lund, D. L., Lund, B. J., Molchany, J. W., Sliney, D. H., "Retinal image motion during deliberate fixation: implications to laser safety for long duration viewing", *Health Physics*, **78(2)**, pp. 131-142, 2000.

23. Polhamus, G. D., Edsall, P. R., Thomas, R. J., Hall, R., Zuclich, J. A., Schmeisser, E. T., Elliot, R., Carothers, V., Zwick, H., and Kang, R., "Laser-induced damage in the peripheral retina", *Health Physics*, **77**, 2000.

24. Roach, W. P., Johnson, T. E., Rockwell, B. A., "Proposed maximum permissible exposure limits for ultrashort laser pulses", *Health Physics*, **76**, pp. 349-354, 1999.

25. Sliney, D. H., Wolbarsht, M.L, "Safety with Lasers and Other Optical Sources", Plenum Publishing Corp, New York, 1980.

26. Sliney, D.H., Mellerio, J, Gabel, V-P., and Schulmeister, K., "What is the meaning of thresholds in laser injury experiments? Implications for human exposure limits", in press *Health Physics* (2001)

27. Stuck, B. E., Belkin, M., "Laser and Noncoherent Ocular Effects: Epidemiology, Prevention, and Treatment I", *SPIE Proceedings*, **2974**, 1997.

28. Stuck, B. E., Belkin, M., "Laser and Noncoherent Ocular Effects: Epidemiology, Prevention, and Treatment III", *SPIE Proceeding, **3591**,* 1999.

29. Wolbarsht, M. L., Sliney, D. H., "1991, 1992, Historical development of the ANSI laser safety standard", *Journal of Laser Applications*, **3**, pp. 5-10; 1991 and **4**, pp. 18-21; 1992.

30. Wolfe, J. A., "Laser retinal injury", *Military Medicine*, **150**, pp. 177-181, 1985.

31. Zuclich, J. A., Lund, D. J., Edsall, P., Hollins, R. C., Smith, P. A., Stuck, B. E., Mclin, L. N., "Laser induced retinal-damage threshold as a function of retinal image size", In: B.E. Stuck and M. Belkin, Eds, *Laser and Noncoherent Ocular Effects: Epidemiology, Prevention, and Treatment. SPIE Proceedings,* **3591**, pp. 335-343, 1999.

32. Zuclich J.A., Lund D. J., Edsall P. R., Hollins R. C., Smith P. A., Stuck B. E., Till S., McLin L. N., Kennedy P. K. and S. Till, "Variation of laser induced retinal-damage threshold with retinal image size", *Journal of Laser Applications,* **12(2)**, pp. 74-80, 2000.

Filtering Potentially Biased Probit's Threshold Estimation with Multiple Analyses

Amir Langus[*a], Camil Fuchs[b] and Israel Gannot[a]

[a] Faculty of Engineering, Department of Bio-Medical Engineering,
[b] Faculty of Exact Sciences, School of Mathematical Sciences, Department of Statistics and Operations Research,
Tel-Aviv University, Tel-Aviv, Israel 69978

ABSTRACT

For more than 10 years there has been a doubt regarding experimental results reported by the USAMRD-WRAIR. The USAMRD-WRAIR report reveals an unexplainable significant variation of the ED_{50} with small changes in wavelength. Reanalyzing the data of the USAMRD-WRAIR with several different analysis methods reveals a large correlation between inconsistent ED_{50} estimations to wavelength with larger ED_{50} values, which can be related to the large ED_{50} variations.

Keywords: Statistical analysis, probit, Laser tissue interactions, Data filtering.

1. INTRODUCTION

The probit analysis method is commonly used in analyzing data gathered at in-vivo dose-response laser-tissue experiments. A sample of subjects (i.e. animals) is treated in a typical in-vivo dose-response laser-tissue experiment. Each subject usually is treated a number of times at different tissue sites with different exposure energies (while other laser parameters are kept constant). The data gathered are the exposure energies and the exposure results, which are the characteristics of the post-exposure laser lesion. Laser lesions may have many different appearances. It is convenient to define a threshold lesion and to classify the exposure results by a binary quantal grade. If an exposure outcome is a lesion that is similar or more severe than the threshold lesion, the exposure's result is defined as response and coded as "1". If an exposure outcome is a lesion that is less severe than the threshold lesion, the exposure result is defined as no-response and coded as "0". The gathered data are then sets of [dose, response] vectors, one vector for each subject, where the doses are rational positive numbers and the responses are binary variables "0" or "1". The probit procedure measures the relationship between the strength of a stimulus and the proportion of cases exhibiting a response to the stimulus. The main assumptions of the probit model are that occurrence or non-occurrence of response depends upon the intensity of the stimulus (e.g. exposure energy). For any one subject there will be a certain level of intensity below which no response occurs, and above which there always is a positive response. This level is usually defined as a tolerance. Tolerance values are assumed to vary from one subject to another and/or within subjects. Hence, the response probability equals to the probability that a randomly selected tolerance is smaller than the stimulus. The probit analysis estimates the parameters of these tolerances' distribution. The most meaningful parameter is the ED_{50}, which is the effective stimulus (exposure) dose that corresponds to a 50% response (lesion) probability. Another important parameter is the slope. The slope is defined as the ratio ED_{84}/ED_{50}, where ED_x corresponds to the x% response (lesion) probability. probit procedure is commonly accepted and widely used in biological assay and clinical trials.

However, we recently preformed an in-silico simulation study that was aimed to verify the relevancy and exactness of the probit analysis method for the case of data gathered at in-vivo laser-tissue experiments[1]. This study reveals that the accuracy of probit's ED_{50} and slope estimations are conditional; and that probit's estimations might sometimes be biased in a way that they raise doubts about the validity of the conclusions based on probit's results. Following these findings we concluded that there is a need for another supporting analysis method, which could trace data, which might be inapplicable to be analyzed with probit; where such an estimation method might even be more accurate than probit.

This report describes the first attempts and results in the search for a different analysis method for data gathered at in-vivo dose-response laser-tissue experiments.

2. METHOD

Two main groups of analysis methods were defined.

The first group is the parameters' distribution estimation method. In this group we followed the basic concept of probit by assuming that the dose-response vectors reflect the properties of a hidden tolerances' distribution. The ED_{50} and slope, which are the parameters of that distribution, are then estimated by a best fit of the dose response vector to the cumulative response frequency that is expected from the assumed distribution. The tolerances' distributions that were considered were

* Correspondence: Email: langusa@eng.tau.ac.il

Laser and Noncoherent Light Ocular Effects: Epidemiology, Prevention, and Treatment,
Bruce E. Stuck, Michael Belkin, Editors, Proceedings of SPIE Vol. 4246 (2001)

of type normal, logistic and uniform and their logarithmic transforms (i.e. log-normal, log-logistic and log-uniform). The best fit of the cumulative distribution to the dose-response data was done by minimizing the sum of squares of the differences between the expected response probability (of the distribution) and the actual response (of the vector); and by the method of maximum likelihood. The distributions' parameters that correspond to the minimum sum of squares or to the maximum likelihood were calculated by the Nelder-Mead simplex (direct search) method.
The second group consists of the methods for threshold estimation. The methods in this group estimate only theED_{50}. These methods are not based on a single specific set of general assumptions.
The first of these methods is the "hypothetical threshold", where a hypothetical threshold is assigned a numerical value (a grade) that represents the number of observations that are consistent with the hypothetical threshold[2]. For each optional value of the hypothetical threshold a grade is calculated by summing the number of events that agree with the hypothetical threshold and subtracting the number of events that do not agree with the hypothetical threshold. Events that agree with the hypothetical threshold are those exposures with energies that are larger than the hypothetical threshold that had a response, and exposures with energies that are smaller than the hypothetical threshold that result in no-response, and vice versa. The threshold is set to be the hypothetical threshold with the largest grade.
The second method was the "min-yes max-no" method. This method calculates the mean of the largest exposure value that did not result in a response with the smallest exposure value that gave a response. If the exposures intensities are equally spaced, this mean is supposed to be located very close to exposure's value that results in a 50% probability of response. In order to consider situations where the exposures intensities are not equally spaced, it is possible to calculate the mean of the second largest exposure value that did not result with response with the second smallest exposure value that resulted in a response. The ED_{50} estimation is then the mean of these two means.
The 3rd method was the "maximum randomness". This method subdivides the dose-response vector into a number of segments and calculates the average response in each segment. The ED_{50} is then the mean of doses in the segment closest to a mean response of 50%. This estimation method requires on one hand that the segments are wide enough in order to get a representative response probability and on the other hand it requires that the segments are narrow enough in order to gain dose accuracy. In the current study we repeated the calculations for several size of segments and chose the segment in which the mean response rate was closest to 50%.
In the 4th method the sum of responses against the doses was calculated. This sum is zero as long as there are no responses and rises linearly at larger doses where all the responses are "1". The first difference of this sum between each two successive doses is zero at the smaller doses, oscillates between "0" and "1" in the dose ranges near the ED_{50} (as the responses aren't constant in that range), and equals to one at the larger doses where all the responses are "1". Taking the second difference of the sum will result in values different from zero only for dose levels near the ED_{50}. The ED_{50} is then the average of the doses, which corresponds to the second differences that are not equal to zero.
Methods 5 and 6 were the Dragstedt-Behrens method and the Reed-Muench method. The details of these methods' are described elsewhere[3].

The evaluation of the accuracy of the analysis methods was done with a Monte-Carlo simulation that included the following steps:
1) Generating in-silico dose-response vectors from a predefined distribution.
2) Estimating the ED_{50} of these vectors with different analysis methods.
3) Comparing the estimated ED_{50} values with the appropriate parameter of the predefined distribution.
4) Comparing the estimated ED_{50} values between the different analysis methods.

The predefined distributions were the normal and the log-normal distributions. The parameters of the distributions were all combinations of ED_{50} values of 15, 20 and 25 and of slope values of 1.001, 1.5 and 2.5.
Two sets of vectors were prepared for each of the 18 combinations of distribution type and parameters. The vectors in one set were of the size of 30 dose-response pairs. The vectors in the second set were of the size of 150 dose- response pairs. Each set contained 1000 vectors. The dose values in each of the in-silico generated vectors were randomly generated from a uniform distribution ranged from 0 to 40. The response values for each of the in-silico generated vectors were determined as follows. For each dose, the probability of response was calculated as the probability that a random tolerance is smaller than that dose. The type and parameters of the tolerance's distribution function were according to the relevant predefined distributions and parameters. Next, a random value originated from a uniform distribution ranged from 0 to 1 was generated. The random number was compared to the calculated response probability. The response was set the value "1" if the random number was smaller then the calculated probability, and "0" otherwise.

The ED_{50}'s for all in-silico vectors were estimated with all of the previously described analysis methods as well as with the probit method. The probit algorithms following Finney's instructions and algorithm[3] with minor adaptations are reported elsewhere[1].
The comparison of the estimated ED_{50} values to the predefined ED_{50} and the comparison between the analysis method were done graphically and will be illustrated in the next section.

3. RESULTS

Figure 1 exhibits the comparison of the ED_{50}s estimated by the 6 parameters' distribution estimation methods to the ED_{50} that was estimated by probit. Each of the three upper graphs (1 to 3) contains 7 sigmoid curves, one curve for each estimation method. Each curve displays the cumulative frequency of 1000 estimated values of the in-silico vectors. The vertical line in the upper graphs displays the pre defined ED_{50}, with which the vectors were prepared. The slope values that were used at the vectors preparation are displayed above the upper graphs.
The correlation between the ED_{50} estimated by the different methods is shown in the three lower graphs (4 to 6). The horizontal axis shows the ED_{50} that was estimated with probit and the vertical axis shows the ED_{50}'s that were estimated with the other distribution estimation methods.

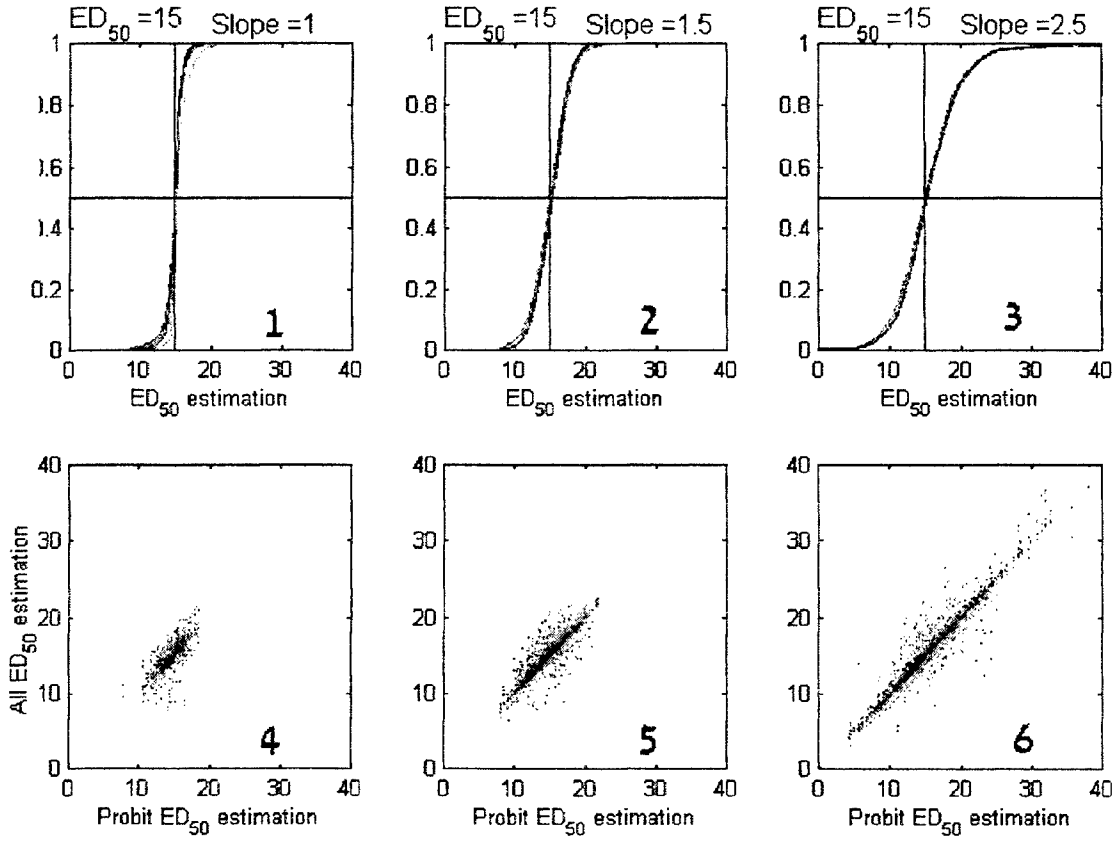

Figure 1: Comparison of the distribution estimating methods to probit

The fact that only one or two of the 7 sigmoid curves can be seen, point out that there is only a slight difference between ED_{50} values that were estimated with different estimation methods, from the group of distribution estimation. However, the slight spread of the dots in graphs 4 to 6 indicates that for each single vector the ED_{50} estimation of the different estimation methods was not the same. From the upper three graphs we conclude that the accuracy of the estimation gets better as the value of the slope approaches 1. The above graphs display the results of the analysis for the normal distribution with a does-response size of 30 pairs. Although the graphs of the other 11 sets of analysis are not displayed here, they show almost the same pattern of the accuracy and of the correlation between different estimations.

Figure 2 exhibits the comparison of the ED_{50}s estimated by the 6 threshold estimation methods to the ED_{50} that was estimated by probit

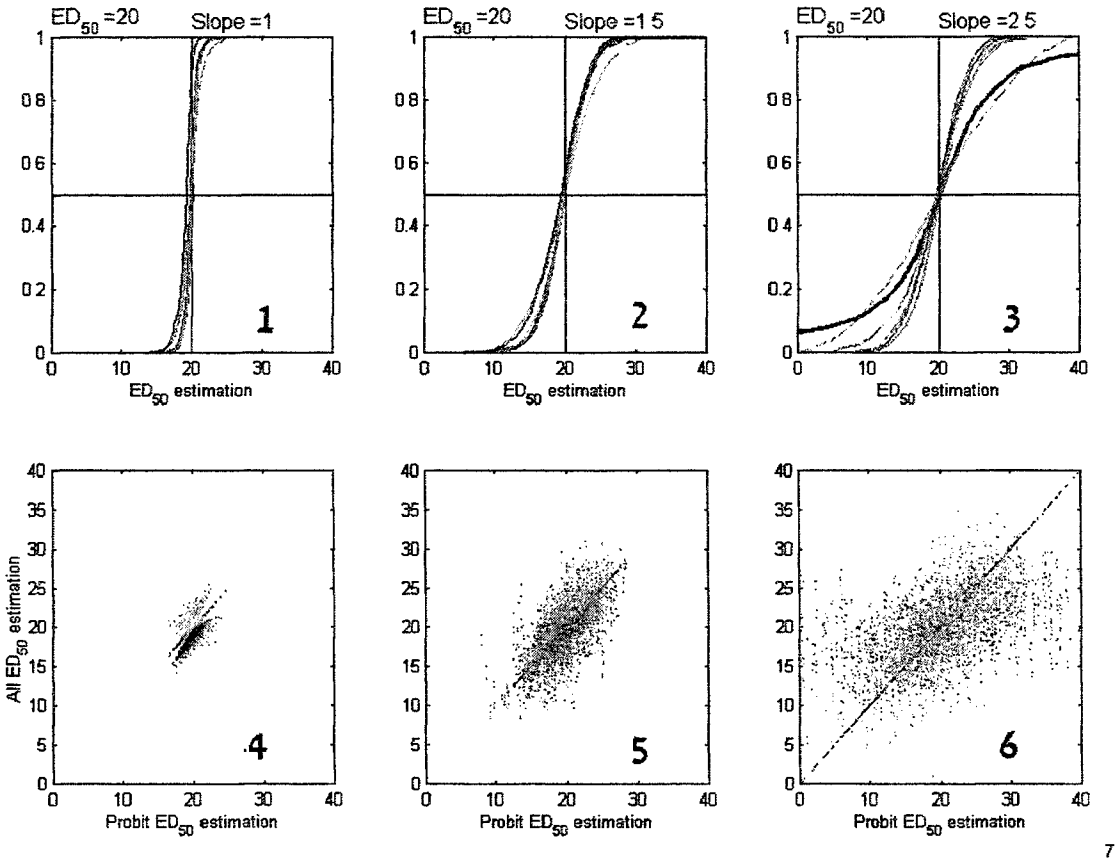

Figure 2: Comparison of the threshold estimating methods to probit

In threshold estimation all of the 7 sigmoid curves can be seen in the upper three graphs (1 to 3), emphasizing the fact that each method has different empirical cumulative frequency for estimating the ED_{50}. The same can be concluded by the large spread of the three lower graphs (4 to 6) compared to those of figure 1.For a slope value of 1.001 all the methods accuracy is fairly good. For a slope value of 1.5 the probit method has the best overall accuracy, the ED_{50} estimate is unbiased compared to those of the other methods where the ED_{50} estimate is over-biased. However from the relatively large spread of graph 5 we see that there were a large number of cases where probit's estimate was biased and some of the other methods gave a more accurate estimate. For a slope value of 21.5 the probit method gives an unbiased estimate but with a large spread, whereas the other methods do have an over-bias but with a lower spread. The above graphs display the results of the analysis for the normal distribution with a does-response size of 30 pairs. The full analysis encompasses 5 more graphs that show the same general trends. That is, the probit estimation is generally better than the threshold estimated methods; yet, the different methods' estimations are loosely correlated. These findings imply that there are vectors that estimated by probit is fit better, while other vectors are better estimated by the other methods.

4. DISCUSSION

The results of the previous section show that none of the other estimation methods are more accurate than probit (graphs 1 to 3 in figures 1 and 2). Nevertheless, the findings that some of the different estimation methods are loosely correlated, while their empirical cumulative frequency distributions are not completely different (some are even identical) suggest that there are some combinations of dose-response vectors that their estimated ED_{50}'s by the different methods are very close to each other, though in other cases the estimated ED_{50}'s by the different methods are quite apart from each other.

It is reasonable to require that the analysis of sound data with different proper analysis methods should result in estimated parameters that are almost identically. Hence, we suggest the multiple analyses estimation methods presented here as a statistical tool, which could be used as a data soundness meter, for data gathered at the laser-tissue dose-response experiments.

For more than 10 years there has been doubt regarding experimental results reported by the USAMRD-WRAIR. The USAMRD-WRAIR report[4] reveals an unexplainable significant variation of the estimated ED_{50} values with small changes in the wavelength.

The results of reanalyzing this data with the multiple analyses method are presented in Figure 3. The upper graph (1) displays the spectral ED_{50} of the USAMRD-WRAIR data. The presented ED_{50} values are the average ED_{50}'s of the different estimation methods. The height of the error bars indicates the $\pm 1\sigma$ values of the ED_{50}'s estimated by the different methods.

The middle graph (2) displays the spectral ED_{50} of 2/3'rd of the wavelengths. The omitted 1/3'rd of the wavelengths are those ED_{50}'s with large standard deviations.

The lower graph (3) displays the spectral ED_{50} of 1/3'rd of the wavelengths. The included 1/3'rd of the wavelengths are those ED_{50}'s with the smallest standard deviations.

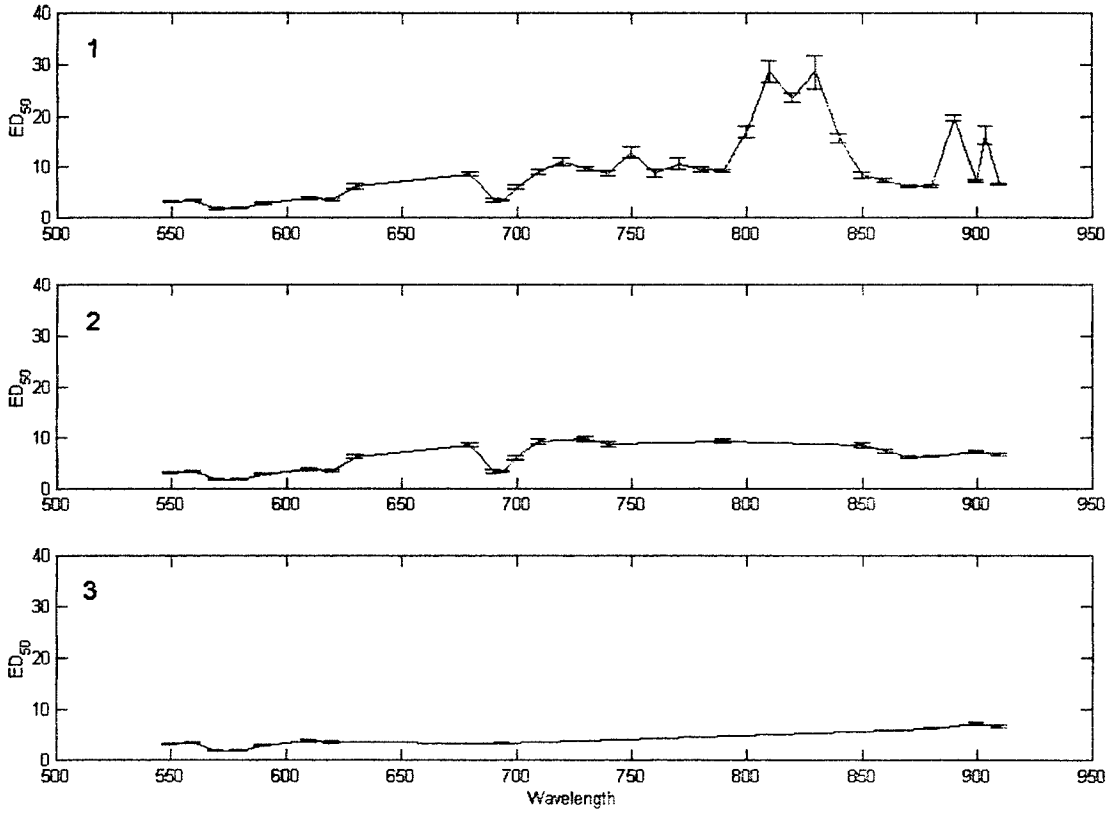

Figure 3: Spectral ED_{50} values, evaluated and filtered with the multiple analyses method

It is easily seen that the large variation of the ED_{50} with small changes in the wavelength vanishes as wavelengths with large standard deviations of the ED_{50} are omitted out.

In another study[1], we simulated the repetitions of the same data gathered by the USAMRD-WRAIR with in-silico vectors. We found a large correlation between wavelengths with larger ED_{50} values, which can be related to the large variations, and the in-silico vectors in which their ED_{50} estimations by probit were biased and had a large standard deviation. (See reference 1 for details). Consequently, we suspected that the large variations in the ED_{50} values were caused by the inapplicability of the probit analysis method to the collected data.

Different presentations of the results of that study are presented in Figure 4. The upper graph (1) displays the spectral ED_{50}'s estimated with probit. The height of the error bars indicates the $\pm 1\sigma$ values of the ED_{50}'s of the in-silico vectors. The middle graph (2) displays the spectral ED_{50}'s of 2/3'rd of the wavelengths. The omitted 1/3'rd of the wavelengths are those ED_{50}'s with large standard deviations. The lower graph (3) displays the spectral ED_{50}'s of 1/3'rd of the wavelengths. The included 1/3'rd of the wavelengths are those ED_{50}'s with the smallest standard deviations.

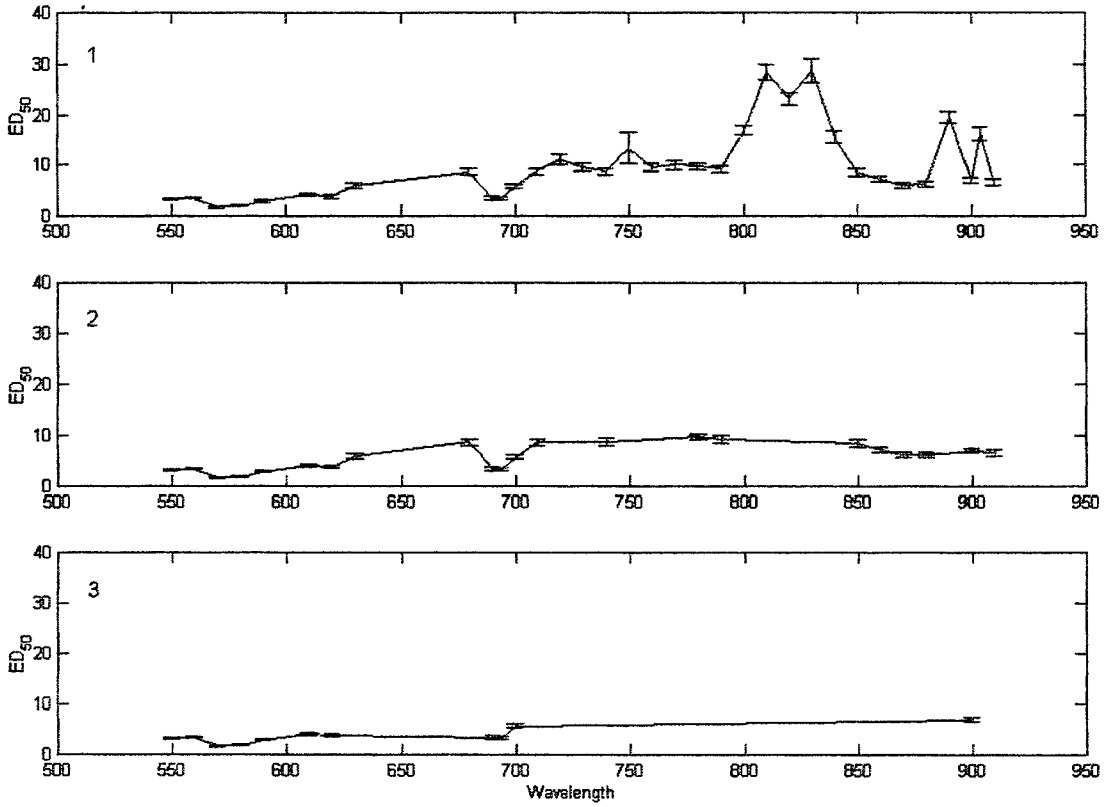

Figure 4: Spectral ED_{50} values, evaluated with probit, and filtered with the in-silico standard deviation.

The similarity of the spectral structure of graph 1 in figure 4 to the spectral structure of graph 1 in figure 3 can easily be explained by the expected similarity of the mean ED_{50}'s of the multiple analyses to the ED_{50}'s from probit. However the similarities of graphs 2 and 3 in figures 3 and 4, can only be explained by the fact that the standard deviations of the ED_{50}'s that were estimated with the multiple analyses method as well as those of the in-silico vectors reveal the same instability of the dose-response data. In fact, comparing those standard deviations to the fiducial intervals of the probit's ED_{50}'s shows similar results. However discarding 2/3'rd of the wavelengths with the larger fiducial intervals omits out all the wavelengths above 700 nm.

In conclusion, it seems that from a pure statistical point of view, the filtering process, either by the in silico simulation or by the multiple analyses method, that smoothed and flattened the large ED_{50} variations, might propose an explanation for the significant variation of the ED_{50}'s with small changes in the wavelength.

However, at the present, we doubt this explanation for several reasons. The first one is that the information regarding the properties of the laser-tissue interaction is not limited only to the soundness of the data. Shaky data shouldn't be automatically omitted out. They do carry some information. The second one is that the statistical results of one experiment can't alone represent the properties of the laser-tissue interaction. Other experiments and physical models should support the statistical results. According to the present physical models the spectral ED_{50} is supposed to vary with the wavelength. For example the ocular chromatic aberration enlarges the retinal spot size as the wavelength departs from 580 nm, which in turn should increase the ED_{50}. Thus, the spectral ED_{50}'s displayed in graphs 3 of figures 3 and 4 are not consistent with the current understanding of the physical mechanisms of the ocular laser-tissue interaction. The third reason is that the results presented here are of a preliminary nature and several more simulations and tests are needed before the multiple analyses method could be implemented with full certainty and confidence.

5. CONCLUSIONS

The multiple analyses method can be used with care as a statistical tool for filtering potentially biased probit's threshold estimation. However, conclusions regarding the properties of the laser-tissue interaction shouldn't be solely based on the results of the filtered data.

ACKNOWLEDGMENTS

We thank the USAMRD-WRAIR for providing us their comprehensive data sets and especially Mr. Jack Lund for his invaluable ideas and support during our research.

REFERENCES

1. Langus A., Fuchs C. and Gannot I., "The Accuracy and Relevancy of the Probit Analysis for the Case of Data Gathered at In-Vivo Dose-Response Laser Tissue Experiments", in this proceedings.
2. Jacques S.L. McAuliffe D.J. "The Melanosome: Threshold Temperature for Explosive Vaporization and Internal Absorption Coefficient during Pulsed Laser Irradiation", Photochem. Photobiol. 53:769-775,1991.
3. Finney D. J., *Probit Analysis*, Cambridge University Press, 1971.
4. Lund D. J., Beatrice E.S., "Near Infrared Laser Ocular Bioeffects", Health Physics Vol. 56, No. 5, pp. 631-636, 1989.

High-Energy Laser Systems: Analytical Risk Assessment and Probability Density Functions

P. A. Smith[a*], D. A. Van Veldhuizen[b] and G. D. Polhamus[a]

[a]Litton/TASC, 4241 Woodcock Drive, Ste B-100,
San Antonio, TX 78228 USA

[b]Optical Radiation Branch, USAF Research Laboratory
Brooks AFB, TX 78235 USA

ABSTRACT

A deterministic approach to laser hazard assessment is used in most laser safety standards. Personnel are protected from hazardous laser radiation is by defining a space within which the direct, reflected, or scattered radiation during laser operation exceeds the safe Maximum Permissible Exposure level. Controlling access to this space insures safety. Although this approach has satisfied the commercial and industrial laser communities for many years, it may not be applicable to the high-power (up to megawatt) laser systems currently being developed by the US military. These systems will have extremely long laser hazard distances, and controlling access to this space will be unrealistic, especially when the likelihood of hazardous human exposure is low. For these situations, an alternative analytical approach that estimates both the level of risk and the degree of risk reduction achievable by controlling key contributors can be applied. Analytic risk assessment tools are finding increasing application in a wide variety of hazard assessments, in both industrial and commercial situations. These tools use scientific data, assumptions, and mathematical models to estimate the likelihood, frequency, and severity of harm to people exposed to the hazard. This paper will discusses application of such tools to laser safety and considers the uncertainties associated with probability density functions applied to key factors such as atmospheric scintillation, reflected radiation, population distribution and ocular injury.

Keywords: Laser safety, risk assessment, uncertainty, probability density function

1. INTRODUCTION

To ensure the safe operation of laser systems in open, uncontrolled environments (i.e. outdoors), the US Air Force utilizes laser hazard evaluation techniques based on the American National Standard.[1] In this standard, and similar International laser safety standards, a laser classification system is used to provide a guide to the hazard† (and indicate appropriate control measures) and a deterministic approach to laser hazard evaluation provides an analysis of the locations where a hazard from direct, reflected, or scattered radiation might exist during laser operation. Hazards are assessed on a worst-case analysis of the possibility of over-exposure, where over-exposure is defined as an exposure above the safe Maximum Permissible Exposure level (MPE). This hazard evaluation is thus expected to provide an absolute indicator of safety (zero risk) in a given environment, despite the fact that the concept of "zero risk" might be regarded as unsound.

Risk is defined as the probability that a substance or situation will produce harm under specified conditions.[2] Risk is a combination of two factors: the probability that an adverse event will occur (such as a specific type of injury), and the consequences of the adverse event. Risk encompasses the impact of the activity on both public health and the environment, and arises from exposure and hazard. Risk does not exist if exposure to a harmful substance or situation does not or will not occur.

Military laser systems are increasing in power, and the range of applications expanding rapidly, with the potential for megawatt systems to be fielded in the not too distant future. As the complexity of the scenario increases, the hazard analysis

*Correspondence: P.A. Smith: Email psmith@tasc.com; 210-536-4783; Fax: 210-534-0420; Supported by the US Air Force under Contract F41624-97-D-9000. Other author information: D.A.V.: Email: david.vanveldhuizen@hedo.brooks.af.mil; Telephone 210-536-3271; Fax: 210-536-3903; Supported by the US Air Force. G.D.P.: Email: gdpolhamus@tasc.com; Telephone: 210-737-1192; Fax: 210-734-0990; Supported by the US Air Force under Contract F41624-97-D-9000.

†The potential to cause harm (physical injury or damage to the health of people).

Laser and Noncoherent Light Ocular Effects: Epidemiology, Prevention, and Treatment,
Bruce E. Stuck, Michael Belkin, Editors, Proceedings of SPIE Vol. 4246 (2001)

includes so many variables, or degrees of freedom, that an exact treatment becomes increasingly intractable, and less useful. Where the number of degrees of freedom is extremely large, statistical approaches to risk assessment become increasingly necessary. Indeed, some contributors to risk, such as atmospheric scintillation, may be inherently probabilistic, and can only be described statistically.

Moreover, conventional laser hazard assessment techniques, when applied to these systems, may indicate that hazards exist, even if the likelihood that the hazard is realized (i.e. the risk) may be extremely small. Hazard distances and zones will be proportionally greater for High-Energy Laser (HEL) systems, and controlling access to this space will be unrealistic. For these situations more sophisticated analytical approaches, based on a logical extension of the hazard assessment, utilizing analytical risk assessment techniques that estimate both the level of risk, and the extent to which risk can be minimized by controlling key contributors can be considered.[3] These techniques use scientific data, assumptions and mathematical models to estimate the likelihood, frequency and severity of harm to people or natural resources exposed to a hazard.

The application of risk assessment tools to public health, safety, and environmental problems has become commonplace in the peer-reviewed scientific and medical literatures. Legislation that would have mandated quantitative risk assessment for all federal environmental, health, and safety regulations came close to being passed several times in the 1990s: SB110 in 1992, HR9 in 1994, the Johnston-Robb Bill in 1996, and S746 in 1999.[4] In addition, the US Environmental Protection Agency (EPA) has recently published its policy for use of probabilistic analysis in risk assessment.[5]

2. RISK ASSESSMENT AND MANAGEMENT

2.1. General Principles

It is useful to begin by drawing a distinction between the terms **risk assessment** and **risk management**. A useful clarification is given by the explanation that risk assessment answers the question "*How risky is the situation?*" whereas risk management answers the question "*What shall we do about the risk?*"

Risk management is the process of identifying, evaluating, selecting, and implementing actions to reduce risk to human health and to ecosystems. The goal of risk management is scientifically sound, cost-effective, integrated actions that reduce or prevent risks while taking into account social, cultural, ethical, political, and legal considerations. Risk management is a systematic and logical process to identify and control hazards. This process includes any or all of the following steps: 1) identify the hazards, 2) define hazard levels, 3) define risks, 4) define and implement risk reduction measures, 5) obtain approval from proper authority, and, 6) ultimately accept the hazard or risk. The AF has implemented these principles in Range Safety standards, most notably those for inert debris[6], and at the Eastern[‡] and Western[§] ranges.[7]

Risk assessment is defined as the objective process that analyzes the form, dimension, and characteristics of the risk. It is primarily a scientific effort in which data from appropriate sources are used to enumerate outcomes and quantify their likelihoods. The probabilistic risk assessment is an integral part of the risk management process, and provides important feedback to the research process.[8] The probabilistic risk assessment phase is more formal, quantitative, and objective than the risk management phase, which involves value judgment and heuristics, and hence is more subjective, qualitative, societal and political. The probabilistic risk assessment should be based on objective likelihoods, usually inferred from statistical data and theories. However, the probabilistic risk assessment is often compelled to use subjective likelihoods based on partial data, expertise and intuition.[9]

Notwithstanding this, a risk assessment should be based on scientific information and public health policy considerations and must consider all relevant, reliable, and reasonably available information, and must explain the basis for selecting the information relied upon. Any significant assumptions must be identified along with their basis in science or policy. An explanation of the basis for the choice of any combination of assumptions should also be given, together with the extent to which the assumption has been validated by, or conflicts with, empirical data. The risk assessment should also describe reasonable alternative assumptions that were considered but not selected.

---

‡ The Eastern Range is the launch head at Cape Canaveral Air Station; owned or leased facilities on downrange sites such as Antigua and Ascension; and in the context of launch operations, the Atlantic Ocean, including all surrounding land, sea, and air space within the reach of any launch vehicle extending eastward into the Indian and Pacific Oceans.

§ The Western Range is the launch head at Vandenberg Air Force Base (VAFB) and extends along the West Coast of the continental United States (US) westward through the Pacific and Indian Oceans.

The risk assessment should include, where appropriate, descriptions of:

i. The hazard;

ii. The populations or natural resources that are the subject of the risk assessment;

iii. Exposure scenarios, including estimates of the population or natural resources at risk and the likelihood of such scenarios;

iv. The nature and severity of the harm from exposure to the hazard; and,

v. The major uncertainties in each component of the risk assessment and their impact on the assessment's outcome.

2.2. EPA Approach

When risk assessments using probabilistic analysis techniques are submitted to the EPA for review and evaluation, they require eight specific conditions to be satisfied to ensure high quality and science.[5] Whilst these conditions may not be specifically required by a HEL probabilistic risk assessment, it would be prudent use them as guidance, considering them in detail, and following their example. The eight EPA conditions are:

i. The purpose and scope of the assessment should be clearly articulated in a "problem formulation" section that includes a full discussion of any highly exposed or highly susceptible sub-populations evaluated (e.g., children, or the elderly). The questions the assessment attempts to answer are to be discussed and the assessment endpoints well defined.

ii. The methods used for the analysis (including all models used, all data upon which the assessment is based, and all assumptions that have a significant impact upon the results) are to be documented and easily located in the report. This documentation is to include a discussion of the degree to which the data used are representative of the population under study. Also, this documentation is to include the names of the models and software used to generate the analysis. Sufficient information is to be provided to allow the results of the analysis to be independently reproduced.

iii. The results of sensitivity analyses are to be presented and discussed in the report. Probabilistic techniques should be applied to the compounds, pathways, and factors of importance to the assessment, as determined by sensitivity analyses or other basic requirements of the assessment.

iv. The presence or absence of moderate to strong correlation or dependencies between the input variables is to be discussed and accounted for in the analysis, along with the effects these have on the output distribution.

v. Information for each input and output distribution is to be provided in the report. This includes tabular and graphical representations of the distributions (e.g., probability density function and cumulative distribution function plots) that indicate the location of any point estimates of interest (e.g., mean, median, 95th percentile). The selection of distributions is to be explained and justified. For both the input and output distributions, variability and uncertainty are to be differentiated where possible.

vi. The numerical stability of the central tendency and the higher end (i.e., tail) of the output distributions are to be presented and discussed.

vii. Calculations of exposures and risks using deterministic (e.g., point estimate) methods are to be reported if possible. Providing these values will allow comparisons between the probabilistic analysis and past or screening level risk assessments. Further, deterministic estimates may be used to answer scenario specific questions and to facilitate risk communication. When comparisons are made, it is important to explain the similarities and differences in the underlying data, assumptions, and models.

viii. Since fixed exposure assumptions (e.g., exposure duration, body weight) are sometimes embedded in the toxicity metrics (e.g., Reference Doses, Reference Concentrations, unit cancer risk factors), the exposure estimates from the probabilistic output distribution are to be aligned with the toxicity metric.

Risk modeling is invariably necessary because the acceptable risk levels are not measurable, and direct sampling of the exposure is not feasible. Nevertheless, the risk assessment must demonstrate a decisional process of diligent data collection and revelation, careful identification of significant facets of the problem, and consideration of possible alternative solutions, and lucid explanation of its assumptions, conclusions and judgments.

2.3. Characterization of Variability and Uncertainty

Where deterministic risk assessment uses high-end point estimates for input values, probabilistic risk assessment uses distributions, and this enables a quantitative analysis of the variability and uncertainty of the risk for the population. Variability refers to true heterogeneity in characteristics with a population, and cannot be reduced by taking more samples. Uncertainty, on the other hand, refers to lack of knowledge and can be reduced, in theory, by further data collection. In practice, cost, time and ethical constraints, together with a minimal impact on the outcome of the assessment, often make additional data collection impractical. Separating variability and uncertainty during the analysis can be necessary to identify parameters where additional data are needed. The importance of adequately characterizing variability and uncertainty in risk assessments has been emphasized by the EPA, in its guidance on the use of Monte Carlo analysis for analyzing variability and uncertainty in risk assessments, although the EPA recognizes that Monte Carlo simulation is not the only acceptable approach for risk assessments.[5]

3. RISK ASSESSMENT FOR HIGH ENERGY LASERS

3.1. Scenario definition

The process of constructing and solving problems for both deterministic and probabilistic risk assessments starts with building a useful mental picture, or model, of the activity and then getting reasonable values into a model. The model should be as simple as possible, while still including all of the important sources of risk. For a HEL engagement scenario, whether it is for a laser on the ground (e.g. the Tactical High Energy Laser), in the air (e.g. Airborne Laser, Advanced Tactical Laser), or in space (e.g. Space Based Laser) the hazard under consideration is that due to the overexposure of human tissue (eye or skin) to laser radiation. The hazard from the laser depends on a number of laser parameters, most notably the power (or energy), wavelength and exposure duration. The subject of the risk assessment is the general public, although other subjects, such as mission essential personnel, and other assets (satellite systems) might also be included.

The assessment begins with a detailed analysis of the key routes to human exposure, which involves identifying the potential pathways and exposure parameters from the exit aperture of the laser to the entrance aperture of the system at risk. Typical parameters for inclusion in the assessment would be the characteristics of the laser, the operation of the laser aiming and tracking system under normal (fault-free) operations, and a consideration of failure modes and effects. For any representative engagement scenario, there will be two principal laser beam paths that will need consideration. The first will be the path of the direct beam from the laser source to the target and beyond. The second path will be that of any reflected radiation from the target. For both paths the characteristics of the propagation of the laser beam through the atmosphere must be considered. Then, if these circumstances give rise to the exposure of a point in space (e.g. on the ground) to laser radiation, the assessment needs to consider whether an individual is located at that point and, finally, whether the individual will suffer harm as a result of this exposure.

3.1.1. Laser beam parameters

Ideally, for each laser system under consideration, the laser output should be well characterized and its behavior understood. If this is not the case, then worst-case estimates for parameters such as the beam power/energy and beam divergence should be used. It is also necessary to know of the existence of any secondary laser beams, or any other inadvertent laser energy leakage emerging from the laser system, together with the above-noted characteristics of this inadvertent output. A sensitivity analysis may be required to evaluate the effect of spatial beam distribution on the outcome of the risk assessment.

3.1.2. Beam pointing accuracy and failure modes

Estimates for boresight errors and tracking accuracy (jitter) are often combined to provide a single pointing parameter. This can be approximated by a radially symmetrical normal distribution with a mean aiming position and associated standard deviation. For automatic tracking systems, as would be the case for HEL systems the manufacturer of the system would be expected to be able to provide detailed information on the laser system performance.

Range safety requirements for the Eastern and Western ranges call for the submission of an analysis and supporting data outlining possible laser system failures for all phases of laser system uses.[7] The data are required in the form of the probability of occurrence versus time of operation for each of the following generic hazard modes (modes of beam control error or failure):

i. Pointing error,
ii. Inadvertent slewing,
iii. Premature firing,
iv. Delayed firing,
v. Beam focusing error,
vi. Loss of focus, and
vii. Other modes such as wrong target acquisition applicable to the system.

If the probability of occurrence is non-zero for any of these hazard modes, then probability distributions for the random hazard mode parameters describing how each mode can occur over time must be provided. The requirements also state that applicable hazard modes must be defined and documented by a Failure Modes, Effects, and Criticality Analysis (FMECA) in accordance with MIL-STD-1543 and MIL-STD-1629 or the equivalent. The probabilities of occurrence and the probability distributions of their descriptive parameters must be quantified with fault tree analyses or the equivalent. The level of analysis conducted in each case is the level at which appropriate component error/failure data are available. If necessary for confidence in the results, analyses of the effects of the uncertainties in the component data must be carried out.

This analysis and associated data would also be directly applicable to the full probabilistic analysis of the scenario under consideration, so this element should not place an additional data collection burden on the risk analysis.

3.1.3. Atmospheric scintillation

The most advanced HEL systems for engagements that include long, near horizontal propagation beam paths, require adaptive optic systems. These systems are designed to compensate for atmospheric turbulence and focus the laser beam over long distances to ensure the maximum energy flux on the target. Adaptive optic systems include some form of wavefront sensor to measure the phase aberrations due to the turbulent atmosphere, and a deformable mirror to adjust the phase of the transmitted beam. In an ideal system the distribution of the compensated beam on the target will be gaussian, and will not vary in intensity due to atmospheric turbulence. Since the need for adaptive optics depends in part upon the planned engagement distances, some systems will not require such technology. However, for very long engagement distances through the atmosphere, as envisioned for systems such as the Airborne Laser, adaptive optics will be necessary. Also, the reflected radiation will be subject to atmospheric turbulence, giving rise to scintillation, as it propagates away from the target.

The variation in energy due to scintillation is generally described in terms of a statistically varying multiplication factor, or gain, for the energy value detected behind an aperture due to scintillation. The probability that the scintillation gain (g_S) lies between (g_S , $g_S + dg_S$) is given by:

$$p_s(g_S)dg_S = \frac{1}{\sqrt{2\pi}}\frac{1}{g_S\eta}exp\left[-\frac{1}{2}\left(\frac{log_e g_S + \frac{1}{2}\eta^2}{\eta}\right)^2\right]dg_S$$

This is a log-normal probability function for the scintillation gain, and is equally applicable to both the spatial distribution of energy over the cross-section of any pulse, and the temporal (pulse-to-pulse) energy distribution along the beam path[10]. It is totally defined by one parameter, η – the standard deviation of the log-irradiance – that may be assigned any value appropriate to the degree of atmospheric turbulence to be expected. A complex relationship between the structural constant of atmospheric refractivity C_N and η has been described.[11] Nonetheless, a worst-case value for η of 1.2 has been used previously, and this corresponds to severe turbulence levels as measured in Death Valley, Arizona. Measurements of air-to-air laser beam propagation over long beam paths (200-400 km) at high altitude (>30,000 ft) in New Mexico and Montana have determined levels of η of 0.638. [12]

These experiments refuted the popular notion that, from an optical turbulence point of view, the upper atmosphere is relatively stable at high altitude, since significant turbulence was detected, albeit not at the worst case level of η (η = 1.2) used elsewhere. The effect of reducing η from 1.2 to 0.638 can be seen in Figure 1, where the probability of getting a high level of gain (focusing) due to scintillation decreases with the reduction in η.

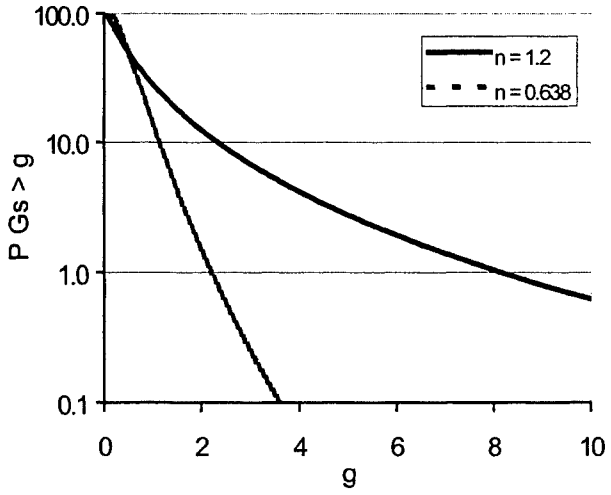

Figure 1. Probability (p Gs) that scintillation gain exceeds a given level (g)

3.1.4. Target Reflectivity

Combining the laser to target geometry with a moving airborne laser source and a moving target, which has both specular and diffuse reflecting properties, will give rise to two main types of exposure scenarios at a given point on the ground. The specular component may give rise to a short-lived, high-energy specular reflection, while the diffuse component will result in a long-duration, low-power exposure. These dynamics, together with the atmospheric variations, will mean that it is necessary to calculate the time integrated intensity profile. This is because the biological response to the exposure is dependent not only on the laser power/energy, but also on the exposure duration and the rate at which energy was delivered to the tissue at risk.[13]

The target reflectivity model being developed for HEL safety assessments[14] is based on the Bi-directional Reflectivity Distribution Function (BRDF) developed by the Environmental Research Institute of Michigan[15]. The BRDF approach classifies the reflected energy into two regimes, diffuse and specular. The diffusely reflected radiation is spread into a full hemisphere, whereas specularly reflected radiation goes in a predominantly forward cone along the nominally forward direction (Figure 2).

These BRDFs have been integrated into initial assessment tools designed to predict hazardous areas associated with testing HEL systems at various test ranges. In using BRDFs in laser safety assessments efforts have been made to ensure conservatism in estimating hazards. In so doing, the application overestimates the specularly reflected component and underestimates the diffusely reflected component. This approach has been justified on the basis that is a worst-case scenario, consistent with safety[16]. However, this cannot be assumed. For instance, if there were a significant risk of over exposure to individuals from the diffusely reflected component, then any underestimation of the amount of radiation will potentially involve many more people than the specularly reflected component, since the diffusely reflected radiation is scattered over a larger area, resulting in potentially more people being exposed over longer exposure times. The specularly reflected component, on the other hand, will have a higher power, and is potentially more hazardous to an individual should it result in human exposure. A sensitivity analysis in the probabilistic risk assessment could be used to assess the relative contribution of each component to the overall risk assessment.

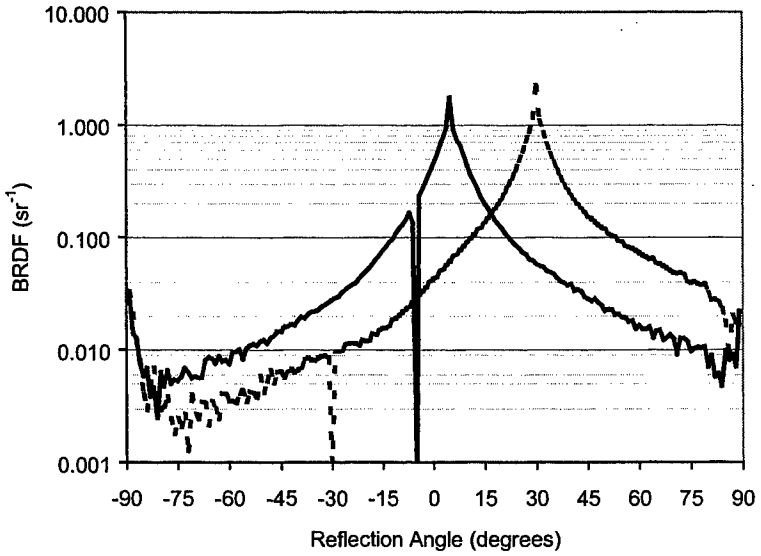

Figure 2. BRDF for diffuse aluminum plate measured at laser illumination angles of 5° and 30°.

Equally, if not more important, is the requirement to fully characterize the uncertainty of the BRDF itself. Recent measurements have indicated that the BRDF from different materials being exposed to HEL radiation may exhibit unexpected variability. Such variability may result from heating of the material surface, changes in the material properties, as well as the existence of minor imperfections or discontinuities (e.g. welds) on the surface that become magnified in the presence of HEL irradiation.

3.1.5. Population Density Modeling

Simplified models of population density have previously been developed by the Eastern and Western ranges to determine the likelihood of casualties if space launch debris lands in a given region[17]. These models generally break the landmasses into regions in which the population is assumed to be equally distributed. Dense population centers and cities are separated from rural areas. Population data are reportedly available in the models for much of the world, although data for some regions, including Europe, are missing. Different population distributions and shelter probabilities are assigned depending on the time of launch (day, evening, or night).

For the risk from debris, shelter categories are defined as follows:

i. Heavy - Blockhouse bunkers and heavily reinforced structures

ii. Medium - Buildings with concrete or reinforced roofs, and all floors except the top floor in multi-story buildings

iii. Light - Single story buildings, trailers, and top floors of multi-story buildings

iv. Exposed - No protection from falling debris

Similar categories could be developed for laser risks, for example heavy shelter could represent windowless buildings, medium shelter - internal rooms in windowed buildings, light shelter - external rooms in windowed buildings, and exposed - out of doors.

3.1.6. Biological Damage Model

In previous applications of probabilistic risk assessment to laser safety it has been stated that that when considering the personnel protection criterion the level of harm should be small, but still capable of being easily detected. In addition, the consequent impairment to the individual should be minor, but not insignificant[18]. A significant level of harm is needed so that a meaningful level of "acceptable" risk level can be defined, since without harm there can be no risk. In contrast, risk

assessments for other hazards (inert debris, blast, toxic effects) usually consider fatality as the personnel protection criterion. Since laser exposure can cause serious injury without fatality a non-fatal personnel protection criterion is required. However, if comparisons of the risk from laser exposure to other risks are to be made, attention should be drawn to the fact that the laser risk assessment is usually made using non-fatal risk criteria. HEL systems are likely to operate at infra-red laser wavelengths, from 1.3 to 3.5 μm. At the lower end of this range, there may be sufficient transmission through the ocular medium to damage the retina of the eye. However, for the longer wavelength systems the cornea or skin may be the more vulnerable tissue. Studies will be needed to determine the tissue at risk, and the dose response characteristics.

It is likely that two principle exposure scenarios need to be examined. The first scenario represents an exposure that could be encountered when both the laser source and the target are moving and the eye receives a momentary direct illumination, or a glancing specular reflection. In this case the dwell time of the laser beam in intercepting the eye will be short, and a short (pulsed) exposure duration would be representative for this scenario. The second exposure scenario arises through illumination to a relatively low-level reflected laser exposure, most likely from a diffuse reflection. Since there will be no visual cues the observer may not exhibit an aversion response or otherwise take evasive action. In this case, a "worst-case" continuous wave exposure duration of up to 10-sec should be investigated. This duration is also defined by current safety standards for invisible laser beams. However, there may be some sort of aversion response invoked, for example, by a sensation of warmth, before any permanent tissue damage occurs. Such a human response can be embraced by the safety assessment, by limiting the duration of the exposure, if the latency of the response can be determined.

For any study of laser induced biological damage the results are usually expressed as a dose-response curve relating the exposure energy to the frequency of detected lesions. A typical dose-response curve is shown in Figure 3, together with the cardinal point known as the ED_{50}, which is the median dose, required to produce a lesion in 50% of the cases, and generally referred to as the "damage threshold'. The data can be fitted well with a cumulative lognormal frequency distribution, and probit analysis[19] is often used to fit the data in the form of a straight line relating the probit value** to the dose (Figure 4).

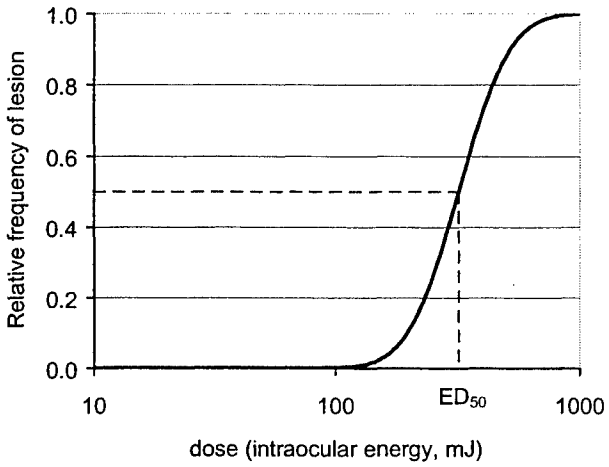

Figure 3. Typical dose-response curve for laser-induced ocular damage

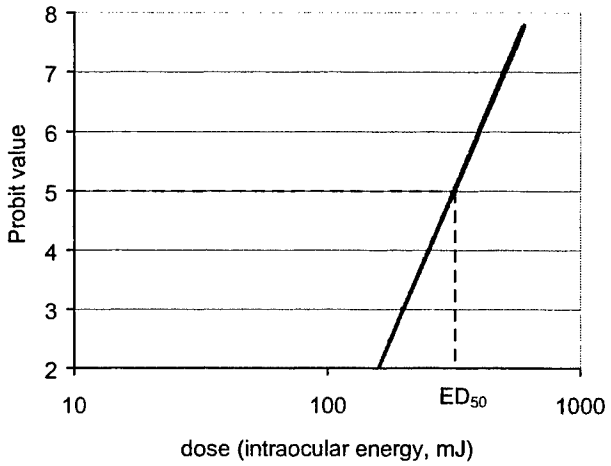

Figure 4. Probit transformation of the dose-response curve for laser-induced ocular damage

Previous applications of probabilistic risk assessment have used the complete probability curve that relates the probit values, and hence lesion probability, to the dose[20,21]. For the application of the dose-response data in a probabilistic risk assessment it is therefore important that studies of biological damage thresholds provide the full dose-response curve. This is usually given by reporting the ED_{50}, and the slope, of the probit line. This curve can then be used to calculate a value for the probability of injury for a given dose. In doing so, as the ocular injury function is followed down to low exposure levels, a corresponding theoretical probability of injury would be predicted, albeit small. However, on biophysical grounds it can be argued that, for exposures in the normal physiological range, the probability for injury must be zero and the function should be truncated, and reduced to zero probability at low exposure levels.

** Probit values are simply probabilities on a transformed scale. For any P, the probit value is the normal equivalent deviate increased by 5, thus a probit value of 5 corresponds to $P = 0.5$.

The question of whether a process has a threshold is fundamental to quantitative and qualitative risk analysis[4]. However, a prohibitively large number of exposures would be needed to accurately determine the risk at low exposure levels, and thus identify this cut-off level. An argument could be made for truncating at the level of the MPE, this being defined as a safe exposure level. An important observation is that the use of a function that is not truncated will overstate the risk at low exposure levels, and err on the side of caution.

It may also be important to consider experimental bias and the uncertainty of the ED_{50} value and slope of the dose-response (probit) curve in a probabilistic analysis. The possible contribution of experimental bias to the ED_{50} and the slope has previously been analyzed, and a probabilistic risk assessment model for space based lasers accounting fully for uncertainty associated with the parameters of the ocular damage model has been developed.[21] Probability distributions, modeling both the biological variability of laser bioeffects on tissue and the uncertainty associated with the variability, are carried through a second order model with a Monte Carlo approach.

4. DISCUSSION AND CONCLUSIONS

Sophisticated probabilistic risk assessment models can be used to provide decision makers with the necessary information to be able to assess the risk from the use of HELs in outdoor environments. These models can be used to estimate the risk from reflected radiation of the proposed lasing scenario to human health, and this information can guide laser safety officers, range safety managers, and military commanders in making risk management decisions. One of the most important challenges facing the risk assessor will be to communicate effectively the insights that an analysis of variability provides. It may be important to remember that the insights may be qualitative in nature (e.g. "a greater risk being involved in a fatal road accident") even though they may be quantitatively based (e.g. "a risk of 1 in 1,000,000").

Like probabilistic risk assessment models developed to support space launches, those supporting HEL safety applications are likely to be complex. Even when a core generic model is developed, additional system and scenario specific data is likely to be required to support a particular application.[5] Although much of this will be required in the form of point estimates for a deterministic hazard assessment, the additional information required to develop a probability density function may be more difficult to obtain, and any probability density function used in the assessment will require additional justification and documentation. Some of these probability density functions may be generic to any laser safety scenario (e.g. atmospheric propagation), others may be specific to the laser and system under consideration (e.g. aiming accuracy and fault modes).

Decisions regarding the allocation of future resources to attempt to reduce the lack-of-knowledge, and gather new data, should take into consideration the most influential input factors in the model and the cost of gaining new information about these factors. Sensitivity analysis can be used to identify which factors are most important in the model. Once so determined, the source of its spread or distribution should be determined. If it has a significant uncertainty component, further research can be used to reduce this uncertainty, whereas, if the distribution represents inherent variability, the spread cannot be reduced.

5. REFERENCES

1. American National Standards Institute. *American national standard for the safe use of lasers.* ANSI Z136.1:2000. Orlando, FL: Laser Institute of America.

2. Presidential/Congressional Commission on Risk Assessment and Risk Management. (1997). *Volume 1: Framework for environmental health risk management.* Washington, DC.

3. Gardner, R., & Smith, P. A. (1995). Quantitative risk assessment - a place in laser safety? *Optics and Laser Technology, 27,* 15-18.

4. Kammen, D. M., & Hassenzahl, D. M. (1999). *Should we risk it? Exploring environmental, health and technological problem solving.* Princeton, NJ: Princeton University Press.

5. US Environmental Protection Agency. (1997). *Guiding principles for the use of Monte Carlo analysis in agency risk assessments.* Report EPA/630/R-97/001. Washington, DC: US Environmental Protection Agency.

6. Range Commanders Council. *Common risk criteria for National test ranges: inert debris.* 321-00:2000: U.S. Army White Sands Missile Range, NM, (Available at: http://technet0.jcte.jcs.mil).

7. Range Safety Office. *Eastern and Western Range Safety Requirements*. EWR 127-1:1997. Patrick AFB, FL: Range Safety Office.

8. National Research Council. (1994). *Science and judgment in risk assessment*. Washington, DC: National Academy Press.

9. Kummamoto, H., & Henley, E. J. (1996). *Probabilistic risk assessment and mangement for engineers and scientists* (2nd ed.). New York, NY: Institute of Electrical and Electronic Engineers, Inc.

10. Smerdon, W. S. (1988). *A probabilistic approach to laser safety*. Proceedings of the First international symposium on laser biological effects and exposure limits, Cedex, France: Commissariat a L'Energie Atomique.

11. Smith, F. G. (Ed.). (1993). The infrared and electro-optical systems handbook (Vol. 2) *Atmospheric propagation of radiation*. Bellingham, WA: SPIE.

12. Weaver, L. D., & Butts, R. R. (1994). ABLEX: High altitude laser propagation experiments. *Laser Digest, 2*, 141-165.

13. Sliney, D. H., & Wolbarsht, M. (1976). *Safety with lasers and other optical sources*. New York: Plenum Press.

14. Hengst, G. H., Crockett, G., Polhamus, G., Kennedy, P., Cupello, J., Lilius, B., Thomas, R., Trevino, J., & Clark, D. (1999). *Laser range safety tool for target reflection analysis*. Proceedings of the International Laser Safety Conference, Orlando, FL: Laser Institute of America.

15. Maxwell, J. R., & Beard, J. (1973). *Bi-directional reflectance model validation and utilization*. Tehnical Report AFAL-TR-73-303. Michigan: Environmental Research Institute of Michigan.

16. Crockett, G. (2000). *Bi-directional reflectivity distribution function (BRDF) modeling in LRST: Maxwell-Beard, Phong, and Gaussian models*. Contract F04701-98-D-0100, CDRL A004. Albuquerque, NM: Logicon RDA.

17. Committee on Space Launch Range Safety. (2000). *Streamlining space launch range safety*. Washington, DC: National Academy Press.

18. Smith, P. A. (1994). Probability and risk in laser safety. *Journal of Laser Applications, 6*, 101-107.

19. Finney, D. J. (1971). *Probit analysis* (3rd ed.). Cambridge: Cambridge University Press.

20. Smith, P. A. (1993). Probabilistic laser safety: ocular damage models for Q-switched neodymium and ruby lasers. *Health Physics, 66*, 414-419.

21. Schulmeister, K., Sonneck, G., Rattay, F., Hödlmoser, H., Sliney, D. H., Mellerio, J., Culoma, A., & Preyssl, C. (2000). *A probabilistic risk analysis model for receiving laser eye injury from space based lasers*. Proceedings of the 5th International Conference on Probabilistic Safety Assessment and Management, Osaka, Japan: Universal Academy Press, Tokyo, Japan.

Modeling of uncertainty associated with dose–response curves as applied for probabilistic risk assessment in laser safety

K. Schulmeister[a*], G. Sonneck[a], H. Hödlmoser[b], F. Rattay[b], J. Mellerio[c] and D. Sliney[d]

[a]Austrian Research Centers Seibersdorf, A-2444 Seibersdorf, Austria
[b]Technical University Vienna, Inst. f. Analysis a. Technical Math., A-1040 Wien, Austria
[c]University of Westminster, School of Biosciences, W1M 8JS London, UK
[d]U.S. Army Center for Health Promotion and Preventive Medicine, Aberdeen Proving Ground, MD 21010-5422, USA

ABSTRACT

In laser safety, dose-response curves describe the probability for ocular injury as a function of ocular energy, and are often used to quantify the risk for ocular injury given a certain level of exposure to laser radiation. In principal, a dose-response curve describes the biological variation of the individual thresholds in a population. In laser safety, a log-normal cumulative distribution is generally assumed for the dose-response curve, for instance when Probit analysis is performed. The log-normal distribution is defined by two parameters, the median, called ED50, and the slope. When animal experiments are performed to obtain dose-response curves for laser induced injury, experimental uncertainty such as focussing errors as well as variability within the group of experimental animals, such as inter-individual variability of absorption of the ocular media, can influence the shape of the dose-response curve.

We present simulations of uncertainties and variabilities that show that the log-normal dose-response curve as obtained in a animal experiments can grossly overestimate the probability for ocular damage for small doses. It is argued that the intrinsic slope for an individual's dose-response curve is rather steep, even for retinal injury, however, the dose-response curve for a group or population can be broader when there is inter-individual variability of parameters which influence the threshold. The quantitative results of the simulation of the grouping of individual dose-response curves can serve as basis to correct potentially biased dose-response curves as well as to characterize the uncertainty associated with the ED50 and the slope of the dose-response curve. A probabilistic risk analysis model, which accounts for these uncertainties by using Monte-Carlo simulation, was developed for retinal laser injuries from pulsed lasers with wavelengths from 200 nm to 20 μm, and the interpretation of the results are discussed on the basis of example calculations.

Keywords: laser safety, probabilistic risk analysis, ocular injury, uncertainty, variability, dose-response curve, Probit analysis, Monte-Carlo simulation

1. INTRODUCTION

The concept of the dose-response curve is widely used in toxicology and health physics. In laser safety, dose-response curves describe the probability of observing a skin or an ocular lesion of a given nature (the response) as a function of laser exposure or energy (the dose). As such, dose-response curves are the basis of both the definition of laser thresholds (exposure limits) as well as of probabilistic risk assessment studies. Aspects of the dose-response curves which are pertinent to the definition of exposure limits are discussed on a phenomenological and biophysical basis in another paper presented at this conference[1]; in this paper we present a quantitative mathematical concept to model uncertainties associated with the dose-response curve with special emphasis towards application for probabilistic risk assessment (PRA).

1.1 Point estimate vs. probability distribution

In risk analysis, parameters such as the exposure dose or the shape parameters of a probability distribution can be described in two ways. The possibility of a range of values for the parameter may be expressed as a probability distribution, for example a normal distribution with a mean of 0.8 μJ and a standard deviation of 0.1 μJ, which means the most likely value of exposure is 0.8 μJ, but there can also be higher or lower values. Alternatively, if the value of the parameter is well known and there is negligible spread of the parameter or for a simplistic risk analysis, a point value estimate might be used, for instance a dose value of 1 μJ. To the knowledge of the authors, previous PRA models for laser exposure only considered point estimates for the dose-response curve and for the ocular exposure level. Our analysis shows that there can

* karl.schulmeister@arcs.ac.at; phone +43 50550 2533; fax +43 50550 2502; http://www.arcs.ac.at/G/GS

Laser and Noncoherent Light Ocular Effects: Epidemiology, Prevention, and Treatment,
Bruce E. Stuck, Michael Belkin, Editors, Proceedings of SPIE Vol. 4246 (2001)

be substantial uncertainty associated with the dose-response curve, which can be partially corrected, but the remaining uncertainty needs to be modeled for a complete PRA characterization. An ocular damage model was developed for exposure to pulsed laser radiation, which models the uncertainty of the dose-response curve by the Monte-Carlo technique.

1.2 Uncertainty and variability

It is helpful for discussion, and also for the completeness of risk models, to note that the spread of possible values of a parameter can be either due to lack of knowledge of the true value, termed uncertainty, or due to (biological) variability[2]. Uncertainty is a description of the imperfection of knowledge about the true single value of a parameter and can be reduced by additional information gathering, better measurements, or analysis. In contrast, variability describes the spread of the parameter which is inherent in the system or population and which cannot be reduced by measurement. For instance, the body weight at birth of a given population can be well described by a normal distribution, and the mean and standard deviation of the distribution, i.e. the shape of the distribution, is well known for countries where measurements are performed on a standardized basis. In a given population, the response to toxic agents (for instance if the sensitivity is directly related to body weight) will show variability, as some individuals will be more sensitive to a given dose than others. Variability can also arise for the exposure parameter of the exposed population, because some individuals will be exposed to a higher dose than others due to variation in the environment or the behavior of the individual. It is typical of variability that it cannot be decreased in extent by additional measurements, but it may be decreased by reducing the population under consideration: for instance, if for one country, babies are generally bigger than for another, the distribution for both countries together will be broader, i.e. there will be a larger spread, than for each of them separately. In the extreme, when the population is reduced to a single individual, the variability distribution of the population for a variable collapses to the value applicable for the individual under consideration. For the case that a risk model does not contain variability, every individual in the population faces an identical risk.

Whilst considering variability and uncertainty, it is interesting to note how they might interact in a specific situation. For example, there may be uncertainty about the amount of variability within a given population. For instance, in developed countries, there are good statistics regarding the weight at birth and the corresponding distribution is well known: however, if measurements of birth weights are not performed on a regular basis, or are performed with poor scales, then there is some uncertainty associated with the actual true shape of the distribution describing the variability in the population. A PRA model, where the uncertainty and variability are modeled separately, is termed second order[3].

In the field of risk analysis, there is some variation in the terminology, as often the nature of the spread of a frequency distribution of a parameter is not further considered and the general term "uncertainty" is used. Using "uncertainty" as the overall term, authors in the field of engineering PRA[4,5] sometimes distinguish between epistemic uncertainty (also called the state of knowledge uncertainty), which is referred to as uncertainty elsewhere and in this paper, and aleatory uncertainty, (also referred to as random or stochastic uncertainty, for instance of the time to failure), which could be compared to variability in the field of environmental health PRA. In some environmental protection studies[6], variability is termed uncertainty Type A, and uncertainty as used here is termed uncertainty Type B.

Previous PRA models for laser exposure have only considered the variability as represented by a dose-response curve[7]. Here, we describe a second order PRA model for laser exposure, which accounts for the uncertainty of the dose-response curve.

1.3 Dose-response curve

A dose-response curve describes the variability of the sensitivity of a given population to a hazardous agent or "agonist". Here "population" has to be understood in a rather broad mathematical sense, and can mean a number of retinal exposure sites within on eye, a number of animals for an experiment, or also potentially exposed humans. In laser safety, the response is of "yes" or "no" type, i.e. "lesion" or "no-lesion". Such a type of response is also called a quantal response, in contrast to a graded response, where an increase in the dose produces a gradual change of the observed phenomena, such as degrees of intoxication following alcohol consumption.
Theoretically, in a given individual when a given tissue site is exposed at a given time, for quantal response there will be a certain sharp threshold dose: below the threshold dose, no response is observed, while if the exposure is above the threshold dose, a response is observed**. Such a situation can be depicted by a step-shaped dose response curve as shown in figure 1.

** It is noted that for a complete information, it is important to specify the nature of response, such a minimal visible lesion, and also the method of observation, such as ophthalmoscopically, with electron microscope, or other techniques, as discussed further in Reference 1.

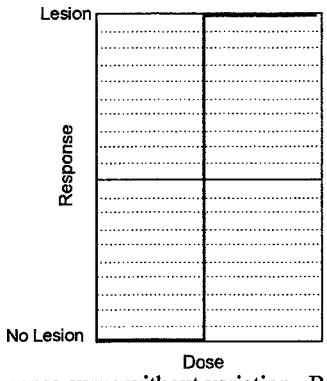

Figure 1. Theoretical dose-response curve without variation. Below a certain threshold dose, no lesion is observed, while above that threshold, exposure always results in a response.

However, it is not possible to determine such a threshold for a single exposure site of a tissue, as a number of exposures are needed to bracket the threshold. and any given point on the retina can only be exposed once, as an exposure damages or potentially changes the properties of the site. Consequently, in laser threshold studies, exposures are performed on a number of different locations on the tissue and also for a number of individuals. Different sites and different individuals will exhibit different thresholds (for instance due to varying retinal absorption, see discussion in Sliney et al. these proceedings[1]) and for a given exposure dose, those sites and individuals with a lower threshold dose than the exposure dose will develop a lesion. When the response axis is defined as the relative frequency (percentage) of observed responses from a given total number of exposures with a given dose, then a dose-response curve results, as schematically shown in figure 2.

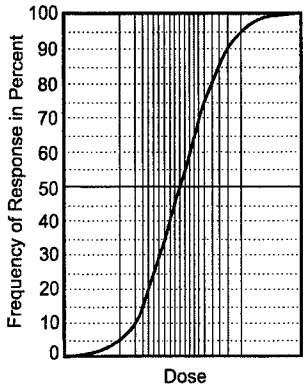

Figure 2. Due to different thresholds of different sites or individuals, for a given exposure dose, only a certain percentage of the exposed population will show a response, and a dose-response curve results.

In figure 2, each vertical line can be conceptualized as an individual sharp threshold step-curve (compare figure 1). The lines are plotted as equidistant frequency, i.e. the intersection with the frequency levels is constant (5 %). Such lines can be also help for graphically determining the shape of the dose-response curve, for instance when two curves from two different "populations" are combined. This is done by counting how many threshold lines lie on the left of any given dose point and dividing by the total number of lines, in this case 20, when the frequency of exposures which will show a response is obtained.

In a mathematical sense, the dose-response curve as shown in figure 2 is a *cumulative* distribution function: when a number of exposures are performed with a given dose, all tissue sites which have a threshold equal to *or smaller than* the exposure dose will show a response. Such a distribution will generally have a sigmoid shape, but it will not be symmetrical, it will be skewed, raising less steeply at the higher dose region because there will always be some tissue samples or individuals, that have a high resistance to damage. An example of a dose-response curve from a laser threshold study is shown in figure 3 with a linear and logarithmic ocular energy scale. As is generally the case for quantal response data[8], if the abscissa of the frequency distribution is plotted on a logarithmic scale, the data can be fitted well with a cumulative normal (Gaussian) distribution function and all the usual statistical calculations are available. A distribution which is normal when the abscissa is on a logarithmic scale is known as a log-normal frequency distribution.

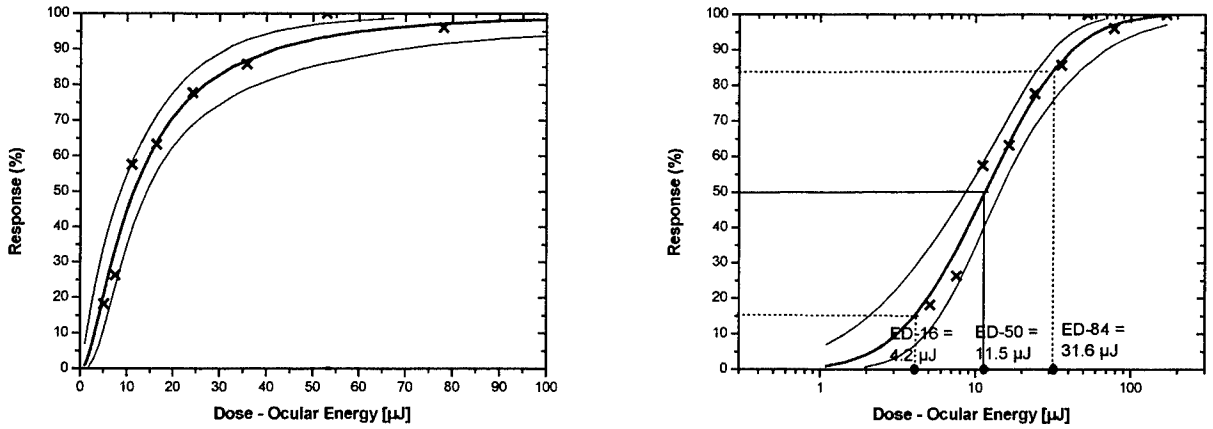

Figure 3. Dose-response curves as obtained from 191 exposures of rhesus monkey retinas to 850 nm, 180 ns laser radiation (private communication J. Lund). The data points (x) are derived by binning of the experimental data into energy intervals and by plotting the resulting relative frequency data for the response between 0 and 1. For instance, if 12 exposures were to fall in a given energy interval or bin, of which 4 showed a response, the relative frequency for response for this bin is 0.33. The lines are the result of a regression with 95 % confidence intervals, where a log-normal cumulative distribution is assumed (probit analysis, see section 1.5)

The log-normal distribution of the response can also be understood on the basis of the central limit theorem of statistics: the variability of a phenomenon or variable is described by a normal distribution, when it arises from many small independent effects in an *additive* way. Since addition of logarithms is equivalent to multiplication of the arguments, a log-normal distribution arises for a variable whenever this variable depends on other small effects in a *multiplicative* way. Consequently, body size and weight are typical examples of normal distributions, as the total observed parameter depends on weight and length of many small portions of the body in an additive way. A typical example of a variable which is described well by a log-normal distribution is the volume of recoverable oil reserves within a field, where the volume is a function of reserve area, thickness, porosity, oil/gas ratio and others[3]. For the example of exposure to laser radiation, the multiplicative dependency of the effect of the radiation producing a lesion could depend on: the transmissivity of the tissue in front of the site under consideration (total transmissivity is multiplicative regarding different kind of tissues, such as cornea, aqueous, lens, vitreous for exposure of the retina), the absorption depth of the tissue under consideration, and the exposure cross-section.

1.4 Log-normal distribution

The formula for the cumulative log-normal distribution is given by

$$P(OE) = \frac{1}{\ln(S)\cdot\sqrt{2\pi}}\cdot\int_0^{OE}\frac{1}{x}\cdot\exp\left[-\frac{\left(\ln(x)-\ln(ED50)\right)^2}{2\cdot\ln(S)^2}\right]dx = 0.5+0.5\cdot erf\left(\frac{\ln(OE)-\ln(ED50)}{\sqrt{2}\cdot\ln(S)}\right) \quad (1)$$

where OE is the ocular energy (dose), *erf* is the error function, which is tabulated for instance in Reference 9, and is also incorporated in many modern mathematical software packages. ED50 is the median dose, i.e., the dose at which 50 % of the exposures result in a response (a detectable lesion), and is referred to as the "effective dose 50 %," or simply, the "ED50". Correspondingly, the dose at which 16 % and 84 % of the exposures result in detected lesions are referred to as ED16 and ED84 respectively. S is the slope, defined as

$$S=\frac{ED84}{ED50}=\frac{ED50}{ED16} \quad (2)$$

A sharp threshold, as pictured in figure 1, would correspond to a slope S of 1, and the dose response curve in figure 3 has a rather shallow slope S of 2.75. The logarithm of the ED84 and ED16 points represent one-standard deviation in the normal distribution from the logarithm of the median dose. The slope S as defined above can therefore be interpreted as a multiplicative standard deviation[10]: instead of "plus/minus" standard deviation as for a normal distribution, the multiplicative standard deviation has to be thought of in terms of "times/divide". For instance, a slope of S = 2 with an ED50 of 10 µJ would mean that 68 % of the log-normal density distribution is within a range of 10 x 2 = 20 µJ and 10/2 = 5 µJ.

1.5 Probit analysis

Today, with modern computers, statistical curve fitting is not a problem, but when toxicology was less developed, a way was sought to allow easy curve fitting with just a ruler and pencil. To simplify the fit of a cumulative log-normal frequency distribution to the data, the data are transformed by turning the cumulative percentage into a probit scale[11], which, as figure 4 shows for the example of the data on which figure 3 is based, yields a straight line when the dose is given in logarithmic scale. Thus by transforming the percentage to probits and fitting a best by-eye fit straight line, reliable estimates of ED50 and the slope could be determined. Graphs with these two transformations, logarithmic on the abscissa (dose) and probit on the ordinate (probability for response), are often referred to as „probit plots".

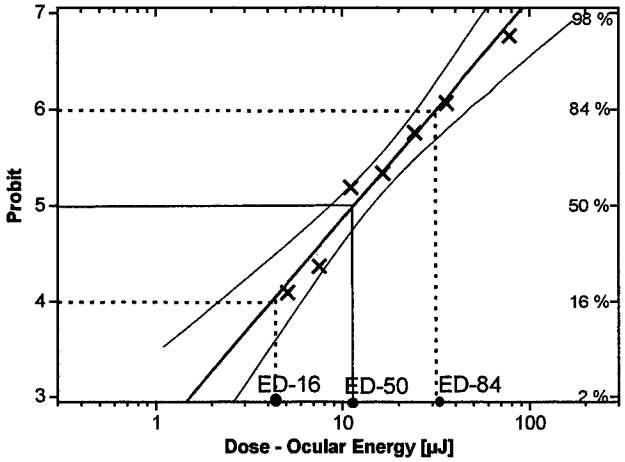

Figure 4. After a probit transformation of the response scale of the data as presented in figure 3, the log-normal distribution becomes a straight line which facilitates graphical fitting and analysis.

A probit value of 5.0 occurs at a probability value of 50 %. A probit value of 6.0 corresponds to ED84 and a probit value of 4.0 occurs at ED16. Data points with 0 % and 100 % response are not shown on a probit scale, as these probability values are not defined on a probit scale. The technique of probit analysis of data is used so widely in laser threshold studies that the term probit plot is used, somewhat erroneously, even when the ordinate is plotted as percentage rather than as probits. Also shown in figures 3 and 4 are the 95 % confidence intervals as calculated by a probit regression.

The most cited point on the probit plot is the ED50. This value is frequently referred to as the "threshold," even though there is *no* sharp threshold and some experimental damage points exist below this "threshold." In order to relate the full information of the variability, the slope is at least as important as the ED50 point, and Mush[7] even argues that "The extent to which ED50 has been used in the past for assessing the safety of substances could almost be termed as abuse".

It is noted that the original definition of the slope as applied in the classic text of Finney[10] is the conventional mathematical meaning of slope, i.e., the change in probability of an effect divided by the change in dose. Also, some software packages, for instance SAS/STAT, use this definition for the slope for the probit regression analysis, and therefore some laser threshold studies also specify the slope in that way and call it "real slope", RS. The real slope and the slope S are related by

$$RS = 1/\log S. \qquad (3)$$

A slope S of 1 corresponds to an infinite real slope, a slope S of 1.1 is a real slope of 24.2, and both are equal for a value of about 2.5. Some other values are listed in table 1.

Table 1. A list of corresponding values for the slope S (multiplicative standard deviation) and the "real slope" RS of the probit plot.

Slope S	RS
1.0	Infinity
1.1	24.2
1.2	12.6
1.4	6.8
1.6	4.9
2.0	3.3
2.5	2.5
3.0	2.1
4.0	1.7

2. DISCUSSION

When the dose-response curve is obtained from a number of exposures to animals in an experiment, the response scale is defined as relative frequency, i.e. total number of exposures producing an effect with a given dose, divided by observed lesions. When a log-normal distribution is fitted to the data, this function can be interpreted as characterizing the probability that an exposed individual will have a threshold less than the dose under consideration, i.e. will suffer an injury for a given dose.

An observed distribution has a spread whose range might be due two sources of dispersion. One is solely due to variability, and the distribution gives the probability that an individual will have their threshold lower than the dose under consideration. Thus the probability is in respect to what damage threshold the exposed individual and exposed site has. Each individual or site has a given specific sharp threshold, and each time the threshold is exceeded, injury occurs. For this pure sense of variability, for each exposure to a given individual and a given site with a given (known) threshold dose, there is no randomness in the response. The dose-response curve in the sense of biological variability represents the fraction of the population where a given dose produces a lesion, hence in this sense, the term "frequency of response" is more appropriate than the term "probability of response". For instance if the frequency of response, calculated from the dose-response curve, is 10^{-4}, this means that it is expected that in a population of 10 000 there is one individual which has a threshold lower than the respective dose. An interpretation of the ordinate as probability is possible, in the sense of the probability that exposure occurs to an individual who has an individual threshold lower than the dose under consideration. The authors would like to stress the difference of a probability distribution describing biological variability from a probability distribution describing aleatory, i.e. stochastic uncertainty, as used to calculate the probability that a thrown dice shows 6. When a dose-response curve is used in the mathematical sense without considering the background of biological variability, it might be erroneously interpreted to characterize a stochastic probability in the sense of "let's throw a coin, does a lesion develop or not".

Besides this interindividual variability, there is another source of variation, which arises because some laser injuries might be induced by stochastic mechanisms. For example, in cases of exposure to ultrashort pulses where the development of optical breakdown might play a role, the probability has the sense of an uncertainty for damage to develop for each exposure of a given individual. Thus, for each specific member of the population and for a given exposure level and site, there is a certain stochastic probability that an injury will occur, like flipping a coin for each exposure.

For thermal, thermomechanical and macroscopical photochemical laser injury mechanisms, which apply for pulse durations greater than about 10 ns, there is very little or no stochastic effect. The following discussion therefore assumes that the stochastic effect is negligible in comparison to inter- and intra-individual variability and other uncertainty components which broaden the distribution.

One main source of an increased spread of the observed distribution is the uncertainty associated with the experimental techniques, including systematic errors. These experimental uncertainties are discussed in Reference 1 of these proceedings, and are summarized and commented from the viewpoint of PRA in the following paragraphs.

2.1 Severity of the consequence

A quantitative risk analysis needs to include a characterization and specification of the severity of the injury for which the probability or frequency is determined. The endpoint in typical laser threshold studies is the minimal visible lesion, MVL, which can be described as a just barely detectable lesion. If the method of examination is ophthalmoscopic, then the endpoint is also called minimal ophthalmoscopically visible lesion, MOVL. However, the severity of the injury depends not only on the level of the ocular exposure, but also on the location of the lesion, as a lesion in the fovea can result in serious vision loss, but may even go unnoticed if located in the periphery of the retina. For a PRA model, the level of severity typically adopted is the MOVL.

2.2 Experimental protocol, comparison with data for humans

Sliney et al. (2001), these proceedings[1], consider whether the results of experimental threshold studies can be influenced by the choice of examination technique and the time of examination. Some techniques are considered more sensitive than others, i.e. for some studies[12], where both ophthalmoscopic examination and histology with microscopy was performed, the ED50 as determined with microscopy was somewhat lower. In other recent studies (for instance exposure to 650 nm, 0.25 s radiation) it was noted that "damage was not detected microscopically at exposed sites not exhibiting an ophthalmoscopically visible lesion" (Ref. 13). Some types of lesions take longer to develop, i.e. the dose-response curve will shift to lower doses for examination at 24 hours after exposure in comparison to an examination at 1 hour after exposure, while Lund et al. in a recent study with blue and green wavelengths and nanosecond pulse durations (Lund, these proceedings[14]) reported that the difference between the ED50 values for 1 hour and 24 hour data was practically zero for

most wavelengths which were studied. Also different sites of the retina exhibit different sensitivities: the macula is generally more sensitive due to a higher pigmentation and therefore higher light absorption than the paramacula region. Therefore, when the dose-response curve is determined in the paramacula region with an ophthalmoscope after 1 hour of exposure, the resulting dose-response curve, depending on the type of exposure and lesion, may be about a factor 2 to 4 above a curve which was determined for the macula, 24 hours after exposure and with microscopy. Animal experiments give ED50 values that are generally lower than those for the few studies where human volunteers were exposed. In particular, Ren-yuan et al.[15] reported for experiments on human Chinese retinas for 150 μs 1.06 μm radiation a factor 1.8 higher for human vs. grey rabbit and a factor 6 for human vs. rhesus monkey. Vassiliadis et al.[16] reported a factor for human vs. rhesus monkey of about 3 for 100 ms 488 nm radiation, a factor greater than 10 for 200 μs 694 nm, a factor of greater 3 for 20 ns 694 nm, and a factor of greater 10 for 30 ns 1.06 μm radiation (the experimental data for humans are rather limited and were not sufficient to perform a probit analysis). Gabel et al.[17] compared ED50 values of chinchilla rabbits to those obtained from human volunteers and obtained a factor of 4 for 488/514 nm 20 ms radiation. In summary, it seems that the higher ED50 values obtained for human exposure, depending on the experimental protocol used to determine the animal dose-response curves, either provide a safety margin or compensate for less sensitive experimental animal experiment protocols. Generally, rhesus monkeys provide a good model for human exposure. However in terms of variability and uncertainty of the variability, i.e. uncertainty of the ED50 and slope and of the shape of the dose-response curve for small probabilities, additional sources of uncertainty, such as varying spot sizes due to focussing errors, need to be considered, as will be discussed below.

2.3 Significance of slope

The slope S is a direct indication of the variability which is expressed by the dose-response curve. It is interesting to note that for medical phenomena which are well described by a log-normal distribution, such as latent periods of infectious diseases and survival time after diagnosis of cancer[9], the median of the distribution (which is the ED50 for dose-response curves) strongly depends on the kind of disease or cancer, ranges from hours to years, but the slope parameter is a typical value for the phenomena under consideration, i.e. the slope is the same for all diseases or cancers[9], as is summarized in table 2.

Table 2 Examples of log-normal distributions from medical sciences (adapted from Limpert et al.[9])

Phenomena	Median (comparable to ED50)	Multiplicative standard deviation (slope S)
latent periods of infectious diseases	Hours to years, depending on kind of disease	1.5
survival time after diagnosis of cancer	Months to years, depending on kind of cancer	3

For laser induced MVL data, the ED50 strongly depends on the wavelength, exposure duration and on the spot size[12]. As there are thermal, photochemical and non-linear damage mechanisms, it would stand to reason that there is an inherent typical slope value for each damage mechanism, even though the ED50 can vary over orders of magnitude depending on wavelength and exposure duration. Unfortunately, it seems that the available data are influenced by uncertainties which mask the expected characteristic intrinsic slopes.

2.4 Variability and uncertainty

For laser induced damage, variability, as quantified by a more or less shallow slope of the dose-response curve, can have different origins. Generally, any interindividual variability of physical and physiological properties which influences the threshold for damage, results in a variation of thresholds for a given "population".

An example of interindividual variability is that of the transmissivity and absorption coefficient of the involved tissues: young individuals will have better transmissivity of the cornea and the lens in the blue and near UV than older ones. These parameters can also vary for a single individual in respect to different exposure locations, for instance for different locations on the retina – these variations can be called "intra-individual variability". Also within a given region of the retina, there is a variability of the absorption characteristic due to melanin granules (see Reference 1).

Additional to the biological variability within a given population, experimental uncertainties will introduce a larger spread of the experimentally determined dose-response curve, for instance:

- Uncertainties in the dosimetry, i.e. in the determination of the laser energy, can broaden the dose-response curve.
- Uncertainties in the spot size diameter. The threshold for retinal damage depends on the area of the irradiated spot when the dose is given as ocular energy. Therefore, if for instance an experiment is designed to produce minimal spot sizes, but not every exposure achieves a minimal spot size, then this produces a larger slope, as is discussed below.

It is important to characterize these uncertainties and to attempt to correct the experimental dose-response curve, when it is to be used to characterize the risk for eye injury of a human. Since there are many factors which influence the dose-response curve for laser induced ocular damage, and the influence of the individual factors is usually poorly characterized, there will be some degree of uncertainty associated with the shape of the dose-response curve which truly characterizes the

biological variability of the population under consideration. In particular, if the log-normal distribution is used to quantify the probability for response to a given dose, then the two parameters of the log-normal distribution, the ED50 and the slope will have an associated uncertainty, which can be modeled by probability distributions.

2.5 Confidence intervals

Since the dose-response curve is derived as statistical regression of data obtained with a limited number of exposures, i.e. of a small part of the total population, confidence intervals (CI) describe the range of possible dose-response curves which are the true dose-response curve for the whole population. For instance, the 95 % CI of the ED50 is a range of values, where one can be 95 % sure that the CI includes the ED50 of the whole population. In this sense, the confidence interval gives some information about the uncertainty of the dose-response curve, but with the important assumptions that the examined group of animals (the sample) is representative of the whole population and also that the measurements and the experimental data are exact, and that there are no systematic errors. Our analysis shows that for laser induced MOVL studies, these assumption might often not be valid, for instance if refractive errors exist. It is noted that confidence limits are called fiducial limits by Finney, with the rather cryptic note[11], that they are most of the time identical to confidence intervals. So far, no other reference could be identified which also refers to fiducial limits and which would elaborate on the possible differences to confidence intervals. For the application for laser threshold studies, it seems justified to interpret Finney's fiducial limits as confidence limits.

2.6 Experimentally determined slopes

For laser thresholds, corneal dose-response curves have generally very steep slopes, of about 1.1 (e.g. Ref. 16). In some studies of corneal damage, for instance with pulsed CO_2 laser radiation[18], there was a sharp threshold which varied by less than 10 % and therefore no probit analysis was undertaken. A variation within 10 % corresponds to a slope of about 1.1. For retinal studies, however, the reported slopes vary from very steep slopes of 1.01 and 1.05 (Ref. 20) of recent studies to slopes as large as 2.8 for the data presented in figure 3. Also in a study by Lund et al.[21], a Ti:Sapphire laser was used to produce dose-response curves for 27 wavelengths from 692.0 to 1010.0 nm with a pulse duration of 100 ms, and the slopes varied from 1.11 to 1.59 in what seems like a random manner. Since the wavelength dependence stems from transmission and absorption properties of the ocular media, which determine the energy deposited in the retinal pigment epithelium, and the process is purely thermal, one would not expect a strong change of biological variability from one wavelength to the next.

2.7 Grouping of individual dose-response curves, variability of absorption

Experimental slope values for "surface" laser injury such as to the cornea or the skin, are usually about 1.1. Such a slope would characterize a distribution where 68 % of the distribution lies within a dose range of approximately ± 10 % around the median point, the ED50[***]. Since the deposited energy, and hence the exposure dose, necessary to produce a given temperature rise depends directly on the absorption, biological variability of the absorption will also result in variability of the threshold, and this is reflected in the dose-response curve. For retinal exposure, the biological variability of the absorption within one macula for the smallest image spot size is of the order of ± 5 % to ± 20 % (Gabel et al.[22]), which would correspond to a dose-response curve slope of about 1.05 to 1.2. These values are also supported by graphical pixel density analysis of a flatprep of a human RPE which was prepared by Gabel et al[22], where the analysis with a spot size (averaging area) of 25 μm, 40 μm and 75 μm resulted in a relative standard deviation of 16 %, 11 % and 8 %, respectively.

However, there is also substantial inter-individual variability in respect to absorption properties of the retina, which is estimated to be of the order of a factor 2 (Gabel[22], Sliney[1]), and this variability is characterized by a dose-response curve with a correspondingly shallower slope.

The applicability of a dose-response curve which characterizes the variability within a given population, and which might be used to indicate the risk, is discussed with the following example: consider that the dose-response curve for a given individual has a slope of 1.1 and the individual ED50 is inversely related to the (mean) retinal absorption of that individual: a small absorption will result in a larger individual ED50 than for an individual with a high absorption, where a smaller dose is sufficient to cause injury. When threshold experiments are conducted with a group where the absorption varies within the group over a certain range, and the data of the whole group are pooled to perform the probit analysis, then a shallower slope with an intermediate ED50 will be the result, as is schematically shown in figure 5.

[***] As discussed above, the slope is a multiplicative standard deviation of the log-normal distribution, in contrast to the additive standard deviation as defined for a normal distribution. For simplified comparisons and small values of slope S, such as 1.1, the difference between the additive and multiplicative standard deviation is not large (as the difference between the normal and log-normal distribution is not large) and a slope of 1.1 can be compared to a (additive) standard deviation of ± 10 %.

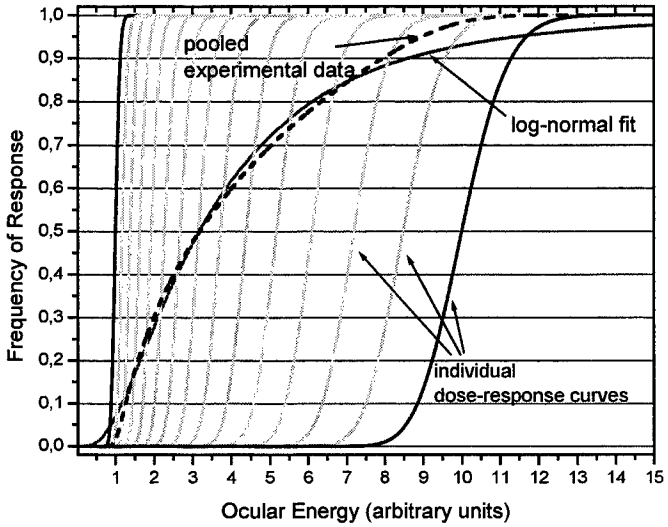

Figure 5. Combination of dose-response curves with steep individual slopes to an overall dose-response curve. Both the combination of simulated pooled data is shown (dashed line) as well as a log-normal curve which is a best fit to the simulated "experimental" data.

The data in figure 5 were derived by simulating individual dose-response curves each with a slope of 1.1 and a range of ED50, starting from ED50 = 1, up to an ED50 = 10 (arbitrary units). The individual dose-response curves were assumed to be continuously overlapping, i.e. the number of individuals within the range of ED50s was assumed to be high, in order to obtain a smooth overall dose-response curve; in figure 5, only 15 individual dose response curves are shown. When the data stem from a small number of non-overlapping individual dose-response curves, the resulting pooled frequency data curve (i.e. the overall dose-response curve) would show steps with horizontal sections where the individual dose-response curve's data do not overlap. For the simulation of the data shown in figure 5, the distribution of the individual dose-response curves was assumed to be logarithmic, i.e. the logarithm of the individual ED50 values was uniformly distributed. A simulation of the pooling of the dose-response curves was performed by creating random dose numbers corresponding to the individual log-normal distributions as well as the logarithmic distribution of the individual dose-response curves. This simulation technique is akin to laser retinal threshold studies where "injury" – "no-injury" data are recorded for a number of exposures per eye and for a number of experimental specimen, and the data are pooled for all animals as the data from single eyes usually are not usually sufficient for an probit analysis or the construction of a dose-response curve. The resulting pooled data are shown in figure 5 as well as a log-normal distribution which has the same ED16, ED50 and ED84 values as the pooled data. It can be seen that within the approximate range of the ED10 to ED90, the log-normal distribution fits well to the pooled individual data, but deviates for the low and high-dose end of the distribution. When the ED50 values of the individual dose-response curves were simulated to be uniformly distributed, instead of logarithmically, then the resulting pooled data were described better by a normal distribution than by a log-normal distribution, i.e. for that case a log-normal dose response is not an appropriate distribution to describe the variability of the population. For laser induced damage, it is difficult to theorize whether the distribution of individual thresholds (i.e. individual dose-response curves with steep slope) is closer to a uniform or to a logarithmic distribution. For instance with the inter-individual variability of ED50 values resulting from refractive errors (as discussed below) it might be the case that there are more individuals who only have a small deviation from perfect vision and only a few who have strong myopia. In this case the distribution would be best described as logarithmic.

As can be judged from a plot like that shown in figure 5, it seems appropriate to describe the variability within the population with a log-normal dose response for the range between the ED16 and the ED84. For doses above the ED84, the log-normal dose response curve with a slope S equal to the slope S of the pooled data, *underestimates* the frequency of ocular damage for a given dose. The pooled data show a frequency of 100 % for a dose of about greater 11, where the log-normal distribution has a frequency of 94 %.

On the other end of the dose range, the log-normal dose-response curve as fitted to the pooled data grossly *overstates* the variability and therefore the risk for doses less than about the ED16. This can be better examined on a logarithmic scale, as shown in figure 6. Towards the lower dose range of individual response curves, the pooled data are governed by the "yes" data (detected lesions) from the individual with the lowest ED50, i.e. for the example of variability of absorption, by the

individual with the highest absorption. It is important to note that there is a lower boundary for the laser threshold variability due to absorption, as there is an upper bound to absorption: in principal, the theoretical maximum absorption is 100 % of the incident radiant energy – a higher absorption is not possible and the corresponding ED50 is the lowest theoretically possible, limiting the variability on the low dose side (assuming that all other parameters are equal).

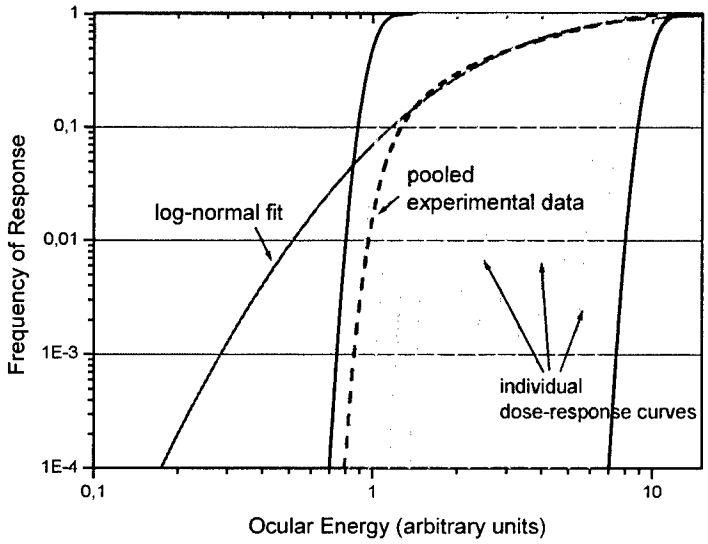

Figure 6. The dose-response curves of figure 5 shown with a logarithmic response and dose scale. It can be seen that for dose values below values where the lowest individual is governing the pooled data, the shallower overall dose-response curve predicts frequencies for response which are far too high.

It is obvious that a log-normal dose response curve which is obtained from pooled data of a population with individual steep dose-response curves but with some variability of individual ED50 values, should not be used to characterize the frequency of response for doses below a certain cross-over point of the log-normal dose-response curve with the pooled data. This crossover points depends on the distribution of the individual ED50 values and on the method of analysis. If the shallower overall dose-response curve were used below the cross-over dose, then the calculated probability values for injury are too large: with overall dose-response curves with shallow slopes, finite probabilities are calculated, for example 10^{-4} for a dose of 10 % of the ED50. Thus a scenario can be envisaged, where 100 000 people are exposed to laser radiation of that dose, and the PRA predicts that ten people would suffer eye injury. If the appropriate steep dose-response curve is applied to this low-dose part, then for a dose of 10 % of the ED50, the calculated frequency for ocular injury would be practically zero. Therefore, for small doses, it is rather the steep individual dose-response curve of the individual, which should be used to quantify the risk.

2.8 Focussing errors

The same arguments as developed above for varying absorption hold for refractive errors: threshold studies are designed to yield a dose-response for a given wavelength, pulse duration and retinal spot size. Often the set-up is for a minimal retinal spot size of about 10 - 20 μm. Due to experimental difficulties, the actual spot size might not be minimal, and has the potential to vary from exposure to exposure, as, for example, when an animal exhibits a refractive error, which may vary during the experiment. If one attempts to obtain a minimal spot size, any refractive error will result in an increased spot size, which leads to a smaller retinal radiant exposure. If a dose-response curve were to be assigned to an animal where a minimal spot is achieved, then the corresponding ED50 will be smaller than for an animal where the energy per pulse is distributed over a larger retinal area, and correspondingly more energy is needed to produce an injury. Rhesus monkeys used in laser threshold studies are usually screened so that the refractive error is not larger than 0.75 diopters. The situation is fully equivalent to the discussion of absorption, when a group of animals is considered, where the refractive error for instance ranges from zero to 0.75 of a diopter. If the threshold is assumed to be varying with the exposed area, then the factor between the threshold for a 10 μm spot and a spot resulting from a refractive error of 0.75 diopter is about 96. If the threshold is assumed to vary with the diameter of the exposed area, as is currently expressed in the laser exposure limits by the factor C_E (ANSI Z136.1) and C_6 (IEC 60825-1), then the factor between zero refractive error and 0.75 diopter is about 10. Values for other refractive errors are given in table 3.

It should be noted that if the refractive error in a given group of experimental animals is assumed to vary between zero and 0.75 diopter, the linear factor 1 to 10 describes the *total range* of individual ED50. The factor from the lowest individual ED50 (corresponding to zero refractive error) to the ED50 of the overall dose-response curve is equal to the square root of

the total range, assuming that all individual data contribute to the overall pooled curve to the same extent. For the example of a refractive error of 0.75 Diopter and a corresponding total range of 10, the increase of the ED50 would be about a factor 3. As is the case for biological variability of tissue absorptivity, the spreading of the dose-response curve is limited towards the side of low doses when focusing errors are considered as reason for the variability: the irradiated area can not be smaller than the minimum spot size.

Table 3. Retinal diameters corresponding to a minimal spot size for no refractive error and for increasing refractive errors. „Factor linear" relates the retinal spot diameter for a given refractive error to the diameter of the minimal spot size, and this factor would be applicable also for laser injury thresholds, as the laser exposure limit spot size dependence is linear with the spot diameter. „Factor area" relates the spot area for a given refractive error to the area of the minimal spot size (which is the relationship of the radiant exposure).

Refractive Error [Diopter]	Diameter [µm]	Factor linear	Square root of factor linear (factor for overall pooled ED50)	Factor area
0	10			
0.25	40	4	2.0	16
0.5	69	7	2.6	48
0.75	98	10	3.2	96
1	127	13	3.6	161

For the situation of an awake human, where refractive errors are usually corrected and where the eye "automatically" attempts to produce a focussed image, i.e. a minimal spot, only the dose-response curve for the minimal spot size appropriately characterizes the risk for exposure to a collimated laser beam. When the experimental dose-response curve is biased by animals with refractive errors, the resulting ED50 and slope values need to be reduced correspondingly. In this sense, when applied to the human case, the influence of the variation of the experimental animal's refraction needs to be treated as bias or uncertainty, not as biological variability.

2.9 Correlation of ED50 and slope for pooled data

From the previous discussion it is clear that whenever data are pooled from a group of animals where the intra-individual variability is small but there is some inter-individual variability, the overall dose-response curve will have a larger slope S (i.e., a shallower slope) and a higher ED50 value as would be applicable for the most sensitive individual. Also the log-normal dose-response curve as implied in probit analysis of data might not be the appropriate distribution to characterize the frequency of response, especially for doses outside the region of the single multiplicative standard deviation, i.e. outside the dose range ED16 to ED84. A statistical analysis of a specific set of experimental raw data of laser exposures regarding the shift of ED50 values following pooling of data from dissimilar subjects, and a simulation of data from an assumed dose-response curve, performed by A. Langus et al.[23], also showed that high ED50 values correlate with the bias and the standard deviation of the simulated data.

In order to obtain information on the relationship between the increase of the slope as a function of the total range of ED50s, the log-normal dose response curve for the pooled data was calculated as described in the previous section for a set of ranges of individual ED50 values, starting with a range of individual ED50s from 1-2 up to 1-100. When a logarithmic distribution of the individual ED50s was assumed within the respective range, and the individual slope S was assumed to be 1.1, a "pivot point" of the overall distribution functions was identified at the ED7 dose, i.e. at a frequency of response of 7 %; for an individual slope of 1.05 and 1.2, the pivot point shifted by less than 1 %.

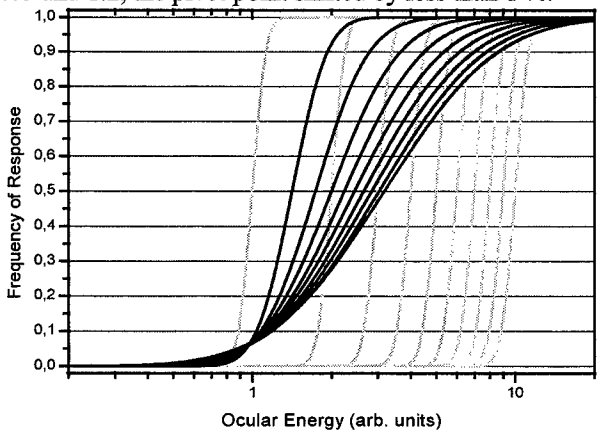

Figure 7. A range of overall log-normal dose-response curves as obtained by grouping of individual data for a set of ranges. The light shaded lines indicate the respective upper ED50 range borders from 2 to 10. The "pivot point" of the resulting overall pooled data response curves is at a response frequency of 7 %.

The relationship of the slope to the range of variation of the individual ED50 is shown in figure 8 and representative values are given in table 4. Both the total range of individual ED50s as well as pooled data ED50 are given in table 4, and they are simply related by a square root dependence. Since the lower range boundary is an ED50 of 1, the upper range boundary can also be interpreted as a general multiplication factor for ED50 values. For instance if the total range of individual variability is described by a factor of 4, then the ED50 of the pooled data will be a factor of 2 above the lower range of individual ED50s, and the slope will increase from the assumed individual value of 1.1 to a slope of 1.6.

Table 4. Calculated increase of slope, from a value of 1.1 for an ED50 of 1, with increasing range of variability of the pooled data.

total range; individual $ED50_{max}$ / $ED50_{min}$	Factor $ED50_{pooled\ data}$ / $ED50_{min}$	Slope
1	1.0	1.10
2	1.4	1.27
3	1.7	1.45
4	2.0	1.60
5	2.2	1.73
6	2.4	1.83
7	2.6	1.93
8	2.8	2.03
9	3.0	2.11
10	3.2	2.18
15	3.9	2.50
20	4.5	2.77
30	5.5	3.15

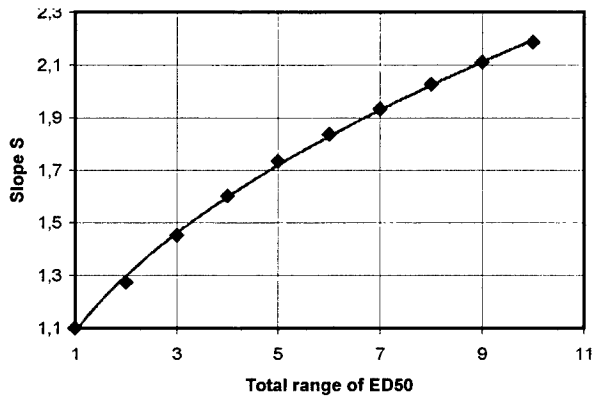

Figure 8. Relationship of slope S of the log-normal dose response curve to the range of ED50 values, where the range is defined as starting from an ED50 of 1 and extending up to the number as given in the plot.

The pivot point and the relationship between the ED50 and the slope also has an application in quantitative risk analysis. Consider the situation where the reported experimental data are derived from pooled data where the individual ED50 varies over a given range, for instance due to focussing errors. Consequently, the experimental dose response curve should be corrected for this variation to obtain a dose response curve which is applicable to a population without this variation (for instance where a minimal spot can always be achieved, as is to be assumed for human exposure). For such a correction, the experimental ED50 and slope would have to be reduced, and the results of the simulation and the correlation between the slope and the ED50, could be used as quantitative guideline for this correction.

When the dose-response curve is "rotated" around the pivot point by reduction of the ED50 and the corresponding reduction of the slopes, the pivot point also divides two trends in terms of probability for response. For a given dose above the pivot point, a reduction of the variability, i.e. of the ED50 and slope, produces an *increase* in the probability for response in comparison to a dose-response curve with larger ED50 and shallower dose, corresponding to an increased level of "risk". For a given dose below the pivot point, a reduction of the ED50 and slope produces an *decrease* in the probability for response in comparison to a dose-response curve with larger ED50 and shallower dose, corresponding to an decreased level of "risk".

2.10 Small probabilities

In the field of quantitative risk analysis and management, acceptable risk levels are often of the order of 10^{-6} per exposure or less, and scenarios are often evaluated where a larger number of people may be exposed. As a result, probabilities of injury often need to be calculated for doses much below the ED50.

The simulation of the pooling of experimental data showed that for the case of a small intra-individual variability but a certain inter-individual variability in a given population, it is not appropriate to extend the (shallow) log-normal dose-response curve to doses lower than about the ED10. However, even for the case where there is little experimental uncertainty and individual variability, or if the overall dose-response curve is corrected by reduction of the slope and correspondingly the ED50, the uncertainty associated with the lower-dose part of the dose-response curve is substantial. The dose-response curve is not known for such low probability values and in practice cannot be determined, as tens of thousands of weak exposures would be needed (compare the "megamouse experiment", Ref. 8). Finney[11] states that "...very extreme probits, say outside the range of 2.5 to 7.5, carry little weight, and may almost be disregarded unless many more subjects were used..." Probit values of 2.5 and 7.5 correspond to probabilities of about 1 % and 99 %, respectively. It has to be kept in mind that the log-normal dose-response curve describes the biological variation of the sensitivity of different individuals and of different locations of exposures for one individual (for instance different regions of the retina). Applying log-normal dose-response curves down to ever decreasing doses would imply that laser radiation of any level could cause injury, i.e. in a small but finite fraction of the population, be it 1 in a billion or less. However, for the case of thermal damage, simple biophysical reasoning shows that energy levels which do not result in a temperature increase of more than, say, 1 °C, cannot produce an ocular injury. If they did, the temperature elevation of 1 °C typical in a mild fever would cause blindness.

Following biophysical reasoning, for thermally induced damage[****], there will be a lower cut-off energy, below which injury is not possible, not even for the most sensitive individual. For PRA, this could be modeled by truncating the dose-response curve at a certain dose, i.e. setting the dose-response curve to zero below a certain ocular energy or exposure value. At present, the knowledge about this lowest possible dose is not sufficient to define such a truncated dose-response curve, but one could model the cut-off point with a probability distribution and perform Monte-Carlo simulation. However, in the PRA model discussed here, this was not done, as the application of steep slopes results in a marked decrease of the probability for damage for very small dose values, in effect similar to a cut-off. For instance, for a slope of 1.1, the calculated probability for the dose value of one 5th of the ED50 is $5 \cdot 10^{-64}$ and for the dose of one 10th of the ED50 could not be calculated with the mathematical software available, but is less than 10^{-100}. Considering that the dose-response curve in the sense of biological variability represents the fraction of the population where a given dose produces a lesion, probability numbers less than the world population do not make sense.

Table 5. Sample values for the log-normal cumulative distribution for a list of slopes, for dose values of a factor 10 and 5, respectively, below the ED50.

slope	Probability for one 10th of ED50	Probability for one 5th of ED50
1.1	< 1E-100	5E-64
1.15	5E-61	7E-31
1.2	9E-37	6E-19
1.25	3E-25	3E-13
1.3	9E-19	4E-10
1.4	4E-12	9E-07
1.6	5E-07	3E-04
1.8	5E-05	3E-03
2	5E-04	1E-02

3. MONTE CARLO SIMULATION OF THE UNCERTAINTY OF DOSE-RESPONSE CURVES

A quantitative risk model was developed to predict the probability for ocular injury upon exposure to pulsed laser radiation. The model was set up for pulse durations less than 1 μs, wavelengths between 190 nm and 19 μm using off-the-shelf mathematical software. The ocular damage model is part of a larger risk model which was developed to characterize the probability for ocular injury from space based lasers and possible exposure with telescopes of varying diameter (Schulmeister et al.[24]).

[****] Also for acute photochemical damage, there is a minimum dose which is necessary to produce a lesion.

The ocular damage model is based on log-normal dose-response curves, and uncertainties associated with the parameters of the dose-response curve, i.e. the ED50 and the slope, are modeled by sampling these values from probability distributions and calculating the probability of response for a given laser ocular energy for each sample. The probability distributions for the ED50 parameter, with wavelength and pulse duration dependence where applicable, are derived from values as reported for rhesus monkeys, and for the corneal damage thresholds for rabbits. For retinal injury, the potential bias of the reported dose-response curve due to experimental uncertainties, such as focussing errors, were considered by using the lowest reported ED50 values as an upper border of the range of ED50 values, and setting the lower range of ED50 values a factor of 2 below the upper border. Following the discussion above, the slope S is set to vary between a value of 1.05 and 1.4, in correlation with the range of ED50 values, i.e. for the lowest ED50 value a slope of 1.05 is chosen and for the largest ED50 value, a slope of 1.4 is chosen. The distributions of ED50 and slope values are taken as uniform, i.e. with equal probability between the lower and upper possible values.

As discussed above, the slope of the retinal dose-response curve for doses below about ED10 should be set to steep values, for instance of the order of 1.05 to 1.2. In the model the range of 1.05 to 1.4 is generally used for the dose-response curve, thereby somewhat overestimating the risk for exposure to small doses. However, for the scenario of space based lasers, the exposure level of the naked eye at the earth surface is usually well below the ED50, and only for exposure with (large) telescopes, is energy sufficient to cause ocular injury collected. The probability for exposure with a telescope with a relatively small field-of-view is quite small. The overall probability for ocular injury during a given mission is dominated by the probability of exposure with that type of telescope, which has the smallest diameter that results in a high probability of ocular damage (close to 1). For this kind of scenario, the overall risk numbers are not sensitive to the shape of the dose-response curve towards the low dose range. This part of the dose-response curve might however become relevant for a scenario where a large number of people is exposed to laser radiation and the exposure level with the naked eye is in a range closer to the lower range boundary of the ED50.

In the ultraviolet (UV) and far infrared range for pulses with durations less than 1 μs, due to sparse experimental data, the uncertainty associated with the slope is less pronounced than the uncertainty of the ED50 values: from available data for some limited wavelengths which affect the cornea or the lens, the slope can generally be assumed to have relatively little uncertainty and vary in the range of 1.05 to 1.2. However, regarding available data for the ED50, for instance for possible thermal corneal and lenticular damage induced by UV pulsed radiation with wavelengths above 310 nm and pulse durations between 1 μs and 1 ns, the experimental data are very few: the only experimental threshold value for thermal damage of the lens by short pulse laser radiation found in the open literature is for 337 nm nitrogen laser with a pulse duration of 10 ns (Zuclich[25]). Additional information on thresholds to short pulse exposure in the UV can be obtained by extrapolation from exposure to 350 nm radiation with a range of pulse durations between 100 μs to seconds (Zuclich[26]) and on the lower exposure level side can be bracketed by data for CO_2 laser radiation, which is absorbed by a small absorption depth in the cornea and can assumed to be having distinctively lower thresholds than near-UV radiation. For the ocular damage model, the uncertainty associated with respective ED50 values for wavelengths between 310 nm and 400 nm and pulse durations between 1 μs and 1 ns and , is represented by a triangular probability distribution with a lower and upper border of 3,000 J m^{-2} and 100,000 J m^{-2}, respectively, and by a most-likely value of 10,000 J m^{-2}.

The uncertainty of the ED50 and slope is simulated with the Monte Carlo technique, where random numbers are calculated for a given distribution of possible values so that the relative frequency of the calculated values correspond to the respective probability distribution. These lists of values for the parameters of the model are used to calculate the output parameter, such as the probability for ocular damage for a given ocular energy. A histogram of the values for the end result represents the distribution of values for the output parameter under consideration. The general scheme is visualized in figure 9, starting with the log-normal dose-response curve with a certain slope and ED50, where for a given ocular energy value, a single value for the probability for response can be identified (Figure 9 (a)). For instance, a value of 0.78 for an ocular energy of 8 μJ. When the parameters ED50 and slope are treated as uncertain, corresponding probability density distributions are defined (Fig 9 (b)), which vary the ED50 and slope, and thereby the shape and location of the dose-response curve in a given range (Fig. 9 (c)). When the probability for ocular damage is to be determined for the ocular energy E_0, then instead of a single point for the probability for ocular damage, a frequency distribution for the probability for ocular damage is found (Fig. 9 (d)), representing the cumulative distribution of dose-response curves over the range of probability for ocular damage values, for a given ocular energy.

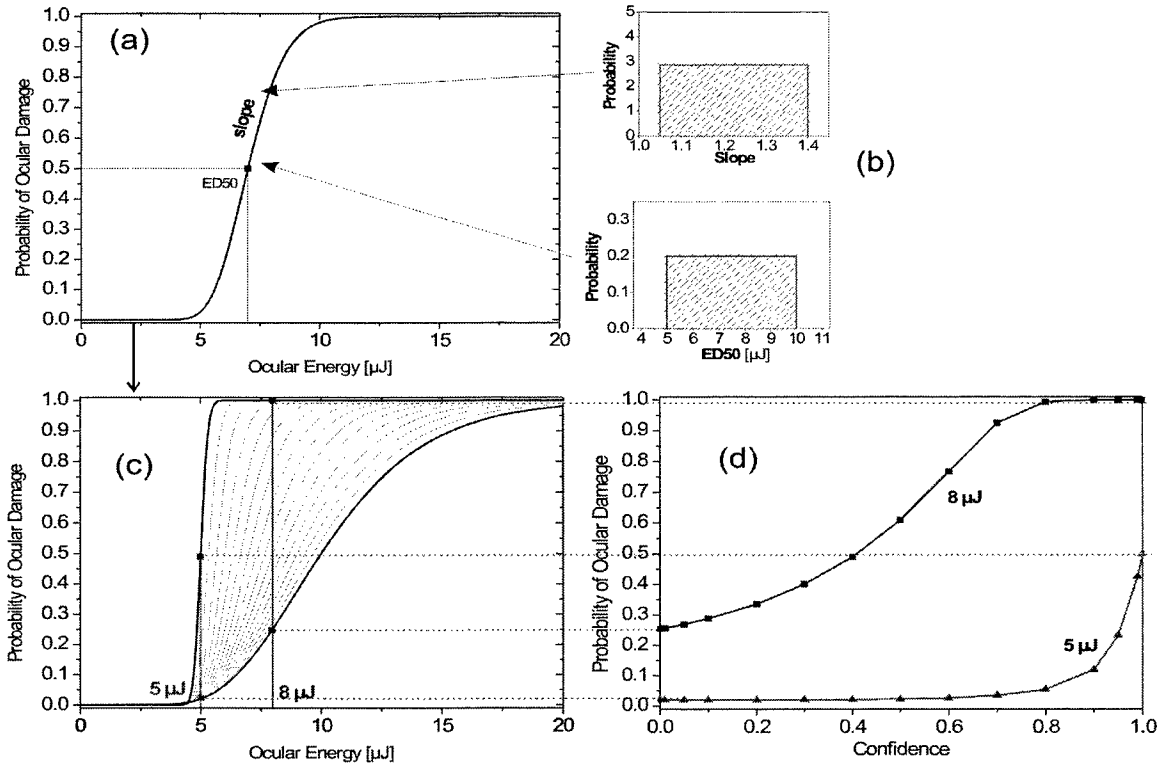

Figure 9 Schematic overview of the calculation of a distribution characterizing the probability for ocular damage given an exposure to a certain energy, and given a certain uncertainty of the shape parameters ED50 and slope S. The arbitrary values of 5 µJ and 8 µJ are taken as examples for the ocular energy.

By simulating the possible range of values for ED50 and slope, the single point value for the probability for ocular damage for a given energy (Fig. 9 (a)) is replaced by a distribution (Fig. 9 (d)). The result of the probabilistic analysis with uncertainty, figure 9 (d), is usually flipped regarding the axis and plotted with the confidence level on the ordinate and the risk figure, i.e. the probability for ocular damage, on the abscissa, as shown in figure 10 for a range of ocular energies. For the example shown in figure 10, a variation of ED50 between 5 µJ and 10 µJ and a variation of the slope between 1.05 and 1.4 for ocular energies between 0.5 µJ and 10 µJ was simulated. These values apply for instance to an exposure to radiation with a wavelength of about 900 nm and pulse durations between about 10 ns to 50 µs radiation with a minimal retinal spot diameter.

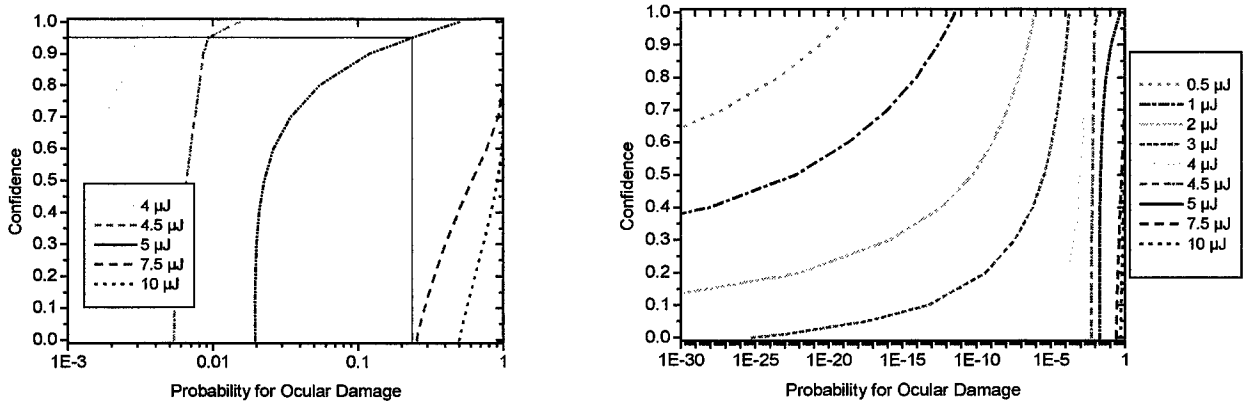

Figure 10. Probability distributions for the probability of receiving ocular injury for a range of ocular energies. The left plot includes ocular energies well below the range of ED50, while the right plot covers a smaller range of probability values.

For plots resulting from the modeling of uncertainty, as shown in figure 10, the ordinate can be interpreted as the "confidence level" for the probability of ocular damage for a given ocular dose. The confidence level can best be explained by an example: in figure 10, with a confidence level of 95 % (the 95 % quantile), the probability for ocular damage given exposure to 5 μJ, is less than or equal 0.23, or 23 %. In other words, there is a 5 % chance that the probability for ocular damage is larger than 23 %. The level of confidence which is used to determine the value on the ordinate is a choice by the risk management. The higher the required level of confidence, the higher the calculated risk numbers become. For instance, if the choice for the level of confidence is 99 %, then one can be 99 % confident, that the probability for ocular damage is less than or equal 40 %. For environmental studies and other risk analysis studies where uncertainty is modeled, often the 95 % quantile is used. The European Space Agency defines a representative quantity of the distribution, called "potentiality" as the logarithmic mean between the 95 % and 50 % quantile. This quantity, attempts to account for both the tail of the distribution towards higher risk numbers as well as the median of the distribution. The model as developed calculates the full set of quantiles, and it is the choice of the user which quantile is used to derive a risk number.

As expected, when exposure to doses within the modeled range of ED50 is considered, the probabilities at the 95 % quantile are high, but decrease for ocular energies which are below the lower border of the range of ED50s. For instance, in figure 10, for 1 μJ (a factor 5 below the lower boundary of the ED50 range and a factor 10 below the upper boundary of the ED50 range) the probability for ocular damage at the 99^{th} quantile is less than 10^{-11}. It should be noted that the distributions for ocular energies below the ED50 range do not have an upper tail towards higher risk values, i.e. the risk hardly increases for levels of confidence above the 95^{th} quantile, and one can have a confidence level of 100 % that the probability for ocular damage is less than or equal to instance 10^{-11} for the ocular energy of 1μJ.

The above calculations where obtained for a given specified (single point) value for the ocular energy. For many exposure scenarios, the actual level of exposure is not known, or can vary within a given range. In the model as developed for exposure from space based lasers, for instance, turbulence effects in the atmosphere induce scintillation are considered. Scintillation randomly varies the ocular energy around a mean value, which is the exposure level without scintillation, and this can be described by a probability density function[27]. Also for a given group of the population, the use of different kinds of optical instrument, which have different glass thicknesses and thus transmissivity, or varying atmospheric transmissivity, can be modeled by a distribution, describing the variability of ocular dose within a specified user group. For such a case of uncertainty and variability of the ocular energy, the resulting probability distributions for ocular damage might show a shallower tail towards higher risk numbers.

5. SUMMARY AND CONCLUSIONS

- For probabilistic risk analysis (PRA) of exposure to laser radiation, it is helpful if the concept of biological variability (heterogeneity within a population) is distinguished from uncertainty, i.e. lack of knowledge.
- When applying the dose-response curve for analysis of experimental data (Probit analysis), and especially for PRA, it should be remembered that the basic meaning of the dose-response curve is to characterize the biological variability of individual thresholds. The ordinate of the dose-response curve (the probability for ocular injury) in this sense, characterizes the probability that the exposed individual or retinal location will have a threshold smaller than the exposure level under consideration. If the threshold of the exposed site and individual were known, the situation is deterministic whether or not injury occurs for a given ocular exposure, i.e. there is no random aspect to the development of injury. For some types of laser-tissue interaction, in addition to the variability described by a dose-response curve, there might be stochastic processes involved.
- It is argued that the individual dose-response curve has a steep slope of the order of 1.05 to 1.2, even for retinal exposures. This slope characterizes the variability of thresholds of different sites of the retina.
- Due to inter-individual variability in a given group of experimental animals or population, there can be a spread of individual thresholds. When experimental threshold data is obtained for such a group and the data are pooled, an overall dose-response curve with a larger ED50 and shallower slope is the result. By performing simulation of the pooling, it is shown that the log-normal distribution only represents the pooled data well in the central part of the dose-response curve; it underestimates the risk for doses above the ED84 and grossly overestimates the risk for doses below the ED16.
- The variability of thresholds is limited towards lower doses due to biophysical reasons. Therefore there is a lower cut-off energy, below which the probability for ocular injury is zero.
- Uncertainties and variabilities which are present during the performance of the threshold experiments, and which are not present for the exposure of humans, need to be taken into account when the dose-response curve is used in PRA. When variability and uncertainty, which is bounded at small doses (such as due to variability of absorption or retinal

spot size) is corrected, the slope S and the ED50 need to be reduced. Simulations were performed to identify the correlation between the slope S and the ED50 for pooling of data.

- The uncertainty associated with the dose-response curve, i.e. to the ED50 and slope, can be modeled with probability distributions and Monte Carlo simulation. The result of such a model is a distribution for each given ocular injury, which characterizes the level of confidence about a calculated probability for ocular injury.

ACKNOWLEDGEMENTS

The study described here was carried out for the European Space Agency under the contract 13604/99/NL/GD.
The authors would like to express their appreciation for many valuable discussions and information regarding experimental laser threshold data to Jack Lund and Bruce Stuck from the Walter Reed Army Institute of Research, US Army Medical Research Detachment in San Antonio, TX, and to Joe Zuclich from TASC San Antonio, TX. Regarding mathematical issues pertaining to PRA and especially modeling of uncertainties, advice provided by Tim Bedford, University of Strathclyde, and David Vose, Le Leche, France, is gratefully acknowledged.

REFERENCES

1. D. H. Sliney, J. Mellerio, and K. Schulmeister, "Implications of using ED-50 and Probit analysis in comparing retinal injury threshold data", these proceedings.
2. D. Hattis and D. E. Burmaster, "Assessment of variability and uncertainty distributions for practical risk analysis", *Risk Analysis*, **14**, pp 713-730, 1994.
3. D. Vose, *Risk Analysis*, 2nd ed. John Weiley & Sons, Chichester, 2000.
4. G. Apostolakis, The concept of probability in safety assessments of technological systems, *Science* **250**, 1359-1364, 1990.
5. T. Bedford and R. M. Cooke, *Mathematical tools for probabilistic risk analysis*, to be published by Cambridge University Press, 2001.
6. F. O. Hoffman and J. S. Hammonds, "Propagation of Uncertainty in Risk Assessments: The need to distinguish between uncertainty due to lack of knowledge and uncertainty due to variability", *Risk Analysis* **14**, pp 707 – 712, 1994
7. P. A. Smith, "Probabilistic laser safety: ocular damage models for Q-switched Neodymium and Ruby lasers", *Health Physics* **66**, pp 414 – 419, 1994.
8. A. Mush, "Dose-time-effect-relationships", in R. M. J. Niesink, J. deVries, M. A. Hollinger, Ed., *Toxicology: Principles and Practice.* CRC Press, Boca Raton, 1996.
9. M. Abramowitz and I. A. Stegun, *Handbook of Mathematical Functions*, p. 295, Dover Publications, New York, 1965.
10. E. Limpert et al., "Life is log-normal", p 20-24 in R. Häberli et al. Ed, Transdisciplinarity: Joint Problem-Solving among Science, Technology and Society Workbook I, Haffmans, Zürich, 2000.
11. D. J. Finney, *Probit Analysis*, 3rd Edn., Cambridge, Cambridge University Press, 1971.
12. D. H. Sliney and M. Wolbarsht, *Safety with Lasers and Other Optical Sources*, New York, Plenum Publishing Corp. 1980.
13. J. A. Zuclich and D. J. Stolarski, Retinal damage induced by red laser, submitted to Health Physics.
14. D. J. Lund, P. R. Edsall, B. E. Stuck, "Ocular hazards of Q-switched blue wavelength lasers", these proceedings.
15. C. Ren-yuan, and 8 other, "Pulsed Nd:YAG laser irradiation injury threshold of Chinese retinas", *Chinese Medical Journal* **100**, pp 855 – 858, 1987.
16. A. Vassiliadis, R. C. Rosan, H. C. Zweng, *Research on ocular laser thresholds*, SRI Report 7191, Stanford Research Institute, Menlo Park, California, USA, 1969.
17. V. P. Gabel and R. Birngruber, "A comparative study of threshold laser lesions in the retinae of human volunteers and rabbits", *Health Physics*, **40**, pp238-240, 1980.
18. N. A. Peppers, A. Vassiliadis, K. G. Dedrick, H. Chang, R. R. Peabody, H. Rose, and H. C. Zweng, "Corneal damage thresholds for CO_2 laser radiation", Applied Optics **8**, pp 377 – 381, 1969.
19. C. B. Bargeron, D. J. Deters, R. A. Farrell, R. L. McCally, "Epithelial damage in rabbit corneas exposed to CO_2 laser radiation", *Health Phys* **56**, pp 85-95, 1989.
20. personal communication, Jack Lund, Walter Reed Army Institute of Research, US Army Medical Research Detachment in San Antonio, TX. ED50 data published in: Zuclich J.A., Lund D. J., Edsall P. R., Hollins R. C., Smith P. A., Stuck B. E., Till S., McLin L. N., "Experimental study of the variation of laser-induced retinal damage threshold with retinal image size (microsecond pulsewidths)", *Nonlinear Optics* **21**, pp 18-27, 1999; and Zuclich J.A., Lund D. J., Edsall P. R., Hollins R. C., Smith P. A., Stuck B. E., Till S., McLin L. N., Kennedy P. K. and S. Till, "Variation of laser induced retinal-damage threshold with retinal image size", *Journal of Laser Applications,* **12**, pp 74-80, 2000.
21. D. J. Lund and P. Edsall, "Action spectrum for retinal thermal injury, pp 209-228" in: Measurement of optical radiation hazards, Ed. Matthes, R. and Sliney, D.H, ICNIRP Oberschleißheim, 1998.

22. V. P. Gabel, R. Birngruber, F. Hillenkamp, *Die Lichtabsorption am Augenhintergrund [Light Absorption in the Retina]*, GSF Report A-55, Gesellschaft fuer Strahlen-und Umwelforschung, Neuherberg; 1976.
23. A. Langus, C. Fuchs and I. Gannot, The accuracy and relevancy of the Probit analysis for „In Vivo dose-response laser tissue experiments", these proceedings.
24. K. Schulmeister, G. Sonneck, F. Rattay, H. Hödlmoser, D. Sliney, J. Mellerio, A. Culoma, C. Preyssl, "A probabilistic risk analysis model for receiving laser eye injury from space based lasers", *Proceedings of the 5th International Conference on Probabilistic Safety Assessment and Management*, Osaka, Nov. 27th- Dec. 1st 2000, Ed.: S. Kondo and K. Futura, Universal Academy Press, Tokyo, Japan, 2000, Volume 1, pages 595 – 602.
25. J. A. Zuclich and J. S. Connolly, "Ocular damage induced by near-ultraviolett laser radiation", *Investigative Ophthamlology* **15,** pp. 760-764, 1976.
26. J. A. Zuclich, "Ultraviolet induced photochemical damage in ocular tissues", *Health Physics,* **56**, pp. 671-682, 1989.
27. L. C. Andrews and R. L. Phillips, *Laser beam propagation through random media*, SPIE Optical Engineering Press, Bellingham, Washington , USA 1998.

Use of the field of view evaluation apparatus (FOVEA) for laser eye protection research: capabilities, limitations and implications

Carita A. DeVilbiss*[a], Elmar Schmeisser**[b], William R. Ercoline**[b], Naiomi Cantu**[b]
[a]USAF Research Laboratory; [b]Litton/TASC, Inc.

ABSTRACT

While the major technological goal of laser eye protection (LEP) is to attenuate any laser radiation that passes through it, consideration of the physical format in which it is realized must not be overlooked. The best protective material can be rendered essentially useless if it does not cover the appropriate field of regard for the wearer. To map the visual field of regard (FOR) coverage provided by LEP devices, the field of view evaluation apparatus (FOVEA) was used. The FOVEA is a one-meter radius arc perimeter containing computer-controlled light emitting diodes at one-degree intervals. Three different mapppings of the visual field can be obtained with this facility: (a) the monocular baseline FOR; (b) the accessibility the LEP demonstrates against the *direct* threat (i.e., a laser source entering the eye beyond frame edge); and (c) the accessibility to *indirect* hazard (i.e., laser energy reflected from the lens backside entering the eye). Comparison of the direct and indirect fields of regard demonstrates the wide coverage variation generated by alternate frame styles and differing head shapes. These results need to be interpreted with respect to FOVEA limitations. First, the full FOR is mapped without regard for the relative importance of the periphery versus the fovea. Second, the coverage from a particular frame style must be measured and specified with an appropriate range of anthropometric face forms to ensure coverage consistency.

1. INTRODUCTION

As the availability of lasers increases with advancements in technology, the importance of effective eye protection in an operational environment also increases. Full field of view protection is required for military personnel engaged in laser operations and is more complex since any protective device must be compatible with the aircrew member's life support equipment. In the past to provide the full field of view coverage, the protection was integrated into flight visors. In such a configuration, verification of full field of view protection focused primarily on the consistency of the protection across the visor since there are typically no gaps between the visor and the helmet. While providing protection in a visor format is efficient, it does not provide sufficient flexibility to meet all operational needs. Hence, alternate formats are explored. For example, protection could be one housed in one of the various spectacle formats that have been successfully used in the commercial world. However, introduction of spectacles is accompanied with new concerns. The best protective material can be rendered essentially useless if it does not cover the appropriate visual field for the wearer. Specific concerns arise from the possibility of significant gaps between the spectacle and the wearer's face through which harmful laser energy could enter the pupil and damage the retina. The need for coverage verification has generated this current project to map the visual field that is covered, i.e., protected, by any particular spectacle format of interest. The resulting methodology would need to be adaptable for standard evaluation of multiple spectacle formats.

Historically, systems designed to measure visual fields (i.e., kinetic perimeters) have been designed for clinical settings and have required tedious and time-consuming operations[1]. Since such systems were developed for detailed clinical needs, the focus was strictly on the visual field, frequently with the head held in a stationary position. Consequently, these systems were not able to accommodate subjects wearing head-mounted equipment nor did they possess the repeatability and versatility needed in research, development, and testing of life support equipment. Hence, such systems were not useful in the evaluation of the visual impact of various operational systems. To fill this need, the Field of View Evaluation Apparatus (FOVEA) facility was constructed for the Cockpit and Equipment Integration Laboratory of the USAF Research Laboratory, Brooks AFB, TX. The FOVEA was established to quantify the visual constraints produced by contemporary life support equipment and to provide a basis upon which to predict the operational ramifications of various design configurations. More recently, the FOVEA has been adapted to map the coverage provided by various spectacle formats that could be employed to provide laser eye protection in an operational setting. This technical note presents the accumulated experience in this project, highlights both the capabilities and limitations of the device, and provides some considerations for data interpretation in the LEP context.

Laser and Noncoherent Light Ocular Effects: Epidemiology, Prevention, and Treatment,
Bruce E. Stuck, Michael Belkin, Editors, Proceedings of SPIE Vol. 4246 (2001)

2. METHODOLOGY

2.1 Facility

The FOVEA facility consists of an adjustable chair centered under a large moveable one-meter radius arc (see figure 1a). The subject is seated at the center of the arc and voluntarily fixates on a point directly in front (indicated with a star). The arc contains a linear series of 7-segment small light emitting diodes (LED) commonly used for numeric displays, placed at one-degree intervals and covering approximately 200 of a potential 250 degrees. Only the central segment is illuminated as a detection target. The apparatus is controlled by an IBM compatible 80286-series computer and Borland TurboC™ software to record and store data. Data files stored in ASCII format are transferred into a spreadsheet for analysis and plotting. The device is designed to measure an eccentricity along each meridian for the visibility of a suprathreshold small light emitting diode (LED) segment for all or part of visual space. Previous uses of the facility have shown its capability to quantify binocular field of regard restriction by various pieces of equipment (helmets, masks, etc.)[2,3]. As described above, this project adapted the FOVEA to measure the field of coverage provided by various spectacle frame styles envisioned for laser eye protection (LEP) use.

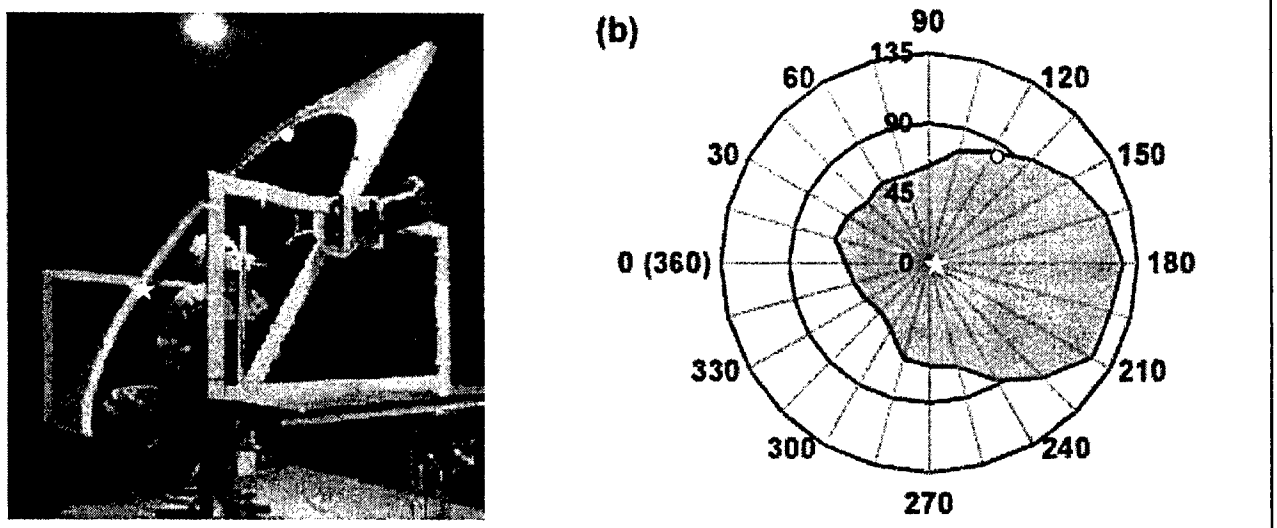

Figure 1: (a) Subject seated within the Field of View Evaluation Apparatus (FOVEA) with **star** indicating center point of focus and a **dot** indicating the location on the arc where the visual target first became visible to the subject. (b) Radial plot of a subject's total field of regard in the shaded area. Superimposed on the radial plot is the center point of focus (the **star**), the 120-degree meridian (where the arc is located); and the 85-degree eccentricity (the **dot**) where the visual target was detected.

2.2 Data

The FOVEA facility is a kinetic perimeter; i.e. it uses a moving stimulus with fixed size and luminance, and the data for the detection of the visual target are recorded in pairs. The first number of the pair is the meridian (i.e., the angle at which the arc is located) and the second number is the eccentricity (i.e., the number of degrees from center along the meridian). The sequence of meridians selected for presentation is randomized for each test run and one eccentricity is marked for each meridian per run. The resulting data pairs are imported to a spreadsheet to provide a three-dimensional radial mapping of the measured visual field (see figure 1b). In the Results section, an illustrative data set will be presented with further discussion of this radial plot. In the interpretation of the resulting visual field mapping it is important to have a full understanding of the instructions each subject followed during the data collection session.

2.2.1 Subject position. Each subject is seated in the center of the one-meter arc wearing any manner of head-mounted equipment that is under evaluation. In this facility, it is the subject's responsibility to maintain the defined position with the head against the headrest and the nose pointed toward the focus point on the arc. It is important that the seat is adjusted up and down to ensure the subject's eyes are located in center of the arc. Whenever the subject is required to wear a helmet, the

head position was adjusted to ensure the eye remains at the center of the arc. For consistency, it is important that the subject maintains this position throughout data collection.

2.2.2 Visual target. With the subject in the required position, the one-meter arc is rotated to one of 360 possible meridian positions. Once the arc is at the designated meridian, the visual target begins behind the subject and proceeds around the one-meter arc toward the center focus point in one-degree steps. In this application, the visual field is mapped with 24 meridians, evenly spaced at fifteen-degree increments. The subject is instructed to notify the investigator when the small LED visual target is first detected in the specified manner. Three examples of instructions for reporting the visual target would be (1) when the visual target approaching from behind the subject is first detectable, (2) when the visual target first intersects with the outer frame, and (3) when the visual target is first visible through the lens within the spectacle frame. Mapping of the visual field associated with the first instruction produces the subject's baseline visual field of regard. The second instruction would yield a visual mapping of the full coverage provided by that spectacle format. The third instruction set produces a visual mapping of the unobstructed visual field that is covered by lens. Note that the last two mapping would be virtually the same for spectacle formats that consist of very narrow frames, but could differ dramatically when a portion of the coverage provided by the format is provided by a thick frame that occludes part of the visual field.

2.2.3 Eye position. The third key element in the instructions to the subject is where the subject is instructed to fix the eye while maintaining fixed head position. To determine the field of coverage provided by a particular spectacle frame, it is important to evaluate the nasal visual fields to ensure any measurable space between the spectacle frame and the nose bridge is detected. Hence, monocular data was recorded with the right eye while the left eye was occluded. There are two traditional instruction sets that are used when recording visual field data with the head in a fixed position: field of view and field of regard data. In the first situation – field of view data – the subject is instructed keep the head fixed and to keep the eye fixated on the focus point and indicate when the visual target is first detected in the periphery. For field of regard data, the subject again keeps the head in the fixed position, but is allowed to rotate the eye to acquire the visual target. In this current application, the field of regard methodology was employed to approximate the extremes to which the eye can rotate in a real world situation. Hence, the illustrative visual field map would not only represent the full extent of the visual space that is available to the subject, it would as provide detail of any gaps between the spectacle and the nasal structure of the face.

2.3 Configurations

As indicated, one of the biggest advantages of using the FOVEA facility is the ability to accommodate life support equipment to simulate "as used" conditions as closely as possible in a laboratory setting. For each subject, an unencumbered field of regard map was obtained to provide the baseline for all comparisons with the configurations being evaluated. The intersection of the light with the spectacle frame marks the limits of coverage provided by that configuration. Comparing the visual mappings with each LEP configuration to the baseline provides a descriptive analysis that represents the percentage of unprotected visual field of regard remaining with each configuration. By implication, these data provide the visual angles from which a laser could illuminate a pilot's retina and, with sufficient power, damage it despite wearing a particular LEP.

3. ILLUSTRATIVE RESULTS

This technical note presents the accumulated experience of this project to adapt visual field mapping techniques to the laser eye protection program. Hence, the objective is to highlight the capabilities and limitations of the device, and to provide some considerations for data interpretation in the LEP context. To provide an appropriate discussion platform, this section presents selected results from an existing data set to illustrate specific concepts.

3.1 Radial Plot

The visual field mapping data are displayed as a two-dimensional projection of the actual three-dimensional space. Refer back to Figure 1 where (a) is a picture of the facility and (b) is the resulting mapping of the subject's baseline visual field. As discussed earlier, the data pairs consisted of a meridian and an eccentricity. Meridians, i.e., the location of the arc, range from 0 degrees (to the left), though 90 degrees at the zenith to 180 degrees (on the right), and continuing to a maximum of 360 degrees (again to the left). Eccentricities (i.e., the location of the visual target along the meridian) range from 0 degrees at the central fixation point, outward in any direction by one degree increments, to 180 degrees directly behind the head. Typically, the visual field is mapped with 24 meridian-eccentricity pairs, with the meridians evenly spaced at fifteen-degree increments and the eccentricities measured within one degree. As an additional reminder, the term "fixation" in these data does not refer to the alignment of the eye's visual axis with a particular vector in visual space. What is fixed is the alignment of the skull itself, since the eyes are free to move during the test. Ideally, this would be done with a bite bar, but since the arc has a large

radius and a best resolution in whole degrees, small errors of placement do not produce large inaccuracies. Stabilization is aided with a headrest and the instructions to "point the nose" at the fixation light.

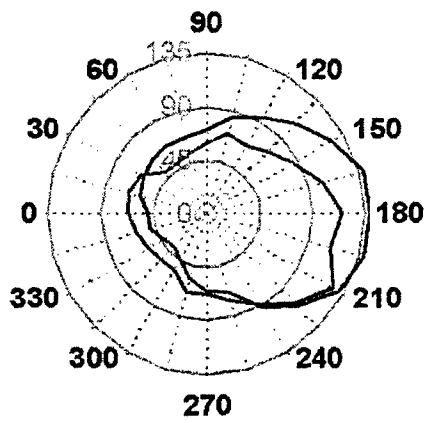

Figure 2: Inter-individual variability. Two baselines obtained from two subjects with differing facial structure in the nasal and brow regions.

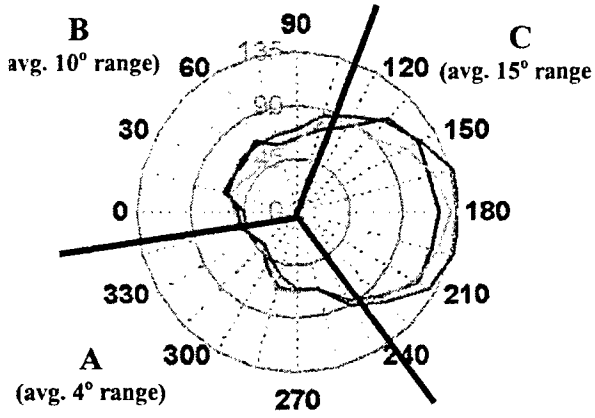

Figure 3: Intra-individual variability. Three baselines with the same subject but measured on separate days. Eccentricity measurement variability along each meridian differs depending on the area of the retinal.

3.2 Sources of Variability

As with all experimental procedures, there are several sources of data error in this device: procedural or equipment, inter-individual and intra-individual variance. A firm appreciation of each source of variability promotes adherence to procedures designed to minimize each and an understanding of the variability that is beyond total control.

3.2.1. Procedural Variability. Procedural variations arise from the unconstrained nature of the test and inherent variability in the equipment. Life support equipment (e.g. LEP, helmet, oxygen mask, etc.) to provide operational relevance may not don reproducibly across multiple sessions, even on the same subject and has variable fit across subjects. Subject positioning is less controlled than typical laboratory settings since a bite bar cannot be used. Based on test-retest runs, it is common to have between 8 and 10% variability in the summed area measurements for any particular visual field. This variability can be minimized with specific instructions to the subject and strict adherence to procedures.

3.2.2. Inter-individual Variability. The natural difference between individuals introduces the inter-individual variability component. Individuals vary in several key aspects: training, equipment familiarization, and criterion for light detection. Another type of variation is unavoidable since it represents the inherent variability in anthropometric structures across the population on interest. Figure 2 illustrates this variability with baselines visual field maps from two subjects with differing prominent facial features. The reproducibility of equipment fit from skull size and shape variations and the relationship of a particular individual to a particular piece of equipment (the average coefficient of variation around all meridians was 15% across four subjects).

3.2.3. Intra-individual Variability. Lastly, variability is introduced within each individual subject from such things as residual body sway (including postural readjustments for comfort), head drifts and facial muscle movement during the test. More importantly, the precision of the eccentricity measurement along each meridian varies across the retina. Figure 3 illustrates this variability by presenting three baseline visual field maps for the same individual. For discussion, the visual field mapping in Figure 3 was subdivided into three equal sections, each containing eight meridians, to illustrate the areas of variability. Within Section A, eccentricity measurements are very repeatable with the average range of 4 degrees between measurements along each meridian. The variability of the eccentricity measures increases to an average range of 10 degrees in Section B. The greatest variability in the eccentricity measures is in Section C with an average range of 15 degrees. These results are consistent with the part of the retinal being stimulated. For example, Section C represents detection in the far periphery where the rods are the dominant visual structure as compared to the cones located near the center of the retina.

3.3 Typical Results. To illustrate the utility of the FOVEA for visual field mapping, the result across four subjects with two different spectacle frames are presented. With the head relatively stabilized, the subject is tested monocularly to reveal areas in which the frame may not provide coverage, but which may be masked by apparent coverage in the other eye's field of view, i.e. over the bridge of the nose. Typically, two visual field mappings are obtained for each format evaluation. The first is the baseline visual mapping, previously discussed, that identifies that subject's full field of regard. The second mapping would be of the outer edge of the spectacle format under evaluation, with the tacit understanding that the spectacle provides the needed laser protection. The final result for each evaluation is typically expressed as the percentage of the baseline field that is covered, i.e., protected, by each spectacle format. Hence, comparisons between configurations can be made on the basis of percent coverage. However, seldom does this percent coverage convey all important factors. To illustrate this point, two spectacle formats with comparable overall coverage will be presented with averaged data from four subjects. Each radial plot includes three visual field maps are superimposed upon each other. The visual maps for the spectacle components are color-coded white and light gray. These illustrations are not intended to be quantitative or in depth analyses of these particular frame styles.

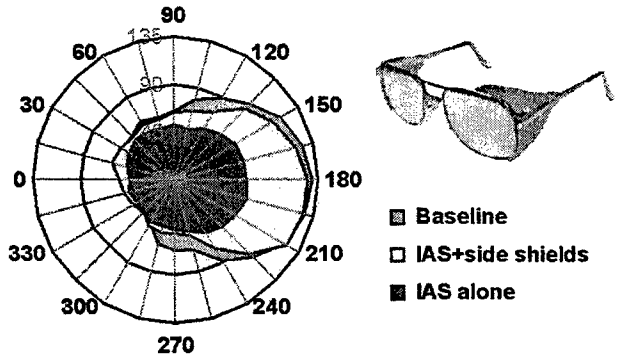

Figure 4. Standard frame example. Average (n=4) visual field of regard map for the Improved Aircrew Spectacle (IAS) with tinted side shields attached to the temples.

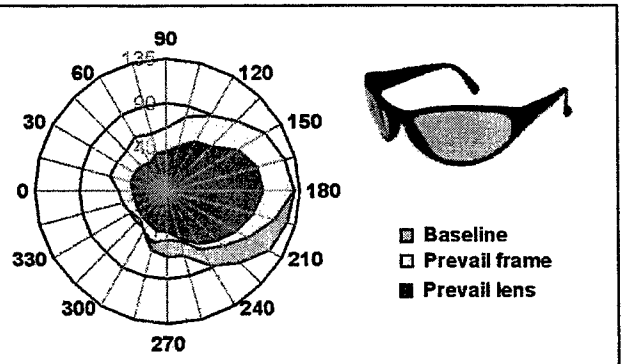

Figure 5. Thick frame example. Average (n=4) visual field of regard map for the Prevail™ frame, with the visual occlusion of the frame material indicated.

3.3.1 Standard frame. The first example format is the "Improved Aircrew Spectacle" (IAS) frame that is similar to commercial spectacle frames with detachable side shields added for peripheral protection (Figure 4). The averaged unencumbered (baseline) monocular visual field of regard is potted as the lowest layer and color-coded with a light gray. The IAS spectacle itself without the side shields, i.e., the top layer color-coded dark gray, covers on average 70% of the baseline visual field. The lenses are slightly curved and the sides relatively open, as is the area over the cheeks. These openings are visible on the radial plot as the difference between the spectacle (dark gray) and the baseline (light gray) visual field maps. There is a small series of openings over the bridge of the nose as well. The third plot, color-coded white, describes the coverage provided by the IAS frame with the additional side shields coverage. This expanded configuration provides an average coverage of 95% of the baseline visual field. Due to the narrow nature of the spectacle frame and assuming a transparent material in the side shield, this is additional coverage, not total occulsion of the visual field. However, if a material different from the lens is used for the side shield, there will be an impact on peripheral vision proportional to the transmissivie differential.

3.3.2 Thick frame. The second example frame is the commercially available Prevail™ frame. This is a sleek plastic frame in a wrap-around design that fits close to the face (see Figure 5). Since the same four subjects were used, the average baseline, i.e., the light gray plot, is the same as just discussed in the previous example. The overall coverage, i.e., color-coded white, provided with this frame is comparable coverage to the IAS frame with side shields -- 93% coverage on average. However, an additional visual field map was obtained to identify the area visibility within the lens. The mapping of the lens, color-coded in dark gray, indicates the 70% of the baseline is both covered and has full visibility. These two examples illustrate the two solutions that provide the similar overall coverage (protection) but with different results. For subjects who were comfortably fit with these spectacles, the wraparound protection was excellent and the occlusion from the thick frame was not deemed to be a significant problem. In the way of further clarification, this sleek plastic fame was dropped from consideration not for the thick frame, but for the lack of adequate adjustment features to allow accommodation of the larger population and in some cases the thickness of the temples interfered with integration with the life support equipment. These two frames were compared to illustrate the complexity of assessing the coverage of a configuration both in the overall amount

of coverage and the potential for negative operational impact of a given solution. Hence, two frames with similar overall coverage levels but could have different operational utility.

3.3.3 Direct vs Indirect Exposure. What has been discussed to this point is a methodology for quantifying the overall percentage of coverage provided by LEP formats from a direct laser threat. Direct threats are laser beams that come directly at the eye from external sources. This visual field mapping methodology can also be expanded to document the smaller indirect threat. Any LEP with openings towards the side of the face has the potential to reflect light from behind the wearer into the eyes in the same manner as a rear view mirror. Consequently, a wearer can see the target LED reflected from the area behind and to one side of the head in the lens. Plotting this field demonstrates the indirect path a laser could take into the eye.

4. DISCUSSION

4.1 Limitations

In essence, the FOVEA reproduces the simple arc perimeter developed in 1857 by Aubert[4], enlarging it and adding a mechanical method to position the arc and the stimulus. Further, unlike Aubert, it is limited to only one type of stimulus (size and shape). It has minimal control over the luminosity or contrast of the stimulus. While it provides some needed capabilities, some of the major limitations of this device need to be understood to fully interpret the results.

4.1.1. Suprathreshold data. A fundamental constraint of the device is that it deals with suprathreshold data only. Further, since it produces only one isopter, it compresses the more or less peaked "hill" of vision into a flat, indeterminately elevated "mesa" of vision. This constraint is actually an optimization that permits the device to be used in a very natural way with bulky equipment and to answer important engineering questions as opposed to investigating fundamental aspects of the visual field.

4.1.2. Overemphasis on periphery. As noted in the methods, the plot visually overemphasizes the periphery, although the calculations of coverage are uniform across the full field of regard. Every square degree is equivalent to every other square degree in importance. From safety considerations only, any lesion anywhere is unacceptable, and the amount of protection for a specific LEP frame style should be calculated in this manner, i.e. in total square degrees covered divided by total square degrees of baseline. However, the retina is not homogeneous. The periphery has much lower acuity resolution, etc. than the center of the retina. Clinically, for example in diabetic retinopathy, physicians routinely put thousands of laser lesions (burns) into the retinal periphery outside the vascular arcades without causing the patient any visual distress[5]. Further, even for the catastrophic hemorrhagic lesions, if they are in the peripheral retina, virtually all of these heal completely without serious visual sequelae without any medical treatment[6,7]. Requiring 100% coverage by an LEP drastically constrains the engineering trade space for design, and may make an acceptable design for combat aviation use impossible.

4.1.3. Sources of variability. The earlier discussion emphasized the necessity of strict procedural adherence to minimize both procedural and individual variability. For example, accommodation of life support equipment in the "as worn" condition precludes the use of laboratory techniques, such as bite bars, which minimize variability. However, diligence in instructing the subject in the importance maintaining the desired posture will help in this regard. Another important source of inter-individual variability can be minimized with clear instruction and training in the appropriate criterion for marking the visual target, e.g., first detection vs. clear identification.

4.1.4. Individual variability. While every effort needs to be employed to minimize variability, it should be noted that some individual variability could provide beneficial information. For example, since the resulting devices will be fielded for a wide population of aircrew members, it is important to sample a wide variety of anthropometric head forms to ensure sufficient adjustment features affords the save level of coverage with different head shapes.

4.2 Capabilities

The benefits gained by employing a facility such as the FOVEA for the quantification of the amount of coverage provided by various LEP configurations far outweigh the limitations. However, without an appreciation for the limitations, the capabilities can be over emphasized and contribute to less than optimal solutions. While the capabilities have been highlighted throughout the text, a summary of the main elements is included.

4.2.1. Monocular visual field. By occluding one eye, the resulting visual map clearly indicates areas of potential vulnerability in the nasal region that may have gone undetected in a binocular mapping. This was not as much of a concern in

earlier application when the protection was provided in a visor format. Advancing to any spectacle format increases the importance of obtaining a clean fit in the nasal region to shield the eye from those rays. This type of visual mapping can be instructive when emphasizing the importance of individual spectacle fit. Adjustments in the nasal region are designed to provide acceptable coverage across the diverse population that will be using these protective devices. These mappings can illustrate the increased vulnerability introduced with poorly fit frames.

4.2.2. Operational relevance. The benefits gained from being able to obtain visual field data in an "as worn" condition cannot be overemphasized. The FOVEA provides a methodology to obtain visual field mapping with the LEP configuration integrated with any type of life support equipment to ensure that there will not be any integration problems. For example, does the LEP become dislodged when worn with a helmet or an oxygen mask.

4.2.3. Representative of the population. The versatility of this methodology provides an excellent way to efficiently verify whether the full population can be accommodated. It is also possible to evaluate unusual cases to determine the amount of their individual visual field coverage with each configuration.

4.2.4. Fit verification. An important side benefit to using this methodology is to demonstrate the importance of proper fit of the spectacles. The best protective material can be rendered essentially useless if it does not cover the appropriate field of regard for the wearer or if it is allowed to slip out of place.

5. CONCLUSIONS

While FOVEA provides unprecedented freedom in determining the relative impact on the visual environment for a particular piece of equipment, its data cannot be over-interpreted nor expected to be accurate to better than about ±5 degrees per meridian measured. The cost/benefit ratio of protection vs. the compound factors of cost, manufacturability, wearability and interference with other combat related tasks is not easily determined. Many additional factors enter into the final decisions. An importance aspect of coverage is to identify what part of the retina is protected. For example, a 10% area that is unprotected may be tolerable if it is located in the far periphery, but totally unacceptable if it the central retina is at risk. The FOVEA facility provides an efficient methodology to quantify the coverage provided by various laser eye protection configurations. These data are important for the safety analysis as well as the evaluation of various candidate prototypes under consideration.

6. REFERENCES

1. D.O. Harrington, *The visual fields: a textbook and atlas of clinical perimetry (5th ed.)* St. Louis: C.V. Mosby Company, 1981.
2. D. Cohen, D. Diesel, "Demonstration of field of view evaluation apparatus (FOVEA) for head borne life support equipment," *SAFE Journal 1996*, **26**(1), pp. 29-33.
3. B.P. Self, "A comparison of the field of view of three chemical defense masks," *SAFE Journal 1999*, **29**(2), pp. 79-84.
4. Aulhorn E, Harms H. Visual Perimetry. In: Jameson D, Hurvich LM (eds). *Handbook of Sensory Physiology, Vol. VII/4: Visual Psychophysics*, Chapter 5, Springer Verlag, Berlin, 1972. Pages 102-145.
5. Mestres FD, Vilaplana D, Civit JR, Torres F, Barraquer J. Static perimetry evaluation of argon green and dye red laser treatment for choroidal neovascular membranes. *Laser and Light in Ophthalmology* 1993; 6(1): 27-32.
6. Mellerio J, Marshall J, Tengroth B, Anderberg B, Wolbarsht M. Battlefield laser weapons: an assessment of systems, hazards, injuries and ophthalmic resources required for treatment. *Lasers and light in ophthalmology* 1991; 4(1): 41-67.
7. Mainster MM. Retinal laser accidents: mechanisms and management. *J Laser Applic 2000*; 12(1): 3-9.

A Morphometric Comparison of the Acute Rabbit and Pig Corneal Response to 1540 nm Laser Light Following Ex Vivo Exposure

Thomas E. Eurell[a], W.Pat Roach[b], Thomas Johnson[b]
[a]University of Illinois at Champaign-Urbana, Urbana, IL, 61802, [b]Uniformed Services University of the Health Sciences, Bethesda, MD, 20814

ABSTRACT

Single pulse, 1540 nm laser light with a pulse width of 1 microsecond altered the morphologic appearance of explant rabbit and pig corneas following ex vivo exposure. Using digital images of the post-exposure corneas projected onto a measuring grid, we could accurately locate the relative position of the circular laser lesion in the embedded tissue. This allowed us to section through the lesion with micrometer precision and accurately resolve the inside edge, middle and outside edge of the laser lesion. All tissue sections used for morphometric analysis were taken through the middle of the lesion. Several features of the response to laser exposure may reflect species-specific tissue differences. The rabbit corneal epithelium showed a homogeneous coagulative necrosis with a distinct demarcation between necrotic and normal epithelium. The pig epithelium also showed a distinct demarcation between necrotic and normal epithelium, however, there were several remarkable differences in the tissue response between the two species including coagulative necrosis pattern and nuclear morphology. These changes suggested a different and less severe response of the pig epithelium to the laser light when compared to the rabbit epithelium.

Keywords: Rabbits, pigs, cornea, laser, infrared laser, histomorphometry, histology

1. INTRODUCTION

Infrared lasers have wavelengths where water is generally considered the principal chromophore. This is useful in refractive surgery of the eye because the cornea is approximately 80% water. Additionally, the infrared laser does not have the potential complication of secondary UV-B irradiation of the lens (a potential complication of the eximer laser). In a transparent tissue, such as the cornea, minimal scattering occurs and the absorption factor is principally associated with light attenuation. In general, photodistruption interactions occur when the pulse width is the shortest (femtosecond - nanosecond range), photoablation interactions fall in the middle range (nanosecond-microsecond range), and photothermal interactions occur with long pulse widths (microsecond-second range) or continuous wave lasers (Sliney and Wolbarsht, 1980; Niemz, 1996). The new generation of infrared lasers operates in the nanosecond-femtosecond pulse width range. These lasers do not produce collateral photothermal damage and are being studied for new and innovative clinical applications such as laser-based flap cutting in the LASIK procedure (Krueger et al., 1998) and intrastromal refractive surgery (Kurtz et al., 1998; Lubatschowski et al., 2000).

Effective clinical application of infrared lasers for both anterior and posterior segment surgery requires prediction of clinical outcomes of post-exposure wound healing. This process is complicated because several of the photoablative and photodisruptive tissue interactions are non-linear in nature (Sliney and Wolbarsht, 1980; Niemz, 1996; Kurtz et al., 1998; Bryant et al., 2000). A key element in approaching this problem is studies with experimental animals. The major animal models for the study of general ocular wound healing include the rabbit, pig, rat, cat, cow, dog, mouse and non-human primate. The rabbit and the pig are the two most commonly reported experimental animals used for laser-induced corneal wound healing. Although there are dozens of reports describing the rabbit or pig response to different surgical approaches and laser equipment, we were not able to find any reports comparing both the rabbit and pig corneal response to equivalent laser exposures under equivalent experimental conditions.

Laser and Noncoherent Light Ocular Effects: Epidemiology, Prevention, and Treatment,
Bruce E. Stuck, Michael Belkin, Editors, Proceedings of SPIE Vol. 4246 (2001)

2. MATERIALS AND METHODS

Experimental Animals

All experimental protocols involving animals were approved by the Institutional Animal Care and Use Committee of the Uniformed Services University of the Health Sciences and were conducted in strict accordance with the "Guiding Principles for the Care and Use of Research Animals." Rabbit and pig eyeballs were obtained from animals undergoing terminal procedures not related to this study and without clinical manifestations of ocular disease. Immediately after euthanasia of the animal and enucleation of the eye, each eyeball was rinsed in 0.1 M phosphate buffered saline and transferred to F12/DMEM media (MediaTech) supplemented with 10% NuSerum (Collaborative Biomedical), 2 mM L-glutamine, 500 IU/ml penicillin, 500 µg/ml streptomycin and 1.25 µg/ml amphotericin. Enucleated eyeballs were maintained at 4°c and used for laser exposure within 6 hours of enucleation

Laser Exposures

All explant corneal exposures were single pulse, 1540 nm laser light with a pulse width of 1 microsecond. The area of the laser beam was either 0.00047 cm^2 or 0.00201cm^2. The radiant exposure (energy density in J/cm^2 at $1/e^2$) ranged from 474 to 65 J/cm^2. The laser used in corneal exposures was manufactured by Laser Sight Technologies (Winter Park, FL). It had an Erbium:Glass rod and q-switched circuitry to produce pulse widths in the µs-ns range at a wavelength of 1540 nm. The pulse widths were measured using a Germanium detector (Thor Labs PDA 255) connected to a TDS 644B -digitizing oscilloscope (Tektronix). Energy measurements were made with a EPM 2000 detector (Molectron) connected to a J-25 energy probe (Molectron).

Histomorphometry

After overnight incubation (4°C) in F12/DMEM media, the corneas were harvested from the laser-exposed eyeballs. Digital images of the corneas were obtained (Kodak EDAS system), the tissues were frozen in OCT embedding medium (Tissue-Tek) and six-micron frozen sections were taken using a motorized cryomicrotome (Bright Instruments). We could accurately locate the relative position of the laser lesion in the embedded tissue by projecting digital images of the corneas onto a measuring grid. This allows us to section through the lesion with micron precision and accurately resolve the inside edge, middle and outside edge of the laser lesion. All tissue sections for histomorphometric analysis of laser effects were taken through the middle of the lesion. Ten control areas (no histological evidence of laser injury) each from 3 pig and 3 rabbit corneas were randomly selected to establish reference histomorphometric values for each species.

Phase differential interference contrast microscopy (BK-2 research microscope, Olympus) was used to evaluate unstained sections for relative position within the lesion, as well as, proper orientation and the occurrence of any sectioning artifacts. Sections were stained using Gill's #3 Hematoxylin for 30 seconds, rinsed in tap water for 5 minutes and counterstained using Eosin/Phloxine for 30 seconds. Stained sections were dehydrated in a series of alcohols, dipped in xylene and mounted using Eukitt (Fisher). Histomorphometric data was captured using a Leitz Orthoplan microscope equipped with a SpotRT digital camera (Diagnostic Instruments). Quantitative evaluation of histomorphometric data was performed using the Image Pro Plus analysis software (Media Cybernetics).

3. RESULTS AND DISCUSSION

Table 1. Reference Histomorphometric Data from Thirty Control Areas in Pig and Rabbit Corneas.

Species	Epithelial Thickness (µ) (mean ±1 S.D.)	Stromal Thickness (µ) (mean ±1 S.D.)	Total Corneal Thickness (µ) (mean ±1 S.D.)
Pig	66.7±9.7	1,198.8±98.8	1,264.4±103.7
Rabbit	36.0±2.6	623.1±37.4	657.9±36.1

Histomorphometric data indicated that although both the epithelial and stromal layers of the pig cornea were approximately twice the thickness of the analogous layers in the rabbit cornea (Table 1), the relative thickness of the pig and rabbit corneal layers was similar. The corneal values determined in the present study were similar to previously reported values for these species (Samuelson, 1999).

Table 2. Histomorphometric Data of Lesions from Six Pig Corneas in Relation to Different Laser Exposure Conditions.

Spot Size (cm^2)	Energy Density (J/cm^2 at area $1/e^2$)	Maximum Depth of Lesion (microns)	Total Area of Lesion ($microns^2$)
0.00047	474	1,180	282,357
0.00047	440	919	274,474
0.00047	435	910	235,445
0.00201	108	645	191,479
0.00201	97	206	129,437
0.00201	65	85	64,397

Table 3. Histomorphometric Data of Lesions from Three Rabbit Corneas in Relation to Different Laser Exposure Conditions.

Spot Size (cm^2)	Energy Density (J/cm^2 at area $1/e^2$)	Maximum Depth of Lesion (microns)	Total Area of Lesion ($microns^2$)
0.00047	456	712	249,148
0.00047	452	660	221,717
0.00047	444	623	218,449

At high energy density (> 450 J/cm^2) the rabbit lesion was deeper that the reference dimension of the normal cornea. When this occurred a characteristic "hump" was formed in the cornea that accounted for the additional thickness. The phenomenon of "hump" formation in rabbit corneas has been previously reported following laser exposure (Kamensky et al., 1998). The formation of a post-laser exposure "hump" was not seen in the pig cornea. At relatively equivalent energy densities ($\geq$ 435 J/cm^2), the pig lesion was deeper than the analogous rabbit lesion, but approximately the same total area. This gave the histologic appearance of a narrower lesion field. In the pig, the larger spot size (0.00201 cm^2) produced a smaller energy density than the 0.00047 cm^2 spot size. This appeared to correlate with a smaller maximum depth and total area of the lesion (Table 2). Only one spot size was used in rabbit tissue exposures.

High magnification (400X) images (Figures 1 and 2) show the characteristic responses of the rabbit and pig anterior corneal segment to laser exposure. Several species differences in the corneal anatomy and laser-tissue interaction are present in these figures. The rabbit epithelium (Figure 1) shows a homogeneous coagulative necrosis with a distinct demarcation between necrotic and normal epithelium. The homogeneity of the coagulative necrosis gives the epithelium an eosinophilic, hyaline appearance. Individual epithelial cells have a uniformly condensed nuclear morphology and indistinct boundaries between cells in the necrotic area. The pig epithelium (Figure 2) also shows a distinct demarcation between necrotic and normal epithelium, however, there are several remarkable differences in the tissue response between the two species. The pig epithelium has an eosinophilic, hyaline appearance only in the posterior segment of the cornea. The coagulative necrosis pattern of the middle wing cells and surface epithelium has a distinct granularity. In addition, the middle and superficial layers of the pig epithelium within the necrotic area have less condensed nuclear morphology and more prominent intercellular boundaries than the analogous regions of the rabbit cornea. In addition to a loss of basement membrane staining underneath the necrotic epithelium, there is a distinct detachment of the basement membrane between the basal epithelial layer and the underlying stromal layer. These changes suggest a different and less severe response of the pig epithelium to the laser light when compared to the rabbit epithelium.

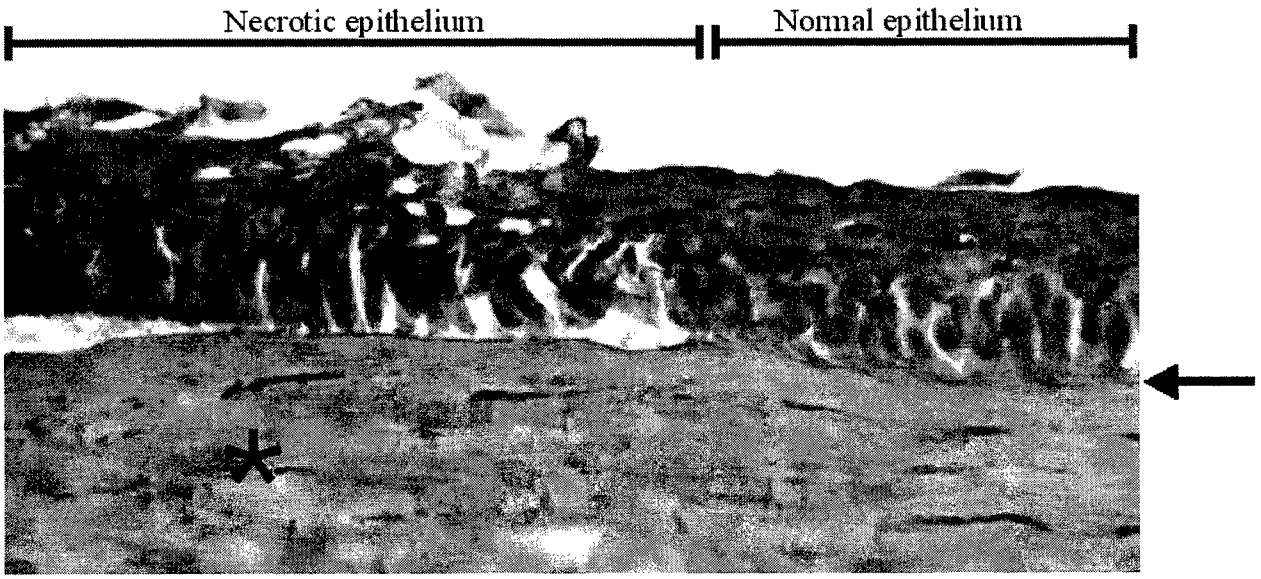

Figure 1. Rabbit anterior cornea at epithelial-stromal junction. Arrow indicates basement membrane; * is coagulated stromal collagen. Note separation of epithelial-stromal layers at basement membrane directly underneath necrotic epithelium. Original magnification= 400X, H&E stain.

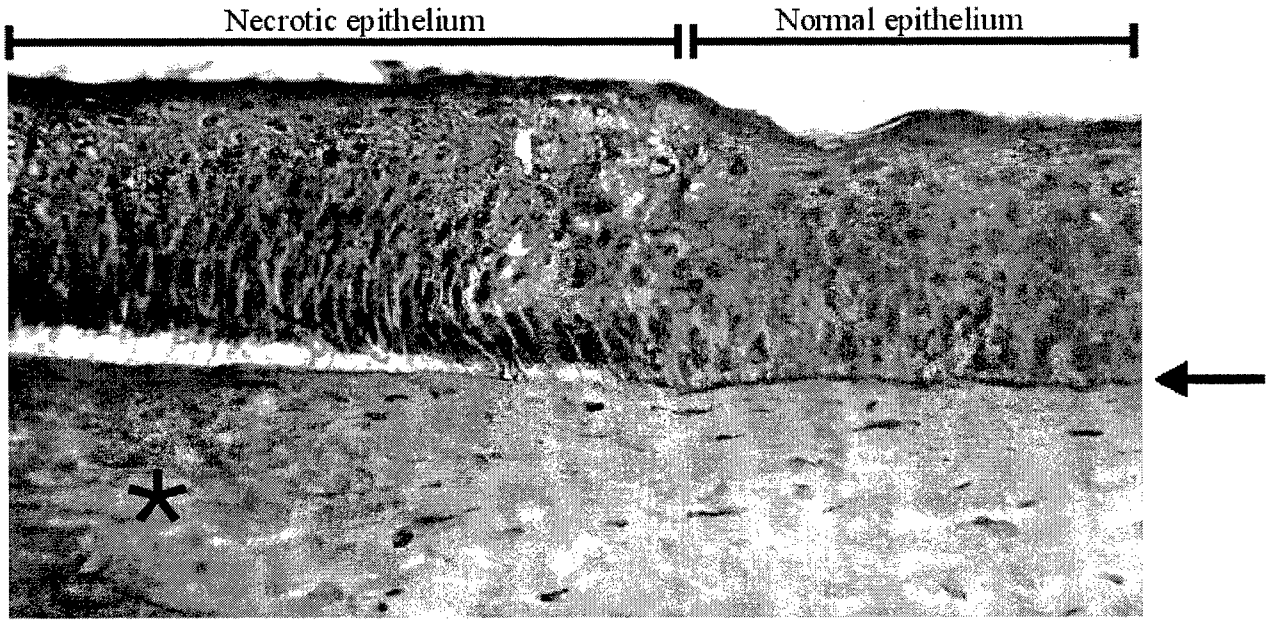

Figure 2. Pig anterior cornea at epithelial-stromal junction. Arrow indicates basement membrane; * is coagulated stromal collagen. Note separation of epithelial-stromal layers at basement membrane directly underneath necrotic epithelium. The epithelial basement membrane of the pig is characteristically more prominent than the rabbit (Figure 1) Original magnification= 400X, H&E stain.

4. LITERATURE CITED

Kamensky, V., R. Kuranov, et al. (1998). In situ observation of IR and UV-solid state laser modifications of lens and cornea. SPIE Vol. 3254, Laser Tissue Interaction, San Jose, CA, SPIE, 390-397.

Krueger, R. R. (1998). "Could apoptosis change the way we do PRK? " J Refract Surg **14**(5): 494-6.

Kurtz, R. M., C. Horvath, et al. (1998). "Lamellar refractive surgery with scanned intrastromal picosecond and femtosecond laser pulses in animal eyes." J Refract Surg **14**(5): 541-8.

Lubatschowski, H., G. Maatz, et al. (2000). "Application of ultrashort laser pulses for intrastromal refractive surgery." Graefes Arch Clin Exp Ophthalmol **238**(1): 33-9.

Niemz, M. (1996). Laser-Tissue Interactions: Fundamentals and Applications. New York, Springer.

Samuelson, D. (1999). Ophthalmic anatomy. in Veterinary Ophthalmology, (ed.) Gelatt, K., 3rd edition, Philadelphia, Lippincott, Williams and Wilkins.

Sliney, D. and M. Wolbarsht (1980). Safety with Lasers and Other Optical Sources. New York, Plenum Press.

Addendum

The following papers were announced for publication in this proceedings but have been withdrawn or are unavailable.

[4246-01] **Neuroprotection treatment for laser-induced retinal injuries: the quest continues**
M. Belkin, G. Dubinski, M. Rosner, I. Ben-Bassat, Y. Solberg, Tel-Aviv Univ. (Israel)

[4246-04] **Medical surveillance of laser workers: pros and cons**
B. E. Stuck, J. Brown, Jr., H. Zwick, D. J. Lund, Walter Reed Army Institute of Research (USA)

[4246-20] **Evaluation of laser injury in the Department of Defense**
J. Dunn, W. P. Roach, T. E. Johnson, Uniformed Services Univ. of the Health Sciences (USA); B. E. Stuck, Walter Reed Army Institute of Research (USA)

Author Index